Structural organization of the FtsB/FtsL transmembrane subcomplex of the bacterial divisome

By

Loren Marie LaPointe

A dissertation submitted in partial fulfillment of

the requirements for the degree of

Doctor of Philosophy

(Biochemistry)

at the

UNIVERSITY OF WISCONSIN – MADISON

2014

Date of final oral examination: 12/1/14

The dissertation is approved by the following members of the Final Oral Committee:

Alessandro Senes, Associate Professor, Biochemistry
Ivan Rayment, Professor, Biochemistry
Patricia Kiley, Professor and Chair, Biomolecular Chemistry
Douglas Weibel, Associate Professor, Biochemistry and Chemistry
Samuel H. Gellman, Professor, Chemistry

To James Granlund, Chemistry, Comstock High School
1957-2005

Table of Contents

List of Figures

Acknowledgements

I would like to thank my funding from the graduate school; I was supported on the WARF Distinguished Fellowship for two years of my graduate career. I would also like to thank my advisor, Professor Alessandro Senes, for his guidance the past five years. He has taught me to think critically about my experiments, and to never settle for not fully understanding a concept or a result. He has truly made me a better, more confident scientist. I am excited to carry forward what I have learned as a graduate student in his lab to my postdoctoral studies. I would also like to thank the current and former members of the Senes Lab. Dr. Sabareesh Subramaniam was integral to the success of my first publication. Ambalika Khadria has been an excellent collaborator of mine and also a helpful support system. Ben Mueller has also been a supportive lab mate, providing insightful discussion, and also adding some fun to being in lab with his sense of humor. Sam Craven and Sam Condon, the newest members of the lab, have really grown into their positons well and are taking great strides toward becoming leaders in the lab. Gladys Díaz-Vázquez is the newest member to join the lab, just a week ago! She is our first biophysics student and I am very excited at the prospect of someone with molecular dynamics experience working in our lab.

I would very much like to thank all of the undergraduate students I have had the pleasure to mentor over the years. Evan Lange started as a high school student with me in 2010 and is now a senior undergraduate at UW working independently in the lab. Claire Armstrong has been in the lab since her sophomore year and has been a huge help in the molecular biology portion of my projects and I am proud to see her also working on her own independent TOXCAT project in the lab. Joel Lange worked with me for his sophomore and junior years at UW and was a huge help with troubleshooting western blotting, to name just one technique that he helped with. Joel has just been accepted to Loyola Medical School where I know he will be very successful. Finally, I would like to thank my current

undergraduate student, Claire Holesovsky, who is going to help me apply brute force to my project to complete Chapter 4 of this dissertation before I transition to my post doc position at Vanderbilt University. I am anxious to follow the careers of these bright young scientists and hope that they have learned a lot under my guidance.

I would like to thank my graduate thesis committee for sticking with me through five years of committee meetings. Professor Ivan Rayment has served as the chair of my committee as well as one of my most fruitful collaborators here at UW. I would like to thank Ivan for his structural expertise, critical questions of my work, and for including me at his lab meeting for extra discussion. His students, Keenan Taylor and Becky Phillips, have assisted me in many aspects of protein purification as well as shared equipment from their lab. I would like to thank the Rayment lab for being such a big part of my graduate school experience. I would like to thank Professor Patricia Kiley for her insightful discussions and challenging questions about the physiology of *E. coli* when I have presented my *in vivo* data. Without her insight, I wouldn't have been able to get that project off the ground. I would like to thank Professor Doug Weibel for his interest and contribution to my dissertation. Our discussions have always been lively because his lab is also interested in the mechanism of bacterial cell division, so his questions always arise from a point of similar interest to mine. Finally, I would like to thank Professor Sam Gellman for joining my committee from the Chemistry department. His vast knowledge of the literature in the field of protein folding has been extremely important to the success of my dissertation as well as his challenging questions during my committee meetings. My past scientific mentors have also been a big part of my success: Dr. Dongil Lee and Dr. Susan Stapelton at Western Michigan University, Dr. Doug Williams and the analytical lab at Kalsec, Inc., and Dr. Karina Kwok and Dr. John Hoogerheide of the Bioprocess Development Group at Pfizer.

I would like to thank my family for their support through the years. My parents, Don and Donna

LaPointe, have always encouraged me to pursue any career I want. My father has been my inspiration for work ethic as he is the most hardworking person I know. My sister, Lindsey, has been a constant motivator as she is currently a medical resident at New York Medical College. Our competition over the years has driven me to this point (even though she beat me to adding doctor to her name). My brother, Lucas, has also been supportive of my career and goals. My extended family is also making the drive to my graduation and I would like to thank them for their support. I would also like to acknowledge my cats, Mookah and Mufasa, because I am a cat lady and would be miserable without them.

I would like to thank my partner, Dustin Green, for his encouragement during the last two years of graduate school. He is always pushing me to work hard and always patient when I say I am going to be late because my experiment is taking longer than I thought. I would also like to thank his parents, Doug and Jackie, for being second parents to me and lending me a place to stay when I needed to get away from a bad roommate situation last summer. They have been extremely supportive throughout this last year as well.

Finally, graduate school would not have been a success without the support of my friends. My IPiB class of 2009 friends have stayed close throughout this phase of our careers and I would like to specifically mention Jess Feldman (basketball game buddy), Kristin Dittenhafer-Reed (running buddy), Matt Mead (comedy buddy), Ben Mueller (lab buddy), Sean Johnston (workout buddy), Darryl Wesener (4th floor buddy), Chris Lapointe (last name buddy), and Keenan Taylor (post doc buddy) and all of their significant others. IPiB students have meant a lot to me over the years as well especially Shruti Waghray and Chelcie Eller for their help in editing this dissertation and Becky Phillips for her help in collaboration on Chapter 4. Other IPiB students that have been close friends include Sarah Wessel, Kelly Stecker, Shruti Waghray, and Erin Ronayne (the Butler street girls); all of whom have

contributed to my scientific career as well as kept my social life in downtown Madison in tact. I also need to thank Pfizer life partner in crime, Kelly Watson, who is attending the University of North Carolina at Chapel Hill. I couldn't have made it all the way to the end without her endless support through google chat (both scientific and emotionally support). Finally, my best girl friends who I have met through ultimate frisbee leagues in Madison and stayed close with through the last four years have really meant the world to me: Cassie McKay, Peggy Boone and Caroline Chappell. There are so many people to acknowledge I could go on for a few more pages, but the take home message here should be that I have had an awesome support group to be very thankful for in Madison during my PhD and I will miss everyone so much when I move on to Nashville to do a post doc with Charles Sanders. It seems unreal that I made it this far, but I'm so thankful I pushed through to the end and look forward to the next step of this very special career.

ON WISCONSIN!

Abstract

Cell division is one of the most fundamental processes in the bacterial life cycle. At its core, cell division requires a set of essential proteins to complete (at least) three major steps. These essential proteins are known as the divisome. The three major events of division include 1) DNA replication, segregation of chromosomes between two dividing cells and cell membrane constriction, 2) full assembly of the complex of division proteins and 3) cell wall reformation including synthesis of new peptidoglycan. While the bacterial divisome has been extensively studied using molecular genetic techniques and interaction studies *in vivo*, most of the structural details of the assembly of the complex remain mysterious. A full literature review of the proteins of the divisome is included in the introductory chapter of the dissertation.

The work, herein, is to characterize two small integral membrane proteins of the divisome, FtsL and FtsB. FtsL and FtsB are central to the bacterial divisome, participating in the second step of assembly of other divisome proteins. Their presence is required to link together steps one and three. Included in this work is the first structural analysis of an integral membrane protein (FtsB) of the complex. The hypothesis is that the transmembrane dimer of FtsB forms a stable core for its association with FtsL, and that FtsL is required to stabilize the periplasmic domain of FtsB, leading to the formation of a complex that is competent for binding to FtsQ and its recruitment to the division septum. This structural analysis is the foundation for functional studies in vivo. The data show that positions in the transmembrane domain of FtsB that are essential for its self-association also disrupt cell division in vivo.

Also included are two collaborations which involve some characterization of an integral membrane protein where I performed an assay to measure self association of the transmembrane domain, which appeared to be important for function of the protein. The first collaboration was on the

PufX protein in purple bacteria. In the *Rhodobacter* (*Rba*.) species of photosynthetic purple bacteria, a single transmembrane α-helix, PufX, is found within the core complex, an essential photosynthetic macromolecular assembly that performs the absorption and the initial processing of light energy. The results of this work suggest that the different oligomerization states of core complexes in various Rba. species can be attributed, among other factors, to the different propensity of its PufX helix to homodimerize. The second collaboration was to measure the association of the second transmembrane domain of the Sigma 1 receptor. Sigma 1 receptor (S1R) is a mammalian member of the ERG2 and sigma1 receptor like protein family (pfam04622). It has been implicated in drug addiction and many human neurological disorders including Alzheimer's and Parkinson's diseases and amyotrophic lateral sclerosis. The results presented in the study support the proposal that S1R function may be regulated by its oligomeric state. The contribution made here was to analyze self association of the transmembrane domains. Structure and function analyses of integral membrane proteins, the main research topic of the laboratory, is a central focus of the dissertation here.

Chapter 1
Introduction:
Structural review of the divisome

This chapter is prepared for publication as:

LaPointe, L.M.; Craven, S.; and Senes, A. The divisome: a complex of membrane associated proteins essential for cell division. *In preparation*

1.1 Introduction to cell division and the divisome

Cell division is one of the most fundamental processes in the bacterial life cycle. At its core, cell division requires a set of essential proteins to complete (at least) three major steps. The three major events of division include 1) DNA replication, segregation of chromosomes between two dividing cells and cell membrane constriction, 2) full assembly of the complex of division proteins and 3) cell wall reformation including synthesis of new peptidoglycan. It will be helpful to consider cell division as occurring in these three major steps for the duration of this section through this Chapter as well as Chapters 2 and 3. Herein, I review the current literature surrounding the complex of proteins required for cell division and their role in cell division, specifically discussing the role that structural data has played in our current understanding[a].

Escherichia coli has served as the model organism for studying cell division in prokaryotes. *E. coli* is a rod shaped gram-negative bacterium, meaning that the cell wall is composed of one layer of peptidoglycan, unlike its gram-positive counterparts which contain several layers of peptidoglycan. Peptidoglycan is a complex polymer consisting of various sugars and amino acids that surrounds the inner cellular membrane of bacteria to protect the cell from the surrounding environment. The cellular membrane is a fluid structure composed of many different types of lipids with proteins embedded throughout. *E. coli* contains an outer cellular membrane and an inner cellular membrane. The fluid region between the two membranes is the periplasm and the central region of the cell (containing genetic material) is the cytoplasm. This complex cellular structure must be modified during cell division. The cellular membrane and peptidoglycan layers must each constrict, separate, and rebuild in order for a cycle of cell division to be complete. This process is completed by a complex of proteins

a This introduction chapter will be submitted as a review article in early 2015. There is more information in this chapter than is relevant to the core dissertation chapters 2, 3, and 4.

called the divisome.

At least ten essential proteins in the divisome work together to complete the major events of cell division. These proteins localize to midcell in a linear fashion (FtsZ, FtsA, ZipA, FtsK, FtsQ, FtsB, FtsL, FtsW, FtsI, FtsN, **Figure 1**). This "hierarchy" will be revisited later in this chapter when I discuss which proteins play a role in each of the aforementioned steps of cell division; they are spread out over the early, intermediate, and late steps. Additionally, several nonessential proteins play a role in cell division and likely many more left to be discovered. These nonessential proteins will also be discussed in later sections. First, I will give a general review of the essential divisome proteins, their placement and potential role in cell division and some discussion on how we have arrived to the current understanding of the field.

1.1.1 Identification of the essential proteins in the divisome through the use of genetic and biochemical techniques

The genes responsible for bacterial cell division were primarily discovered through identification of a group of thermosensitive mutants which produced very long, filamentous cells at high temperature (filamentous thermosensitive, fts)[1]. The first cell division gene product to be identified was FtsA, by gamma-transducing phage, when Joe Lutkenhaus (now a professor at University of Kansas Medical Center) did his postdoctoral studies in the Donachie lab[2]. The *ftsA* and *ftsZ* genes were differentiated from one another as well as neighboring murein genes (late division) using the same method,[3] and discovery of the rest of the cell division gene products followed[4,5]. Genetic experiments to study cell division and chromosome replication were pioneered by the W.D. Donachie group in the late 1960s and 1970s at the University of Edinburgh. These experiments showed that cell division and chromosome replication were separate events.[6,7] In the beginning it was believed that FtsA

was associated with chromosome separation[8], instead of FtsK, but now it is known that both proteins are essential in the divisome and have separate functions. Pioneering genetic work identified the specific loci of each gene and later the gene products were identified by transduction.

The characterization of the divisome proteins, many of which share similar topologies, but varied functions, started with a similar workflow of experiments. The initial work performed on the characterization of individual cell division proteins was pioneered by the laboratory of Professor Jon Beckwith at Harvard University. First, they used immunofluorescence microscopy to observe whether or not a temperature sensitive strain could be complemented with a modified version of the deficient protein[9–13]. Next, they constructed merodiploid strains which contained a wild type allele and an allele that contained a fusion to GFP[14–18]. For example, the cytoplasmic domain of the protein was removed from the divisome protein the ability of the protein to localize was visualized by the GFP tag. Studies using these strains, allowed for determination of what other divisome proteins needed to be present and functional in order for the GFP-tagged protein of interest to localize to the division site. An early and important finding using this method was that FtsQ required FtsZ and FtsA (but not FtsL or FtsI) to be present for localization[14]. This put FtsQ in the "middle" of the chain of localization. The merodiploid strain method is useful for analyzing different versions of essential proteins, say lacking or modifying one of the major domains. An example is the malF transmembrane domain swapped in place of the transmembrane domain of a divisome protein to determine whether the transmembrane domain is functionally important in the localization of the protein to the septum[19–21]. In later sections, I will discuss the architecture of the proteins of the divisome in detail and will highlight the results from these experiments, uncovering the functional domains of each individual protein. Localization and domain swapping experiments confirmed the hierarchy of localization of the divisome proteins.

1.2 The divisome proteins localize to the septum in a hierarchical fashion

The divisome hierarchy of assembly (FtsZ, FtsA, ZipA, FtsK, FtsQ, FtsB, FtsL, FtsW, FtsI, FtsN, **Figure 1**) has been a guiding theme in the literature and is very important to the current understanding of the divisome. One protein's function might involve an interaction with another protein already localized to the division site, which then recruits a downstream divisome protein to the septum. For the purposes of this review I will break the hierarchy into three parts: early, intermediate, and late proteins, which align with the three main steps of cell division aligned earlier. However, the simplicity of this hierarchy is challenged as some divisome proteins interact with members that do not fall in their category, as shown by biochemical methods[22–24]. A second complication is that many proteins can compensate for the loss of others in null mutant strains[25–27]. This indicates that there is likely some redundancy in the divisome proteins as well as some feedback regulation, an obvious requirement for a fundamental process like cell division. The following sections outline the essential divisome proteins in each stage of the hierarchy. This will provide a general overview to help facilitate a better understanding of the intricate details in later sections.

1.2.1 The early stage of cell division is constriction of the outer cell layers and chromosome separation through action by FtsZ, FtsA, ZipA, and FtsK

The early essential divisome proteins are FtsZ, FtsA, ZipA, and FtsK. These proteins coordinate the first major event in cell division which is the formation of the FtsZ ring at the midcell and separation of chromosomes to daughter cells. FtsZ is a GTPase that is homologous to tubulin and forms a ring structure at the site of cell division[28]. The polymeric form of FtsZ monomers[29] forms varied conformations, either straight or curved filaments[30] depending on certain regulatory proteins (to be discussed later). FtsA and ZipA tether FtsZ to the membrane as the FtsZ filaments assemble[31,32]. Either

one or both of FtsA and ZipA need to be present for the tethering to occur, showing some possible redundancy of function between these two proteins. The assembly of FtsZ, FtsA, and ZipA is better known as the assembly of the proto-ring (**Figure 2**). Before the proto-ring has formed and division begins the cell must replicate and distribute their DNA to the daughter cells. This function is assisted by the DNA translocase FtsK[33], which actively separates chromosomes in order for cells to export genetic material to the new cell[34]. Importantly, the soluble parts of FtsZ and FtsA are located in the cytoplasm (**Figure 1** – shown in depth in **Figure 2**). As such, the formation of the proto-ring occurs in the cytoplasm whereas the final step in cell division occurs in the periplasm.

FtsZ is both the most conserved cell division protein as well as the most well studied. Recent reviews emphasize that we have learned a great deal about how bacteria determine where within the cell the division complex should form [35], which begins with the formation and localization of the FtsZ-ring in rod shaped bacteria [36], and how that formation is regulated [37,38]. Because the topic has been extensively reviewed, this chapter is going to focus on the lesser known divisome proteins; the intermediate stage proteins, which are the primary focus of the dissertation.

1.2.2 The intermediate proteins FtsQ, FtsL, and FtsB form a stable subcomplex that serves as a scaffold for the remaining divisome proteins

The intermediate divisome proteins FtsQ, FtsL, and FtsB share a similar topology and are grouped together for two reasons. First, evidence suggests that they form a subcomplex[39]. Another reason is that between the early proteins and the late proteins a change in the topological orientation across the inner membrane is observed. In other words, these proteins are the first to localize that contain a large globular domain in the periplasm rather than cytoplasm (**Figure 1**, details shown in **Figure 3**). It has been hypothesized that this structural detail is important for the function of FtsL,

FtsB, and FtsQ[40,41]. Perhaps this function is to serve as a structural scaffold linking early and late division proteins together. The FtsQ, FtsL, FtsB subcomplex will be discussed in greater detail in sections to follow[b].

1.2.3 The late step in cell division: synthesis of peptidoglycan and closing the division septum

FtsW, FtsI(PBP3), and FtsN are considered the "late" proteins of cell division. These proteins primarily function in rebuilding the peptidoglycan layer between two daughter cells. FtsW is an essential enzyme for transport of lipid II (part of the peptidoglycan layer) in the final process of cell division[42]. FtsI is a penicillin binding protein (PBP), a class of proteins targeted by Beta-lactam antibiotics[43]. Both FtsW and FtsI have already been targeted for development of antibiotics because of their diverse enzymatic activity (reviewed in[44]). FtsW and FtsI topology is shown in **Figure 4**. Although it is always listed last in the hierarchy due to late recruitment to the cell division site[18,45], evidence suggests that FtsN interacts with the early cell division protein FtsA[46].

1.2.4 Summary of the major events of cell division

In summary, the major events of cell division and the proteins involved include: (1 or Early) DNA replication[47] and cell membrane constriction[48,49] initiated by the formation of the FtsZ protofilament (association of FtsZ with FtsA and/or ZipA)[50,51] which all occurs during chromosome separation (facilitated by FtsK); (2 or Intermediate) assembly of the proteins on the division septum facilitated by the intermediate proteins FtsQ, FtsL, and FtsB; and (3 or Late) cell wall reformation (carried out largely by the penicillin binding proteins, FtsI/PBP3 and others, and its association with

b Chapters 2, and 3 of this dissertation discuss FtsB and FtsL in structural and functional detail and describe future studies.

FtsQ, FtsW, and FtsN) [52,53]. This process is highly dynamic and also extremely regulated: a regulatory checkpoint may be seen in the FtsB/FtsL interaction as well as the FtsN/FtsA interaction. From here, the “minor” events in cell division become much more intricate and complicated.

1.3 The cell division proteins comprise a complicated web of interactions, in and around the membrane

The proteins of the bacterial divisome participate in a complex web of interactions, some are essential while some are accessory. These interactions include protein-protein interactions (both intermolecular and intramolecular), protein interactions with the inner membrane, and protein interactions with the outer wall and peptidoglycan layer upon reformation of a daughter cell. Many proteins also self associate into higher oligomers before associating with other components (**section 1.9.3)**. It is well understood that the aforementioned hierarchy of divisome interactions is transient and multifaceted. Although some interactions in the divisome seem to be transient, some seem to be quite stable. There are stable interactions that occur within stable subcomplexes of divisome proteins capable of associating on their own without other players in the divisome (see **section 1.9.2**). The goal of this Chapter is to shed light on the structural details that are known about the divisome proteins, how structure contributes to function, and where there is still missing information. The Senes lab is interested in the structure and folding of integral membrane proteins, so the divisome serves our purpose well and is an extremely complex system with several questions that still need to be answered, complicated by the fact that this complex is so closely associated with the cell membrane.

In recent years, knowledge of the structure of the divisome proteins has been greatly improved, but the data is not yet complete. This is largely because the essential divisome proteins are almost entirely membrane spanning, with a few exceptions (FtsZ, FtsA, and some nonessential proteins). Structural characterization of membrane proteins has lagged far behind their soluble counterparts, therefore studies of the divisome proteins are more complicated (see **section 1.9.1**). Structures of the soluble domains of the essential divisome proteins of *E. coli* have been elucidated (see figures in [36,54])

but we still lack high resolution data for the membrane components. It is true that transmembrane domains often serve as an anchor domain, but in recent years the association of transmembrane domains within the membrane has been more important for protein function[55]. This is especially true in oligomerization of higher order subcomplexes; a few of which occur among the divisome proteins. Oligomerization has been an important structural motif in the divisome, but it is not yet understood how oligomers of proteins or complexes behave in the divisome as a whole (see **section 1.9.2**). The association of one required protein with several others in the divisome has been shown for several members using bacterial two hybrid assays (BACTH)[24,56]. The interactions of divisome proteins and their complexities will be revisited in the discussion of divisome proteins on an individual basis, but first I will discuss some of the diverse methods that have been used to study these proteins since their discovery.

1.3.1 New methods used to characterize our understanding of the divisome

Once the proteins in the divisome were established as a hierarchy, studies probed the protein protein interactions occurring within the divisome. A useful method for understanding the interactions of the divisome is the bacterial two hybrid assay (BACTH) which showed that Fts proteins can associate to form a multiprotein complexes[24,57]. To explore the contacts between individual proteins at the division septum, a new method was developed by the Beckwith lab that was termed "aritficial septal targeting[58]." This method works by using nonessential protein ZapA, FtsZ and the protein protein interaction of interest. ZapA will recruit to the FtsZ ring without the assistance of other division proteins, so it can be fused to protein 1 of interest, the "bait" protein. The "prey" protein is fused to GFP so if an interaction is observed at midcell, a GFP ring will be observed. This method precisely defined the hierarchy of the divisome down to the specific interactions.[59] Artificial septal targeting

further analyzed divisome proteins in other bacterial divisomes in an *E. coli* background to sort out any other stabilizing interactions that might be occuring *in vivo*[60]. Artificial septal targeting is a great tool for identifying interactions in vivo, and now it is even more important to characterize these interactions using high resolution techniques to improve our understanding of the intricate details of the divisome.

Recently, *in vitro* reconstitution has been used to visualize divisome proteins in their membrane environment, pioneered by the group of Professors Miguel Vicente and Germán Rivas Caballero of the Centro de Investigaciones Biológicas in Spain. Specific studies include reconstitution of fluorescently labeled FtsZ with FtsA into giant unilamellar inner membrane vesicles (GUIMVs) which allowed observation of the spatial distribution in a membrane environment by confocal microscopy[61]. They found that when GTP was present, FtsZ assembled inside the GUIMVs, forming dense spots, but that FtsA was found attached to the inner face of the GUIMVs. This suggests that the FtsZ polymers regulate the FtsA tethering interaction with the membrane. Microscopy techniques, in general, have really evolved to enhance the way researchers can observe the behavior of proteins in live cells. Confocal fluorescence microscopy in conjunction with fluorescence recovery after photobleaching (FRAP) is another new technique used to study cell division by being able to determine if the cell septum has separated during another cell division event through the FRAP[62]. FRAP has also been used in experiments where the size and shape of the bacteria has been in question as a response to inhibitors[63]. Certainly, there are many more microscopy techniques on the horizon that will be at our disposal in the near future.

I previously summarized the pioneering methods that have built the current picture of the divisome, from genetic assays to phenotypic analysis to biochemical experiments. These methods are extremely important for understanding the functional importance of individual proteins, and are still

widely used today. In order to build a full picture of a system as complicated and dynamic as the divisome, a combination of techniques must be used. The divisome represents an excellent system for understanding membrane protein association and dynamics through various different methods, both biophysical and biological. If we can improve our understanding of the sum of the intricate biophysical and structural components of the E. coli divisome we will be able to functionally test hypotheses using the well established in vivo techniques. We will be able to target bacterial cell division proteins in the drug development field and contribute to potentially more effective antibiotics (see **Discussion**). This includes characterizing the transmembrane domains and membrane associated domains and understanding how they work with other proteins to affect successful cell division. Taken together, these experiments will enhance our understanding of the divisome in unprecedented ways. The goal of this Chapter is to summarize this overwhelming amount of interactions, to start to build a map for quick reference in future studies and to emphasize the role that structural analysis has played in determining divisome protein function. This includes self association of divisome proteins and association with other members, down to pinpointing residues and interfaces involved in interactions. The structural knowledge of these protein interactions has advanced significantly in the past ten years, and this will also be summarized here. I will stress the structural and mutational information available that is attributed to protein association and function. As technology advances we will learn more about the intricate structural details of the complex membrane associated proteins of the divisome. From here, our understanding of the most fundamental process in the lifecycle of bacteria will greatly improve. Next, I will give a deep analysis of each protein in the divisome, in a sequential manner beginning with the first event, the formation of the FtsZ ring.

1.4 FtsZ must polymerize to initiate division septum formation and is stabilized through protein-protein interactions

FtsZ polymerization is the first major step in bacterial cell division. It occurs along with DNA replication and chromosome segregations, discussed in **section 1.5**. FtsZ is the most conserved cell division protein in bacteria and is homologous to tubulin in eukaryotes[28]. The structure of FtsZ is very important for its function – the physics (constriction) of the dividing bacterial cell is regulated by the polymerization of FtsZ and its association with regulatory proteins. FtsZ is by far the most well studied protein of the divisome to date with expansive research articles and numerous reviews available, some discussed in the following paragraphs. Therefore, my focus here will be on interaction details between FtsZ and participating proteins rather than, for example, cell wall constriction or GTPase activity.

FtsZ monomers assemble into protofilament sheets and smaller rings in the same way that tubulin does[50] and the cell membrane begins to constrict. This constriction mechanism is powered through GTP hydrolysis [30]. In order for the Z ring to assemble, FtsZ must bind to FtsA or ZipA. Both proteins bind to FtsZ through the same C-terminal peptide of FtsZ[64,65]. FtsA and ZipA can compensate for loss of one another through recovery mutants, a possible regulatory event. The FtsZ monomers assembly at the center of the bacterial cell is guided by an antagonistic mechanism produced by proteins called the bacterial Min system[35,37]. In rod shaped bacteria, the Min proteins oscillate between cell poles opposing cell division at equal intensities, preventing FtsZ polymerization near the poles. This complex mechanism defines where division should occur. As the Min proteins do not assemble directly on the division septum, these proteins will not be discussed in this chapter in terms of interactions in the divisome; but in their absence cell division occurs in only some cells and multiple Z-rings form throughout the cell[66].

The structure of FtsZ was elucidated by the laboratory of Professor Jan Löwe in 2004[67]. The structure and biochemical data from this study revealed that the N and C terminal domains of FtsZ function independently from one another. The two domains fold independently and are stable on their own. The C-terminal domain and its polar residues can function as a GTP-binding pocket on its own. Later, the mechanism evolved to include the N-terminal domain as part of the GTP-binding domain and the C-terminal domain as the GTPase complementing domain. **Figure 1** shows an assembly of FtsZ monomers forming a Z ring and tethering to the membrane via interaction with FtsA and ZipA[68].

A recent review from the Vicente group provides a summary of where the research regarding the formation of the FtsZ proto-ring currently stands[51]. The proto-ring consists of FtsZ, FtsA, and ZipA, and this complex directs the downstream assembly of the divisome (intermediate cell division). The assembly of the proto-ring and its structural components is shown in Figure 2 in detail. Another recent review from Meier and Goley[48] adds in a summary of in vitro reconstitution experiments that have been performed on FtsZ and its protein binding partners in addition to high resolution imaging techniques. A combination of confocal microscopy images and fluorescence recovery after photobleaching (FRAP) provides new insight into the final Z-ring constriction event by showing that FtsZ and ZapA dissociate from the membrane before the cells compartmentalize, indicating that FtsZ is not present in this final step of constriction[69]. Recent research using high resolution microscopy has revealed much about this initial division event, but we still do not have a complete, detailed map of the mechanism of the proto-ring. In order to define the complete molecular details of the proto ring, a combination with super high resolution imaging, in vitro reconstitution, and advanced structural and biophysical techniques will be essential. I will now discuss the binding partners of FtsZ that stabilize the proto ring at the site of cell division.

1.4.1 Actin homologue FtsA regulates formation of FtsZ filaments and co-assemble on the cell membrane

FtsA was hypothesized to have a role in the formation of the cell septum in the 1980s[8]. FtsA, which laterally associates with the cell membrane, is required for Z ring attachment to the inner cell membrane. FtsA localization depends on presence of FtsZ and vice versa[70]. FtsA is the second most conserved protein in the divisome, likely due to its role here in the first major step of cell division. The crystal structure of FtsA from *Thermotoga maritima* was solved in 2000 by Jan Löwe's group showing structural homology to another eukaryotic cytoskeleton protein, actin[69]. Subsequently, the same group showed that FtsA contains a conserved peptide binding region in the C-terminus linked to the rest of FtsA by an unstructred linker region. This likely allows FtsA access to binding multiple proteins, including its function of tethering FtsZ to the membrane[71]. Bacteria lacking FtsA contain a protein with a similar architecture known as SepF which has also been analyzed using structural techniques to perform the same function as FtsA[72]. The recent crystal structure of FtsA from *Staphylococcus aureus* shows twisted FtsA filaments rather than straight, stacked filaments, indicating that the organization may be different from species to species.[73]

FtsA is able to self-associate based on BACTH experiments[74,75]. A study from the laboratory of Professor William Margolin, showed that oligomerization of FtsA actually regulates the extent of FtsZ assembly[76]. There, it was shown that a dominant negative missense mutation of FtsA inhibited homodimerization of FtsA, blocking the formation of the Z ring. However, mutants that cause inhibition of Z ring formation (M17A) could be suppressed by altering levels of other divisome proteins. A more recent study from the laboratory of Professor KC Huang used computational modeling and molecular dynamics to probe the dimer dynamics of FtsA from known crystal structures[77]. In this

study key interfacial residues were identified as having an important role in oligomerization of FtsA. The interfacial residues were shown to form two major clusters, one surrounding the ATP binding site of FtsA and the other at the monomer-monomer interface. This study also found a conserved pair of negatively charged residues (D140 and D150 of FtsA) in the 1c domain of FtsA which were proposed to interact with a postively charged segment of late division protein, FtsN[22]. Indeed, mutants D140 and D150 were sensitive in the molecular dynamics simulations[78]of FtsA described above.

The large amount of structural data available for FtsA may be a result of the fact that FtsA is likely slightly easier protein to work with experimentally. It has an amphipathic helix associated with the membrane, unlike some of the other divisome proteins containing a membrane spanning domain. It is also interesting that the unstructured portion (in FtsZ tethering segment and in FtsA the peptide binding region with unstructured linker region at the C-terminus) is important for the function of FtsA, which would not be known without high resolution structural data. One can see the importance of flexible regions in the tethering of FtsZ to the membrane by FtsA in **Figure 2**. If FtsA is not present, bacteria can compensate with another protein, membrane spanning protein, ZipA.

1.4.2 Domains of ZipA are separate functional domains

ZipA was discovered later than the majority of the essential divisome proteins[79]. ZipA seems to be a partially redundant protein for bacterial cell division as it is not as highly conserved as FtsA and FtsA and ZipA can compensate for loss of one another. Either protein is sufficient for proper tethering of FtsZ to the membrane, but both proteins must be present for long term Z ring stability[78]. The domains of ZipA are diverse in function, as is the case with many divisome proteins with single-pass membrane protein topology. The N-terminal domain of ZipA is the transmembrane domain. The C-terminal domain of ZipA is charged and contains a segment rich in Pro and Glu (P/Q domain) that has

been proposed to be unfolded and flexible through microscopy studies [80]. So, like FtsA, it is the lack of structure that seems to be important for the function as this domain is that which tethers FtsZ to the membrane and is unfolded[81].

1.4.3 FtsZ is stabilized by nonessential, accessory Zap proteins

FtsZ associating proteins, or "Zap" proteins, stabilize FtsZ by increasing lateral interactions found in FtsZ filament bundling. Cells are still able to divide without the presence of the Zap proteins, but this may result in oddly shaped Z-rings or bacteria cells. Known Zap proteins are ZapA[82], ZapB[83], ZapC[84], and ZapD[85]. Not all of these proteins are essential for cell division and are likely redundant because of the importance of the stabilization of the FtsZ ring. In its functional form as a stabilizer of FtsZ bundling, ZapA exists as a tetramer and structural studies have identified a mutant in ZapA (I83E) where ZapA is fully folded and binds to FtsZ but is a constitutive dimer[86]. Through the use of this mutant it was shown that ZapA is required for FtsZ bundling and GTPase activity. Another crystal structure of ZapA in conjunction with mutagenesis showed key residues in the charged helix of ZapA that affect FtsZ bundling. Another study using single molecule based super resolution imaging method Photoactivated Localization Microscopy (PALM) analyzed the roles of ZapA and ZapB in assembly dynamics of FtsZ[87] where it was found that in cells lacking zapA or zapB presented abnormal septa as well as unstable dynamic FtsZ structures. Before high resolution structures and imaging were available, not much was known about ZapA's specific role in the first event of cell division. The literature still states that this process is unknown. This is the case for many divisome proteins, due to the details lacking in their structural data.

1.5 FtsK is a multipass transmembrane protein that functions as a DNA translocase

Before the proto-ring has formed and the cells start dividing, they must replicate and distribute their DNA to the daughter cell. This function is assisted by FtsK. FtsK is a DNA translocase that actively separates chromosomes in order for cells to export genetic material to the new cell[33,34]. Its N-terminal domain (200 amino acids) contains four transmembrane spanning segments and is essential for cell division; its presence at the septum being required[88,89]. It's C-terminal domain contains the DNA translocase and is considered a RecA-fold ATPase[90]. The hexameric structure of FtsK's DNA translocase has been solved by Jan Löwe's group[91]. Now, much more is known about the DNA translocase activity of FtsK, its ability to segregate chromosomes, and affects on DNA recombination, which has all been summarized in reviews[92,93].

In order for FtsK to perform its work as a DNA translocase, it will occasionally encounter proteins bound to DNA that it must dislodge for translocation to continue. These proteins are a major source of stalled replication forks which lead to genome instability[94,95]. A recent study used single molecule imaging to visualize FtsK interacting with these DNA bound proteins[96]. They found that FtsK collides with DNA bound proteins and can push them off or bypass them. They were able to relate the outcome of the collisions to the relative affinity that the DNA binding protein has for its binding site. Specifically they show that protein-protein interactions between FtsK and XerD helps with removal of XerCD (DNA recombinases) from DNA. It has been shown previously that FtsK's C-terminal domain interacts with XerCD site-specific recombinases, but it was unclear how this mechanism actually worked[97]. This use of single molecule technology is somewhat unprecedented in the divisome – only a few studies currently exist,[98,99] and all have been performed in only the last year or so.

The function of FtsK's C-terminal is well known, but unfortunately, the function of the N-

terminal domain, containing the four transmembrane spanning segments, is unknown even though this domain is the only portion that is essential for cell division[89]. A very recent study reveals a revised topology for the N-terminal domain using site-directed fluorescence labeling[100]. They found that a loop exists between transmembrane 3 and 4 that contains residues that, when mutated, result in asymmetric cell division of the cytoplasm (visualized by high resolution transmission electron microscopy). Additionally, there is a linker domain between the N and C-terminal domains of FtsK rich in Pro and Glu that varies in length in different bacterial species, but no role has been given to this linker region[101,102]. The bifunctional nature of FtsK has allowed some speculation that FtsK could serve as a cell division checkpoint[103]. Its N-terminal domain is important for forming the scaffold where downstream divisome proteins will be recruited, and has functional importance for proper invagination of the membrane as shown in the revised topology, described above. Meanwhile, it's C-terminal domain is able to sense whether or not chromosome segregation has been completed[102]. Other divisome proteins have multiple domains, with possibly diverse functions, as is seen in the intermediate division proteins, discussed next.

1.6 FtsL, FtsB, and FtsQ form a higher order oligomer subcomplex central to cell division

FtsL, FtsB, and FtsQ comprise the intermediate stage of cell division: they serve as a scaffold, along with FtsK, for the remaining downstream divisome proteins to localize. The discovery of FtsQ, FtsL, and FtsB occurred about ten years apart from one another, respectively[17,104,105]. It was first determined that FtsL had a binding partner, FtsB, in 2002 after a computer search of the E. coli genome predicted it as a potential interacting partner for FtsL[17]. It is established that FtsB and FtsL interacted with FtsQ, forming a subcomplex independent of their localization to the septum[39]. Because we now know that different elements of the divisome machinery can interact independently in a lot more cases (**section 1.9.3**) it is possible to characterize these protein complexes further structurally and biophysically and improve our understanding of these essential proteins in vivo.

The FtsQLB subcomplex serves as an example of a completely membrane spanning complex that is absolutely critical for division. These proteins are termed "intermediate" divisome proteins because they are recruited to the divisome after the Z ring forms and is stabilized and before the peptidoglycan binding proteins begin the division process. They are the first proteins in the divisome hierarchy that have a larger periplasmic segment than cytoplasmic segment. It is thought that this "flip" of topology over the inner membrane is relevant in the pinching step of the membrane in cell division, though the actual mechanism is not understood in any detail[40,41]. All three proteins have a similar topology including a short cytoplasmic tail, a membrane spanning segment, and a periplasmic domain. Here I will discuss each protein in the FtsQLB subcomplex; FtsB and FtsL being the main focus of my dissertation project.

1.6.1 Central cell division protein, FtsQ, interacts with numerous components of the divisome

Early experiments to measure localization of FtsQ were performed using immunofluorescence microscopy and showed that the periplasmic domain was essential for proper localization[13]. The domains of FtsQ were further explored using "domain swapping" experiments, which was a very common technique used for divisome proteins with the bitopic membrane spanning topology[19]. The domains of FtsQ were attributed separate functions in a later mutational analysis, separating the localization ability of FtsQ from its other functions (namely recruiting downstream partners, FtsL, FtsB, and FtsI)[106]. In this way it was learned that the cytoplasmic as well as the periplasmic domain of FtsQ was required, but the transmembrane domain could be swapped with a nonessential transmembrane domain, such as MalF. The domains of FtsQ were further understood using the wrinkled colony phenotypic method from the Beckwith lab[107]. This method was used to screen method for mutant *ftsQ* alleles that are not able to complement a temperature sensitive strain containing *ftsQ* at restrictive temperature. It was using this assay that it was learned that FtsQ interacts with FtsL and FtsB via the C-terminal domains. Recent studies have probed this interaction further. The extracellular beta domain of FtsQ found to interact with the unstructured C-terminal regions of FtsB and FtsL shown by computational modeling and site specific photo cross-linking[108]. In this study it was shown that the C-terminal domains of FtsL and FtsB interact with FtsQ, and both domains are predicted to be unstructured. This result was also confirmed after the crystal structure of the periplasmic domain of FtsQ was solved and interactions with the periplasmic domains of FtsL and FtsB were probed using X-ray scattering and surface plasmon resonance[109]. The crystal structure also showed that FtsQ's C-terminal domain contains a POTRA domain (polypeptide-transport-associated-domain), which is

typically associated with polypeptide transport over the outer membrane[110]. It was also observed the mutants affecting the two main functions of FtsQ, localization to septum and recruitment of downstream protein, were found in different domains. The former were found in the POTRA domain and the later in the C-terminal domain[111].

FtsQ is certainly a key protein for the complexity of the divisome because it has numerous interactions with other divisome proteins. FtsQ has been shown to self interact and interact with FtsI, FtsL, FtsN, FtsB, and FtsW through bacterial two hybrid analyses.[23] Point mutations involved in these interactions have been examined using a two-hybrid two-phage assay and random mutagenesis[112]. FtsQ's diverse interactions make it an attractive candidate for antibiotic development because it could potentially inhibit many aspects of the cell division process.

1.6.2 FtsB/FtsL subcomplex has a structural role in the divisome

In terms of function, FtsB and FtsL are the two proteins in the divisome that we know the least about. The interaction of FtsL and FtsB with each other and with FtsQ is essential for the divisome to function properly[39]. FtsL and FtsB contain a topology that mirrors one another: a short cytoplasmic tail, a single pass transmembrane domain, and a periplasmic coiled-coil domain. Because the coiled-coil is a motif that is often involved in dimerization, it was initially hypothesized that the structure of the FtsL/B subcomplex follows that of a helical heterodimer[113]. My studies have shown that FtsB forms a dimer through self-association mediated by a conserved polar residue, Gln16, in the transmembrane domain, whereas the periplasmic domain forms a canonical coiled-coil [114] (**Chapter 2**). Polar amino acids present in transmembrane domains have proven to be driving forces of association in other systems[115,116]. FtsB contains a conserved glycine rich region between the transmembrane domain and coiled-coil, which has been computationally modeled.[114] FtsL stabilizes the FtsB dimer by forming a

complex with 1:1 stoichiometry, possibly a tetramer, though the precise structure of this subcomplex remains unknown[117]. FtsL, on its own, is also highly unstable in the cell[118] and has been shown to degrade in the absence of FtsB by proteolysis in Bacillus subtilis[119]. **Figure 3** summarizes the topology of FtsL and FtsB, shows the computational model of the FtsB transmembrane homodimer, and also includes the hypothesis of interaction between FtsB, FtsL, and FtsQ[114,117].

The FtsL/B subcomplex is an example of where structural and biophysical techniques brought our knowledge up to speed with the other, more thoroughly studied divisome proteins. **Chapter 2** discusses the structural organization of FtsB oligomer in much more detail. However, they also represent a great example of how difficult the divisome proteins are to study in isolation. Both FtsB and FtsL are unstable on their own, overexpression leads to toxicity in most cases (data not shown), but single point mutations do not upset the complex as a whole *in vivo* (see **Chapter 3**), indicating that as a complex the proteins actually are quite stable. The stability of this complex is tested in a structural experiment which fuses the coiled coil domains of FtsL and FtsB to a eukaryotic heterotetramer coiled-coil complex. Preliminary data for this experiment include a stable, co-expressed, co-purified heterotetramer complex (not included in this thesis) which is the future of this project as it stands.

1.6.3 Nonessential intermediate divisome proteins

FtsE and FtsX are ABC transporter homologues that participate in the intermediate stage of cell division, especially in media lacking salts, but are not essential for cell division[120]. FtsE comprises the nucleotide binding domain of the transporter and FtsX supplies the transmembrane domain[121]. This complex acts as a regulator of cell wall hydrolysis at the cell division site[121]. FtsX is also a participant in the late division stage, by interacting with nonessential proteins involved in the hydrolysis of peptidoglycan[122]. The whole complex serves as a linker between early and late division events with

FtsE interacting with FtsZ and FtsX modulating cell wall synthesis[121], so FtsQ, FtsL, and FtsB are not alone in this process. Though it is a nonessential complex, it clearly has a profound role in proper cell division in bacteria.

1.7 The penicillin binding proteins interact with FtsW and the outer membrane and cell wall in the final step of cell division

The last step, or "late" step, in cell division, reformation of the cell wall, is a highly dynamic process involving many protein and cellular components. A major component of the cell wall is peptidoglycan, and once the cells complete the division cycle, they must rebuild the cell wall. This process is catalyzed by two classes of penicillin binding proteins (the targets of β-lactams) class A and class B[123]. Escherichia coli contain three class A PBPs (PBP1A, PBP1B, and PBP1C) and two class B PBPs (PBP2 and PBP3/FtsI)[124,125]. These proteins work with other proteins during elongation of the cells and division of the cells to rebuild the peptidoglycan layer[41]. PBP1B and FtsI (PBP3, called FtsI from here forward) are the essential PBPs working with the other essential divisome proteins. However, PBP1B is not generally listed in the hierarchy because it does not assemble on the inner membrane like FtsI does. Instead, it localizes at the lateral cell wall during elongation and then at the division site only during septation[126]. It's localization is dependent on the presence of FtsI.

The PBPs and synthesis of peptidoglycan have been reviewed extensively in the literature[41,124,127,128]. What I want to discuss are the specific interactions that we know between proteins in this stage of cell division. A recent study showed that the transmembrane and cytoplasmic domains of two PBPs (2X and 2B) were essential for viable cell division, rather than merely membrane anchors, using reciprocal domain swapping and mutagenesis[129]. The crystal structure of PBP3 from *E. coli* was recently solved (not including the transmembrane domain) to reveal the transpeptidase activity domain as well as a site for potential dimerization[98].

FtsW is another participant in the late step in cell division. FtsW is a multi pass transmembrane protein with ten transmembrane domains[130]. FtsW belongs to the SEDS (shape, elongation, division and

sporulation) family of proteins[131]. FtsW has been proposed to communicate signals from divisome proteins of cytoplasm (early division proteins) and division proteins of the periplasm (intermediate division proteins)[132]. The proposed function of FtsW is as a lipid II flippase that translocates lipid II (part of the peptidoglycan layer) from the cytoplasm to the periplasm[42]. The enzymatic activity of FtsW has been targeted in development of antimicrobials[44]. FtsW interacts with FtsI, FtsQ, FtsL, and FtsN in BACTH assays[24,56].

Not only have FtsW and FtsI been shown to interact via BACTH assays, they have been shown to interact in vitro and in vivo through FRET analyses and co-immunoprecipitation experiments[133]. Their topology and interaction sites are displayed in **Figure 4**. Specifically, the 9/10 transmembrane loop of FtsW appears to be involved in the interaction with FtsI, possibly playing an important role in the positioning of these proteins on the septum during cell division. This is another example of subcomplex forming independently of other proteins in the divisome.

1.8 Late division protein FtsN may play a regulating role and its domains are diverse in function

FtsN is a small, bitopic, integral membrane protein that is recruited to the division site very late in the hierarchy[18,45]. Localization of FtsN does not require the transmembrane domain as shown by domain swapping experiments[11]. The cytoplasmic region of FtsN is sufficient for binding to early cell division protein FtsA, but only when tethered to the TM of FtsN or a leucine zipper[22]. FtsN has been studied using the "divide and conquer" strategy, though no work has been published on the structure of the transmembrane domain. The NMR structure of part of the soluble domains of FtsN was solved, breaking up the non-transmembrane domain into 5 separate domains with possibly different functions[134]. These domains include: a short cytoplasmic domain, a transmembrane domain, three partially formed helices, and a Q-rich domain linking the C-terminal globular domain. The C-terminal domain is homologous to other peptidoglycan binding domains[134].

Despite its late recruitment it has been shown to interact with several proteins in the divisome, including early divisome protein FtsA[22]. The previously reported "nonessential" N terminus of FtsN was also later determined to act cooperatively with another early cell division protein, FtsK, to stabilize the divisome[135]. FtsN has also been shown to interact with early protein ZapA, as well as late proteins FtsI and FtsW through FRET analyses at endogenous protein levels[136]. Given that FtsN interacts with an early division protein, yet is recruited to the hierarchy last, but can also bind peptidoglycan, it seems that this protein's role is to link all of these events together.

1.9 Many of the essential divisome proteins span the membrane with at least one transmembrane domain

Determining the structure and thermodynamic stability of a protein is one of the most important factors in determining the function of the protein in live cells. If the transmembrane (TM) domain is thought to be a membrane anchor in the function of the protein the practice has often been to remove the TM and characterize the soluble portion of the protein separately. In the case of the proteins of the *E. coli* divisome, this is severely complicated by the fact that almost all of these proteins span the inner cell membrane. Folding of membrane proteins in the correct and energy favorable fashion is crucial for proper protein function at the cellular level, and this is of course true in the case of cell division. An excellent review on the progress made toward understanding the driving forces in membrane protein folding was recently published by H. Hong [137].

1.9.1 Membrane protein folding knowledge lags behind that of soluble proteins

Over 25% of genomes across a number of organisms are predicted to code integral membrane proteins like those found in the majority of the divisome ([138,139]). Despite this fact, the knowledge of membrane protein structure and folding dynamics severely lags behind that of soluble proteins. Currently the comparision is ~471 solved structures of membrane proteins (Prof. Stephen White website: http://blanco.biomol.uci.edu/) to over 22,000 solved structures of soluble proteins (Protein Data Bank). One reason for this lag is due to the difficulty in studying membrane proteins in the lab using traditional biochemical and structural techniques. It is difficult to understand the behavior of a protein without being able to replicate the specific membrane environment that they exist within. The first step to analyzing protein structure is to overexpress the protein to isolate in a high yield and herein lies another challenge in gaining structural information. In the case of integral membrane proteins the

overexpression often leads to cell lysis because of toxicity ([140,141]). Variations on the *E. coli* overexpression system have allowed researchers to overcome the toxicity challenge[142]. Once the target protein is overexpressed, it is extremely difficult to mimic this heterogeneous membrane environment in the test tube. Detergents and lipids have been used a membrane mimic, but it is well established that plasma membranes can contain hundreds of lipid components[143]. We do not currently have a complete understanding of the intricate membrane environment of a living cell and as a result the target protein often ends up in an aggregated state when isolated. Aggregated protein will not behave in a manageable way in downstream biophysical experiments. Lastly, measurements of reversible folding, while possible, are extremely challenging to make in membrane environments ([144]).

1.9.2 Oligomerization is important in the divisome

For a long time single-pass membrane proteins (also known as single-pass transmembrane proteins) have been considered to function as membrane anchors. It was believed that these membrane anchors purely tether catalytic and other functional domains to the membrane. Helix association in the membrane has also been shown to drive membrane protein folding[145]. The two stage model of membrane protein folding proposed that membrane helices insert into the membrane (stage one) followed by a stage where the helices interact and from higher order structures (stage two)[146]. This oligomerization of transmembrane helices has been shown to be important across diverse families of proteins. Oligomerization is a common motif in the divisome proteins, so it is likely that association of the transmembrane helices is occuring, but again, structural details on the transmembrane domains are lacking.

Oligomerization is seen in FtsZ, FtsA, ZapA, ZipA, FtsN, FtsB, which I will now summarize. FtsZ functions as a polymeric Z-ring[29]. A very recent study showed that oligomerization of the

conserved C-terminal tail of FtsZ enhanced binding to multiple ZipA proteins in vitro[147]. ZipA forms homodimers prior to the association with FtsZ[148]. FtsA showed self-association in BACTH[75] assays and was dimerization was confirmed to be important for the function of FtsA by molecular dynamics[77]. ZapA exists as a functional tetramer, competent for lateral association with FtsZ bundles[86]. Finally, FtsB self-associates via a polar residue in the transmembrane domain[114](see **Chapter 2**). Not only do many proteins have self-association properties, a few subcomplexes between proteins can also form in the divisome.

1.9.3 Stable protein subcomplexes form in the divisome

As I have stated, many proteins in the divisome have multiple interaction partners, but in some cases a stable subcomplex can form. The ability for a complex of proteins to form independently in the divisome makes for a clear route to high resolution structure characterization. It is possible to measure the thermodynamic stability of the complex in vitro, which can tell us a lot about a protein's function in vivo. FtsL, FtsB, and FtsQ form an independent subcomplex[39], but the oligomeric state of this complex is currently unknown. Based on their presence in the intermediate division step it is hypothesized that this subcomplex has a structural as a scaffold[49], though that is not confirmed. Within this subcomplex, FtsL and FtsB form another subcomplex and their interaction is essential for cell division[113]. Because it is believed that FtsL and FtsB form a complex that is a tetramer at the smallest size[114,117], it is quite possible that the complex with FtsQ could be a large complex with multiple subunits. FtsW and FtsI form a stable, functional subcomplex that is specific for peptidoglycan synthesis[133] (**Figure 4**). The association between FtsN and FtsA is also quite significant, so a subcomplex could form here as well[22].

1.9.4 The divide and conquer strategy to study divisome proteins

In order to bypass the difficulties in biophysical characterization of membrane proteins,

researchers will analyze the soluble domain(s) of the protein in isolation from the transmembrane domain. In my work, this process is dubbed the “divide and conquer” strategy. This can take two forms: in some cases it is easier to work with the membrane domain in isolation from the rest of the protein, and in other cases there may be separate functions for separate domains. This has been seen in the work done beyond genetic and phenotypic experiments with the divisome proteins. In these studies, most of the soluble domains have been characterized and/or crystallized separated from the rest of the protein. I have described this strategy in previous sections with FtsK, FtsB, FtsQ, FtsI, and FtsN. FtsL has not been characterized independently and could potentially be analyzed using this strategy.

This “divide and conquer” strategy can be very useful for building a picture of how the structure contributes to the function of the protein, but requires much more hypothesis driven research regarding the unexplored domains. For example, the transmembrane domain of FtsQ is essential for the localization of this protein to the inner membrane, but it's periplasmic POTRA domain has been shown to interact with several other members of the divisome[23,109]. Another example is the interaction of early division protein FtsA with late division protein FtsN, though they are not sequential in the hierarchy[22]. A third example is the case of FtsK, a bifunctional protein whose N-terminal domain and C-terminal domain function independently in cell division[103].

1.10 Discussion

The divisome is a complex and intriguing set of proteins whose dynamic interactions serve as the mechanism for bacterial cell division. Not only is this a fundamental process in the bacterial lifecycle, it is also a process that can be targeted for synthesis of more effective antimicrobials, especially since many components do not have a counterpart in eukaryotes. As we know, the current rate at which bacteria evolve resistance the antimicrobials is unprecedented. The question now is, how exactly do we target the cell division machinery to engineer these new antibiotics? Most current antibiotics targeting cell division proteins are designed to disrupt enzymatic activity in proteins like FtsI and FtsW[44]. However, disruption of essential protein-protein interactions in the divisome could be a target for antibiotic engineering[149]. The fact that many of these interactions appear to be conserved is also promising for targeting this machinery. This review discusses these interactions at length. Protein-protein interactions can be difficult to target, but methods to screen small molecules for inhibiting such reactions are developing as well[150]. Our lab's interest in the divisome stems from our interest in understanding the folding and function of integral membrane proteins, both computationally and biochemically. My project to characterize the divisome proteins FtsB and FtsL has employed an array of techniques in collaboration, all across this spectrum.

1.11 Summary of the dissertation

My graduate thesis work has mainly focused on the structural characterization of the FtsL/FtsB subcomplex of the bacterial divisome. However, I have also participated in collaborations with other groups (Professor Klaus Schulten group of University of Illinois and a large collaboration with Professor Brian Fox and Professor Arnold Ruoho of University of Wisconsin-Madison) wherein I performed a detailed mutational analysis of a transmembrane domain of interest. Additionally, I will

include analyses that were unpublished collaborations with my own group. These include other proteins of the divisome with single-pass transmembrane domains (FtsN and ZipA) as well as some unpublished computational collaborations with Dr. Sabareesh Subramaniam, a former member of our group. I have received very diverse training throughout the course of these projects and will take these skills to the lab where I will do my postdoctoral research also studying membrane protein structure, but this time using NMR.

In **Chapter 2** I will discuss the structural organization of FtsB, which has been published in ACS Biochemistry. Prior to my work, not much was known about the function or structure of FtsB other than its interaction with FtsL is essential for cell division. It was believed they formed a single, possibly helical heterodimer. I found that FtsB actually forms an oligomer, driven by association of a polar residue (Glu 16) in the transmembrane domain. I mapped out the interaction interface for the FtsB oligomer, finding precise disruption scores for each residue involved. I solved the structure of the FtsB dimer coiled-coil and found that it was mildly stable. We hypothesize that this oligomer is stabilized through lateral interactions with FtsL, which was confirmed by FRET work from my labmate, Ambalika Khadria, and published in ACS Biochemistry.

In **Chapter 3** I will discuss the work I have completed to analyze the functional importance of the FtsB oligomer in vivo. From the interaction interface found in Chapter 2, I tested point mutations in vivo to see if cell division would be disrupted; in other words, cells would become filamentous. The purpose of this chapter is mainly to describe the set up of the assay and what mutations I have tested. Most point mutations did not cause a large effect on filamentation, so future work and further characterization of the structural organization in vitro, will need to be complete in order to complete the functional analysis.

In **Chapter 4**, I include the collaboration with Jen Hsin and Klaus Schulten of University of Illinois. Jen performed molecular dynamics simulations of four species of Rhodobacter PufX proteins which form the photosynthetic core of these purple bacteria. I confirmed the MD simulations by analyzing the transmembrane domains of the four species of PufX using the TOXCAT assay. This work was published in the Journal of the American Chemical Society in 2012.

In **Chapter 5**, I include the collaboration with Professor Brian Fox, Professor Arnold Ruoho, and others. They determined that the Sigma-1 receptor oligomerizes and is stabilized by ligands through ligand binding assays and chromatography. I performed the work on the second single-pass transmembrane domain (TM2) which was found to drive oligomerization of this complex. I performed TOXCAT and mutagenesis on the TM2 domain to measure oligomerization. I also confirmed expression of constructs that I tested using western blotting. This work was published in the Journal of Biological Chemistry in 2014.

In the **Appendix**, I will briefly summarize self-association of division proteins ZipA and FtsN via the TOXCAT assay.

I will not discuss the preliminary data I have for the refinement of our model of the structural organization of the FtsB/FtsL subcomplex, but this work is ongoing and expected to be completed in 2015. The goal here is to build a higher resolution picture of this subcomplex and some exciting preliminary work has been done. To date, I have been able to develop a protocol for purification of FtsB from inclusion bodies in *E. coli* and I have also been able to purify a stable heterotetramer complex of the coiled coil domains of FtsB and FtsL. These two projects will be completed before I start my postdoctoral research.

Figure 1.1

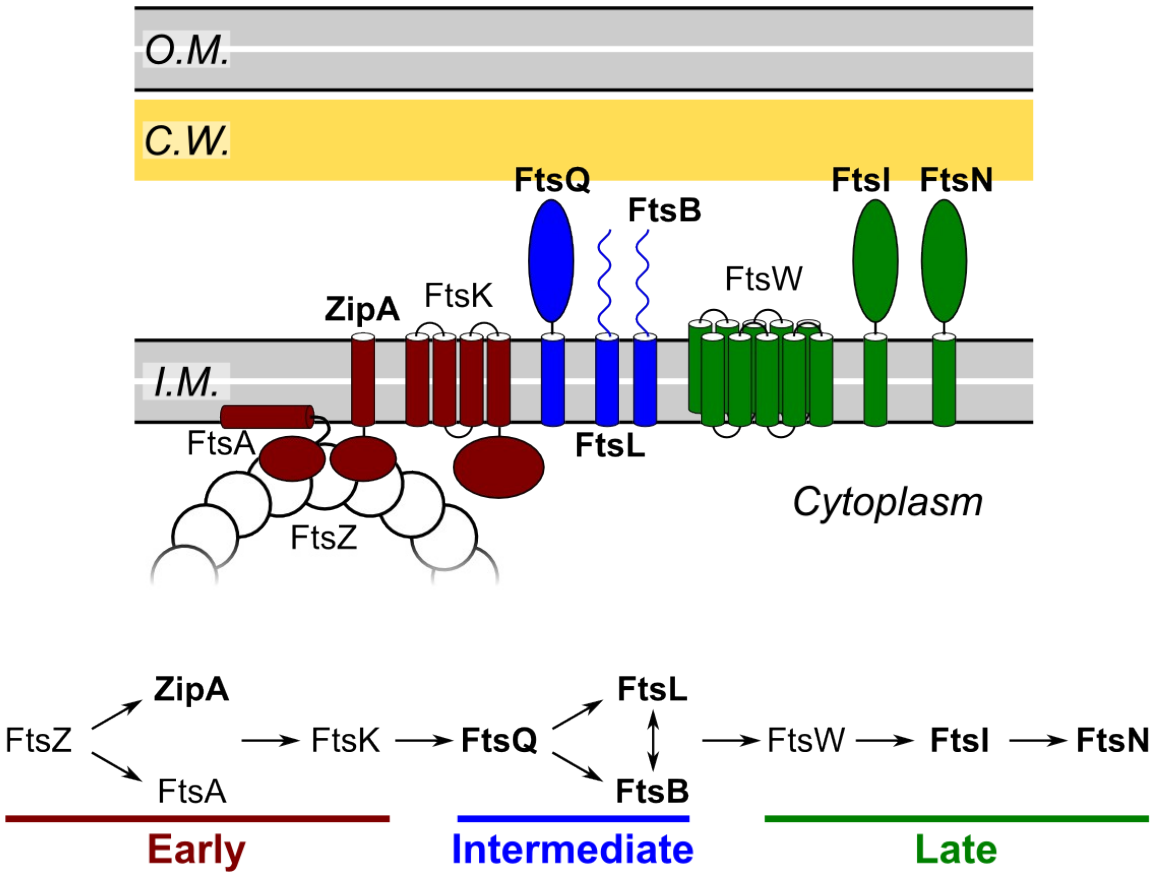

Figure 1.1 Summary of the three stages of cell division. The early stage of cell division is the segregation of chromosomes by FtsK and assembly of the Z ring by FtsZ, FtsA, and ZipA (red). The intermediate stage of cell division is assembly of the rest of the divisome starting with the formation of the FtsQ, FtsL, FtsB subcomplex (blue). The final stage of cell division is synthesis of peptidoglycan after cells have separated assisted by FtsW and FtsI (green). Membrane topology of each protein has been shown here. All of the soluble domains have solved crystal structures which can be found in another review[54]. The membrane component of each protein in the divisome is still structurally uncharacterized, except for that of FtsB, as shown in my work.

Figure 1.2

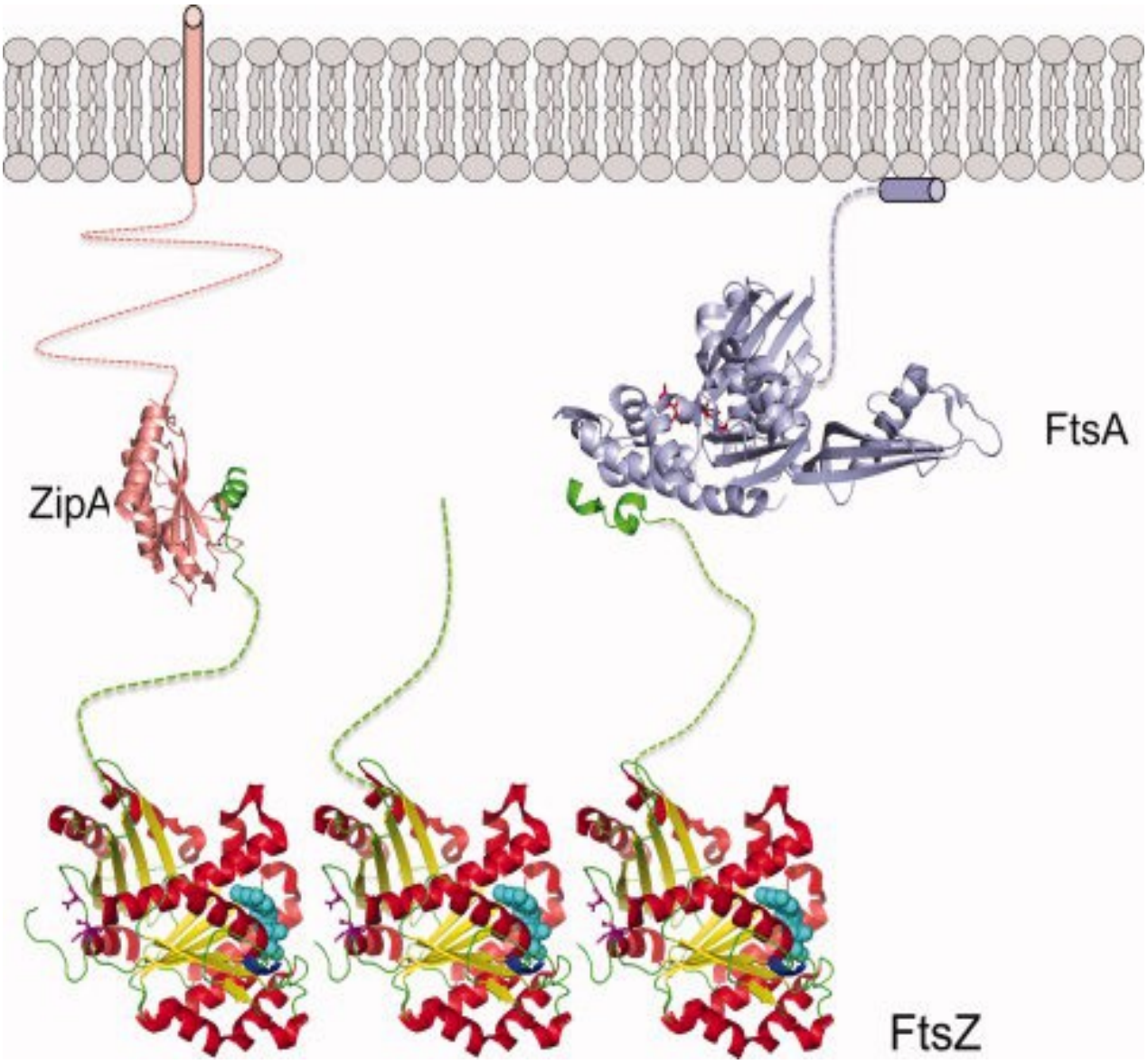

Figure 1.2 Assembly of the FtsZ proto ring. FtsZ filaments assemble from FtsZ monomers and are tethered to the inner membrane by FtsA and ZipA. FtsA and ZipA bind to the conserved C-terminal tail of FtsZ which is connected to FtsZ by a flexible linker. Known structures are shown in this image and

were discovered from the same group. Figure from Lutkenhaus, J.; Pichoff, S.; and Du, S. Bacterial Cytokinesis: From Z ring to divisome. Cytoskeleton (Hoboken). 2012. 69(1): 778-90 (permission to resuse requested).

Figure 1.3

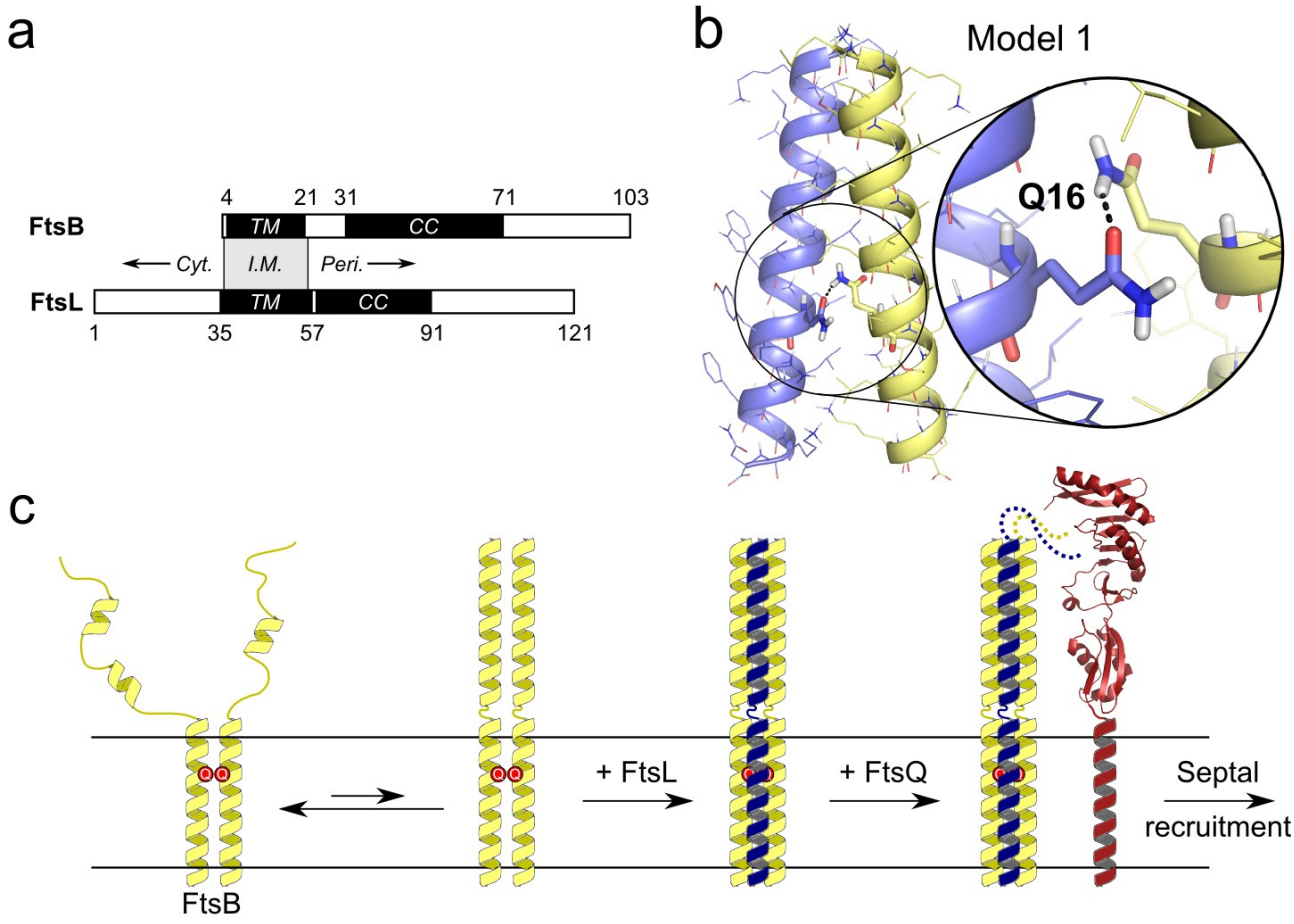

Figure 1.3 The intermediate stage of cell division is regulated by FtsQ, FtsL, and FtsB. FtsB and FtsL share a similar topology (a): both proteins contain a short cytoplasmic tail, a transmembrane domain, and a coiled-coil domain. FtsB self associates through a critical polar residue in the transmembrane domain (Glu16) modeled computationally, highlighting hydrogen bonding between interacting glutamine resides (b). The working hypothesis for the association of FtsB, FtsL, and FtsQ (c): FtsB self associates via Glu 16 in the transmembrane domain and is laterally stabilized by FtsL and the fully folded complex is able to bind FtsQ and localize to the division septum. Permission to reuse

figure granted from Khadria AS and Senes A. The transmembrane domains of the bacterial cell division proteins FtsB and FtsL form a stable high-order oligomer. *Biochemistry*. (2013) 52(43):7542-50.

Figure 1.4

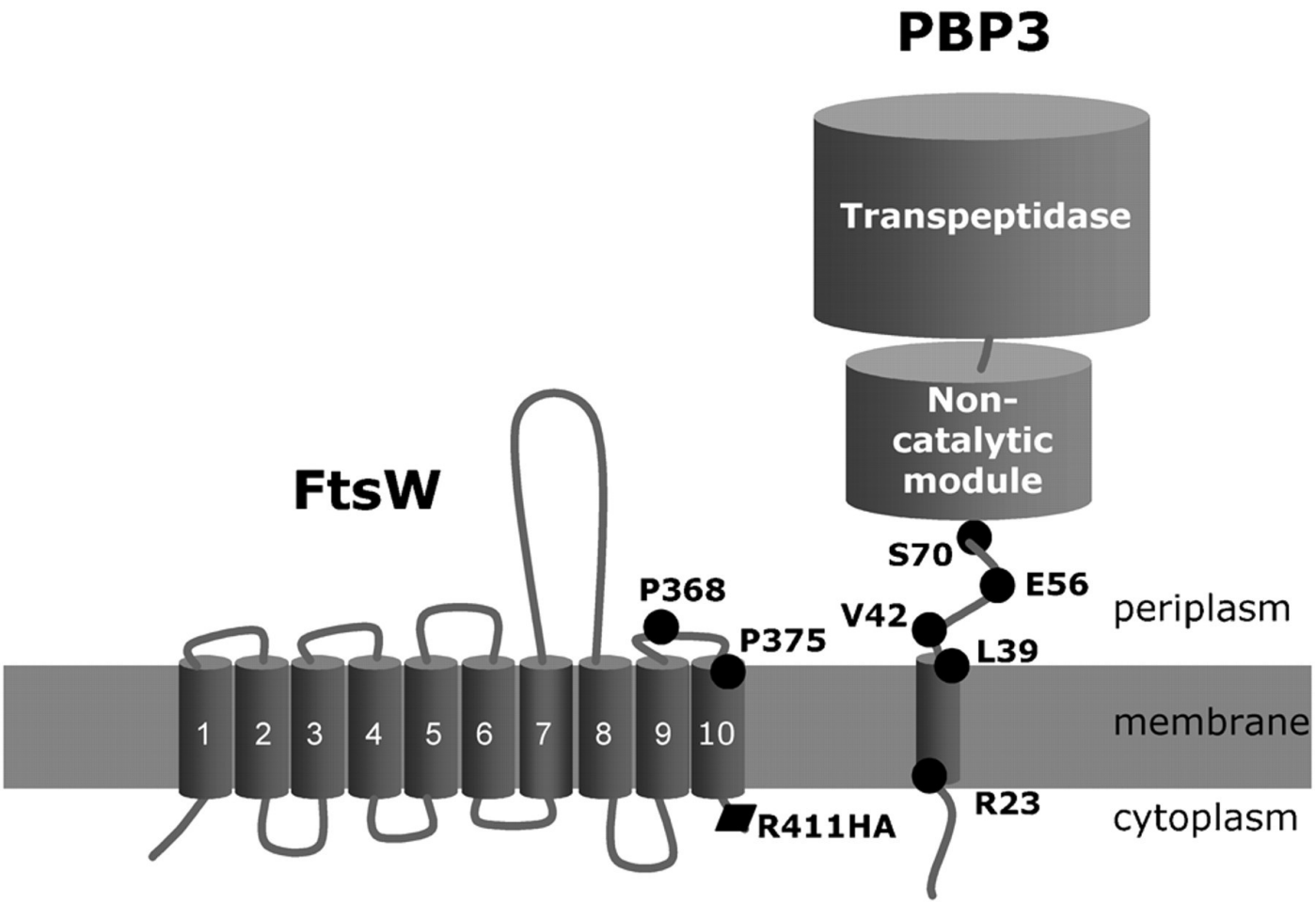

Figure 1.4 Membrane topology of FtsW and FtsI(PBP3). These are essential proteins that participate in the late step of cell division. They are shown to interact in vitro through the specific positions to form a subcomplex shown in the figure[133].

1.12 References

1. Hirota, Y., Ryter, A. & Jacob, F. Thermosensitive mutants of E. coli affected in the processes of DNA synthesis and cellular division. Cold Spring Harb. Symp. Quant. Biol. **33,** 677–693 (1968).
2. Lutkenhaus, J. F. & Donachie, W. D. Identification of the ftsA gene product. J. Bacteriol. **137,** 1088–1094 (1979).
3. Lutkenhaus, J. F., Wolf-Watz, H. & Donachie, W. D. Organization of genes in the ftsA-envA region of the Escherichia coli genetic map and identification of a new fts locus (ftsZ). J. Bacteriol. **142,** 615–620 (1980).
4. Yi, Q. M., Rockenbach, S., Ward, J. E. & Lutkenhaus, J. Structure and expression of the cell division genes ftsQ, ftsA and ftsZ. J. Mol. Biol. **184,** 399–412 (1985).
5. Storts, D. R., Aparicio, O. M., Schoemaker, J. M. & Markovitz, A. Overproduction and identification of the ftsQ gene product, an essential cell division protein in Escherichia coli K-12. J. Bacteriol. **171,** 4290–4297 (1989).
6. Donachie, W. D. Relationship between cell size and time of initiation of DNA replication. Nature **219,** 1077–1079 (1968).
7. Donachie, W. D. & Begg, K. J. Growth of the bacterial cell. Nature **227,** 1220–1224 (1970).
8. Tormo, A. & Vicente, M. The ftsA gene product participates in formation of the Escherichia coli septum structure. J. Bacteriol. **157,** 779–784 (1984).
9. Pogliano, J., Pogliano, K., Weiss, D. S., Losick, R. & Beckwith, J. Inactivation of FtsI inhibits constriction of the FtsZ cytokinetic ring and delays the assembly of FtsZ rings at potential division sites. Proc. Natl. Acad. Sci. U. S. A. **94,** 559–564 (1997).
10. Weiss, D. S. et al. Localization of the Escherichia coli cell division protein Ftsl (PBP3) to the division site and cell pole. Mol. Microbiol. **25,** 671–681 (1997).
11. Addinall, S. G., Cao, C. & Lutkenhaus, J. FtsN, a late recruit to the septum in Escherichia coli. Mol. Microbiol. **25,** 303–309 (1997).

12. Weiss, D. S., Chen, J. C., Ghigo, J. M., Boyd, D. & Beckwith, J. Localization of FtsI (PBP3) to the septal ring requires its membrane anchor, the Z ring, FtsA, FtsQ, and FtsL. J. Bacteriol. **181,** 508–520 (1999).
13. Buddelmeijer, N., Aarsman, M. E., Kolk, A. H., Vicente, M. & Nanninga, N. Localization of cell division protein FtsQ by immunofluorescence microscopy in dividing and nondividing cells of Escherichia coli. J. Bacteriol. **180,** 6107–6116 (1998).
14. Chen, J. C., Weiss, D. S., Ghigo, J. M. & Beckwith, J. Septal localization of FtsQ, an essential cell division protein in Escherichia coli. J. Bacteriol. **181,** 521–530 (1999).
15. Ghigo, J. M., Weiss, D. S., Chen, J. C., Yarrow, J. C. & Beckwith, J. Localization of FtsL to the Escherichia coli septal ring. Mol. Microbiol. **31,** 725–737 (1999).
16. Chen, J. C. & Beckwith, J. FtsQ, FtsL and FtsI require FtsK, but not FtsN, for co-localization with FtsZ during Escherichia coli cell division. Mol. Microbiol. **42,** 395–413 (2001).
17. Buddelmeijer, N., Judson, N., Boyd, D., Mekalanos, J. J. & Beckwith, J. YgbQ, a cell division protein in Escherichia coli and Vibrio cholerae, localizes in codependent fashion with FtsL to the division site. Proc. Natl. Acad. Sci. U. S. A. **99,** 6316–6321 (2002).
18. Dai, K., Xu, Y. & Lutkenhaus, J. Topological characterization of the essential Escherichia coli cell division protein FtsN. J. Bacteriol. **178,** 1328–1334 (1996).
19. Guzman, L. M., Weiss, D. S. & Beckwith, J. Domain-swapping analysis of FtsI, FtsL, and FtsQ, bitopic membrane proteins essential for cell division in Escherichia coli. J. Bacteriol. **179,** 5094–5103 (1997).
20. Ghigo, J.-M. & Beckwith, J. Cell Division in Escherichia coli: Role of FtsL Domains in Septal Localization, Function, and Oligomerization. J Bacteriol **182,** 116–129 (2000).
21. Shiomi, D. & Margolin, W. Compensation for the loss of the conserved membrane targeting sequence of FtsA provides new insights into its function. Mol. Microbiol. **67,** 558–569 (2008).
22. Busiek, K. K., Eraso, J. M., Wang, Y. & Margolin, W. The early divisome protein FtsA interacts

directly through its 1c subdomain with the cytoplasmic domain of the late divisome protein FtsN. J. Bacteriol. **194,** 1989–2000 (2012).

23. D'Ulisse, V., Fagioli, M., Ghelardini, P. & Paolozzi, L. Three functional subdomains of the Escherichia coli FtsQ protein are involved in its interaction with the other division proteins. Microbiol. Read. Engl. **153,** 124–138 (2007).
24. Karimova, G., Dautin, N. & Ladant, D. Interaction network among Escherichia coli membrane proteins involved in cell division as revealed by bacterial two-hybrid analysis. J. Bacteriol. **187,** 2233–2243 (2005).
25. Bernard, C. S., Sadasivam, M., Shiomi, D. & Margolin, W. An altered FtsA can compensate for the loss of essential cell division protein FtsN in Escherichia coli. Mol. Microbiol. **64,** 1289–1305 (2007).
26. Geissler, B. & Margolin, W. Evidence for functional overlap among multiple bacterial cell division proteins: compensating for the loss of FtsK. Mol. Microbiol. **58,** 596–612 (2005).
27. Geissler, B., Shiomi, D. & Margolin, W. The ftsA* gain-of-function allele of Escherichia coli and its effects on the stability and dynamics of the Z ring. Microbiol. Read. Engl. **153,** 814–825 (2007).
28. Nogales, E., Downing, K. H., Amos, L. A. & Löwe, J. Tubulin and FtsZ form a distinct family of GTPases. Nat. Struct. Biol. **5,** 451–458 (1998).
29. Erickson, H. P., Taylor, D. W., Taylor, K. A. & Bramhill, D. Bacterial cell division protein FtsZ assembles into protofilament sheets and minirings, structural homologs of tubulin polymers. Proc. Natl. Acad. Sci. U. S. A. **93,** 519–523 (1996).
30. Lu, C., Reedy, M. & Erickson, H. P. Straight and curved conformations of FtsZ are regulated by GTP hydrolysis. J. Bacteriol. **182,** 164–170 (2000).
31. Pichoff, S. & Lutkenhaus, J. Unique and overlapping roles for ZipA and FtsA in septal ring assembly in Escherichia coli. EMBO J. **21,** 685–693 (2002).
32. Pichoff, S. & Lutkenhaus, J. Tethering the Z ring to the membrane through a conserved

membrane targeting sequence in FtsA. Mol. Microbiol. **55,** 1722–1734 (2005).

33. Wang, L. & Lutkenhaus, J. FtsK is an essential cell division protein that is localized to the septum and induced as part of the SOS response. Mol. Microbiol. **29,** 731–740 (1998).
34. Stouf, M., Meile, J.-C. & Cornet, F. FtsK actively segregates sister chromosomes in Escherichia coli. Proc. Natl. Acad. Sci. U. S. A. **110,** 11157–11162 (2013).
35. Monahan, L. G., Liew, A. T. F., Bottomley, A. L. & Harry, E. J. Division site positioning in bacteria: one size does not fit all. Front. Microbiol. **5,** 19 (2014).
36. Lutkenhaus, J., Pichoff, S. & Du, S. Bacterial cytokinesis: From Z ring to divisome. Cytoskelet. Hoboken NJ **69,** 778–790 (2012).
37. Rowlett, V. W. & Margolin, W. The bacterial Min system. Curr. Biol. CB **23,** R553–556 (2013).
38. Bramkamp, M. & van Baarle, S. Division site selection in rod-shaped bacteria. Curr. Opin. Microbiol. **12,** 683–688 (2009).
39. Buddelmeijer, N. & Beckwith, J. A complex of the Escherichia coli cell division proteins FtsL, FtsB and FtsQ forms independently of its localization to the septal region. Mol. Microbiol. **52,** 1315–27 (2004).
40. Vicente, M. & Rico, A. I. The order of the ring: assembly of Escherichia coli cell division components. Mol. Microbiol. **61,** 5–8 (2006).
41. Den Blaauwen, T., de Pedro, M. A., Nguyen-Distèche, M. & Ayala, J. A. Morphogenesis of rod-shaped sacculi. FEMS Microbiol. Rev. **32,** 321–344 (2008).
42. Mohammadi, T. et al. Identification of FtsW as a transporter of lipid-linked cell wall precursors across the membrane. EMBO J. **30,** 1425–1432 (2011).
43. Wang, L., Khattar, M. K., Donachie, W. D. & Lutkenhaus, J. FtsI and FtsW are localized to the septum in Escherichia coli. J. Bacteriol. **180,** 2810–2816 (1998).
44. Den Blaauwen, T., Andreu, J. M. & Monasterio, O. Bacterial cell division proteins as antibiotic targets. Bioorganic Chem. **55,** 27–38 (2014).

45. Dai, K., Xu, Y. & Lutkenhaus, J. Cloning and characterization of ftsN, an essential cell division gene in Escherichia coli isolated as a multicopy suppressor of ftsA12(Ts). J. Bacteriol. **175,** 3790–3797 (1993).

46. Corbin, B. D., Geissler, B., Sadasivam, M. & Margolin, W. Z-ring-independent interaction between a subdomain of FtsA and late septation proteins as revealed by a polar recruitment assay. J. Bacteriol. **186,** 7736–44 (2004).

47. Syeda, A. H., Hawkins, M. & McGlynn, P. Recombination and Replication. Cold Spring Harb. Perspect. Biol. (2014). doi:10.1101/cshperspect.a016550

48. Meier, E. L. & Goley, E. D. Form and function of the bacterial cytokinetic ring. Curr. Opin. Cell Biol. **26,** 19–27 (2014).

49. Rico, A. I., Krupka, M. & Vicente, M. In the beginning, Escherichia coli assembled the proto-ring: an initial phase of division. J. Biol. Chem. **288,** 20830–20836 (2013).

50. Erickson, H. P. The FtsZ protofilament and attachment of ZipA--structural constraints on the FtsZ power stroke. Curr. Opin. Cell Biol. **13,** 55–60 (2001).

51. Natale, P., Pazos, M. & Vicente, M. The Escherichia coli divisome: born to divide. Environ. Microbiol. **15,** 3169–3182 (2013).

52. Goehring, N. W. & Beckwith, J. Diverse Paths to Midcell: Assembly of the Bacterial Cell Division Machinery. Curr. Biol. **15,** R514–R526 (2005).

53. Den Blaauwen, T. Prokaryotic cell division: flexible and diverse. Curr. Opin. Microbiol. **16,** 738–744 (2013).

54. Szwedziak, P. & Löwe, J. Do the divisome and elongasome share a common evolutionary past? Curr. Opin. Microbiol. **16,** 745–751 (2013).

55. Moore, D. T., Berger, B. W. & DeGrado, W. F. Protein-Protein Interactions in the Membrane: Sequence, Structural, and Biological Motifs. Structure **16,** 991–1001 (2008).

56. Di Lallo, G., Fagioli, M., Barionovi, D., Ghelardini, P. & Paolozzi, L. Use of a two-hybrid assay to study the assembly of a complex multicomponent protein machinery: bacterial septosome

differentiation. Microbiol. Read. Engl. **149,** 3353–3359 (2003).

57. Karimova, G., Pidoux, J., Ullmann, A. & Ladant, D. A bacterial two-hybrid system based on a reconstituted signal transduction pathway. Proc. Natl. Acad. Sci. U. S. A. **95,** 5752–5756 (1998).
58. Goehring, N. W., Gueiros-Filho, F. & Beckwith, J. Premature targeting of a cell division protein to midcell allows dissection of divisome assembly in Escherichia coli. Genes Dev. **19,** 127–137 (2005).
59. Goehring, N. W., Gonzalez, M. D. & Beckwith, J. Premature targeting of cell division proteins to midcell reveals hierarchies of protein interactions involved in divisome assembly. Mol. Microbiol. **61,** 33–45 (2006).
60. Robichon, C., King, G. F., Goehring, N. W. & Beckwith, J. Artificial septal targeting of Bacillus subtilis cell division proteins in Escherichia coli: an interspecies approach to the study of protein-protein interactions in multiprotein complexes. J. Bacteriol. **190,** 6048–6059 (2008).
61. Jiménez, M., Martos, A., Vicente, M. & Rivas, G. Reconstitution and organization of Escherichia coli proto-ring elements (FtsZ and FtsA) inside giant unilamellar vesicles obtained from bacterial inner membranes. J. Biol. Chem. **286,** 11236–11241 (2011).
62. Söderström, B. et al. Disassembly of the divisome in Escherichia coli: evidence that FtsZ dissociates before compartmentalization. Mol. Microbiol. **92,** 1–9 (2014).
63. Zhou, M., Eun, Y.-J., Guzei, I. A. & Weibel, D. B. Structure-activity studies of divin: an inhibitor of bacterial cell division. ACS Med. Chem. Lett. **4,** 880–885 (2013).
64. Ma, X. & Margolin, W. Genetic and functional analyses of the conserved C-terminal core domain of Escherichia coli FtsZ. J. Bacteriol. **181,** 7531–7544 (1999).
65. Haney, S. A. et al. Genetic analysis of the Escherichia coli FtsZ.ZipA interaction in the yeast two-hybrid system. Characterization of FtsZ residues essential for the interactions with ZipA and with FtsA. J. Biol. Chem. **276,** 11980–11987 (2001).
66. Yu, X. C. & Margolin, W. FtsZ ring clusters in min and partition mutants: role of both the Min

system and the nucleoid in regulating FtsZ ring localization. Mol. Microbiol. **32,** 315–326 (1999).

67. Oliva, M. A., Trambaiolo, D. & Löwe, J. Structural insights into the conformational variability of FtsZ. J. Mol. Biol. **373,** 1229–1242 (2007).
68. Lutkenhaus, J., Pichoff, S. & Du, S. Bacterial cytokinesis: From Z ring to divisome. Cytoskeleton **69,** 778–790 (2012).
69. Van den Ent, F. & Löwe, J. Crystal structure of the cell division protein FtsA from Thermotoga maritima. EMBO J. **19,** 5300–5307 (2000).
70. Addinall, S. G. & Lutkenhaus, J. FtsA is localized to the septum in an FtsZ-dependent manner. J. Bacteriol. **178,** 7167–7172 (1996).
71. Löwe, J. & van den Ent, F. Conserved sequence motif at the C-terminus of the bacterial cell-division protein FtsA. Biochimie **83,** 117–120 (2001).
72. Duman, R. et al. Structural and genetic analyses reveal the protein SepF as a new membrane anchor for the Z ring. Proc. Natl. Acad. Sci. U. S. A. **110,** E4601–4610 (2013).
73. Fujita, J. et al. Crystal structure of FtsA from Staphylococcus aureus. FEBS Lett. **588,** 1879–1885 (2014).
74. Yan, K., Pearce, K. H. & Payne, D. J. A conserved residue at the extreme C-terminus of FtsZ is critical for the FtsA-FtsZ interaction in Staphylococcus aureus. Biochem. Biophys. Res. Commun. **270,** 387–392 (2000).
75. Yim, L. et al. Role of the carboxy terminus of Escherichia coli FtsA in self-interaction and cell division. J. Bacteriol. **182,** 6366–6373 (2000).
76. Shiomi, D. & Margolin, W. Dimerization or oligomerization of the actin-like FtsA protein enhances the integrity of the cytokinetic Z ring. Mol. Microbiol. **66,** 1396–1415 (2007).
77. Hsin, J., Fu, R. & Huang, K. C. Dimer dynamics and filament organization of the bacterial cell division protein FtsA. J. Mol. Biol. **425,** 4415–4426 (2013).
78. Hale, C. A. & de Boer, P. A. Recruitment of ZipA to the septal ring of Escherichia coli is dependent on FtsZ and independent of FtsA. J. Bacteriol. **181,** 167–176 (1999).

79. Hale, C. A. & de Boer, P. A. Direct binding of FtsZ to ZipA, an essential component of the septal ring structure that mediates cell division in E. coli. Cell **88,** 175–185 (1997).

80. Ohashi, T., Hale, C. A., de Boer, P. A. J. & Erickson, H. P. Structural evidence that the P/Q domain of ZipA is an unstructured, flexible tether between the membrane and the C-terminal FtsZ-binding domain. J. Bacteriol. **184,** 4313–4315 (2002).

81. López-Montero, I. et al. Intrinsic disorder of the bacterial cell division protein ZipA: coil-to-brush conformational transition. FASEB J. Off. Publ. Fed. Am. Soc. Exp. Biol. **27,** 3363–3375 (2013).

82. Gueiros-Filho, F. J. & Losick, R. A widely conserved bacterial cell division protein that promotes assembly of the tubulin-like protein FtsZ. Genes Dev. **16,** 2544–2556 (2002).

83. Ebersbach, G., Galli, E., Møller-Jensen, J., Löwe, J. & Gerdes, K. Novel coiled-coil cell division factor ZapB stimulates Z ring assembly and cell division. Mol. Microbiol. **68,** 720–735 (2008).

84. Durand-Heredia, J. M., Yu, H. H., De Carlo, S., Lesser, C. F. & Janakiraman, A. Identification and characterization of ZapC, a stabilizer of the FtsZ ring in Escherichia coli. J. Bacteriol. **193,** 1405–1413 (2011).

85. Durand-Heredia, J., Rivkin, E., Fan, G., Morales, J. & Janakiraman, A. Identification of ZapD as a cell division factor that promotes the assembly of FtsZ in Escherichia coli. J. Bacteriol. **194,** 3189–3198 (2012).

86. Pacheco-Gómez, R. et al. Tetramerization of ZapA is required for FtsZ bundling. Biochem. J. **449,** 795–802 (2013).

87. Buss, J. et al. In vivo organization of the FtsZ-ring by ZapA and ZapB revealed by quantitative super-resolution microscopy. Mol. Microbiol. **89,** 1099–1120 (2013).

88. Diez, A. A., Farewell, A., Nannmark, U. & Nyström, T. A mutation in the ftsK gene of Escherichia coli affects cell-cell separation, stationary-phase survival, stress adaptation, and expression of the gene encoding the stress protein UspA. J. Bacteriol. **179,** 5878–5883 (1997).

89. Draper, G. C., McLennan, N., Begg, K., Masters, M. & Donachie, W. D. Only the N-terminal

domain of FtsK functions in cell division. J. Bacteriol. **180,** 4621–4627 (1998).

90. Aussel, L. et al. FtsK Is a DNA motor protein that activates chromosome dimer resolution by switching the catalytic state of the XerC and XerD recombinases. Cell **108,** 195–205 (2002).
91. Massey, T. H., Mercogliano, C. P., Yates, J., Sherratt, D. J. & Löwe, J. Double-stranded DNA translocation: structure and mechanism of hexameric FtsK. Mol. Cell **23,** 457–469 (2006).
92. Sherratt, D. J., Lau, I. F. & Barre, F. X. Chromosome segregation. Curr. Opin. Microbiol. **4,** 653–659 (2001).
93. Sherratt, D. J., Arciszewska, L. K., Crozat, E., Graham, J. E. & Grainge, I. The Escherichia coli DNA translocase FtsK. Biochem. Soc. Trans. **38,** 395–398 (2010).
94. Mizuno, K., Miyabe, I., Schalbetter, S. A., Carr, A. M. & Murray, J. M. Recombination-restarted replication makes inverted chromosome fusions at inverted repeats. Nature **493,** 246–249 (2013).
95. Alzu, A. et al. Senataxin associates with replication forks to protect fork integrity across RNA-polymerase-II-transcribed genes. Cell **151,** 835–846 (2012).
96. Lee, J. Y., Finkelstein, I. J., Arciszewska, L. K., Sherratt, D. J. & Greene, E. C. Single-molecule imaging of FtsK translocation reveals mechanistic features of protein-protein collisions on DNA. Mol. Cell **54,** 832–843 (2014).
97. Grainge, I. Simple topology: FtsK-directed recombination at the dif site. Biochem. Soc. Trans. **41,** 595–600 (2013).
98. Sauvage, E. et al. Crystal structure of penicillin-binding protein 3 (PBP3) from Escherichia coli. PloS One **9,** e98042 (2014).
99. Bisicchia, P., Steel, B., Mariam Debela, M. H., Löwe, J. & Sherratt, D. The N-terminal membrane-spanning domain of the Escherichia coli DNA translocase FtsK hexamerizes at midcell. mBio **4,** e00800–00813 (2013).
100. Berezuk, A. M., Goodyear, M. & Khursigara, C. M. Site-directed fluorescence labeling reveals a revised N-terminal membrane topology and functional periplasmic residues in the Escherichia coli cell division protein FtsK. J. Biol. Chem. **289,** 23287–23301 (2014).

101. Begg, K. J., Dewar, S. J. & Donachie, W. D. A new Escherichia coli cell division gene, ftsK. J. Bacteriol. **177,** 6211–6222 (1995).

102. Dubarry, N., Possoz, C. & Barre, F.-X. Multiple regions along the Escherichia coli FtsK protein are implicated in cell division. Mol. Microbiol. **78,** 1088–1100 (2010).

103. Grainge, I. FtsK--a bacterial cell division checkpoint? Mol. Microbiol. **78,** 1055–1057 (2010).

104. Begg, K. J., Hatfull, G. F. & Donachie, W. D. Identification of new genes in a cell envelope-cell division gene cluster of Escherichia coli: cell division gene ftsQ. J. Bacteriol. **144,** 435–437 (1980).

105. Guzman, L. M., Barondess, J. J. & Beckwith, J. FtsL, an essential cytoplasmic membrane protein involved in cell division in Escherichia coli. J. Bacteriol. **174,** 7716–7728 (1992).

106. Chen, J. C., Minev, M. & Beckwith, J. Analysis of ftsQ mutant alleles in Escherichia coli: complementation, septal localization, and recruitment of downstream cell division proteins. J. Bacteriol. **184,** 695–705 (2002).

107. Goehring, N. W., Petrovska, I., Boyd, D. & Beckwith, J. Mutants, suppressors, and wrinkled colonies: mutant alleles of the cell division gene ftsQ point to functional domains in FtsQ and a role for domain 1C of FtsA in divisome assembly. J. Bacteriol. **189,** 633–45 (2007).

108. Van den Berg van Saparoea, H. B. et al. Fine-mapping the contact sites of the Escherichia coli cell division proteins FtsB and FtsL on the FtsQ protein. J. Biol. Chem. **288,** 24340–24350 (2013).

109. Masson, S. et al. Central domain of DivIB caps the C-terminal regions of the FtsL/DivIC coiled-coil rod. J. Biol. Chem. **284,** 27687–27700 (2009).

110. Sánchez-Pulido, L., Devos, D., Genevrois, S., Vicente, M. & Valencia, A. POTRA: a conserved domain in the FtsQ family and a class of beta-barrel outer membrane proteins. Trends Biochem. Sci. **28,** 523–526 (2003).

111. Van den Ent, F. et al. Structural and mutational analysis of the cell division protein FtsQ. Mol. Microbiol. **68,** 110–123 (2008).

112. Grenga, L., Guglielmi, G., Melino, S., Ghelardini, P. & Paolozzi, L. FtsQ interaction mutants: a way to identify new antibacterial targets. New Biotechnol. (2010). doi:10.1016/j.nbt.2010.05.002

113. Robichon, C., Karimova, G., Beckwith, J. & Ladant, D. Role of leucine zipper motifs in association of the Escherichia coli cell division proteins FtsL and FtsB. J. Bacteriol. **193,** 4988–4992 (2011).

114. LaPointe, L. M. et al. Structural organization of FtsB, a transmembrane protein of the bacterial divisome. Biochemistry (Mosc.) **52,** 2574–2585 (2013).

115. Zhou, F. X., Cocco, M. J., Russ, W. P., Brunger, A. T. & Engelman, D. M. Interhelical hydrogen bonding drives strong interactions in membrane proteins. Nat. Struct. Biol. **7,** 154–60 (2000).

116. Choma, C., Gratkowski, H., Lear, J. D. & DeGrado, W. F. Asparagine-mediated self-association of a model transmembrane helix. Nat. Struct. Biol. **7,** 161–6 (2000).

117. Khadria, A. S. & Senes, A. The transmembrane domains of the bacterial cell division proteins FtsB and FtsL form a stable high-order oligomer. Biochemistry (Mosc.) **52,** 7542–7550 (2013).

118. Daniel, R. A. & Errington, J. Intrinsic instability of the essential cell division protein FtsL of Bacillus subtilis and a role for DivIB protein in FtsL turnover. Mol. Microbiol. **36,** 278–289 (2000).

119. Wadenpohl, I. & Bramkamp, M. DivIC stabilizes FtsL against RasP cleavage. J. Bacteriol. **192,** 5260–5263 (2010).

120. Schmidt, K. L. et al. A predicted ABC transporter, FtsEX, is needed for cell division in Escherichia coli. J. Bacteriol. **186,** 785–793 (2004).

121. Yang, D. C. et al. An ATP-binding cassette transporter-like complex governs cell-wall hydrolysis at the bacterial cytokinetic ring. Proc. Natl. Acad. Sci. U. S. A. **108,** E1052–1060 (2011).

122. Mavrici, D. et al. Mycobacterium tuberculosis FtsX extracellular domain activates the peptidoglycan hydrolase, RipC. Proc. Natl. Acad. Sci. U. S. A. **111,** 8037–8042 (2014).

123. Goffin, C. & Ghuysen, J. M. Multimodular penicillin-binding proteins: an enigmatic family of orthologs and paralogs. Microbiol. Mol. Biol. Rev. MMBR **62,** 1079–1093 (1998).

124. Sauvage, E., Kerff, F., Terrak, M., Ayala, J. A. & Charlier, P. The penicillin-binding proteins: structure and role in peptidoglycan biosynthesis. FEMS Microbiol. Rev. **32,** 234–258 (2008).

125. Höltje, J. V. Growth of the stress-bearing and shape-maintaining murein sacculus of Escherichia coli. Microbiol. Mol. Biol. Rev. MMBR **62,** 181–203 (1998).

126. Bertsche, U. et al. Interaction between two murein (peptidoglycan) synthases, PBP3 and PBP1B, in Escherichia coli. Mol. Microbiol. **61,** 675–690 (2006).

127. Matteï, P.-J., Neves, D. & Dessen, A. Bridging cell wall biosynthesis and bacterial morphogenesis. Curr. Opin. Struct. Biol. **20,** 749–755 (2010).

128. Zapun, A., Noirclerc-Savoye, M., Helassa, N. & Vernet, T. Peptidoglycan assembly machines: the biochemical evidence. Microb. Drug Resist. Larchmt. N **18,** 256–260 (2012).

129. Berg, K. H., Straume, D. & Håvarstein, L. S. The function of the transmembrane and cytoplasmic domains of pneumococcal penicillin-binding proteins 2x and 2b extends beyond that of simple anchoring devices. Microbiol. Read. Engl. **160,** 1585–1598 (2014).

130. Lara, B. & Ayala, J. A. Topological characterization of the essential Escherichia coli cell division protein FtsW. FEMS Microbiol. Lett. **216,** 23–32 (2002).

131. Henriques, A. O., Glaser, P., Piggot, P. J. & Moran, C. P. Control of cell shape and elongation by the rodA gene in Bacillus subtilis. Mol. Microbiol. **28,** 235–247 (1998).

132. Margolin, W. Themes and variations in prokaryotic cell division. FEMS Microbiol. Rev. **24,** 531–548 (2000).

133. Fraipont, C. et al. The integral membrane FtsW protein and peptidoglycan synthase PBP3 form a subcomplex in Escherichia coli. Microbiol. Read. Engl. **157,** 251–259 (2011).

134. Yang, J.-C., Van Den Ent, F., Neuhaus, D., Brevier, J. & Löwe, J. Solution structure and domain architecture of the divisome protein FtsN. Mol. Microbiol. **52,** 651–660 (2004).

135. Goehring, N. W., Robichon, C. & Beckwith, J. Role for the nonessential N terminus of FtsN in divisome assembly. J. Bacteriol. **189,** 646–649 (2007).

136. Alexeeva, S., Gadella, T. W. J., Jr, Verheul, J., Verhoeven, G. S. & den Blaauwen, T. Direct interactions of early and late assembling division proteins in Escherichia coli cells resolved by FRET. Mol. Microbiol. **77,** 384–398 (2010).

137. Hong, H. Toward understanding driving forces in membrane protein folding. Arch. Biochem. Biophys. (2014). doi:10.1016/j.abb.2014.07.031

138. Wallin, E. & von Heijne, G. Genome-wide analysis of integral membrane proteins from eubacterial, archaean, and eukaryotic organisms. Protein Sci. Publ. Protein Soc. **7,** 1029–1038 (1998).

139. Krogh, A., Larsson, B., von Heijne, G. & Sonnhammer, E. L. Predicting transmembrane protein topology with a hidden Markov model: application to complete genomes. J. Mol. Biol. **305,** 567–580 (2001).

140. Dill, K. A. Dominant forces in protein folding. Biochemistry (Mosc.) **29,** 7133–7155 (1990).

141. Massey-Gendel, E. et al. Genetic selection system for improving recombinant membrane protein expression in E. coli. Protein Sci. Publ. Protein Soc. **18,** 372–383 (2009).

142. Studier, F. W. Protein production by auto-induction in high density shaking cultures. Protein Expr. Purif. **41,** 207–234 (2005).

143. Ingólfsson, H. I. et al. Lipid organization of the plasma membrane. J. Am. Chem. Soc. **136,** 14554–14559 (2014).

144. Stanley, A. M. & Fleming, K. G. The process of folding proteins into membranes: challenges and progress. Arch. Biochem. Biophys. **469,** 46–66 (2008).

145. Popot, J. L., Gerchman, S. E. & Engelman, D. M. Refolding of bacteriorhodopsin in lipid bilayers. A thermodynamically controlled two-stage process. J. Mol. Biol. **198,** 655–676 (1987).

146. Popot, J. L. & Engelman, D. M. Membrane protein folding and oligomerization: the two-stage model. Biochemistry (Mosc.) **29,** 4031–7 (1990).

147. Du, S., Park, K.-T. & Lutkenhaus, J. Oligomerization of FtsZ converts the FtsZ tail motif (CCTP) into a multivalent ligand with high avidity for partners ZipA and SlmA. Mol. Microbiol. (2014).

doi:10.1111/mmi.12854

148. Skoog, K. & Daley, D. O. The Escherichia coli cell division protein ZipA forms homodimers prior to association with FtsZ. Biochemistry (Mosc.) **51,** 1407–1415 (2012).
149. Lock, R. L. & Harry, E. J. Cell-division inhibitors: new insights for future antibiotics. Nat. Rev. Drug Discov. **7,** 324–338 (2008).
150. Arkin, M. R. & Wells, J. A. Small-molecule inhibitors of protein-protein interactions: progressing towards the dream. Nat. Rev. Drug Discov. **3,** 301–317 (2004).

Chapter 2

Structural organization of FtsB, a transmembrane protein of the bacterial divisome

This chapter was prepared for publication as:
Loren M. LaPointe, Keenan C. Taylor, Sabareesh Subramaniam, Ambalika Khadria, Ivan Rayment, Alessandro Senes. Structural organization of FtsB, a transmembrane protein of the bacterial divisome. Biochemistry. (2013) 52(15):2574-85.
Dept of Biochemistry, University of Wisconsin-Madison 53706

Abstract

Cell division in bacteria depends on the concerted effort of a membrane bound protein complex to orchestrate the coordinated remodeling of the cell envelope and the separation of the daughter cells. While the bacterial divisome has been extensively studied using molecular genetic techniques and interaction studies *in vivo*, most of the structural details of the assembly of the complex remain mysterious. Here we report the first structural analysis of an integral membrane protein of the complex. Using a combination of mutagenesis, computational modeling and X-ray crystallography, we have determined the structural organization of the transmembrane and periplasmic domains of an FtsB homo-dimer from *Escherichia coli*. We found that the transmembrane domain of FtsB has an evolutionarily conserved interaction interface where a polar residue (Gln 16) plays a critical role in promoting association through the formation of an inter-helical hydrogen bond. The crystal structure of the periplasmic domain, solved at 2.3Å as a fusion with Gp7, shows that 30 juxta-membrane amino acids of FtsB form a canonical coiled coil. Molecular modeling and the presence of conserved Gly residues suggests that flexibility in the linker region between the transmembrane and coiled coil regions is functionally important. We hypothesize that the transmembrane dimer of FtsB forms a stable core for its association with FtsL, and that FtsL is required to stabilize the periplasmic domain of FtsB, leading to the formation of a complex that is competent for binding to FtsQ and its recruitment to the division septum.

2.1 Introduction

Cell division is one of the most fundamental processes in the life of bacteria. In gram-negative bacteria division requires a complex and coordinated remodeling of the three-layer cell envelope, and therefore mechanisms must exist to sort the duplicated chromosome, to provide constrictive force, to synthesize the septal cell wall and, finally, to induce membrane fusion. These events are enabled by a multi-protein complex called the *divisome.* The assembly of the divisome begins with the formation of a ring-like structure at the site of division (the Z-ring), where the polymeric FtsZ provides constrictive force (1, 2) and forms a scaffold for the recruitment of the complex (3). In *Escherichia coli* the recruitment of the essential proteins follows a strikingly linear hierarchy, illustrated in Fig. 1a (4). The cytoplasmic side of the ring is formed by FtsZ and the other early components. These are FtsA, a member of the actin family (5) that tethers FtsZ to the plasma membrane (6); ZipA, a single-pass membrane protein that also contribute to FtsZ tethering (7, 8); and FtsK, a DNA translocase that is essential for unlinking chromosome dimers after homologous recombination (9). In contrast, the late proteins (FtsW, FtsI and FtsN) perform functions related to the reconstruction of the cell-wall and thus their topology is biased toward the periplasm. FtsW is a transporter of cell-wall precursors across the membrane (10, 11); FtsI is important for the cross-linking of the cell wall during division (12); and FtsN is required for septal recruitment of two non-essential septal components, the murein hydrolase AmiC (13, 14), and the Tol-Pal complex required for proper invagination during constriction (15).

In between the early and late proteins there is a trio of single pass transmembrane proteins – FtsQ, FtsB, and FtsL – whose function remains still mysterious. As highlighted in Fig. 1a, FtsB and FtsL are mutually dependent for their recruitment at the division site, and both proteins depend on the localization of FtsQ (16, 17). A similar picture has been reported in *Bacillus subtilis*, where the

localization of the homologues of FtsL and FtsB ($FtsL_B$ and DivIC) depends on the FtsQ homologue (DivIB) at the temperature at which DivIB is essential (18, 19). There is strong evidence that FtsQ, FtsB and FtsL form a stable sub-complex *in vivo.* A complex comprising FtsQ, FtsL, and FtsB was isolated from *E. coli* by co-immunoprecipitation (20). The physical interaction of the *E. coli* and *B. subtilis* proteins was also confirmed by two-hybrid analysis (21–23). Further evidence of a stable interaction between FtsB, FtsL and FtsQ was obtained with a series of artificial septal targeting experiments by the Beckwith group (24–29). In these experiments one of the partners was fused with the FtsZ-binding protein ZapA to force its localization (the "bait"), and its ability to recruit a second GFP-labeled protein (the "prey") was determined by epifluorescence microscopy (24). These experiments demonstrated that, even when FtsQ has been depleted from the cell, FtsL and FtsB still interact with each other and can recruit the downstream proteins (25). It was also demonstrated that the *B. subtilis* homologues, $FtsL_B$ and DivIC, form a stable complex in *E. coli* in the absence of the other *B. subtilis* cell division proteins (26). These findings provides further confirmation that a complex can form independently of other components, considering the fact that $FtsL_B$ and DivIC are unlikely to interact with the significantly divergent *E. coli* division proteins.

While the interactions of FtsB and FtsL have been extensively dissected *in vivo*, their function is still unknown. There is some indication that the FtsB-FtsL pair may be involved in a regulatory checkpoint of division, because the depletion of FtsB from *E. coli* cells results in the disappearance of FtsL (16). The cellular instability of FtsL was also observed in *B. subtilis* (18, 21, 30), where $FtsL_B$ is rapidly degraded by the intramembrane protease RasP (31) unless it is stabilized by its interaction with DivIC. These observations lead to the hypothesis that active proteolysis of FtsL may be a regulatory factor in the timing of bacterial cell division (32). The ability of FtsB and FtsL to recruit the late

divisome elements and their domain organization also suggest that they may have a structural role in the divisome. The topology of FtsB and FtsL, shown in Fig. 1*b*, appears to be very similar although the two proteins are not homologous. Both proteins contain a small (FtsL) or minimimal (FtsB) cytoplasimic N-terminal tail, a transmembrane domain and a juxta-membrane coiled coil. The transmembrane and coiled coil regions of FtsB are necessary and sufficient for its interaction with FtsL, while its C-terminus is necessary for the interaction of FtsB with FtsQ (28). Similarly, the transmembrane and coiled coil regions of FtsL are both essential for its interaction with FtsB (20). The data strongly suggest that a FtsB/FtsL complex mediated by the transmembrane helices and the juxta-membrane coiled coil assembles first, and it is subsequently recruited to the divisome by the interaction with FtsQ.

The structure of the FtsQ/FtsB/FtsL complex is still unknown but a low resolution model of their *Streptococcus pneumoniae* homologues was proposed by Masson et al. (33), based on a combination of NMR, small angle neutron and X-ray scattering, and surface plasmon resonance. In the model, the coiled coil domains of FtsB and FtsL form a hetero-dimer, while their C-terminal tails interact with one side of the β-domain of FtsQ. The model does not include the transmembrane domains. These were truncated and replaced by a soluble coiled coil pair (the e5 and k5 peptides) which also induced hetero-dimerization (33, 34). More recently, a bioinformatic analysis suggested two alternative models of the soluble domains of FtsB, FtsL and FtsQ with 1:1:1 or 2:2:2 oligomeric stoichiometries (35). To date, however, there is still no structural information regarding the transmembrane helices of the proteins. In fact, prior to the present study the molecular architecture of the membrane region of the entire divisome was completely unexplored.

Here we report the first structural study on the transmembrane domains of a bacterial division protein, with the computational model of an FtsB homodimer based on extensive mutagenesis. The interfacial residues appear to be evolutionarily conserved, including a key polar amino acid that stabilize the interaction through the formation of an inter-helical hydrogen bond. We have also determined the X-ray crystal structure of the juxta-membrane domain of FtsB, which forms a canonical coiled coil. Our analysis suggest the hypothesis that the association of the transmembrane helix of FtsB may form a core for the assembly of the FtsB/FtsL complex. It also suggests that the linker region between the transmembrane domain and the coiled coil of FtsB is likely flexible and that the lateral association of FtsL may be required for the stabilization of the periplasmic domains.

2.2 Results and Discussion

2.2.1 The transmembrane domains of FtsB and FtsL self-associate

To determine if the transmembrane domains of FtsB and FtsL from *E. coli* self-associate, we analyzed them with TOXCAT (36). TOXCAT is a biological assay based on a chimeric constructs in which the transmembrane domain of interest is fused to the ToxR transcriptional activator domain from *Vibrio cholera* (Fig. 2*a*). Oligomerization, driven by the transmembrane helices, results in the expression of the reporter gene chloramphenicol acetyltransferase (CAT). The expression level (measured enzymatically) is compared to a stable dimer, Glycophorin A (GpA), as a standard. Our analysis shows that the TOXCAT signal of both FtsB and FtsL are significantly above background (Fig. 2*b*). While the association of FtsL appears to be rather weak, the activity of FtsB is approximately half of the GpA signal, indicating that the homo-oligomerization of its transmembrane domain is rather stable.

2.2.2 The transmembrane self-association of FtsB is mediated by a critical polar amino acid

To investigate what amino acids are important for the self-association of FtsB and FtsL, we systematically mutated each position and monitored the effects on association. The expectation is that the changes at interfacial positions would perturb oligomerization more than the changes at positions that are solvent exposed, as commonly observed (for example (37–41)). We adopted an initial large-to-Ala and small-to-Leu mutational strategy to identify the key positions, and then rationally expanded the mutagenesis to a larger variety of hydrophobic amino acids to further refine the analysis.

The analysis of FtsB revealed that its transmembrane domain oligomerizes with a distinct

interaction interface. The mutagenesis data is reported in Figs. 3 and 4. Fig. 3 shows the TOXCAT data for about half of the 57 variants tested. Fig. 4*a* schematically summarizes the entire mutagenesis using a classification of the phenotypes as "WT-like", "slightly destabilizing", "significantly destabilizing" and "strongly disruptive". The scheme permits a visual assessment of the overall sensitivity of each position. A calculated average disruption value is also displayed at the bottom the scheme. When the average disruption is projected on a helical wheel diagram (Fig. 4*b*) it becomes evident that the sensitive mutations cluster on the helical face defined by positions T5, L6, L8, L9, L12, L15, Q16, L19 and W20. When fit to a sine function (Fig. 4*c*), the average disruption shows a periodicity of 3.5 amino acids per turn, which suggests that the helices of the FtsB oligomer interact with a left-handed crossing angle.

As expected, the low TOXCAT signal of FtsL did not allow a similarly comprehensive analysis. While a number of significantly disruptive mutations were identified (most noticeably C41, T52, V53 and V54), the disruption pattern does not clearly map to a helical interface as in the case of FtsB (supplementary Fig. S1). Therefore the analysis of FtsL was not expanded further.

2.2.3 FtsB self-association is mediated by inter-helical hydrogen bonding

Among the positions of the transmembrane domain of FtsB that are sensitive to mutation, Gln 16 is of particular interest. Polar amino acids, such as Gln, Asn, Glu, Asp, Lys, Arg and His, are not frequent in transmembrane domains, which are primarily composed by hydrophobic residues (42, 43). When present, however, polar residues can stabilize the association of transmembrane helices through the formation of hydrogen bonds, which are enhanced in an apolar environment (44, 45). While the energetic contribution of hydrogen bonding to membrane protein folding appears to be on average

rather modest (~1 kcal/mol) (45, 46), polar amino acids can be important for the association of model peptides (47, 48) and of biological systems (49–53). When present, polar amino acids are also likely to play an important structural or functional role, and it has been observed that phenotypic alterations and disease are likely to result from mutations that reverse the polarity of an amino acid in membrane proteins (54, 55).

When Gln 16 is substituted by hydrophobic amino acids (Ala, Phe and Val), the oligomerization of FtsB is almost entirely disrupted (Figs. 3 and 4). Even when the Gln is replaced by a hydrophobic amino acid with similar size and flexibility (Met) the mutation is severely disruptive. Conversely, when the position is substituted by Asn, which has the same amide terminal moiety of Gln, the variant retains most of the association. This result confirms that hydrogen bond formation plays a major role in stabilizing the transmembrane oligomer. Two side chains that could potentially hydrogen bond with Gln 16 across the interface are Tyr 17 and Ser 18. However, the removal of their hydroxyl groups (Y17F and S18A variants) did not affect oligomerization. This observation suggests that Gln 16 is likely to donate to a carbonyl oxygen atom from the backbone or to hydrogen bond with itself (from the opposing helix), an hypothesis that is supported by the computational modeling presented in the next section.

2.2.4 Computational model of a FtsB left-handed homo-dimer

Molecular modeling can interpret the wealth of information contained in large scale mutagenesis and synthesize it into a structural hypothesis (37–39, 56). The modeling of the transmembrane domain of FtsB was performed with a search protocol implemented with the molecular software library developed in this laboratory (MSL) (57). The program generates helices in standard

conformation and systematically varies their relative orientation to explore conformational space. In this calculation we imposed the formation of a symmetrical oligomer and also required that Gln 16 forms an inter-helical hydrogen bond in the structure. The calculation produced two well packed dimeric low-energy solutions (Fig 5). In one solution (Model 1, panel *a*) Q16 is hydrogen bonded non-symmetrically with Gln 16 on the opposite side. In Model 2 (panel *b*) Q16 is hydrogen bonded symmetrically to the carbonyl oxygen of Val 13. The two models are closely related (1.5Å RMSD), having a similar left-handed crossing angle and inter-helical distance, and differing by a relative rotation of approximately 60˚ applied around the helical axis. To identify which solution was most compatible with the experimental data, we applied *in silico* the same set of mutations that was experimentally tested, and computed the average disruption for the two models. The theoretical and experimental disruption patterns are compared in Fig. 5 *c* and *d*. Model 2 is in reasonable agreement with the data overall, but its periodicity appears be slightly off-phase with respect to the experimental data, and the match becomes poor toward the C-terminal end of the helix (panel *d*). Model 1 (panel *c*) is in excellent agreement with the experimental data, and therefore we propose it as the most likely structural interpretation. Model 1 is illustrated in more detail in Fig. 6 where the specific orientation of the side chains at the dimer interface is shown in panel *a* and a full-sphere representation demonstrates the void-free complementary packing in panel *b*. A PDB file of the two models is included as supplementary information or can be downloaded from http://seneslab.org.

2.2.5 Gln 16 and the interfacial amino acids of the transmembrane domain of FtsB are evolutionarily conserved

To investigate if the interfacial amino acids, and Gln 16 in particular, are evolutionarily

important, we performed a multi-sequence alignment of related FtsB sequences and computed a consensus. A condensed version of the alignment is shown in Fig. 7 and the complete analysis is provided as supplementary material (Fig. S2). The transmembrane region of FtsB appears to be relatively well conserved across a broad group of gamma and beta proteobacteria. Most importantly, the pattern of conservation corresponds remarkably well to the positions that have the highest sensitivity to mutagenesis. Gln 16 in particular is almost invariable. This observation supports the hypothesis that the structural organization of the transmembrane domain of FtsB is evolutionarily conserved and therefore must be of biological importance for division.

2.2.6 The X-ray crystal structure of the periplasmic region of FtsB reveals a canonical coiled coil

After establishing that the organization of the transmembrane domain of FtsB, we investigated the structure of the periplasmic coiled coil region using X-ray crystallography. Unlike transmembrane helices, which are stabilized by the hydrophobic environment, the soluble coiled coils tend to be unstable in isolation (33). For this reason we adopted a fusion strategy, replacing the transmembrane region with a soluble globular protein (bacteriophange Φ29 Gp7) which nucleates the helix and stabilizes the coiled coil. This fusion strategy has been demonstrated to greatly improve the solubility and crystallization propensity of coiled coil domains (58, 59).

A Gp7 fusion construct encompassing amino acids 28-63 of FtsB (Gp7-FtsB$_{CC}$) crystallized readily and its structure was solved at a 2.3 Å, with two dimeric molecule in the asymmetric unit (supplementary Fig. S3*a*). The X-ray data collection and refinement statistics are provided in supplementary Table S1. The structure of the Gp7-FtsB$_{CC}$ dimer is shown in Fig. 8, where the Gp7 moiety is highlighted in gray and the FtsB component in blue. FtsB adopts a canonical coiled coil

conformation. As expected, the two Asn residue that are present at "*a*" heptad positions (Asn 43 and 50) form a hydrogen bond across the interface with their corresponding residue on the other chain (Fig. 8b). The coil is straight for one of the dimers (chain A and B) but exhibits a slight kink in the second (supplementary Fig. S3*b*), presumably due to the effect of crystal packing. The structure demonstrates that, as for the transmembrane domain, the coiled coil region of FtsB is also compatible with the formation of a homo-dimer. The structure also determines that the coiled coil region of FtsB can extend at least to position 60. It is not clear whether the coiled coil would extend further, at least in the absence of FtsL. CD analysis of a longer constructs that encompassed 7 heptad repeats (positions 28-77) revealed that it is poorly helical (supplementary Fig. S4). A Gp7-FtsB$_{CC}$ construct that contains the entire soluble region of FtsB is also only moderately helical.

2.2.7 Flexibility may be important between the transmembrane and coiled coil region of FtsB

There is a gap of six amino acids (positions 22-27) between the computational model of the transmembrane domain and the X-ray structural model of the periplasmic coiled coil, raising the question of how these two regions are connected. The simplest hypothesis would be that the two domains form a seamless helical structure that transverses the transmembrane region and extends into the periplasm. Our geometric analysis, however, revealed that the two models cannot be connected by a simple fusion of their helices. While the crossing angle and inter-helical distance of the two domains match each other, the orientation of the helices around their main axes is not compatible. The interface of the transmembrane region is rotated by approximately 100˚ with respect to the interface that would result from a natural extension of the coiled coil.

The analysis of the sequence alignment (Fig. 7) also supports the hypothesis that a helical break

is likely present in the linker region between the domains. The alignment reveals that two Gly residue at positions 22 and 25 are highly conserved (highlighted cyan). Moreover, a third Gly residue is also frequently present in many species at position 24. The presence of a conserved Gly-rich region suggests that the linker requires either flexibility or adopts a backbone conformation that would be inaccessible to non-Gly amino acids, or perhaps both. According to this view, we mined the structural database for protein fragments that contained two Gly with the correct spacing (G*xx*G) to find candidate linkers for the two models. We extracted all *x*G*xx*G*x* fragments existing in high-resolution structures from the PDB, where *x* is any amino acid. We also imposed a constraint that two additional residues at each side of the fragment must assume a helical conformation (thus the pattern becomes *hhx*G*xx*G*xhh*, where *h* is any amino acid in helical conformation). These helical amino acids were geometrically aligned with the ends of the transmembrane and coiled coil structure. With this procedure we were able to identify the low-energy solution that connects the two models illustrated in Fig. 9.

2.3 Conclusions

2.3.1 Is FtsL required to stabilize the periplasmic domain of FtsB?

In this article we demonstrate that the transmembrane helix of the bacterial division protein FtsB self-associates in *E. coli* membranes. The interaction is mediated by an inter-helical hydrogen bond formed by a critical polar residue embedded in the middle of the hydrophobic region. We also report the structure of the juxta-membrane domain of FtsB which forms a canonical coiled coil. The two domains are connected by a likely flexible linker.

While the model of the linker region shown in Fig. 9 is hypothetical, it raises the question of whether the Gly-rich segment could effectively nucleate and stabilize the juxta-membrane coiled coil. The question is even more compelling when it is considered that the Gp7-FtsB$_{CC}$ construct has low thermal stability. Although the fusion protein crystallizes readily and is helical at low temperature, it reversibly unfolds quite rapidly and it appears to be completely unfolded at 40 ˚C (supplementary Fig. S4). Longer constructs, including one that extends to the entire soluble region of FtsB, showed lower helicity and even lower stability. The relatively low stability of the coiled coil, however, is not surprising when it is considered that the structure includes a large number of polar amino acids (Q35, N43, N50) at the buried "*a*" and "*d*" positions, which are generally hydrophobic (60, 61). These sequence features appear conserved in the sequence alignment (Fig. 7). Therefore it is possible that association with FtsL may be required for the stabilization of the periplasmic region of FtsB. The fact that the periplasmic domain of FtsB may be partially unfolded could also account for some of the cellular instability of FtsB, which is rapidly degraded in the absence of FtsL (28).

On the basis of our analysis, we hypothesize that a FtsB homo-dimer forms an initial core that

laterally recruits FtsL into a higher-order oligomer, such as a trimer or tetramer (Fig. 10). Given the presence of several Thr residues in the transmembrane helix of FtsL, an interesting possibility is that its lateral association could augment the membrane-embedded polar network by forming additional hydrogen bonds with the donor or acceptor groups that are left unsatisfied on Gln 16 (Fig. 6*c*). Alternatively, instead of forming a higher-order oligomer, FtsL could compete with the FtsB homo-dimer to form a FtsL/FtsB hetero-dimer. In either case, the formation of the heterologous complex and the folding of the periplasmic domains may be a determinant for making FtsB competent for binding to the periplasmic domain of FtsQ (28), which is required for their septal localization and the recruitment of the late proteins. Further biophysical studies on a FtsB/FtsL binary complex are required to address these important questions.

2.4 Materials and Methods

Vectors and strains

All oligonucleotides were purchased in desalted form Integrated DNA Technologies and used without purification. The expression vectors pccKAN, pccGpA-wt, and pccGpA-G83I, and *malE* deficient *Escherichia coli* strain MM39 were kindly provided by Dr. Donald M. Engelman (36). Genes encoding the transmembrane domain of FtsB and FtsL were cloned into the NheI-BamHI restriction sites of the pccKAN vector resulting in the following protein sequences: FtsB "...NRASLALTLLLLAILVWLQYSLWFGILIN..."; FtsL "...NRASFGKLPLCLFICIILTAVTVVTTAGILIN...". All mutagenesis was done with the QuikChange kit (Stratagene).

The periplasmic sequence of FtsB was obtained from the *E. coli* genome (K12 strain) by PCR using PfuUltra II Fusion DNA polymerases (Stratagene), and cloned into a pET31b vector containing the fusion protein Gp7, using a modified QuikChange protocol that includes the use of PfuUltra II Fusion DNA polymerase, 1 min annealing time, 2 min/kb extension time at 65 ˚C, 50 ng of template and 100–150 ng of the first round PCR product, in the presence of 4% DMSO (62). All constructs generated throughout the studies were sequence-verified over the entire ORF insert and at least 50 bp upstream and downstream of the ORF. The resulting plasmids containing Gp7-FtsB fusions were transformed into BL21-DE3 cells for overexpression and further analyses.

Expression of Chimeric Proteins in MM39 cells and MalE complementation assay

The TOXCAT constructs were transformed into MM39 cells. A freshly streaked colony was inoculated into 3 mL of LB broth containing 100 μg/mL ampicillin and grown overnight at 37 ˚C.

Overnight cultures were inoculated into 3 mL of LB broth at a ratio of 1:1000 and grown to an OD_{420} of approximately 1 at 37 ˚C (OD_{600} of 0.6) at 37 ˚C. After recording the optical density, 1 mL of cells were spun down for 10 min at 17000*g* and resuspended in 500 mL of sonication buffer (25 mM Tris-HCl, 2 mM EDTA, pH 8.0). Cells were lysed by probe sonication at medium power for 10 seconds over ice, and an aliquot of 50 μL was removed from each sample and stored in SDS-PAGE loading buffer for western blotting. The lysates were then cleared by centrifugation and the supernatant was kept on ice for chloramphenicol acetyltransferase (CAT) activity assay. To confirm for proper membrane insertion of the TOXCAT constructs, overnight cultures were plated on M9 minimal medium plates containing 0.4% maltose as the only carbon source and grown at 37 ˚C for 48 hours (36).

Chloramphenicol Acetyltransferase (CAT) spectrophotometric assay

CAT activity was measured as described (53, 63). 1 mL of buffer containing 0.1 mM acetyl coA, 0.4 mg/mL 5,5'-dithiobis-(2-nitrobenzoic acid), and 0.1 M Tris-HCl pH 7.8 was mixed with 40 μL of cleared cell lysates and the absorbance at 412 nm was measured for two minutes to establish basal activity rate. After addition of 40 μL of 2.5 mM chloramphenicol in 10% ethanol were added, the absorbance was measured for an additional two minutes to determine CAT activity. The basal CAT activity was subtracted and the value was normalized by the cell density measured as OD_{420}. All measurement were determined at least in duplicate and the experiments were repeated at least twice.

Quantification of expression by immunoblotting

Protein expression was confirmed by immunoblotting. The cell lysates (10 μL) were loaded onto a NuPAGE 4-12% Bis-Tris SDS-PAGE gel (Invitrogen) and then transferred to PVDF membranes (VWR) for 1 hour at 100 millivolts. Blots were blocked using 5% Bovine serum albumin (US

Biologicals) in TBS-Tween buffer (50 mM Tris, 150 mM NaCl, 0.05% Tween 20) for two hours at 4 ˚C, incubated with biotinylated anti-Maltose Binding Protein antibodies (Vector labs), followed by peroxidase-conjugated streptavidin (Jackson ImmunoResearch). Blots were developed with the Pierce ECL Western Blotting Substrate Kit and chemiluminescence was measured using an ImageQuant LAS 4000 (GE Healthsciences).

Expression of chimeric proteins in BL21-DE3 cells for E. coli overexpression and Ni-NTA purification

The Gp7-FtsB chimerae, with an added C-terminal six-His tag preceded by the recognition site for TEV protease, were expressed in *E. coli* BL21-DE3 cells using a modified pET31b vector. A single colony was grown at 37 ˚C in 50 mL overnight and then inoculated into 4L of LB broth. Cells were grown to an OD_{600} of 0.8-1.0 before addition of 1 mM IPTG to induce over-expression which was carried out for 18 hours at 18 ˚C. The cell pellets were washed and stored at -80 ˚C until purification. All Gp7 fusion proteins were purified using an identical protocol. Typically, 8-12 g of frozen cell pellets were mixed with 10 mL lysis buffer (50 mM NaCl, 5 mM β-mercaptoethanol, 0.5 mg/mL lysozyme, 50 mM HEPES pH 8.0, 1 mM phenylmethylsulfonyl fluoride) per gram of cell pellet and lysed by sonication. Lysates were cleared using centrifugation at 45000*g* for 30 min (JA 25.5 rotor). Cleared lysates were loaded onto 5 mL of Ni-NTA resin washed extensively with Buffer A (300 mM NaCl, 1 mM β-mercaptoethanol, 20 mM imidazole, 25 mM HEPES, pH 8.0), and eluted with Buffer B (same as Buffer A, but with 300 mM imidazole). The eluted fractions were mixed with TEV protease at a molar ratio of ~1:40 and dialyzed at 4 ˚C overnight against Buffer C (10 mM HEPES, 100 mM NaCl, 0.5 mM TCEP, 0.1 mM EDTA pH 8.0). The TEV protease was prepared as described (64). The dialysate was repurified on Ni-NTA, this time collecting fractions that elute during washes with lower

imidazole (Buffer A). The pure fractions were pooled and dialyzed against Buffer C again and concentrated to ~10 mg/mL using an Ultracel - 10K (Millipore), clarified by centrifugation at 5000 *g* and finally flash frozen as 30 µL droplets in liquid nitrogen and stored at -80 ˚C.

Circular dichroism (CD)

The purified Gp7-FtsB constructs were diluted to 0.2-0.4 mg/mL for CD analysis. CD measurements were carried out on an Aviv 202SF spectropolarimeter. Samples were measured in 1 mM Hepes pH 8, 10 mM NaCl, and 0.1 mM TCEP. The thermostability studies were performed under the same buffer conditions with a temperature ramp of 3 ˚C/min, and the ellipticity was monitored at 222 nm and 208 nm.

Crystallization of Gp7-FstB.

Gp7-FtsB was screened for initial crystallization conditions by vapor diffusion at 20 ˚C with a 144-condition sparse matrix screen developed in the Rayment laboratory. Crystals of Gp7-FtsB were grown by vapor diffusion at 20 ˚C from a 1:1 mixture of protein at 10 mg/mL with 100 mM Bis-Tris, 5 mM gamma-caprolactone, 2.1 M ammonium sulfate, 0.6 M malonate, 5% glycerol, pH 6.5. After one day hexagonal crystals measuring 0.1 x 0.1 x 0.5 mm were observed. The crystals were soaked in mother liquor for 24 hours subsequent to flash freezing in liquid nitrogen. Gp7-FtsB crystallized in the space group $P6_1$ with unit cell dimensions of a = 87.6 Å, b = 87.6 Å, and c = 185.1 Å where two Gp7-FtsB dimers were present in the asymmetric unit.

Data collection and structure determination for Gp7-FtsB.

X-ray data for Gp7-FtsB were collected at 100 ˚K on the Structural Biology Center beam line 19ID at the Advanced Photon Source in Argonne, IL. Diffraction data were integrated and scaled with

HKL3000 (65). Data collection statistics are given in supplementary Table S1. A molecular replacement solution was obtained using residues 2 – 48 of Gp7 (PDB entry 1NO4) (66) as a search model in the program Molrep (67). The electron density was improved with the program Parrot and the initial model was built using Buccaneer (68, 69). Final Models were generated with alternate cycles of manual model building and least-squares refinements using the programs Coot (70) and Refmac (71). Refinement statistics are presented in supplementary Table S1.

Computational modeling

The transmembrane oligomer of FtsB was modeled with the program *predictHelixOligomer* written in house using the MSL molecular modeling libraries (57). The program creates standard helices and performs a global rigid search altering the inter-helical separation, the crossing angle, the crossing point and the axial orientation of the helices. The backbone was kept rigid during the procedure while the side chains were optimized using a greedy trials method implemented in MSL (57, 72). Side chain mobility was modeled using the Energy-Based conformer library applied at the 90% level (73). The models were evaluated using a van der Waals function with CHARMM 22 parameters and the SCWRL hydrogen bond function implemented in MSL. The models were sorted by energy and all low-energy models were visually inspected to exclude any poorly packed solutions containing cavities. To impose the formation of an inter-helical hydrogen bond involving Gln 16, prior to the analysis the conformational space was pre-screened to exclude the region of space that were incompatible. This was performed on helices in which all amino acids were converted to Ala except Gln 16, Tyr 17 and Ser 18.

The computational model of the transmembrane domain and the coiled coil region were

connected together using fragments from the PDB database. To do this, protein fragments of the pattern *hhx*G*xx*G*xhh* (where *x* is any amino acid, and *h* is any amino acid in a helical conformation) were extracted from high resolution X-ray structures deposited in the PDB database with a resolution of 2 Å or better. The MSL program *connectWithFragments* takes these fragments and aligns the helical end residues with the corresponding residues in the coiled coil domain and then the modeled transmembrane domain. Only the N, C, CA and O atoms were considered for the alignment and the fragments with the lowest R.M.S.D. were selected. The side chains on the fragment were replaced with the one corresponding to the FtsB sequence and their conformation was optimized using a greedy trials method.

Figure 2.1

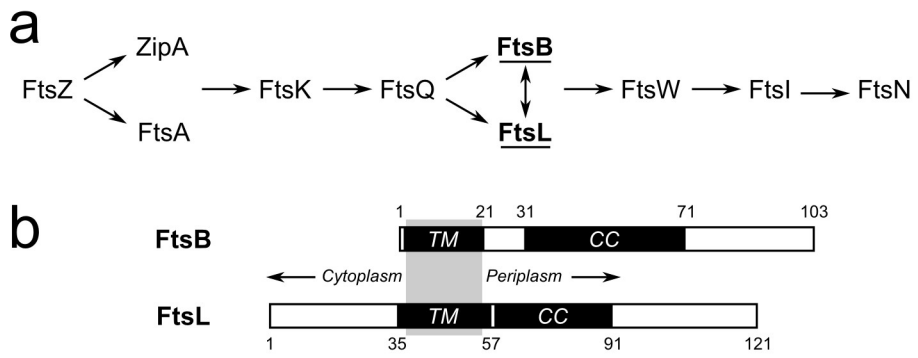

Figure 2.1 The recruitment hierarchy of the divisome and the predicted topology of FtsB and FtsL. a) In *E. coli* the recruitment of the divisome to the division site follows a strict hierarchical dependency (4). A functional FtsZ is required for the recruitment of FtsA and ZipA, which in turn are required for the recruitment of FtsK, and so on. FtsB and FtsL are co-dependent for their recruitment and both depend on FtsQ. b) FtsB and FtsL are short transmembrane proteins with a single transmembrane domain domain (*TM*) and a predicted juxta-membrane coiled coil region (*CC*). FtsL has also a short cytoplasmic N-terminal tail.

Figure 2.2

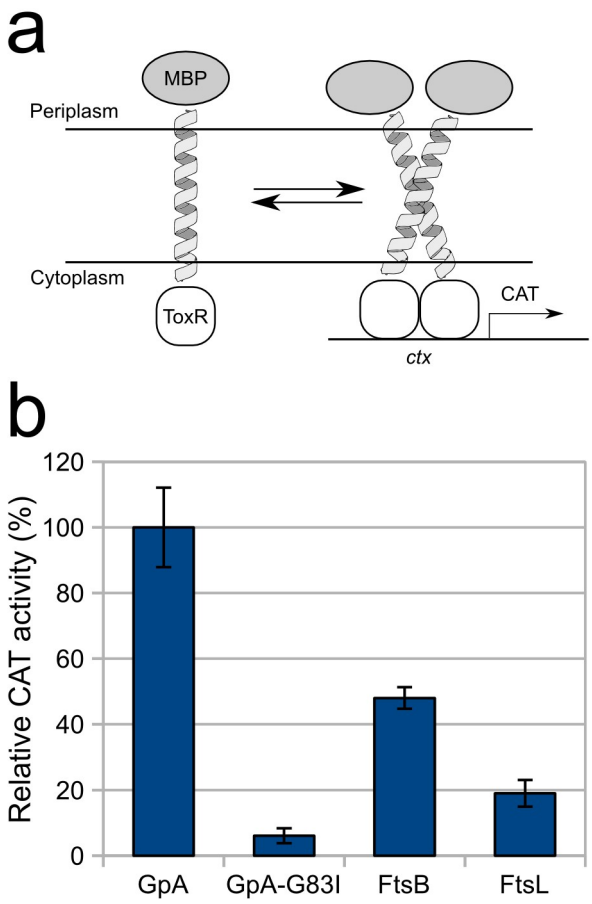

Figure 2.2 FtsB and FtsL self-associate in TOXCAT. a) TOXCAT is an *in vivo* assay based on a construct in which the transmembrane domain under investigation is fused to the ToxR transcriptional activator of *V. cholerae*. Transmembrane association results in the expression of a reporter gene in *E. coli* cells, which can be quantified. b) TOXCAT assay of FtsB and FtsL transmembrane domains. FtsB shows significant CAT activity, half of the activity of the strong transmembrane dimer of Glycophorin A (GpA). The activity of FtsL is low but above baseline, indicating a weak propensity to homo-oligomerize. The monomeric G83I mutant of GpA is used as a negative control.

Figure 2.3

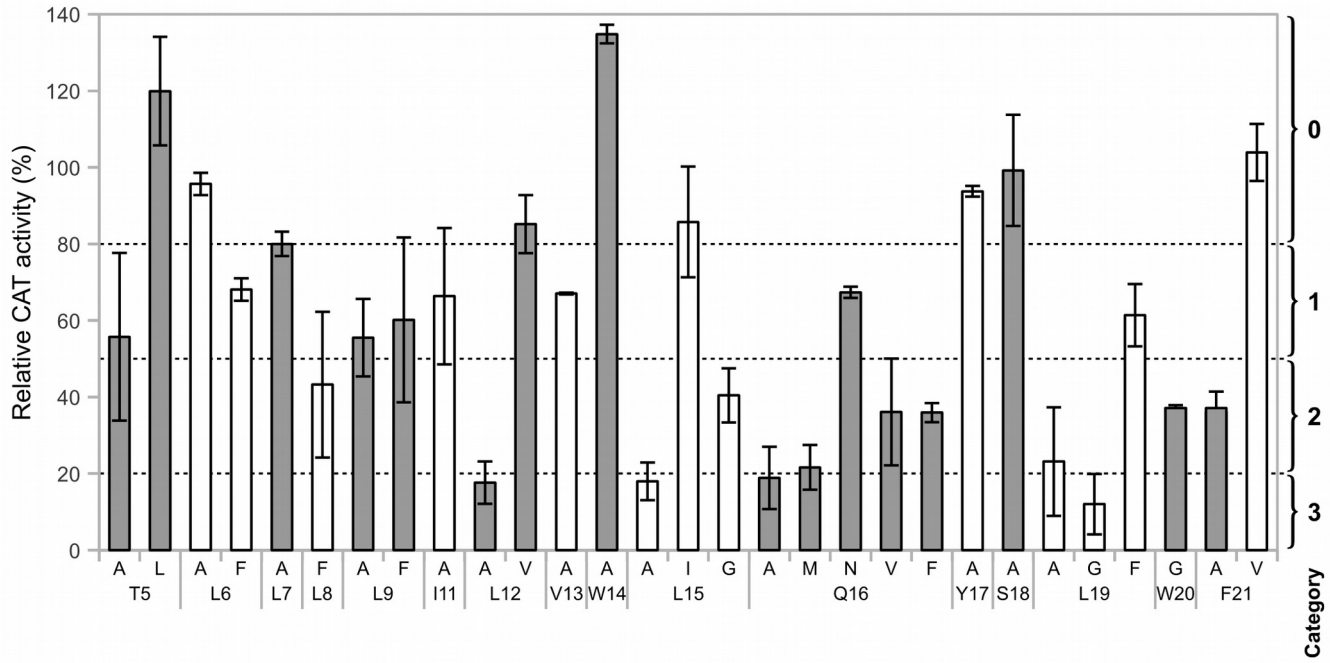

Figure 2.3 Mutagenesis of the transmembrane helix of FtsB. The figure shows a selection of 29 point mutations analyzed in TOXCAT. Each mutation has been categorized as non disruptive (0) or slightly (1), significantly (2) or strongly disruptive (3). The dashed lines represent the thresholds adopted for the categorization. The association of all 57 variants is summarized using the above scoring scheme in Fig. 4.

Figure 2.4

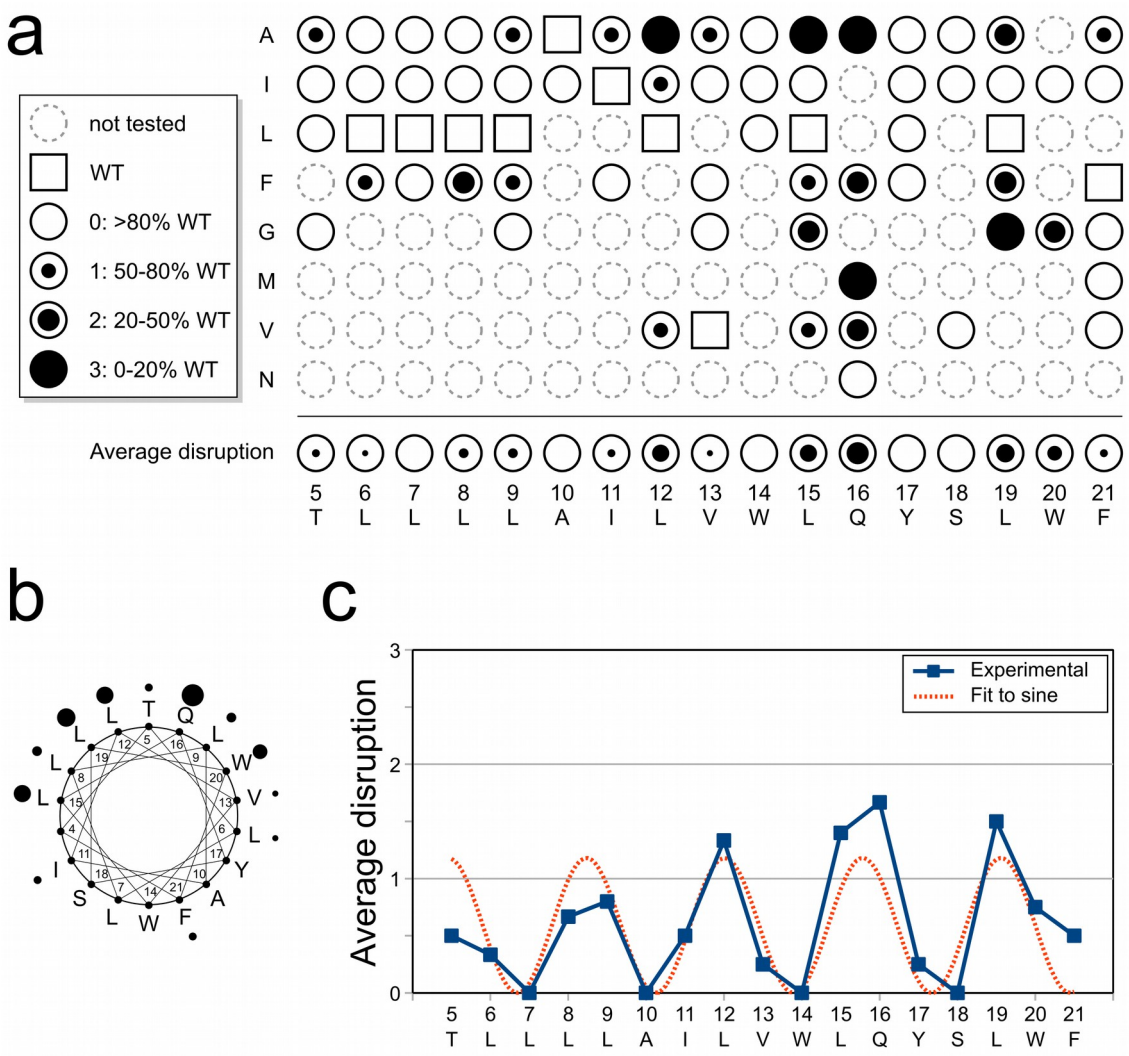

Figure 2.4 FtsB mutagenesis identifies a helical interface and an essential polar residue. a) The scheme summarize the effect of all mutations of FtsB-TM measured in TOXCAT. The data has been categorized as in the legend. An average disruption score is displayed at the bottom of the scheme. While Q16 is the most sensitive position, the introduction of an Asn side chain restores association almost entirely, indicating that a hydrogen bond is important for the association. b) Diagram mapping the average disruption score to a helical wheel. The disruption pattern clusters on one helical face

defined by positions T5, L6, L8, L9, L12, L15, Q16, L19 and W20. c) Fit of the average disruption index to a sine function. The estimated periodicity is approximately 3.5 amino acid per turn, which corresponds to a helical interaction with a left-handed crossing angle.

Figure 2.5

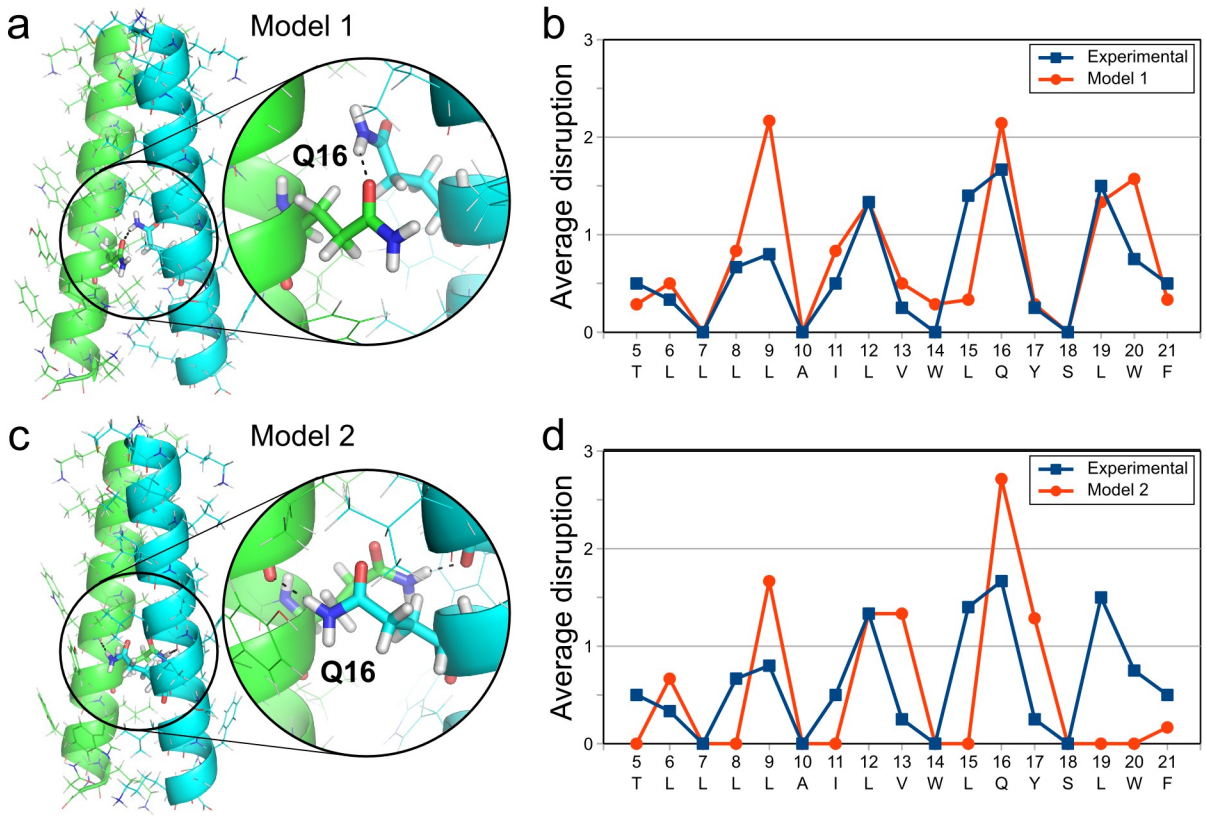

Figure 2.5 Molecular model of the FtsB transmembrane dimer. Modeling identified two well packed low-energy structures in which Gln 16 forms an inter-helical hydrogen bond (panels a and c). Model 1 and 2 are closely related (Cα RMSD of 1.5Å), with a left-handed crossing angle (25˚ and 20˚, respectively) and an inter-helical distance of 10.1Å. In Model 1 the side chains of Gln 16 interact with a non-symmetrical hydrogen bond. The helices of Model 2 are rotated axially of about 60˚ with respect to Model 1. The side chains of Gln 16 interact symmetically with the carbonyl oxygen of Val 13. Panels b and d compare the average disruption index for the computational mutagenesis applied to the models to the average disruption observed experimentally. Model 1 shows an excellent agreement with the experimental data, which is better than Model 2, particularly in the C-terminal side of the

transmembrane domain.

Figure 2.6

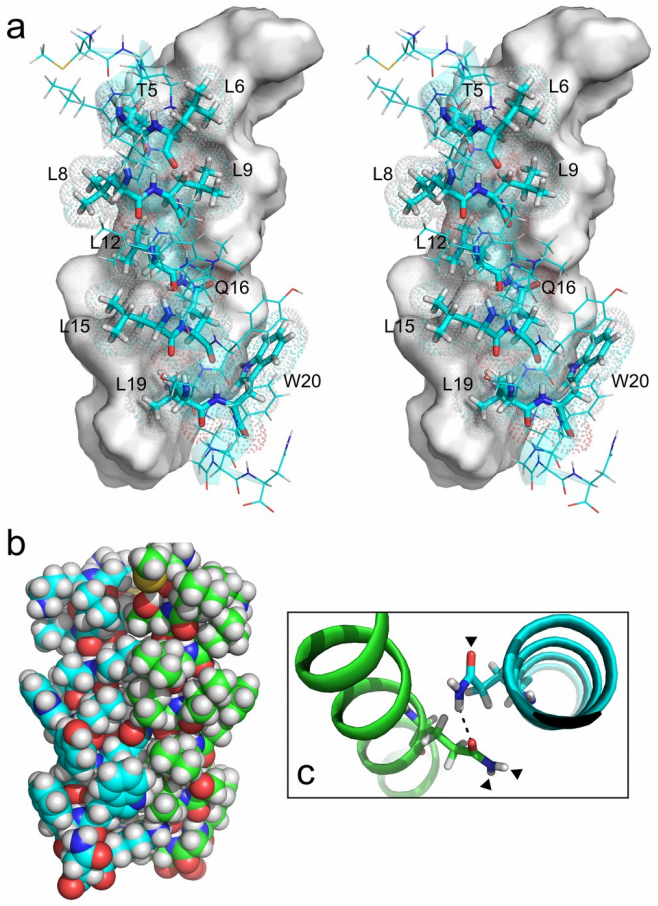

Figure 2.6 Computational model of FtsB-TM (Model 1). *a*) Stereo representation. Chain A is represented as a gray surface. The interacting positions on the opposite chain are shown in sticks and a dotted surface to highlight the arrangement and packing of the side chains. *b*) Sphere representation highlights complementary packing. The two chains are colored in green and cyan. *c*) Cross-section of the dimer. The black arrows highlight unsatisfied hydrogen bonding donor and acceptors of Gln 16 that are solvent accessible. These groups could be potentially available to interact with an hydroxyl group from one of the several Thr present in the transmembrane domain of FtsL (LLPLCLFICIIL**T**AV**T**VV**TT**A).

Figure 2.7

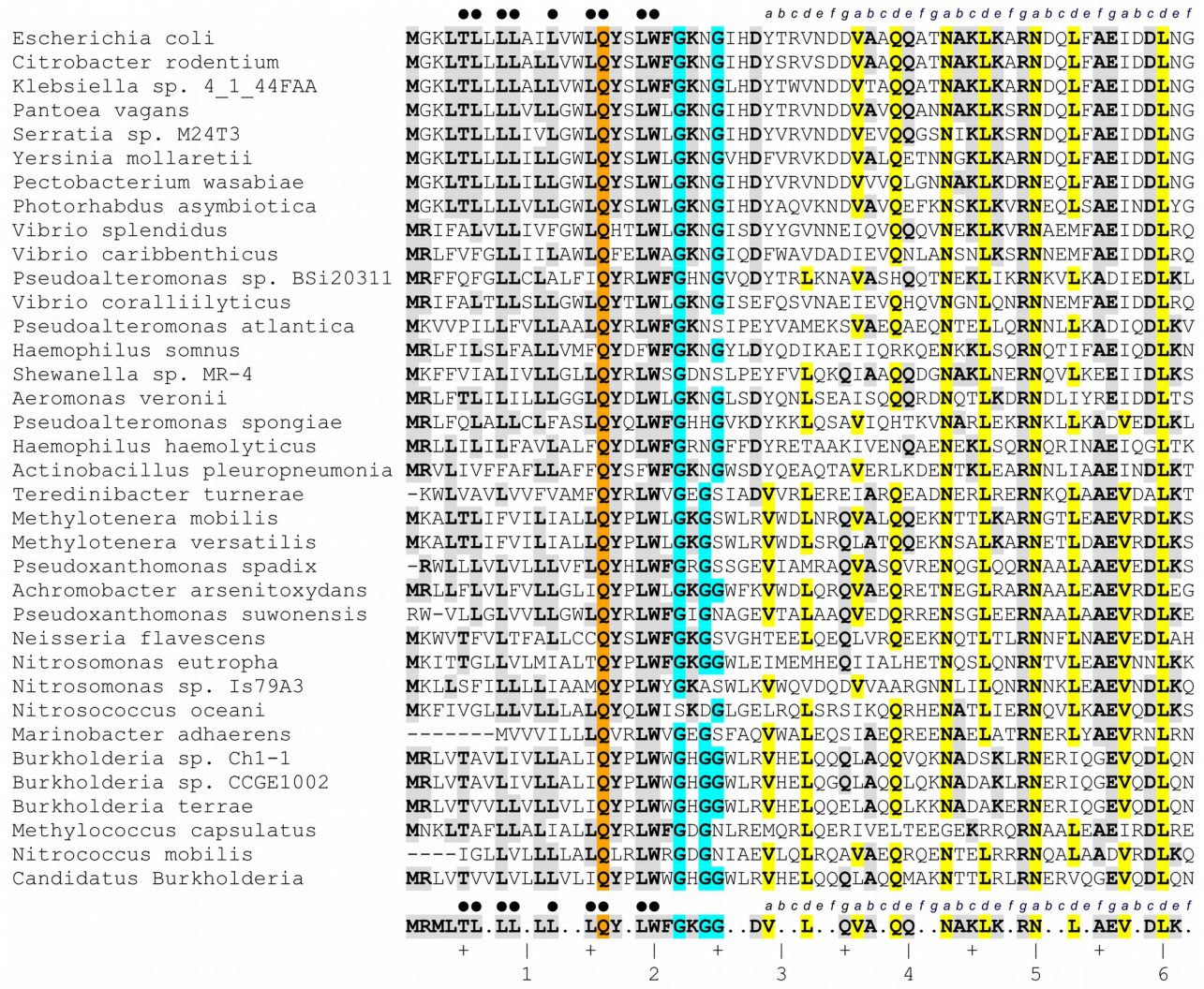

Figure 2.7 Sequence alignment of FtsB indicates that the interfacial positions are evolutionary conserved. Partial representation of a sequence alignment of FtsB. The complete alignment is provided in supplementary Figure S2.2. FtsB is relatively well conserved among a diverse group or beta and gamma proteobacteria. The consensus sequence is shaded and printed at the bottom of the alignment. The positions that are involved at the FtsB dimer interface (Fig. 5) are marked with a full circle ( ). A remarkable match between conservation and the interfacial positions is evident. In

particular, positions Q16 (highlighted in orange), L20 and W21 are almost invariable. The heptad repeat designation (positions *a* to *g*) of the coiled coil region is also given, and the conserved amino acid at the interfacial *a* and *d* positions are highlighted in yellow. In cyan are highlighted three conserved Gly amino acids (positions 22, 24 and 25) that are likely to confer flexibility to the linker region between the transmembrane domain and the coiled coil region.

Figure 2.8

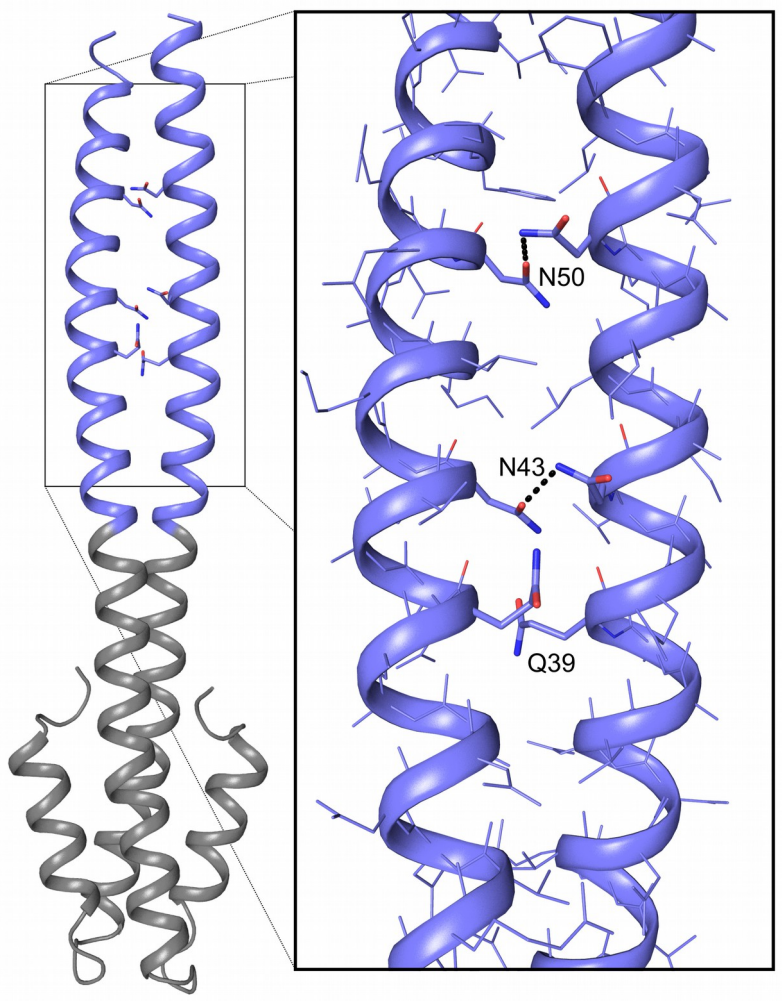

Figure 2.8 X-ray crystal structure of a Gp7-FtsB$_{CC}$ fusion protein. Ribbon representation of one of the two dimeric molecules in the asymmetric unit. This molecule forms a straight canonical coiled coil. The second molecule in the asymmetric unit exhibits a slight bend, possibly as a result of crystal packing (supplementary Figure S2.3). The N-terminal Gp7 unit which replaces the transmembrane domain is highlighted in gray, and the FtsB sequence in blue. The inset highlights a number of polar amino acids that are present at the interface in "*d*" (Q39) and "*a*" (N43 and N50) positions.

Figure 2.9

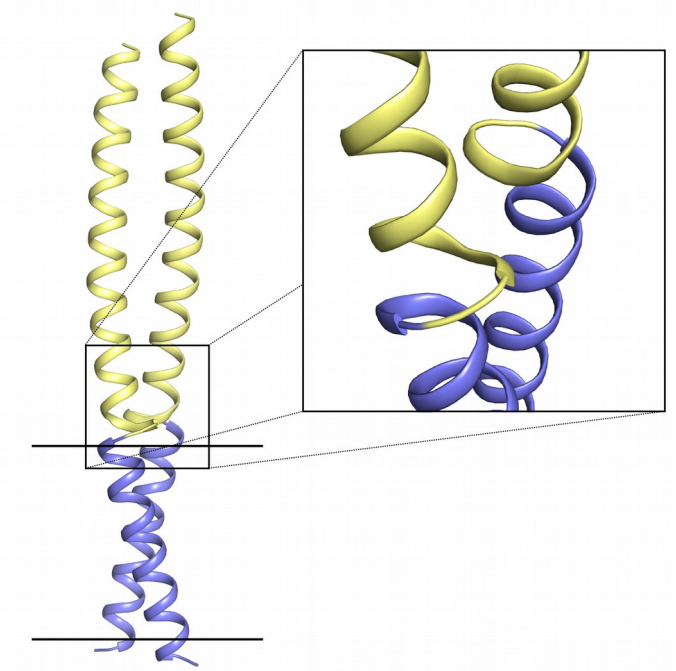

Figure 2.9 A theoretical model of a FtsB dimer that encompasses the transmembrane and coiled coil domains. The crystal structure of the coiled coil region of FtsB (yellow) and the computational Model 1 of the transmembrane domain (blue) were stitched together using a fragment based approach (see **Methods**). The resulting theoretical model includes a hinge between the coiled coil and the transmembrane helix where the helix unfolds (highlighted in the box). This hinge corresponds to conserved a Gly rich region in the sequence alignment, suggesting that a flexible connection may be functionally important.

Figure 2.10

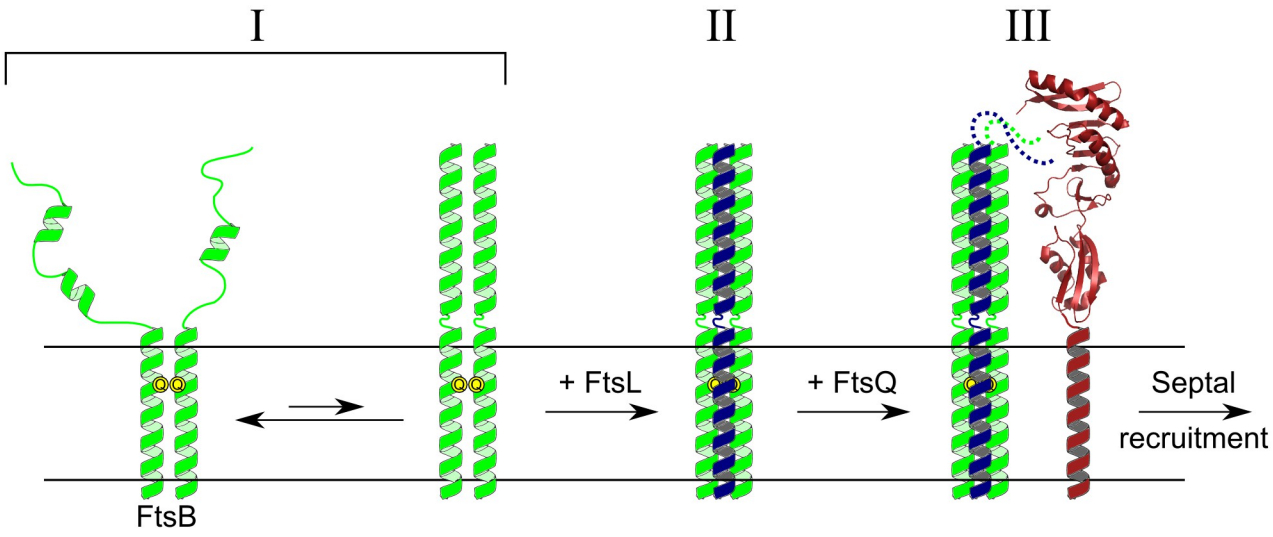

Figure 2.10 A functional hypothesis for the formation of FtsB/FtsL complex and its recruitment to the divisome. The transmembrane domain of FtsB self-associates in *E. coli* membranes, driven by an inter-helical hydrogen bond (Gln 16, represented by a yellow circle) but the coiled coil region is likely to be marginally stable or unstable (I). This finding rises the hypothesis is that the interaction with FtsL is required to stabilize the periplasmic domain. It is likely that FtsL (blue) laterally associates with a pre-existing FtsB dimer (II). Alternatively, FtsL may compete with the self-association of FtsB to form an FtsB/FtsL hetero-dimer (not represented). Once the periplasmic domain is folded, the C-terminal tails of the FtsB/FtsL complex (dotted lines) would bind to FtsQ (red) and the proteins would subsequently be recruited to the division septum (III).

2.5 Supplementary Information

Table S2.1. Data collection and refinement statistics

Wavelength (Å)	0.9791
Space group	$P6_1$
Cell dimensions (Å)	
a, b, c (Å)	87.6, 87.6, 185.1
α β γ (°)	90.0, 90.0, 120.0
Resolution (Å)[a]	50 - 2.3 (2.34-2.3)
R_{sym} (%)[a]	9.5% (63.1%)
<I>/<σ> (I)[a]	28.7 (5.0)
Completeness (%)[a]	100.0 (100.0)
Redundancy[a]	11.1 (11.1)
Refinement	
Resolution (Å)	30 - 2.3
No. of reflections (|F|>0σ)	33598
R_{factor} / R_{free} [b]	21.9 / 25.6
Total no. of protein atoms	2613
Water molecules (no.)	163
Average B Factors (Å^2)	
Protein	41.41
Water	35.9
RMSD	
Bond Lenghts (Å)	0.009
Bond Angles (°)	1.029
Ramachandran (%)	
Within favored	99.37
Within allowed	0.63
Outliers	0

[a]Data in parentheses represent the highest resolution shell.

[b]$R_{factor} = \Sigma \mid F_{obs} - F_{calc} \mid / \Sigma \mid F_{obs} \mid$

Where R_{free} refers to the R_{factor} for 5% of the data that were excluded for the refinement.

Figure S2.1

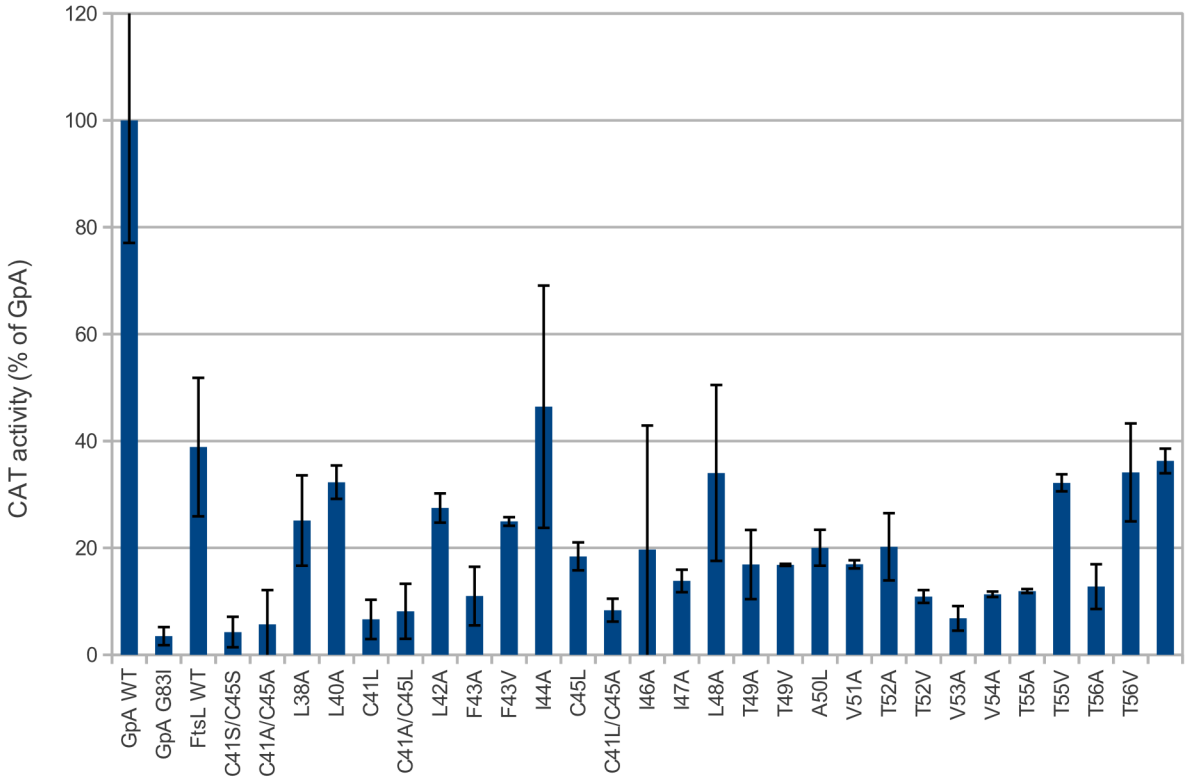

Figure S2.1 Mutagenesis of the transmembrane helix of FtsL. The figure shows the single and double mutations analyzed in TOXCAT. The CAT activity is reported as percentage of the transmembrane domain of Glycophorin A (GpA). A monomeric negative control (GpA, G83I mutation) is also shown.

Figure S2.2

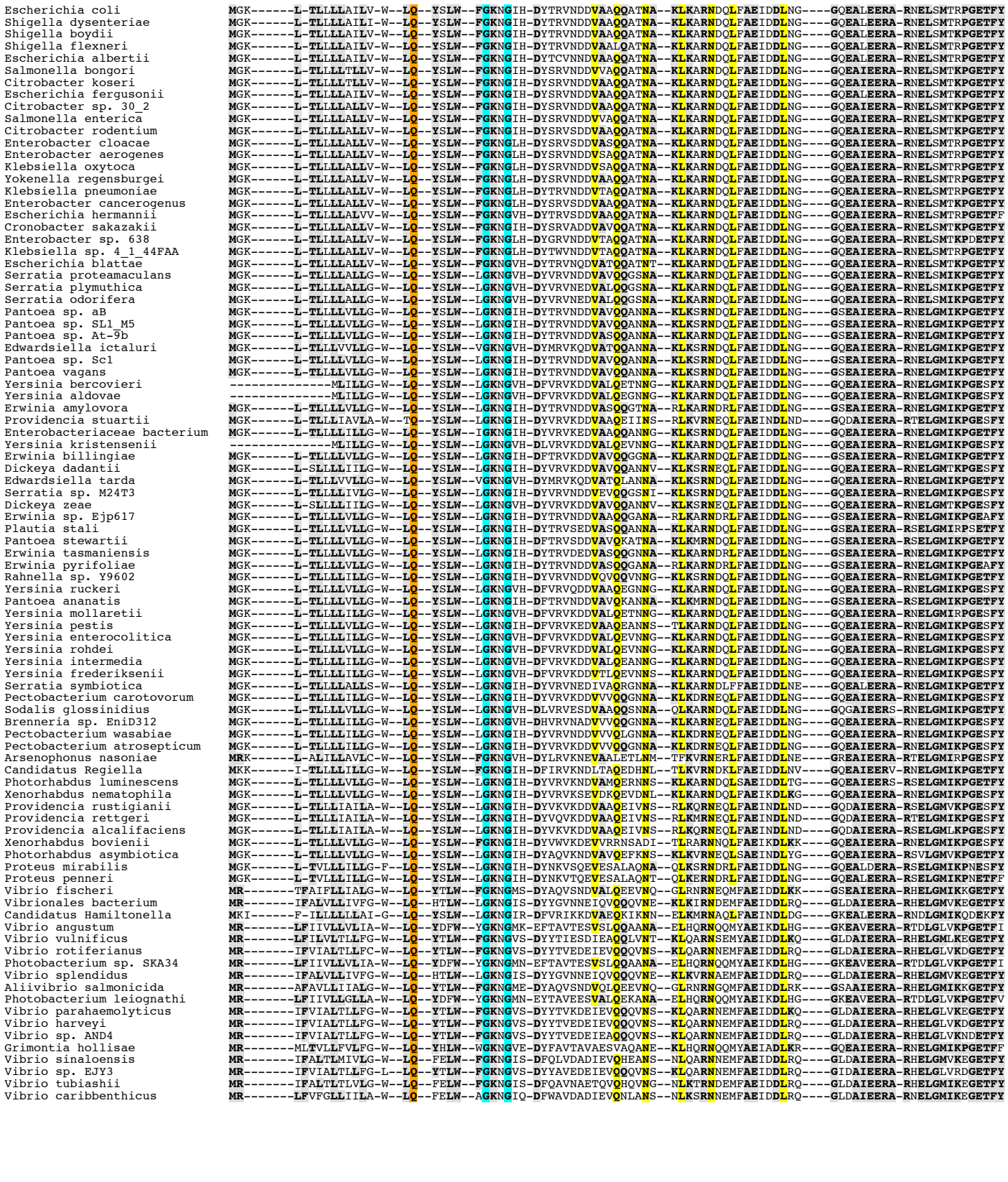
Escherichia coli
Shigella dysenteriae
Shigella boydii
Shigella flexneri
Escherichia albertii
Salmonella bongori
Citrobacter koseri
Escherichia fergusonii
Citrobacter sp. 30_2
Salmonella enterica
Citrobacter rodentium
Enterobacter cloacae
Enterobacter aerogenes
Klebsiella oxytoca
Yokenella regensburgei
Klebsiella pneumoniae
Enterobacter cancerogenus
Escherichia hermannii
Cronobacter sakazakii
Enterobacter sp. 638
Klebsiella sp. 4_1_44FAA
Escherichia blattae
Serratia proteamaculans
Serratia plymuthica
Serratia odorifera
Pantoea sp. aB
Pantoea sp. SL1_M5
Pantoea sp. At-9b
Edwardsiella ictaluri
Pantoea sp. Sc1
Pantoea vagans
Yersinia bercovieri
Yersinia aldovae
Erwinia amylovora
Providencia stuartii
Enterobacteriaceae bacterium
Yersinia kristensenii
Erwinia billingiae
Dickeya dadantii
Edwardsiella tarda
Serratia sp. M24T3
Dickeya zeae
Erwinia sp. Ejp617
Plautia stali
Pantoea stewartii
Erwinia tasmaniensis
Erwinia pyrifoliae
Rahnella sp. Y9602
Yersinia ruckeri
Pantoea ananatis
Yersinia mollaretii
Yersinia pestis
Yersinia enterocolitica
Yersinia rohdei
Yersinia intermedia
Yersinia frederiksenii
Serratia symbiotica
Pectobacterium carotovorum
Sodalis glossinidius
Brenneria sp. EniD312
Pectobacterium wasabiae
Pectobacterium atrosepticum
Arsenophonus nasoniae
Candidatus Regiella
Photorhabdus luminescens
Xenorhabdus nematophila
Providencia rustigianii
Providencia rettgeri
Providencia alcalifaciens
Xenorhabdus bovienii
Photorhabdus asymbiotica
Proteus mirabilis
Proteus penneri
Vibrio fischeri
Vibrionales bacterium
Candidatus Hamiltonella
Vibrio angustum
Vibrio vulnificus
Vibrio rotiferianus
Photobacterium sp. SKA34
Vibrio splendidus
Aliivibrio salmonicida
Photobacterium leiognathi
Vibrio parahaemolyticus
Vibrio harveyi
Vibrio sp. AND4
Grimontia hollisae
Vibrio sinaloensis
Vibrio sp. EJY3
Vibrio tubiashii
Vibrio caribbenthicus

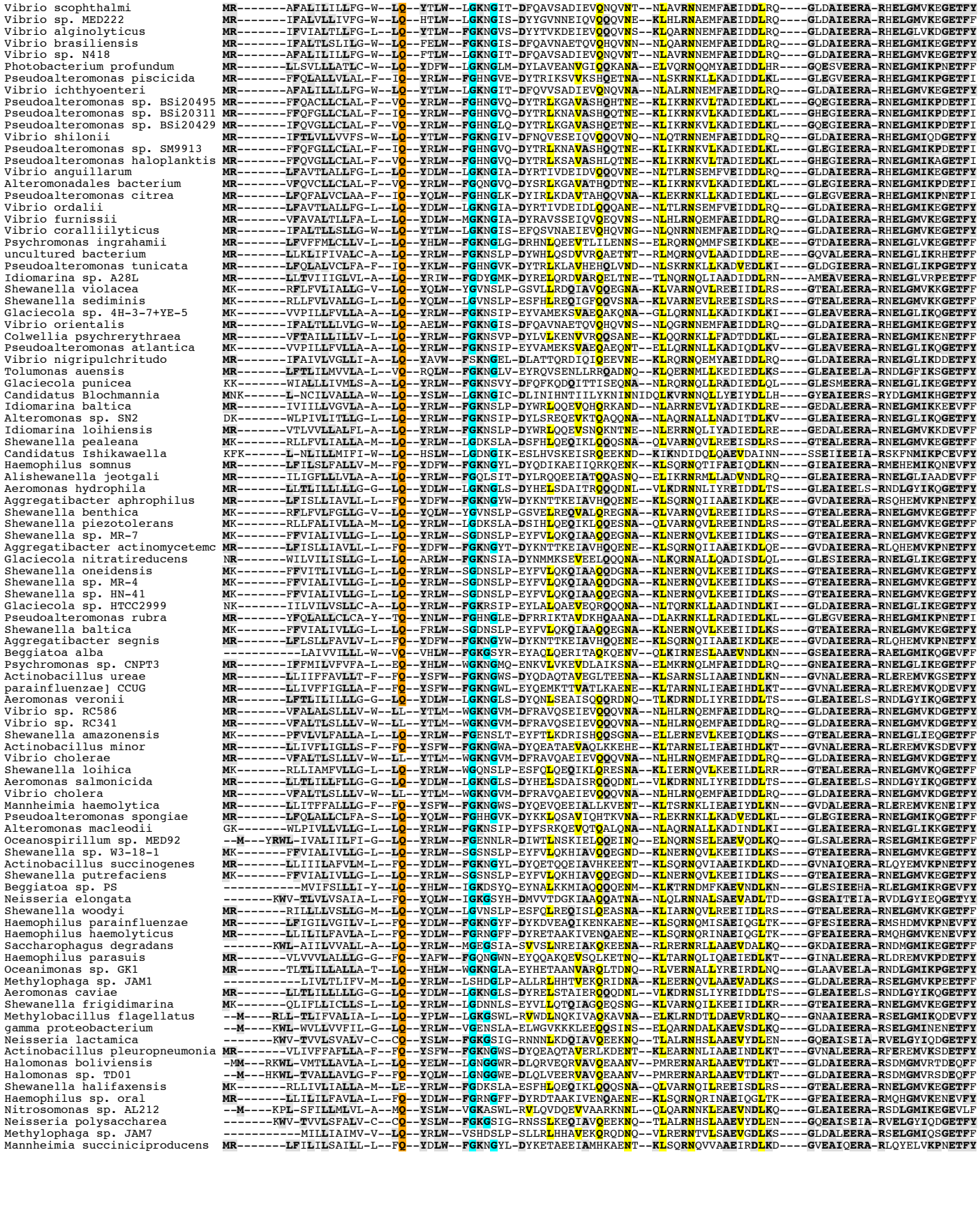
Vibrio scophthalmi
Vibrio sp. MED222
Vibrio alginolyticus
Vibrio brasiliensis
Vibrio sp. N418
Photobacterium profundum
Pseudoalteromonas piscicida
Vibrio ichthyoenteri
Pseudoalteromonas sp. BSi20495
Pseudoalteromonas sp. BSi20311
Pseudoalteromonas sp. BSi20429
Vibrio shilonii
Pseudoalteromonas sp. SM9913
Pseudoalteromonas haloplanktis
Vibrio anguillarum
Alteromonadales bacterium
Pseudoalteromonas citrea
Vibrio ordalii
Vibrio furnissii
Vibrio coralliilyticus
Psychromonas ingrahamii
uncultured bacterium
Pseudoalteromonas tunicata
Idiomarina sp. A28L
Shewanella violacea
Shewanella sediminis
Glaciecola sp. 4H-3-7+YE-5
Vibrio orientalis
Colwellia psychrerythraea
Pseudoalteromonas atlantica
Vibrio nigripulchritudo
Tolumonas auensis
Glaciecola punicea
Candidatus Blochmannia
Idiomarina baltica
Alteromonas sp. SN2
Idiomarina loihiensis
Shewanella pealeana
Candidatus Ishikawaella
Haemophilus somnus
Alishewanella jeotgali
Aeromonas hydrophila
Aggregatibacter aphrophilus
Shewanella benthica
Shewanella piezotolerans
Shewanella sp. MR-7
Aggregatibacter actinomycetemc
Glaciecola nitratireducens
Shewanella oneidensis
Shewanella sp. MR-4
Shewanella sp. HN-41
Glaciecola sp. HTCC2999
Pseudoalteromonas rubra
Shewanella baltica
Aggregatibacter segnis
Beggiatoa alba
Psychromonas sp. CNPT3
Actinobacillus ureae
parainfluenzae] CCUG
Aeromonas veronii
Vibrio sp. RC586
Vibrio sp. RC341
Shewanella amazonensis
Actinobacillus minor
Vibrio cholerae
Shewanella loihica
Aeromonas salmonicida
Vibrio cholera
Mannheimia haemolytica
Pseudoalteromonas spongiae
Alteromonas macleodii
Oceanospirillum sp. MED92
Shewanella sp. W3-18-1
Actinobacillus succinogenes
Shewanella putrefaciens
Beggiatoa sp. PS
Neisseria elongata
Shewanella woodyi
Haemophilus parainfluenzae
Haemophilus haemolyticus
Saccharophagus degradans
Haemophilus parasuis
Oceanimonas sp. GK1
Methylophaga sp. JAM1
Aeromonas caviae
Shewanella frigidimarina
Methylobacillus flagellatus
gamma proteobacterium
Neisseria lactamica
Actinobacillus pleuropneumonia
Halomonas boliviensis
Halomonas sp. TD01
Shewanella halifaxensis
Haemophilus sp. oral
Nitrosomonas sp. AL212
Neisseria polysaccharea
Methylophaga sp. JAM7
Mannheimia succiniciproducens

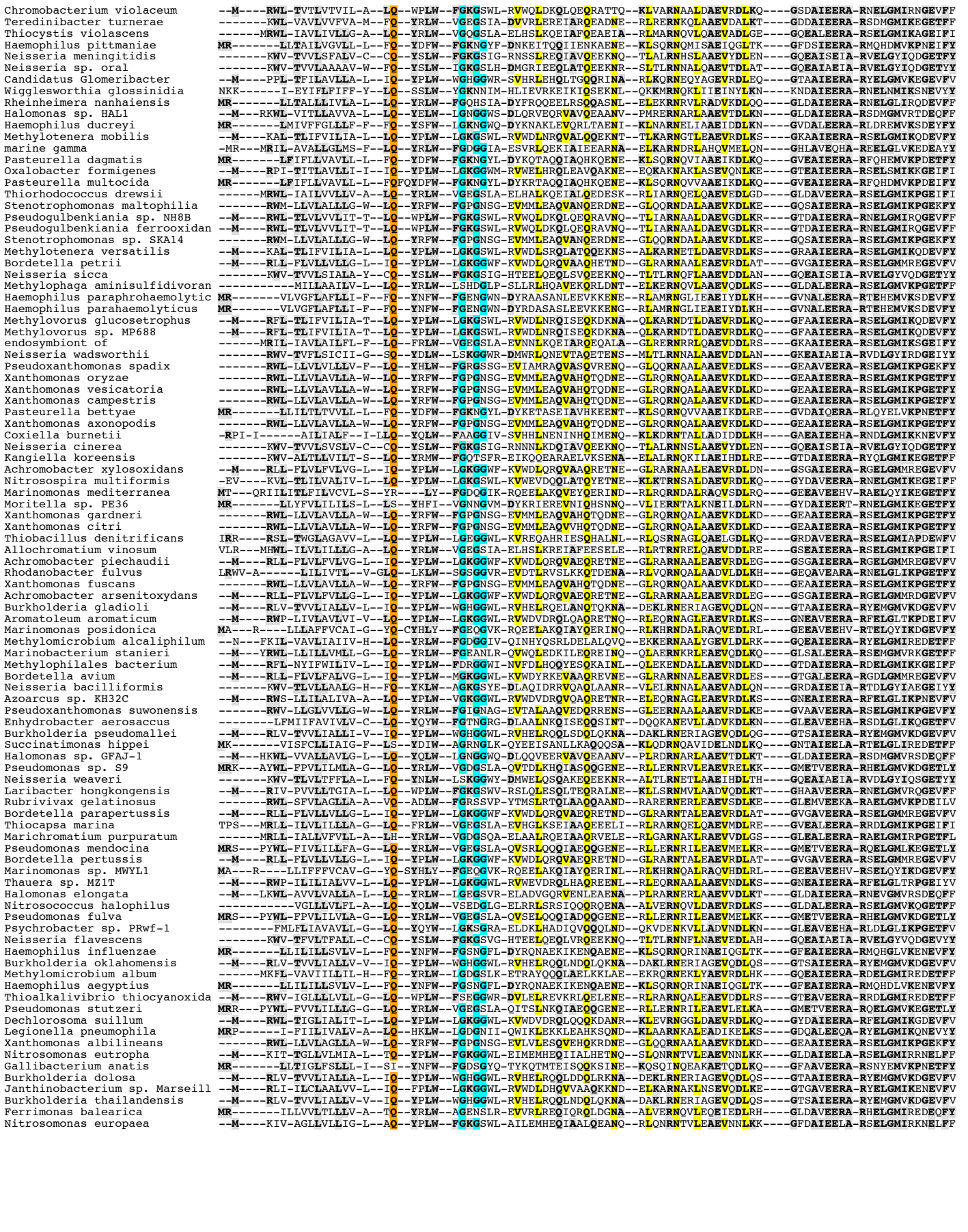
Chromobacterium violaceum
Teredinibacter turnerae
Thiocystis violascens
Haemophilus pittmaniae
Neisseria meningitidis
Neisseria sp. oral
Candidatus Glomeribacter
Wigglesworthia glossinidia
Rheinheimera nanhaiensis
Halomonas sp. HAL1
Haemophilus ducreyi
Methylotenera mobilis
marine gamma
Pasteurella dagmatis
Oxalobacter formigenes
Pasteurella multocida
Thiorhodococcus drewsii
Stenotrophomonas maltophilia
Pseudogulbenkiania sp. NH8B
Pseudogulbenkiania ferrooxidan
Stenotrophomonas sp. SKA14
Methylotenera versatilis
Bordetella petrii
Neisseria sicca
Methylophaga aminisulfidivoran
Haemophilus paraphrohaemolytic
Haemophilus parahaemolyticus
Methylovorus glucosetrophus
Methylovorus sp. MP688
endosymbiont of
Neisseria wadsworthii
Pseudoxanthomonas spadix
Xanthomonas oryzae
Xanthomonas vesicatoria
Xanthomonas campestris
Pasteurella bettyae
Xanthomonas axonopodis
Coxiella burnetii
Neisseria cinerea
Kangiella koreensis
Achromobacter xylosoxidans
Nitrosospira multiformis
Marinomonas mediterranea
Moritella sp. PE36
Xanthomonas gardneri
Xanthomonas citri
Thiobacillus denitrificans
Allochromatium vinosum
Achromobacter piechaudii
Rhodanobacter fulvus
Xanthomonas fuscans
Achromobacter arsenitoxydans
Burkholderia gladioli
Aromatoleum aromaticum
Marinomonas posidonica
Methylomicrobium alcaliphilum
Marinobacterium stanieri
Methylophilales bacterium
Bordetella avium
Neisseria bacilliformis
Azoarcus sp. KH32C
Pseudoxanthomonas suwonensis
Enhydrobacter aerosaccus
Burkholderia pseudomallei
Succinatimonas hippei
Halomonas sp. GFAJ-1
Pseudomonas sp. S9
Neisseria weaveri
Laribacter hongkongensis
Rubrivivax gelatinosus
Bordetella parapertussis
Thiocapsa marina
Marichromatium purpuratum
Pseudomonas mendocina
Bordetella pertussis
Marinomonas sp. MWYL1
Thauera sp. MZ1T
Halomonas elongata
Nitrosococcus halophilus
Pseudomonas fulva
Psychrobacter sp. PRwf-1
Neisseria flavescens
Haemophilus influenzae
Burkholderia oklahomensis
Methylomicrobium album
Haemophilus aegyptius
Thioalkalivibrio thiocyanoxida
Pseudomonas stutzeri
Dechlorosoma suillum
Legionella pneumophila
Xanthomonas albilineans
Nitrosomonas eutropha
Gallibacterium anatis
Burkholderia dolosa
Janthinobacterium sp. Marseill
Burkholderia thailandensis
Ferrimonas balearica
Nitrosomonas europaea

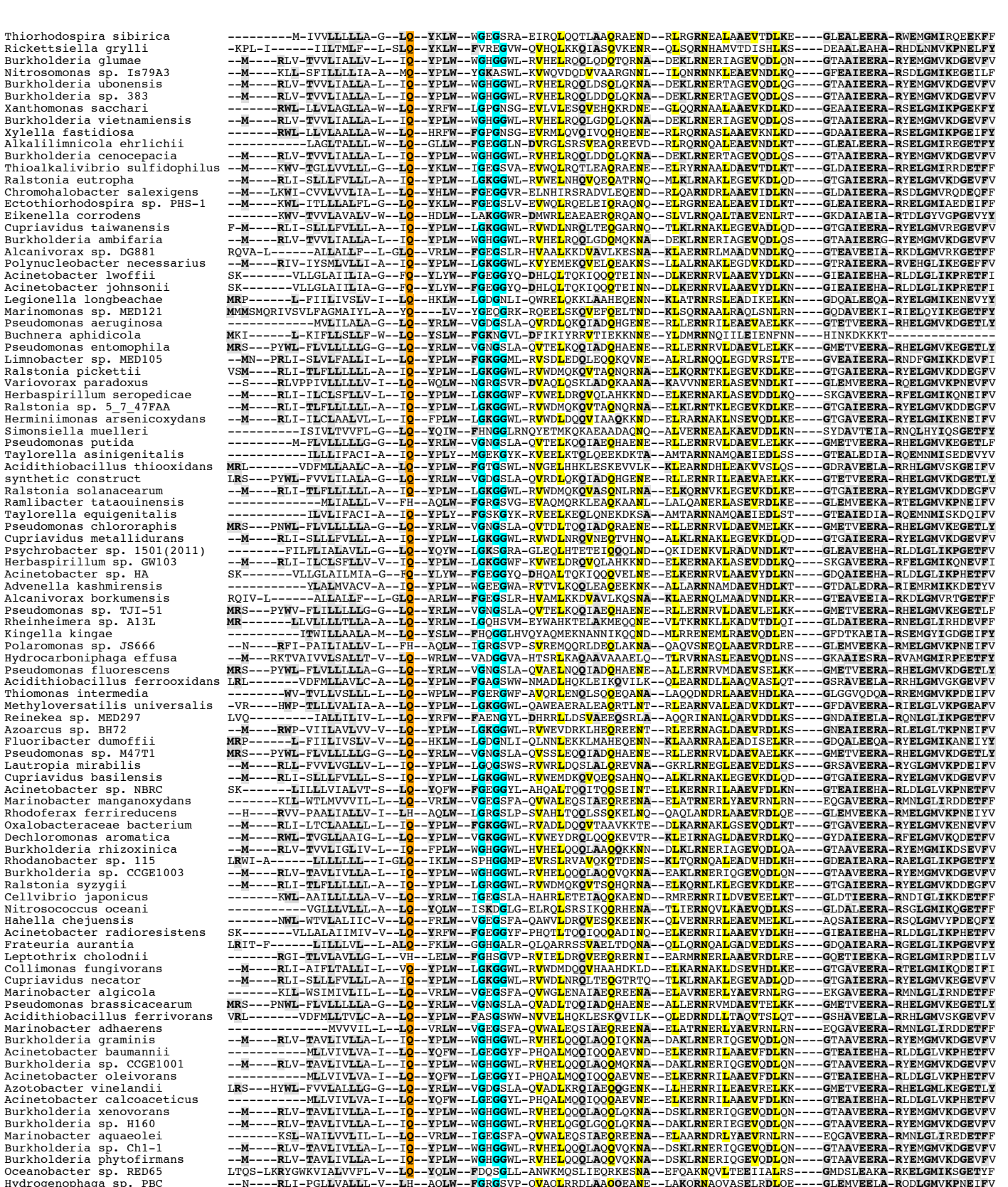
Thiorhodospira sibirica
Rickettsiella grylli
Burkholderia glumae
Nitrosomonas sp. Is79A3
Burkholderia ubonensis
Burkholderia sp. 383
Xanthomonas sacchari
Burkholderia vietnamiensis
Xylella fastidiosa
Alkalilimnicola ehrlichii
Burkholderia cenocepacia
Thioalkalivibrio sulfidophilus
Ralstonia eutropha
Chromohalobacter salexigens
Ectothiorhodospira sp. PHS-1
Eikenella corrodens
Cupriavidus taiwanensis
Burkholderia ambifaria
Alcanivorax sp. DG881
Polynucleobacter necessarius
Acinetobacter lwoffii
Acinetobacter johnsonii
Legionella longbeachae
Marinomonas sp. MED121
Pseudomonas aeruginosa
Buchnera aphidicola
Pseudomonas entomophila
Limnobacter sp. MED105
Ralstonia pickettii
Variovorax paradoxus
Herbaspirillum seropedicae
Ralstonia sp. 5_7_47FAA
Herminiimonas arsenicoxydans
Simonsiella muelleri
Pseudomonas putida
Taylorella asinigenitalis
Acidithiobacillus thiooxidans
synthetic construct
Ralstonia solanacearum
Ramlibacter tataouinensis
Taylorella equigenitalis
Pseudomonas chlororaphis
Cupriavidus metallidurans
Psychrobacter sp. 1501(2011)
Herbaspirillum sp. GW103
Acinetobacter sp. HA
Advenella kashmirensis
Alcanivorax borkumensis
Pseudomonas sp. TJI-51
Rheinheimera sp. A13L
Kingella kingae
Polaromonas sp. JS666
Hydrocarboniphaga effusa
Pseudomonas fluorescens
Acidithiobacillus ferrooxidans
Thiomonas intermedia
Methyloversatilis universalis
Reinekea sp. MED297
Azoarcus sp. BH72
Fluoribacter dumoffii
Pseudomonas sp. M47T1
Lautropia mirabilis
Cupriavidus basilensis
Acinetobacter sp. NBRC
Marinobacter manganoxydans
Rhodoferax ferrireducens
Oxalobacteraceae bacterium
Dechloromonas aromatica
Burkholderia rhizoxinica
Rhodanobacter sp. 115
Burkholderia sp. CCGE1003
Ralstonia syzygii
Cellvibrio japonicus
Nitrosococcus oceani
Hahella chejuensis
Acinetobacter radioresistens
Frateuria aurantia
Leptothrix cholodnii
Collimonas fungivorans
Cupriavidus necator
Marinobacter algicola
Pseudomonas brassicacearum
Acidithiobacillus ferrivorans
Marinobacter adhaerens
Burkholderia graminis
Acinetobacter baumannii
Burkholderia sp. CCGE1001
Acinetobacter oleivorans
Azotobacter vinelandii
Acinetobacter calcoaceticus
Burkholderia xenovorans
Burkholderia sp. H160
Marinobacter aquaeolei
Burkholderia sp. Ch1-1
Burkholderia phytofirmans
Oceanobacter sp. RED65
Hydrogenophaga sp. PBC
Acinetobacter junii

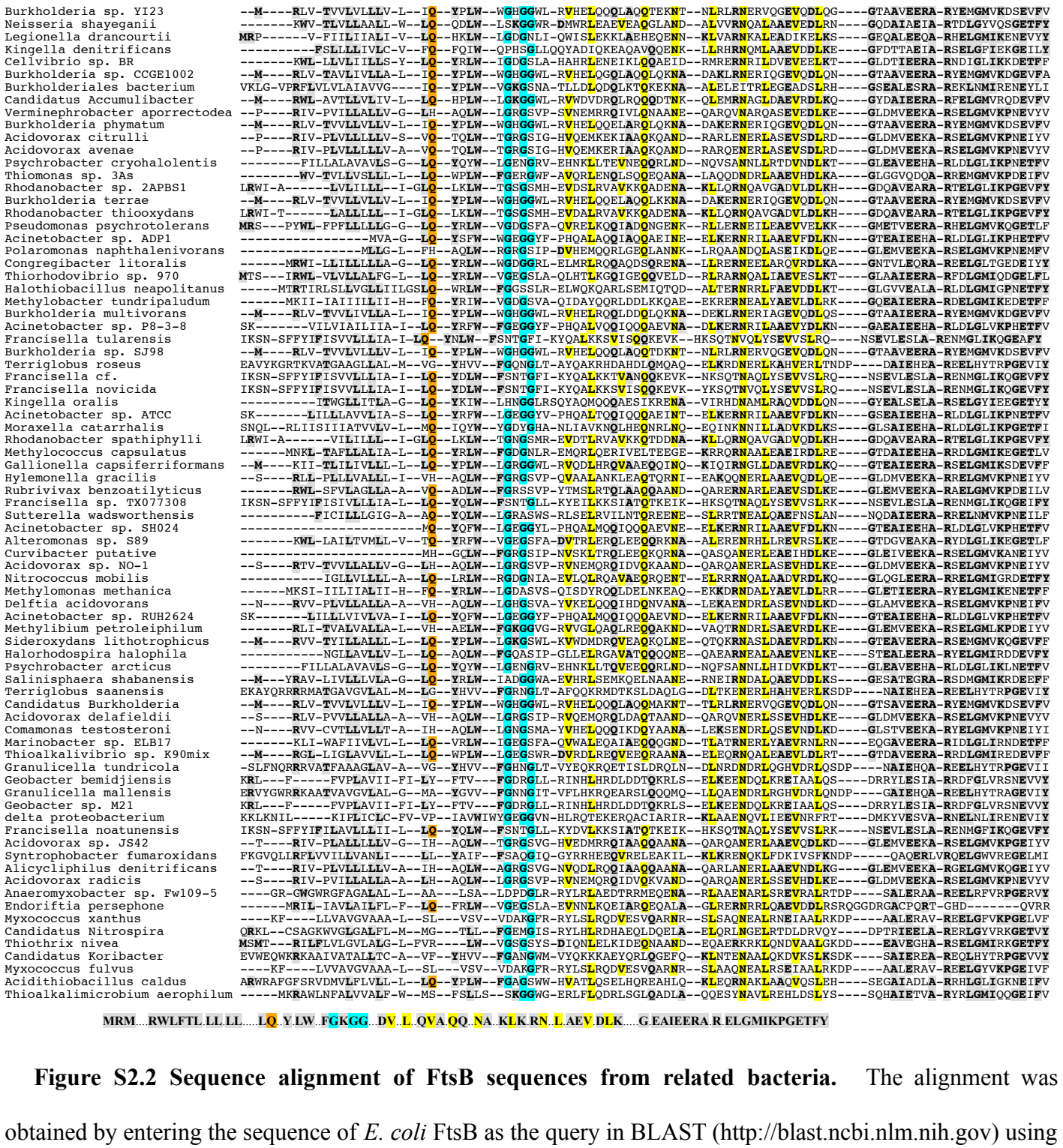

Figure S2.2 Sequence alignment of FtsB sequences from related bacteria. The alignment was obtained by entering the sequence of *E. coli* FtsB as the query in BLAST (http://blast.ncbi.nlm.nih.gov) using the blastp algorithm with default settings. The resulting 464 sequences were aligned with the multiple

alignment facility in BLAST (COBALT). The amino acids that are present in at least 30% of sequence at each position are in bold and shaded. These amino acids are also highlighted in the consensus sequence at the bottom of the alignment. The critical Gln 16 is highlighted in orange. The Gly amino acids in the linker region (positions 22, 24 and 25) are highlighted in cyan. The conserved amino acids at the interfacial *a* and *d* positions of the coiled coil region are highlighted in yellow.

Figure S2.3

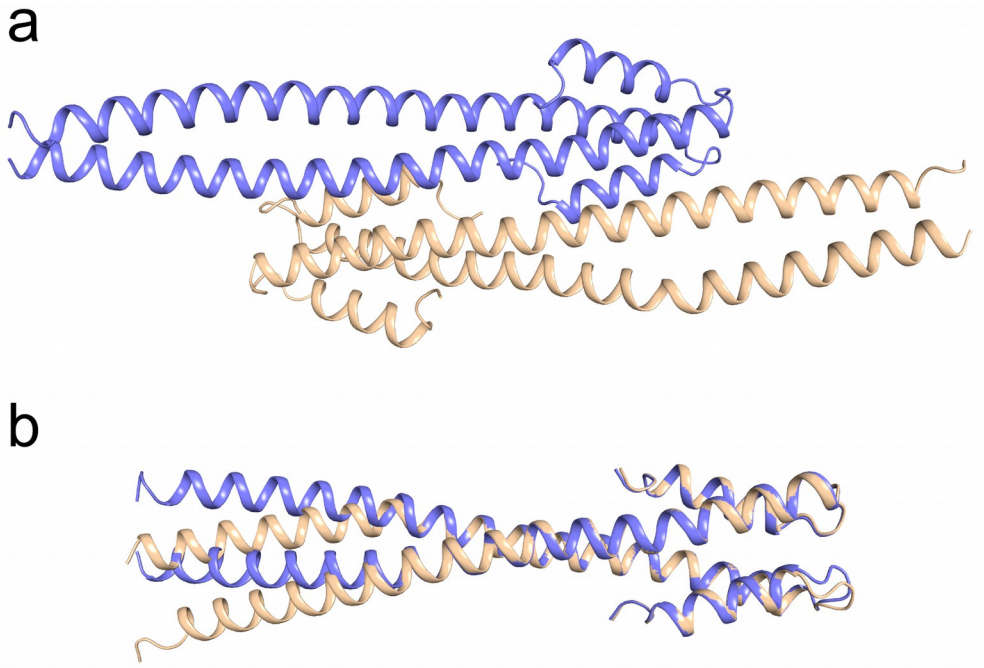

Figure S2.3 X-ray crystal structure of a Gp7-FtsB$_{CC}$ fusion protein. Ribbon representation of the two dimeric molecules in the asymmetric unit. a) The coil is straight for one of the dimers (chain A and B, blue) but it exhibits a slight kink in the second (yellow), presumably due to the effect of crystal packing. b) The kink becomes more evident when the two dimers in the asymmetric unit are aligned according to their Gp7 moiety.

Figure S2.4

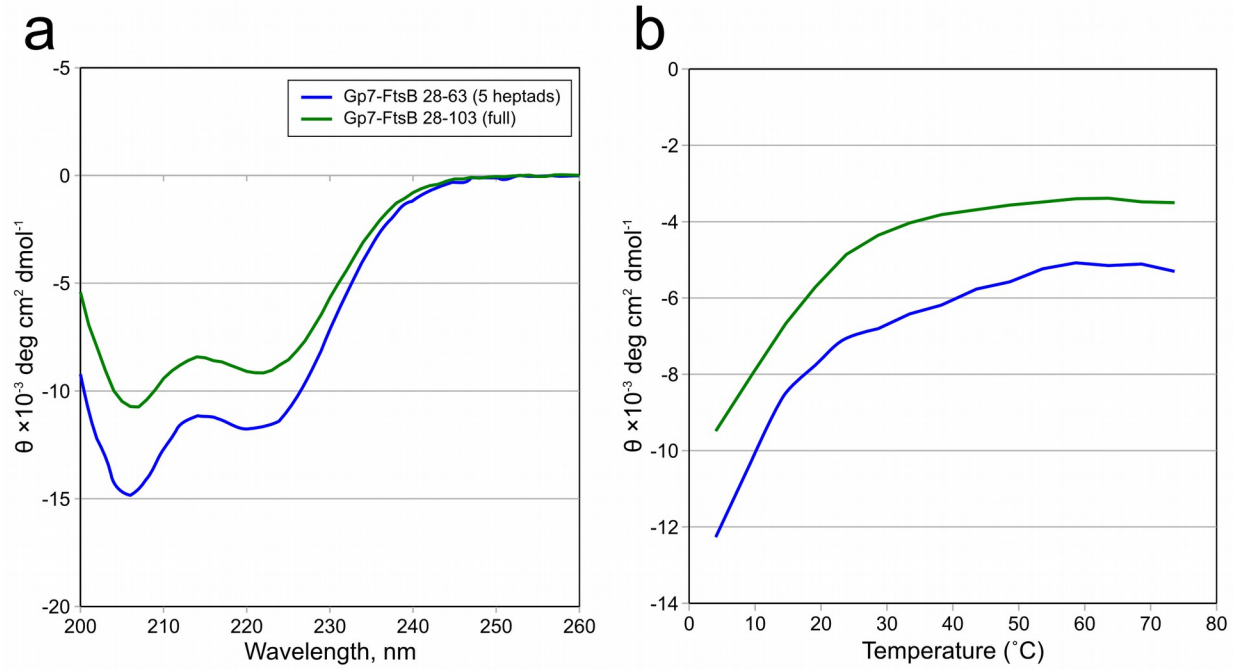

Figure S2.4 CD analysis Gp7-FtsB$_{CC}$ fusion proteins. a) Scans of Gp7-FtsB constructs containing 5-heptad repeats of the periplasmic coiled coil domain (positions 28-63, blue), and the entire periplasmic region (positions 28-103, green) at 4 ˚C. b) Thermal melts of the same constructs.

2.6 Acknowledgements

We are grateful to Dr. Darrell McCaslin of the Biophysical Instrumentation Facility of the Department of Biochemistry for assistance in the collection of the CD data. We thank Dr. Engelman and Miriam Alonso for providing the TOXCAT plasmids. We are grateful to Ben Mueller for useful discussion and assistance with TOXCAT, and to Dr. Vadim Klenchin for assistance with the QuikChange method. We thank Dr. Gevorg Gregorian for helpful discussion. IR and KCT were supported by funds from the NIH GM083987. Use of the Structural Biology ID19 beamline Argonne National Laboratory Advanced Photon Source was supported by the U.S. Department of Energy, Office of Energy Research, under Contract No. W-31-109-ENG-38.

2.7 References

1. Erickson HP, Anderson DE, Osawa M (2010) FtsZ in bacterial cytokinesis: cytoskeleton and force generator all in one. *Microbiol Mol Biol Rev* 74:504–528.
2. Löwe J, Amos LA (2009) Evolution of cytomotive filaments: the cytoskeleton from prokaryotes to eukaryotes. *Int J Biochem Cell Biol* 41:323–329.
3. Mingorance J, Rivas G, Vélez M, Gómez-Puertas P, Vicente M (2010) Strong FtsZ is with the force: mechanisms to constrict bacteria. *Trends Microbiol* 18:348–356.
4. Goehring NW, Beckwith J (2005) Diverse Paths to Midcell: Assembly of the Bacterial Cell Division Machinery. *Current Biology* 15:R514–R526.
5. Szwedziak P, Wang Q, Freund SM, Löwe J (2012) FtsA forms actin-like protofilaments. *EMBO J* 31:2249–2260.
6. Hale CA, de Boer PAJ (2002) ZipA is required for recruitment of FtsK, FtsQ, FtsL, and FtsN to the septal ring in Escherichia coli. *J Bacteriol* 184:2552–2556.
7. Hale CA, Rhee AC, de Boer PA (2000) ZipA-induced bundling of FtsZ polymers mediated by an interaction between C-terminal domains. *J Bacteriol* 182:5153–5166.
8. Liu Z, Mukherjee A, Lutkenhaus J (1999) Recruitment of ZipA to the division site by interaction with FtsZ. *Mol Microbiol* 31:1853–1861.
9. Sherratt DJ, Arciszewska LK, Crozat E, Graham JE, Grainge I (2010) The Escherichia coli DNA translocase FtsK. *Biochem Soc Trans* 38:395–398.
10. Mohammadi T et al. (2011) Identification of FtsW as a transporter of lipid-linked cell wall precursors across the membrane. *EMBO J* 30:1425–1432.

11. Fraipont C et al. (2011) The integral membrane FtsW protein and peptidoglycan synthase PBP3 form a subcomplex in Escherichia coli. *Microbiology (Reading, Engl)* 157:251–259.

12. Nguyen-Distèche M, Fraipont C, Buddelmeijer N, Nanninga N (1998) The structure and function of Escherichia coli penicillin-binding protein 3. *Cell Mol Life Sci* 54:309–316.

13. Bernhardt TG, de Boer PAJ (2003) The Escherichia coli amidase AmiC is a periplasmic septal ring component exported via the twin-arginine transport pathway. *Mol Microbiol* 48:1171–1182.

14. Heidrich C et al. (2001) Involvement of N-acetylmuramyl-L-alanine amidases in cell separation and antibiotic-induced autolysis of Escherichia coli. *Mol Microbiol* 41:167–178.

15. Gerding MA, Ogata Y, Pecora ND, Niki H, de Boer PAJ (2007) The trans-envelope Tol-Pal complex is part of the cell division machinery and required for proper outer-membrane invagination during cell constriction in E. coli. *Mol Microbiol* 63:1008–1025.

16. Buddelmeijer N, Judson N, Boyd D, Mekalanos JJ, Beckwith J (2002) YgbQ, a cell division protein in Escherichia coli and Vibrio cholerae, localizes in codependent fashion with FtsL to the division site. *Proc Natl Acad Sci USA* 99:6316–6321.

17. Ghigo JM, Weiss DS, Chen JC, Yarrow JC, Beckwith J (1999) Localization of FtsL to the Escherichia coli septal ring. *Mol Microbiol* 31:725–737.

18. Daniel RA, Errington J (2000) Intrinsic instability of the essential cell division protein FtsL of Bacillus subtilis and a role for DivIB protein in FtsL turnover. *Mol Microbiol* 36:278–289.

19. Katis VL, Wake RG, Harry EJ (2000) Septal localization of the membrane-bound division proteins of Bacillus subtilis DivIB and DivIC is codependent only at high temperatures and requires FtsZ. *J Bacteriol* 182:3607–3611.

20. Buddelmeijer N, Beckwith J (2004) A complex of the Escherichia coli cell division proteins FtsL, FtsB

and FtsQ forms independently of its localization to the septal region. *Mol Microbiol* 52:1315–1327.

21. Daniel RA, Noirot-Gros M-F, Noirot P, Errington J (2006) Multiple interactions between the transmembrane division proteins of Bacillus subtilis and the role of FtsL instability in divisome assembly. *J Bacteriol* 188:7396–404.
22. Karimova G, Dautin N, Ladant D (2005) Interaction network among Escherichia coli membrane proteins involved in cell division as revealed by bacterial two-hybrid analysis. *J Bacteriol* 187:2233–2243.
23. Robichon C, Karimova G, Beckwith J, Ladant D (2011) Role of leucine zipper motifs in association of the Escherichia coli cell division proteins FtsL and FtsB. *J Bacteriol* 193:4988–4992.
24. Goehring NW, Gueiros-Filho F, Beckwith J (2005) Premature targeting of a cell division protein to midcell allows dissection of divisome assembly in Escherichia coli. *Genes Dev* 19:127–137.
25. Goehring NW, Gonzalez MD, Beckwith J (2006) Premature targeting of cell division proteins to midcell reveals hierarchies of protein interactions involved in divisome assembly. *Molecular Microbiology* 61:33–45.
26. Robichon C, King GF, Goehring NW, Beckwith J (2008) Artificial septal targeting of Bacillus subtilis cell division proteins in Escherichia coli: an interspecies approach to the study of protein-protein interactions in multiprotein complexes. *J Bacteriol* 190:6048–6059.
27. Rowland SL et al. (2010) Evidence from Artificial Septal Targeting and Site-Directed Mutagenesis that Residues in the Extracytoplasmic {beta} Domain of DivIB Mediate Its Interaction with the Divisomal Transpeptidase PBP 2B. *J Bacteriol* 192:6116–6125.
28. Gonzalez MD, Beckwith J (2009) Divisome Under Construction: Distinct Domains of the Small Membrane Protein FtsB Are Necessary for Interaction with Multiple Cell Division Proteins. *J Bacteriol*

191:2815–2825.

29. Gonzalez MD, Akbay EA, Boyd D, Beckwith J (2010) Multiple interaction domains in FtsL, a protein component of the widely conserved bacterial FtsLBQ cell division complex. *J Bacteriol* 192:2757–2768.
30. Daniel RA, Harry EJ, Katis VL, Wake RG, Errington J (1998) Characterization of the essential cell division gene ftsL(yIID) of Bacillus subtilis and its role in the assembly of the division apparatus. *Mol Microbiol* 29:593–604.
31. Bramkamp M, Weston L, Daniel RA, Errington J (2006) Regulated intramembrane proteolysis of FtsL protein and the control of cell division in Bacillus subtilis. *Mol Microbiol* 62:580–591.
32. Wadenpohl I, Bramkamp M (2010) DivIC Stabilizes FtsL Against RasP Cleavage. *J Bacteriol* 192:5260–5263.
33. Masson S et al. (2009) Central domain of DivIB caps the C-terminal regions of the FtsL/DivIC coiled-coil rod. *J Biol Chem* 284:27687–27700.
34. Noirclerc-Savoye M et al. (2005) In vitro reconstitution of a trimeric complex of DivIB, DivIC and FtsL, and their transient co-localization at the division site in Streptococcus pneumoniae. *Mol Microbiol* 55:413–424.
35. Villanelo F, Ordenes A, Brunet J, Lagos R, Monasterio O (2011) A model for the Escherichia coli FtsB/FtsL/FtsQ cell division complex. *BMC Struct Biol* 11:28.
36. Russ WP, Engelman DM (1999) TOXCAT: A Measure of Transmembrane Helix Association in a Biological Membrane. *PNAS* 96:863–868.
37. Adams PD, Arkin IT, Engelman DM, Brünger AT (1995) Computational searching and mutagenesis suggest a structure for the pentameric transmembrane domain of phospholamban. *Nat Struct Biol*

2:154–162.

38. Fleming KG, Engelman DM (2001) Computation and mutagenesis suggest a right-handed structure for the synaptobrevin transmembrane dimer. *Proteins* 45:313–317.
39. Jenei ZA, Warren GZL, Hasan M, Zammit VA, Dixon AM (2011) Packing of transmembrane domain 2 of carnitine palmitoyltransferase-1A affects oligomerization and malonyl-CoA sensitivity of the mitochondrial outer membrane protein. *FASEB J* 25:4522–4530.
40. Lemmon MA, Flanagan JM, Treutlein HR, Zhang J, Engelman DM (1992) Sequence specificity in the dimerization of transmembrane alpha-helices. *Biochemistry* 31:12719–25.
41. Li R et al. (2004) Dimerization of the transmembrane domain of Integrin alphaIIb subunit in cell membranes. *J Biol Chem* 279:26666–26673.
42. Senes A, Gerstein M, Engelman DM (2000) Statistical analysis of amino acid patterns in transmembrane helices: the GxxxG motif occurs frequently and in association with beta-branched residues at neighboring positions. *J Mol Biol* 296:921–36.
43. Senes A et al. (2007) E(z), a depth-dependent potential for assessing the energies of insertion of amino acid side-chains into membranes: derivation and applications to determining the orientation of transmembrane and interfacial helices. *J Mol Biol* 366:436–448.
44. Senes A, Engel DE, DeGrado WF (2004) Folding of helical membrane proteins: the role of polar, GxxxG-like and proline motifs. *Curr Opin Struct Biol* 14:465–479.
45. Bowie JU (2011) Membrane protein folding: how important are hydrogen bonds? *Curr Opin Struct Biol* 21:42–49.
46. Joh NH et al. (2008) Modest stabilization by most hydrogen-bonded side-chain interactions in membrane proteins. *Nature* 453:1266–1270.

47. Choma C, Gratkowski H, Lear JD, DeGrado WF (2000) Asparagine-mediated self-association of a model transmembrane helix. *Nat Struct Biol* 7:161–6.

48. Zhou FX, Cocco MJ, Russ WP, Brunger AT, Engelman DM (2000) Interhelical hydrogen bonding drives strong interactions in membrane proteins. *Nat Struct Biol* 7:154–60.

49. Fleming KG, Engelman DM (2001) Specificity in transmembrane helix-helix interactions can define a hierarchy of stability for sequence variants. *Proc Natl Acad Sci USA* 98:14340–14344.

50. Stanley AM, Fleming KG (2007) The role of a hydrogen bonding network in the transmembrane beta-barrel OMPLA. *J Mol Biol* 370:912–924.

51. Li E, You M, Hristova K (2006) FGFR3 dimer stabilization due to a single amino acid pathogenic mutation. *J Mol Biol* 356:600–612.

52. Lawrie CM, Sulistijo ES, MacKenzie KR (2010) Intermonomer hydrogen bonds enhance GxxxG-driven dimerization of the BNIP3 transmembrane domain: roles for sequence context in helix-helix association in membranes. *J Mol Biol* 396:924–936.

53. Sulistijo ES, Mackenzie KR (2009) Structural basis for dimerization of the BNIP3 transmembrane domain. *Biochemistry* 48:5106–5120.

54. Partridge AW, Therien AG, Deber CM (2002) Polar mutations in membrane proteins as a biophysical basis for disease. *Biopolymers* 66:350–358.

55. Partridge AW, Therien AG, Deber CM (2004) Missense mutations in transmembrane domains of proteins: phenotypic propensity of polar residues for human disease. *Proteins* 54:648–656.

56. Lemmon MA, Treutlein HR, Adams PD, Brünger AT, Engelman DM (1994) A dimerization motif for transmembrane alpha-helices. *Nat Struct Biol* 1:157–163.

57. Kulp DW et al. (2012) Structural informatics, modeling, and design with an open-source Molecular

Software Library (MSL). *J Comput Chem* 33:1645–1661.

58. Frye J, Klenchin VA, Rayment I (2010) Structure of the tropomyosin overlap complex from chicken smooth muscle: insight into the diversity of N-terminal recognition. *Biochemistry* 49:4908–4920.
59. Klenchin VA, Frye JJ, Jones MH, Winey M, Rayment I (2011) Structure-function analysis of the C-terminal domain of CNM67, a core component of the Saccharomyces cerevisiae spindle pole body. *J Biol Chem* 286:18240–18250.
60. Harbury PB, Zhang T, Kim PS, Alber T (1993) A switch between two-, three-, and four-stranded coiled coils in GCN4 leucine zipper mutants. *Science* 262:1401–1407.
61. Grigoryan G, Keating AE (2008) Structural specificity in coiled-coil interactions. *Curr Opin Struct Biol* 18:477–483.
62. Chen GJ, Qiu N, Karrer C, Caspers P, Page MG (2000) Restriction site-free insertion of PCR products directionally into vectors. *BioTechniques* 28:498–500, 504–505.
63. Shaw WV (1975) Chloramphenicol acetyltransferase from chloramphenicol-resistant bacteria. *Meth Enzymol* 43:737–755.
64. Blommel PG, Fox BG (2007) A combined approach to improving large-scale production of tobacco etch virus protease. *Protein Expr Purif* 55:53–68.
65. Otwinowski Z, Minor W (1997) in *Methods in Enzymology*, ed Charles W. Carter J (Academic Press), pp 307–326. Available at: http://www.sciencedirect.com/science/article/pii/S007668799776066X [Accessed September 26, 2012].
66. Morais MC et al. (2003) Bacteriophage phi29 scaffolding protein gp7 before and after prohead assembly. *Nat Struct Biol* 10:572–576.
67. Vagin A, Teplyakov A (2000) An approach to multi-copy search in molecular replacement. *Acta*

Crystallogr D Biol Crystallogr 56:1622–1624.

68. Cowtan K (2008) Fitting molecular fragments into electron density. *Acta Crystallogr D Biol Crystallogr* 64:83–89.
69. Cowtan K (2010) Recent developments in classical density modification. *Acta Crystallogr D Biol Crystallogr* 66:470–478.
70. Emsley P, Cowtan K (2004) Coot: model-building tools for molecular graphics. *Acta Crystallogr D Biol Crystallogr* 60:2126–2132.
71. Murshudov GN, Vagin AA, Lebedev A, Wilson KS, Dodson EJ (1999) Efficient anisotropic refinement of macromolecular structures using FFT. *Acta Crystallogr D Biol Crystallogr* 55:247–255.
72. Xiang Z, Honig B (2001) Extending the accuracy limits of prediction for side-chain conformations. *J Mol Biol* 311:421–430.
73. Subramaniam S, Senes A (2012) An energy-based conformer library for side chain optimization: Improved prediction and adjustable sampling. *Proteins* 80:2218–2234.

Chapter 3
Functional studies of FtsB *in vivo*

3.1 Introduction

Through the literature review in **Chapter 1**, I have established the importance of the FtsB/FtsL subcomplex in bacterial cell divison. The presence and the interaction of both proteins is essential for cell division[1,2]. To briefly summarize, FtsL and FtsB are part of the intermediate step of the assembly of the divisome; the step that links the early (Z-ring formation) and the late steps (rebuilding the cell wall). This step is much less characterized, but it is hypothesized that FtsL and FtsB form a structural scaffold for the divisome proteins[3]. Research from our lab has probed some structural details of this complex as discussed in depth in **Chapter 2** and in this chapter. We have shown that FtsB and FtsL form a stable subcomplex *in vitro*, where FtsB oligomerizes and FtsL stabilizes FtsB laterally[3,4]. I have shown that a specific interaction interface exists in the FtsB oligomer and have identified key residues that are essential for this association, including a conserved gluatmine residue in the transmembrane domain. We do not yet know precisely how FtsL interacts with FtsB, nor the exact oligomeric state of the complex, but we do know that the stoichiometry of the oligomer is 1:1. It is also known that FtsQ complexes with FtsB and FtsL before localization to the midcell[5], but we have not yet characterized this interaction.

In this Chapter, I ask about the functional importance of the FtsB oligomer *in vivo*, based on what we know from my previous work. In **Chapter 2**, I mapped out the interaction interface of FtsB using the TOXCAT assay[6]. Here I test whether the point mutations that disrupted the FtsB oligomer in TOXCAT phenotypically affect cell division. To do this, I use a depletion strain system developed by the laboratory of Jon Beckwith at Harvard. The depletion strain contains a repressable chromosomal FtsB. The effect of FtsB point mutants (introduced on a plasmid) on cell division can be observed using microscopy. I discovered that a number of point mutations disrupt cell division both in the transmembrane domain as well as the flexible linker domain, which has not been previously

characterized *in vitro*. FtsL point mutations were also analyzed using the same *in vivo* assay, but the data was not conclusive. This work is preliminary and builds a foundation for this project to be carried out (see section **3.5 Future Studies** for discussion).

3.2 Materials and Methods

Plasmids and strains

Strains and plasmids used in this study were graciously obtained from the laboratory of Jon Beckwith at Harvard University and used as previously described [1]. Antibiotics and chemicals were purchased from Dot Scientific (Burton, MI). Spectinomycin was used at a final concentration of 100 μg/mL for all plasmids used. Medium was supplemented with 0.2% L-arabinose or 0.2% D-glucose to induce or repress expression of genes regulated by the P_{BAD} promoter, respectively. Isopropyl-β-D-thiogalactoside (IPTG) was added at indicated concentration or, in some cases, not added because the plasmid expression is leaky. Mutants were constructed for this study using Quikchange mutagenesis. Oligonucleotide primers were purchased from Integrated DNA Technologies.

Depletion strain experiments

A single colony of cells from either FtsB or FtsL depletion strain listed in Table 1 (with or without plasmid) was grown overnight at 37°C in 3 mL of LB medium supplemented with 0.2% L-arabinose and 100 μg/mL spectinomycin then diluted 1:100 into fresh medium containing the same supplement and grown to optical density at 600 nm (OD600) of ~0.3. An aliquot of 1 mL was taken from this culture and centrifuged at 17000g for 10 min and washed twice with LB media lacking sugar. Washed aliquots were resuspended in 1 mL (or normalized) and inoculated into a fresh 3mL tube containing LB supplemented with 0.2% D-glucose and either 10μM IPTG or 0μM IPTG. Under these conditions the time required to deplete the cells of endogenous protein (FtsL or FtsB) is approximately 3 hours as reported[1]. Glucose was kept in the media to repress additional expression of FtsB from the P_{BAD} promoter. Cells were also analyzed at 42°C as long as normal cell division was observed in all control samples. This slightly restrictive temperature will cause a more visible phenotype as it adds additional stress to the cells, but does not disrupt the phenotype of the controls. Controls for analyzing

FtsB and FtsL mutations were constructed as listed in Table 1.

Strain	**Plasmid**	**Media Supplement**	**Phenotype observed**
NB946	None	0.2% L-arabinose	Normal division
NB946	None	0.2% D-glucose	Filamentous
NB946	flag-FtsB	0.2% L-arabinose	Normal division
NB946	FtsB-flag	0.2% L-arabinose	Normal division
NB946	PNG162 empty vector	0.2% L-arabinose	Filamentous
MDG277	None	0.2% L-arabinose	Normal division
MDG277	None	0.2% D-glucose	Filamentous
MDG277	flag-FtsL	0.2% L-arabinose	Normal division
MDG277	FtsL-flag	0.2% L-arabinose	Normal division

Table 1 Phenotypes expected for NB946 strain (FtsB depletion strain [1]) and MDG277 strain (FtsL depletion strain [2]).

Microscopy

All microscopy experiments were performed in collaboration with the laboratory of Professor Doug Weibel. After cultures were grown for the appropriate time, samples were mounted on a slide with a 3% agarose cushion to prevent movement of the live cells. Cells were optically imaged cells using a Nikon Eclipse Ti inverted microscope equipped with crossed polarizers and a Photometics CoolSNAP HQ2 CCD camera (Tucson, AZ) using a Nikon Plan Apo λ, 100X/1.45 oil objective lens. Images were collected with the EM gain off and with a 100 ms exposure time (10 frames/sec). Images of cells were collected using Nikon NIS Elements software where bright field and crossed polar images were collected for the same field of view.

3.3 Results

3.3.1 Mutations in the transmembrane domain of FtsB disrupt cell division

We previously discovered that FtsB could associate into homo-oligomers *in vitro*. The specific interaction interface was mapped using mutagenesis and used to build a computational model of an FtsB homodimer[4](See **Chapter 1**). Our hypothesis is that the oligomer of FtsB forms a stable higher oligomer with FtsL *in vivo*, which then is able to interact with FtsQ via the C-terminal domains (**Chapter 1**, Figure 10), but we do not yet know the precise oligomeric state of this complex. We do know what residues in the transmembrane domain are sensitive to mutation. To better understand the biological function of FtsB, here I investigated whether mutations that disrupt the self-association of the homo-oligomer using the TOXCAT assay[6] (**Chapter 1**, Figure 4) would also abolish division in living cells. A mutation that causes disruption of the association of the FtsB homo-oligomer could disrupt the overall FtsB/FtsL oligomer and inhibit cell division, causing long, filamentous cells.

To probe this question, I used a system developed by the Beckwith lab.[1,2] This *in vivo* assay utilizes a strain of E. coli deficient in gene of interest from the chromosome; either ftsB depletion strain or ftsL depletion strain. These depletion strains contain a chromosomal copy of the wild type protein under control of an inducible promoter. A plasmid containing this gene or mutant is transformed into the cells and expressed in place of the wild type version by repressing the chromosomal copy and inducing the plasmid copy. The cells are then visualized using microscopy to determine if the phenotype changes from normal to filamentous.

The results show that the majority of the point mutations that were disruptive in TOXCAT on FtsB did not show a filamentous phenotype in the cells (Figure 1). The controls used for this experiment include introduction of an unmutated FtsB (normal cell division) and strains transformed with an empty plasmid (filamentous cells) shown in **Figure 1**. Two mutants in FtsB caused filamentous

cells at normal cell division temperature (37ºC) that are important to discuss: Q16F and W20A. These mutants are in the transmembrane domain of FtsB showed filamentous cells at the higher temperature (**Figure 2** and **Figure 3**). These positions were important at the interface of association of FtsB as measured previously by TOXCAT (**Chapter 1**, Figure 4) and are also highly conserved (**Chapter 1**, Figure 7). Microscopy of some of the FtsB mutations at position Q16 and W20 is shown in **Figure 2**. Two other FtsB mutations also showed filamentous cells at a more restrictive temperature (42ºC), which puts stress on the cells making them more sensitive to the defects of the cell division machinery. This was the case with L12F and L15A, which both occur at the interface of the FtsB dimer. An overall summary of the FtsB mutants that were sensitive to the TOXCAT assay tested and their affect on cell division phenotype at the two temperatures is presented in **Figure 4**.

3.3.2 Mutations in the conserved flexible linker region of FtsB do not disrupt cell division, but adding alanine insertions does disrupt cell division

Our theoretical model of the FtsB homo-oligomer shows a conserved linker region between the transmembrane domain and coiled-coil domain (**Chapter 1**, Figure 7 and Figure 9). We made mutants of this region in residues G22 and G25, which may be important for flexibility, to see if this linker was important *in vivo*. Initially, filamentous cells were observed in the mutation G25A, but not G22A or G22A/G25A. This result is difficult to interpret. Several more mutants were cloned into the G22 and G25 positions: G22A, G22I, G22V, G25A, G25L, G25I, G25F, and G22A/G25A. All of these were tested *in vivo* and none of the mutants produced filamented cells at 37ºC or 42ºC.

Adding an Ala linker between the transmembrane and coiled-coil domain does disrupt cell division

Sequential additions of one, two, and three alanines were also tested. These alanines were inserted directly C-terminal to the transmembrane domain of FtsB in order to twist the helix around so that the interface of coiled-coil and transmembrane domains does not line up. These mutants did

produce a semi-filamentous phenotype *in vivo* at 37°C, with the most defective phenotype for two alanines relative to wild type (**Figure 6**), indicating that the linker region is important for FtsB function.

Filamentation of negative control cell samples begins in the first or second division cycle after addition of glucose and IPTG

To investigate when the cells began to filament in the depletion assay, images of the cells were taken for each cycle of division right after induction. The data showed that the cells began to filament immediately in the negative controls (NB946 strain with and without empty vector, **Figure 6A** and **Figure 6C**). An intermediate phenotype was also tested and this result showed filamentation immediately, but after a few cycles of cell division there were some cells that were exhibiting normal cell division (NB946 cells with Y85stop plasmid, **Figure 6D**). No filamentation was observed in the positive controls (NB946 strain with FtsB plasmid, **Figure 6B**). I am confident in the controls for this experiment and the fact that if the cells are thoroughly washed (at least three cycles) the mutants begin affecting cell division right away.

3.3.3 FtsL point mutations in the transmembrane domain do not affect cell division

We also tested a series of point mutations in FtsL, hoping to be able to build a disruption map between FtsL and FtsB to help guide *in vitro* experiments. The assay works exactly the same as with FtsB, but with a FtsL depletion strain and plasmid with mutated copy of FtsL. These point mutations are shown in **Figure 7**. There appears to be a small amount of inhibition of cell division in mutant L53F, shown in **Figure 7G** but this has not been explored further.

3.4 Discussion

3.4.1 The FtsL/FtsB subcomplex is stable *in vivo*, but a few mutations in FtsB cause a filamentous phenotype

Our working hypothesis is that a FtsB homo-oligomer forms an initial core that then laterally recruits FtsL into a higher-order oligomer, such as a tetramer (**Chapter 1**, Figure 10). The mutational analysis that we previously performed was in the transmembrane domain of FtsB only, but we were still able to map a theoretical model for the FtsB oligomer (**Chapter 1**, Figure 9). I hypothesized that the same disruptive mutants would cause a change in cell division phenotype, so I tested almost all of these mutations *in vivo* (Figure 4). Because the TOXCAT assay measures association of a transmembrane domain in isolation (**Chapter 1**, Figure 2), our results indicate that when the full complex of FtsB/FtsL and FtsQ is present it is significantly more difficult to disrupt as a whole and in turn, affect cell division. The helical interface of FtsB is likely very important for the function of the dimer, so it is not surprising that the alanine linker mutants were more disruptive than single point mutations of FtsB. Our previous data and previous data from the Beckwith group indicate that this complex is very stable, so we were not incredibly surprised by this result.

The core of our hypothesis that FtsB is stabilized by FtsL is centered around the less stable soluble domain of FtsB. This domain contains a coiled-coil domain and a glycine rich linker which links the transmembrane domain to the soluble domain. We tested mutations in the glycine rich linker region *in vivo*, hypothesizing that substitutions that remove this flexible would have a profound effect on cell division. The linker region is conserved and the flexibility probably allows correct association of FtsB with FtsL. None of the mutants in G22 or G25 that we tested *in vivo* affected cell division. Our accidental result that occurred when a stop codon was inserted prior to the coiled-coil domain of FtsB and a filamentous phenotype was observed confirms previous results from Gonzalez and Beckwith who

determined on a very small portion of the FtsB C-terminus was dispensible for full function of FtsB *in vivo*[1].

3.4.2 Point mutations in the transmembrane domain of FtsL do not disrupt cell division

The association of the transmembrane domain of FtsL in TOXCAT is very small compared to FtsB (**Chapter 1**, Figure 2) being only slightly higher than our negative control mutant GpA G83I. I initially performed a mutational analysis of the transmembrane domain of FtsL, but I was unable to map an interaction interface (data presented in prelim). Given our current working hypothesis, this result makes sense, as we do not think FtsL self-associates. A number of mutants of the transmembrane domain of FtsL were tested *in vivo* without any affect on cell division. This was performed to support our initial goal that we could add dimension to our hypothetical model of the interaction of FtsB/FtsL by scanning mutants using this *in vivo* assay, which is not the case thus far.

3.4.3 The model of FtsB/FtsL must be refined *in vitro* before we can test mutants *in vivo*

Our initial goal with this work was to build a map of mutants that disrupted cell division that would help guide *in vitro* experiments to refine the structural model of the FtsB/FtsL subcomplex (**Chapter 3**). We learned that without more knowledge of the stability of this complex *in vitro*, most of the mutants we observe *in vivo* will not have an effect on cell division. It is also possible that these two projects can continue to move forward simultaneously, giving us new information about not only the overall interaction of FtsB/FtsL and its stability but its function *in vivo*. A computational model docking FtsL along the FtsB dimer is currently underway using mutational information that we do have. This type of modeling could potentially guide the choice of which mutants to explore *in vivo*. We are also working on isolating the entire complex *in vitro* and measuring stability using biochemical techniques such as gel filtration, circular dichroism, X-ray crystallography, and FRET (see **Future Studies**).

Figure 3.1

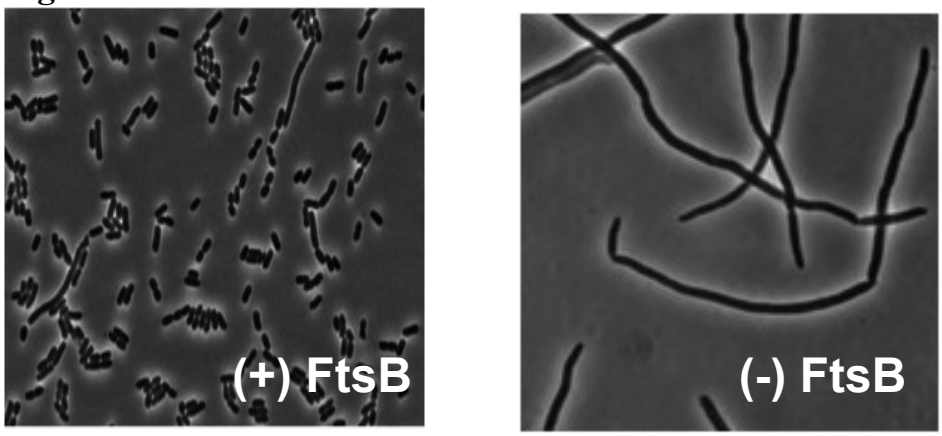

Figure 3.1 Phenotypes of positive and negative control samples. Positive and negative controls of depletions strain NB946 with flag-FtsB plasmid unmutated (left) and empty plasmid (right). These results are typical of 42ºC where there are very occasional filaments in the positive control sample. For cells grown at 37ºC this does not occur. They are shown here for comparison to other figures.

Figure 3.2

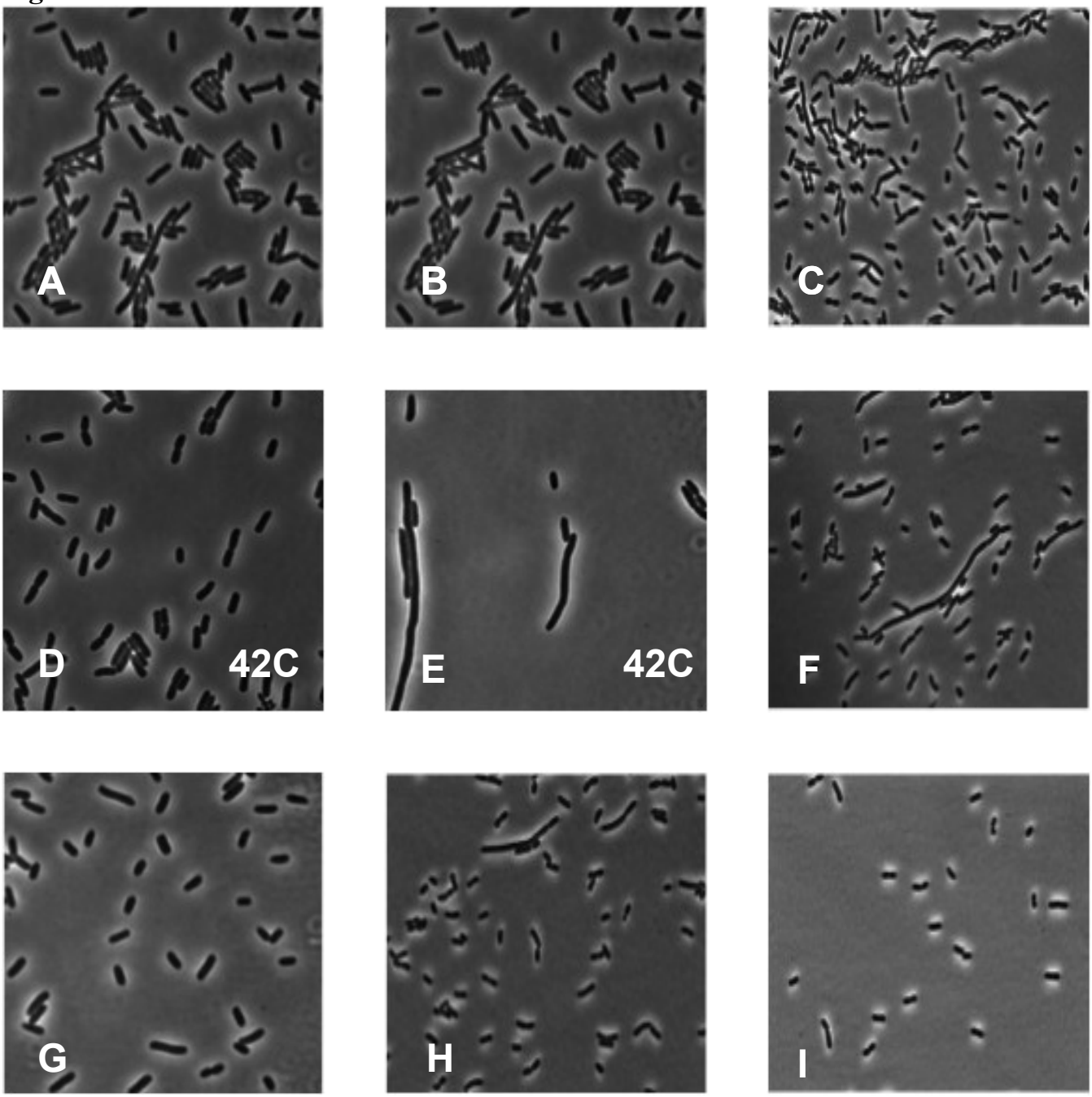

Figure 3.2 Representative FtsB point mutants of FtsB dimer tested *in vivo*. Panels D and E show result at 42ºC. All mutants were tested at both temperatures, but 42ºC did not make a difference for the rest. Specific point mutations per panel are: **A** Q16A, **B** Q16F, **C** Q16I, **D** Q16A, **E** Q16F, **F** Q16L, **G** Q16FW20F, **H** Q16V, **I** Q16M.

Figure 3.3

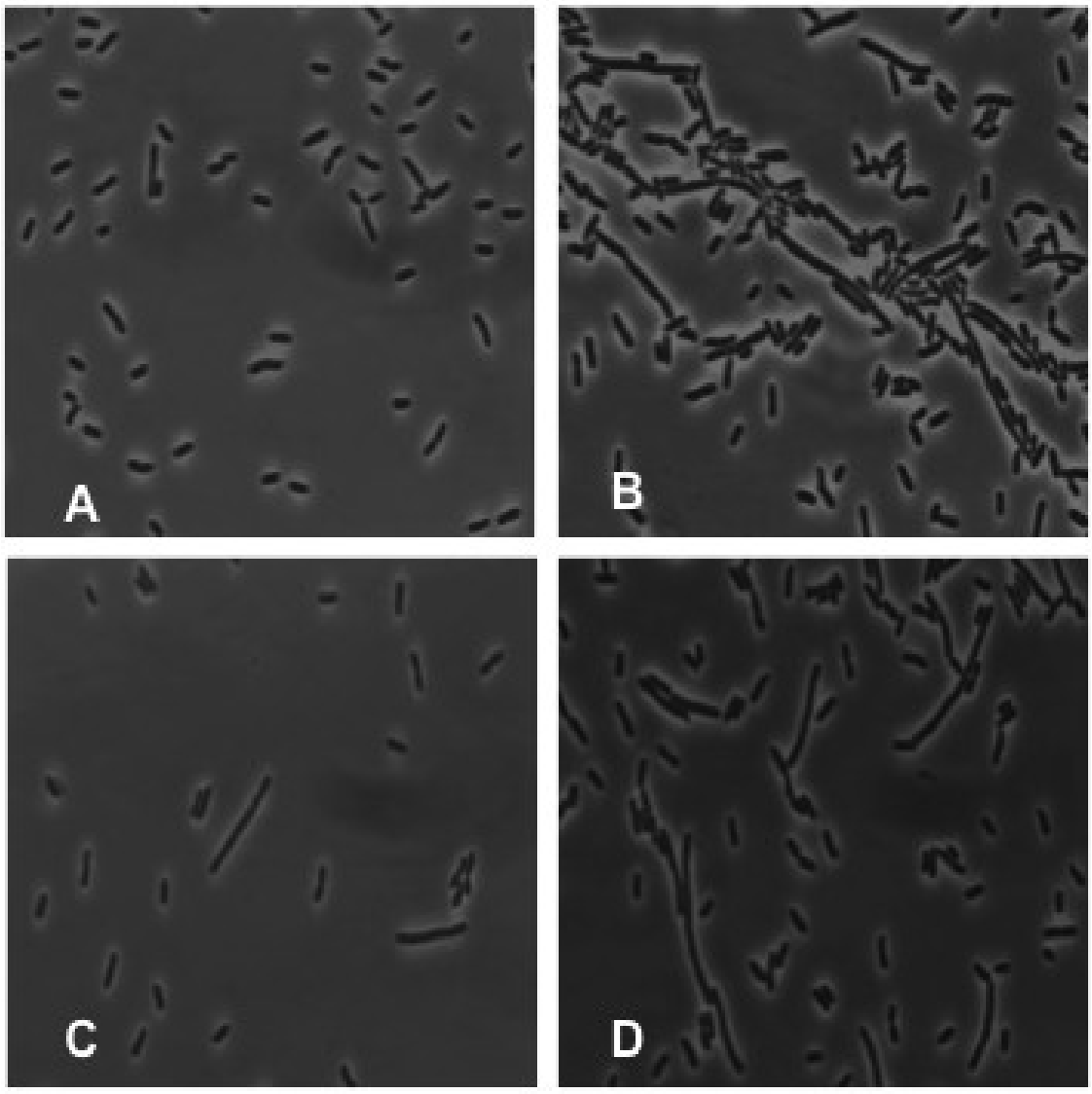

Figure 3.3 Representative point mutations in FtsB transmembrane dimer interface tested *in vivo*.

A FtsB L12F at 37°C; **B** FtsB L12F at 42°C; **C** FtsB L15A at 37°C; **D** FtsB L15A at 42°C.

Figure 3.4

FtsB TM Residue	Mutation	TOXCAT score	Phenotype 37C	Phenotype 42C
L12	A	3	WT	WT
L12	F	2	F	F
V13	A	1	WT	WT
V13	F	0	WT	WT
L15	A	3	F	F
L15	F	1	WT	-
Q16	A	3	WT	WT
Q16	I	-	WT	WT
Q16	L	-	WT	WT
Q16	F	2	F	F
Q16	M	3	WT	WT
Q16	V	2	WT	WT
Y17	A	0	WT	WT
Y17	F	0	WT	WT
L19	A	2	WT	WT
L19	F	2	WT	WT
W20	A	-	F	F
W20	I	0	WT	WT
W20	L	-	WT	WT
W20	F	-	WT	WT
W20	G	2	WT	WT
Q16W20	F	-	WT	WT
G22	A	-	WT	WT
G25	A	-	WT	WT

Figure 3.4 A table of mutants of FtsB and their affect on cell division and association of FtsB in TOXCAT. An exhaustive summary of the mutants tested in TOXCAT and *in vivo* is given here for side by side comparison. Many of the mutants disruptive in TOXCAT did not affect cell division.

Figure 3.5

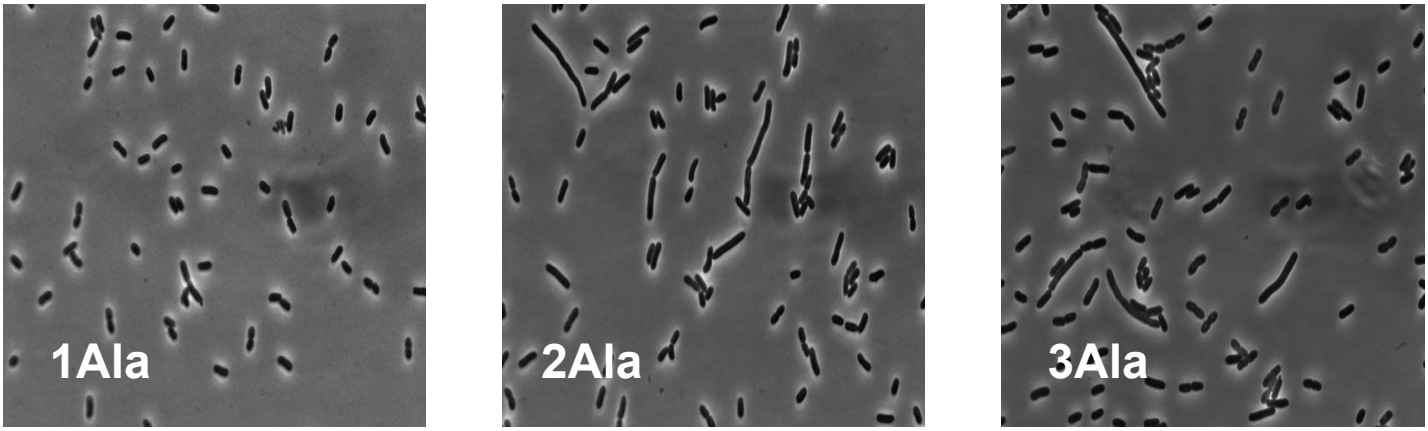

Figure 3.5 Alanine insertions in region between coiled-coil and transmembrane domain of FtsB. These insertions rotate the helical dimer of FtsB between the transmembrane domain and coiled-coil domain. The disruption of dimerization affects cell division in this case, especially when two and three alanines are inserted. These type of drastic changes are very likely to disrupt the folded complex of FtsL and FtsB *in vivo*.

Figure 3.6

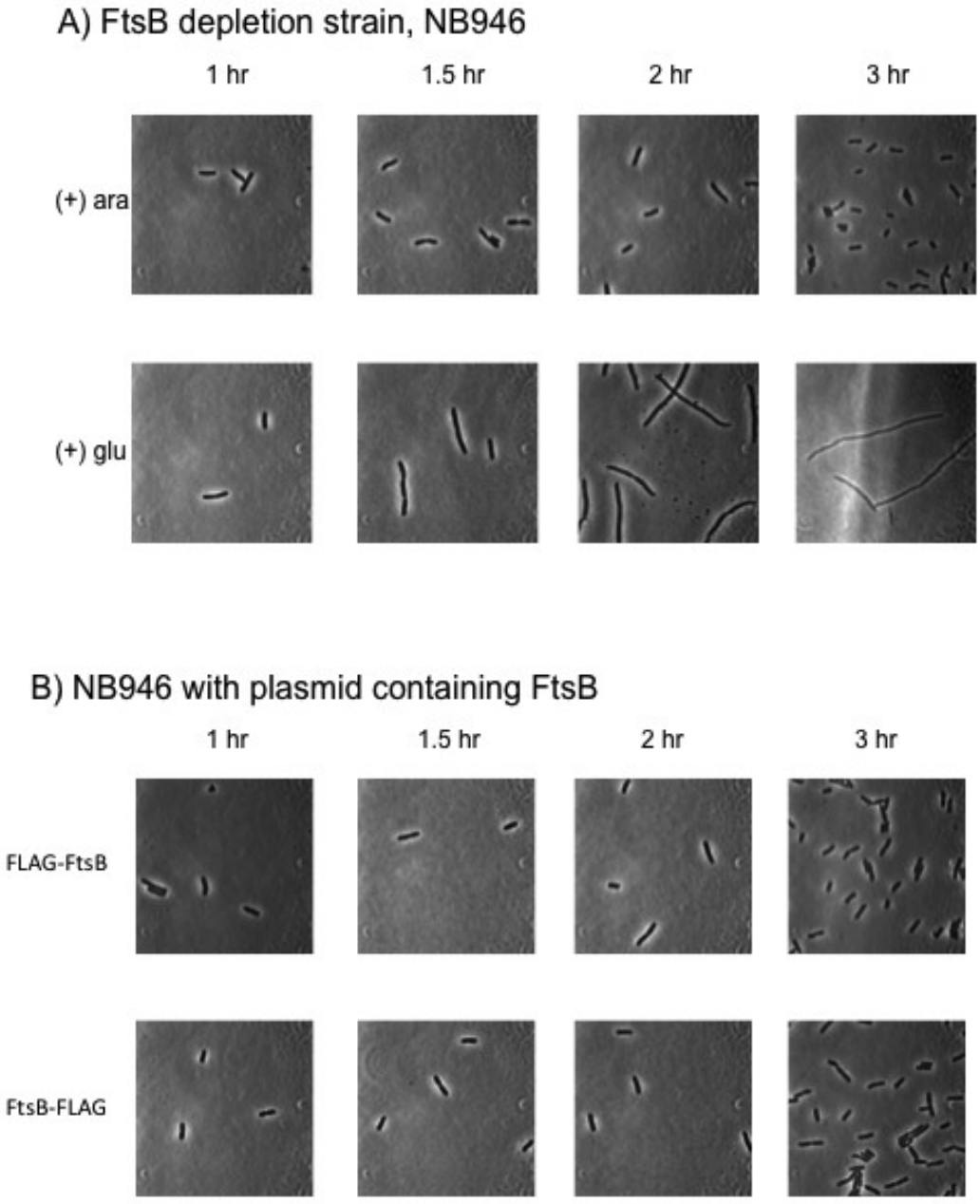
A) FtsB depletion strain, NB946
1 hr
1.5 hr
2 hr
3 hr
(+) ara
(+) glu
B) NB946 with plasmid containing FtsB
1 hr
1.5 hr
2 hr
3 hr
FLAG-FtsB
FtsB-FLAG

C) NB946 with empty vector control plasmid

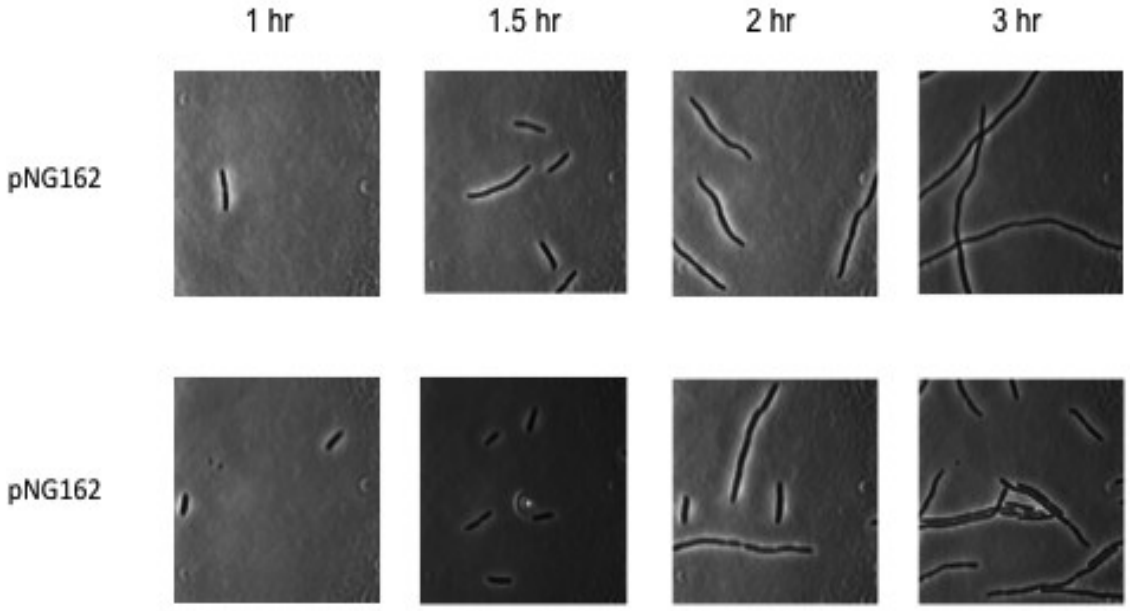

D) NB946 with intermediate phenotype control plasmid

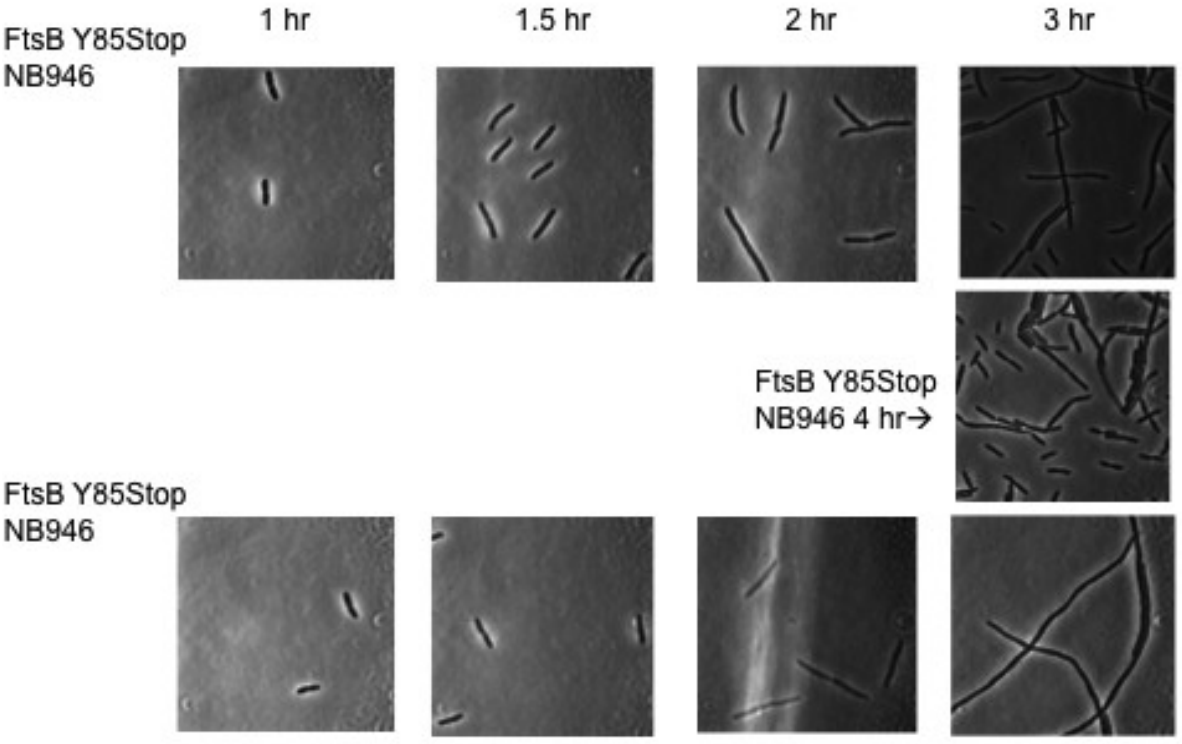

Figure 3.6 Timelapse experiment of FtsB depletion strain assay. Images were taken one hour after induction and then every half hour. It is clear that the filamentation begins in just one or two cycles of cell division and there is not a large lag, indicating that the cells are deficient of the wild type FtsB. A) Depletion strain only B) Depletion strain plus plasmids with FtsB (positive controls) C) Depletion strain plus empty vector plasmid (negative controls) D) Depletion strain plus intermediate phenotype plasmid.

Figure 3.7

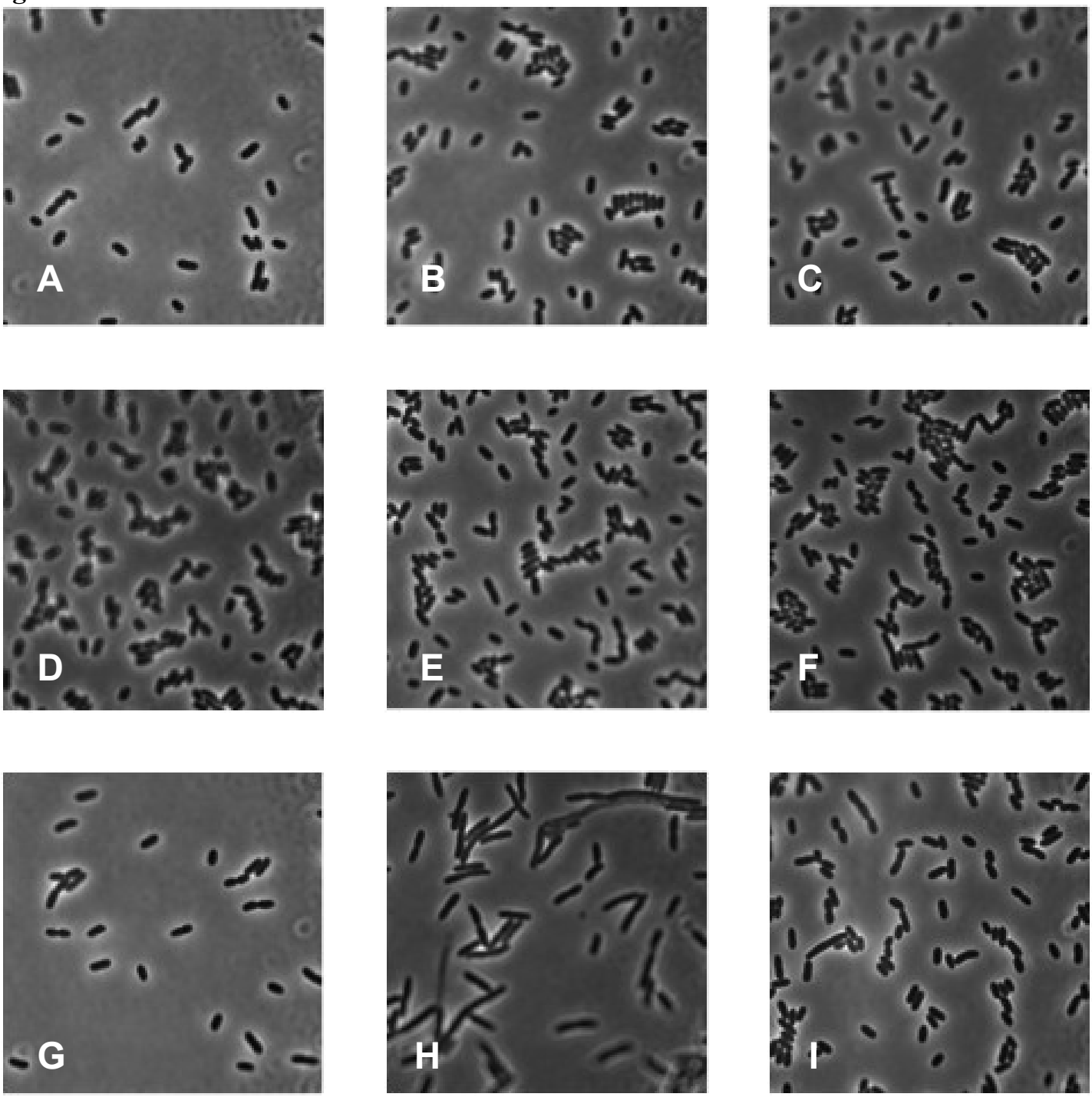

Figure 3.7 Point mutations of FtsL tested *in vivo*. These mutants were tested at 37ºC and 42ºC and shown here is an average image of each. Specific panels contain the following mutants: **A** T55F, **B** T56F, **C** L44F, **D** L43F, **E** L42F, **F** I47F, **G** A57F, **H** L53F, **I** C41F.

3.5 Future Studies

The work on this project will be carried out by another graduate student from this point forward. I have assisted with the set up for the *in vivo* assay, and have discovered that we might need to use more information from our structural model before testing point mutations. I think it would also be beneficial to employ some co-immunoprecipitation experiments with these strains and the mutations that we are curious about to more directly probe the interaction. Another experiment that should be optimized is a western blot to check for expression of these plasmids in the depletion strain assays. I attempted this without being successful. Finally, once we have a clearer map of the complex and how it is disruptive, it will be interesting to figure out which positions are involved in the localization of FtsL and FtsB and which are involved in the recruitment of downstream proteins. We have received the GFP-tagged plasmids from the Beckwith lab, so we just need to clone in the mutations of interest. For recruitment experiments we can use artificial septal targeting[7]. We already know that the interaction of FtsL and FtsB is essential for cell division, but the details on how this interaction is stabilized exactly, is not clear. Another aspect of the project has been to refine the structural model we currently have (**Chapter 2**) but this preliminary work is not included in this document.

3.6 Acknowledgements

I would like to acknowledge Senes lab undergraduate student, Joel Lange, for his help with the molecular biology for this project. He also helped with the western blotting of the flag-tagged FtsB and FtsL proteins to check for consistent overexpression. I would also like to acknowledge Deena Al-Mahbuba who tested FtsB TM mutants during her rotation project at higher temperature, which yielded the exciting L12F and L15A results. Finally, I would like to thank graduate student from the Senes lab, Sam Craven, for his insightful discussion and for taking over this project. This project has been supported by the Senes lab grant NIH_R01_GM099752. I was also supported by the WARF Distinguished Graduate Fellowship.

3.7 References

1. Gonzalez, M. D. & Beckwith, J. Divisome under construction: distinct domains of the small membrane protein FtsB are necessary for interaction with multiple cell division proteins. J. Bacteriol. **191,** 2815–2825 (2009).
2. Gonzalez, M. D., Akbay, E. A., Boyd, D. & Beckwith, J. Multiple interaction domains in FtsL, a protein component of the widely conserved bacterial FtsLBQ cell division complex. J. Bacteriol. **192,** 2757–2768 (2010).
3. Khadria, A. S. & Senes, A. The transmembrane domains of the bacterial cell division proteins FtsB and FtsL form a stable high-order oligomer. Biochemistry (Mosc.) **52,** 7542–7550 (2013).
4. LaPointe, L. M. et al. Structural organization of FtsB, a transmembrane protein of the bacterial divisome. Biochemistry (Mosc.) **52,** 2574–2585 (2013).
5. Buddelmeijer, N. & Beckwith, J. A complex of the Escherichia coli cell division proteins FtsL, FtsB and FtsQ forms independently of its localization to the septal region. Mol. Microbiol. **52,** 1315–27 (2004).
6. Russ, W. P. & Engelman, D. M. TOXCAT: a measure of transmembrane helix association in a biological membrane. Proc. Natl. Acad. Sci. U. S. A. **96,** 863–8 (1999).
7. Goehring, N. W., Gonzalez, M. D. & Beckwith, J. Premature targeting of cell division proteins to midcell reveals hierarchies of protein interactions involved in divisome assembly. Mol. Microbiol. **61,** 33–45 (2006).

Chapter 4

Oligomerization State of Photosynthetic Core Complexes Is Correlated with the Dimerization Affinity of a Transmembrane Helix

This chapter was prepared for publication as:
Jen Hsin[1], Loren M. LaPointe[2], Alla Kazy[2], Christophe Chipot[1], Alessandro Senes[2], and Klaus Schulten.[1] Oligomerization state of photosynthetic core complexes is correlated with the dimerization affinity of a transmembrane helix. J. Am. Chem. Soc., (2011), 133 (35), pp 14071–14081.
[1]Department of Physics and Beckman Institute for Advanced Science and Engineering, University of Illinois at Urbana−Champaign, Urbana, Illinois 61801, United States
[2]Department of Biochemistry, University of Wisconsin−Madison, Madison, Wisconsin 53706, United States

Contribution:
This collaboration was part computational and part experimental. I performed the experimental work through TOXCAT of transmembrane domains found in PufX proteins in four species of purple bacteria.

Abstract

In the *Rhodobacter* (*Rba*.) species of photosynthetic purple bacteria, a single transmembrane α-helix, PufX, is found within the core complex, an essential photosynthetic macromolecular assembly that performs the absorption and the initial processing of light energy. Despite its structural simplicity, many unresolved questions surround PufX, the most important of which is its location within the photosynthetic core complex. One proposed placement of PufX is at the center of a core complex dimer, where two PufX helices associate in the membrane and form a homodimer. Inability for PufX of certain Rba. species to form a homodimer is thought to lead to monomeric core complexes. In the present study, we employ a combination of computational and experimental techniques to test the hypothesized homodimerization of PufX. We carry out a systematic investigation to measure the dimerization affinity of PufX from four Rba. species, Rba. blasticus, Rba. capsulatus, Rba. sphaeroides, and Rba. veldkampii, using a molecular dynamics-based free-energy method, as well as experimental TOXCAT assays. We found that the four PufX helices have substantially different dimerization affinities. Both computational and experimental techniques demonstrate that species with dimeric core complexes have PufX that can potentially form a homodimer, whereas the one species with monomeric core complexes has a PufX with little to no dimerization propensity. Our analysis of the helix–helix interface revealed a number of positions that may be important for PufX dimerization and the formation of a hydrogen-bond network between these GxxxG-containing helices. Our results suggest that the different oligomerization states of core complexes in various Rba. species can be attributed, among other factors, to the different propensity of its PufX helix to homodimerize.

4.1 Introduction

Compared to algae and plants, bacterial photosynthesis, while similar in its chemical principles of energy conversion, is a lot simpler in the structure and organization of the associated protein–pigment assemblies. Nonetheless, there are many unknown features regarding the macromolecular arrangement of some of the most critical photosynthetic complexes, one example being the core complex of purple photosynthetic bacteria. The photosynthetic core complex is a combination of two major transmembrane (TM) protein–pigment complexes that carry out the initial steps of the photosynthetic process: light-harvesting complex 1 (LH1) and the reaction center (RC). In some species of purple bacteria, most notably the *Rhodobacter* (Rba.) genus, the core complex contains an additional TM protein that is largely α-helical and is named PufX for *Rhodobacter*s. Some *Rhodobacter* core complexes can form dimers,(1, 2) resulting in a large assembly with a dimension of approximately 20 nm × 10 nm in the membrane plane (Figure 1)(1, 3-10).

The TM protein PufX is known to be crucial in the formation of dimeric photosynthetic core complexes in *Rba. sphaeroides*,(14) and deletion of this protein leads to monomeric core complexes.(2, 9, 15) Yet, as the location of PufX is still being debated, the molecular mechanism with which PufX determines the oligomerization state of the core complex is still an active topic of discussion.(15) Two models have been proposed for the placement and organization of PufX, each model involving a different mechanism for the PufX-assisted dimerization of the core complex (Figure 1). Figure 1a depicts a central placement of PufX, and the dimerization of the TM region of PufX “fuses” the two core complex monomers together.(4, 6, 16, 17) In contrast, Figure 1b shows a placement of PufX near the gap of the two open LH1 rings,(7) and in this scheme PufX is thought to induce core complex dimerization via interaction of its long N-terminal region in the cytoplasmic space.(7, 11, 12) A

crystallographic structure of a dimeric core complex is not yet available to determine unambiguously the validity of either model, although it has also been speculated that different species of *Rba*. bacteria might have different protein organizations in the core complex.(15, 18)

Interestingly, the oligomerization states of different *Rba*. core complexes are not the same. Through atomic force microscopy (AFM) imaging of the *Rba. blasticus* photosynthetic membrane, dimeric core complexes have been identified, although monomeric core complexes were also observed at an approximately 3:1 dimer to monomer ratio.(6) The *Rba. sphaeroides* core complex has also been shown to form dimers,(2, 4, 7, 9) with monomeric core complexes present as well at a 1:1 dimer to monomer ratio.(18) Unlike *Rba. blasticus* and *Rba. sphaeroides*, the *Rba. veldkampii* core complex was observed to be monomeric in a structural and functional analysis,(19) and microscopy studies also reported no sighting of dimeric core complex in the *Rba. veldkampii* photosynthetic membrane,(13, 17, 20) suggesting that *Rba. veldkampii* core complex is unable to dimerize. While there is no structural information available for the *Rba. capsulatus* core complex, its PufX can replace that of *Rba. sphaeroides*, and the resulting *Rba. sphaeroides* is still photosynthetically viable,(15) prompting the idea that *Rba. sphaeroides* and *Rba. capsulatus* core complexes are likely very similar, and that the core complex of *Rba. capsulatus* is also capable of dimerizing.

Examining the sequences of PufX in four *Rba*. bacteria, it can be noted that some sequence similarities exist (Figure 1c).(13, 15) In fact, it has been suggested that the GxxxG motif found in *Rba. sphaeroides* PufX between amino acids 31 and 35 (the N-terminal Met = 0 convention is adopted here) might serve as the dimerization region,(17, 21) similar to that in glycophorin A (GpA).(22) Computational investigations have subsequently shown that a *Rba. sphaeroides* PufX dimer appears to be stable in a 1-palmitoyl-2-oleoyl-sn-glycero-3-phosphoethanolamine (POPE) membrane.(23)

However, the GxxxG motif between locations 31 and 35 is only present in *Rba. sphaeroides*, not in *Rba. blasticus* or *Rba. capsulatus*, which also have a dimeric core complex. In addition, mutation of the glycines in this motif does not appear to abolish the ability for *Rba. sphaeroides* core complex to dimerize, as shown both computationally(23) and experimentally.(18) Furthermore, as shown in Figure 1c, GxxxG motifs are also present in *Rba. capsulatus* and *Rba. veldkampii*, although not between positions 31 and 35. A purely sequence-based argument for the dimerization affinity of PufX and the variability in core complex oligomerization state, thus, seems to be still inconclusive and requires further investigation.

In an effort to provide new insight into the potential dimerization of the PufX TM region, a prerequisite for the validity of the core complex organization shown in Figure 1a, and to relate dimerization of PufX segments to the core complex oligomerization state, we employed both computational and experimental methods to measure the dimerization affinity of four species of PufX: *Rba. blasticus, Rba. capsulatus, Rba. sphaeroides,* and *Rba. veldkampii*. We first constructed monomeric and dimeric PufX models for *Rba. blasticus, Rba. capsulatus*, and *Rba. veldkampii*, and then probed the stability of these structures in a membrane environment using all-atom molecular dynamics (MD), similar to the strategy previously followed for *Rba. sphaeroides* PufX.(23) Subsequently, TOXCAT(24) was performed on the four PufX TM segments to quantitatively measure the strength of helix–helix association. To complement the experiment, we also computed the apparent dimerization free energy for the four PufX helices using an MD-based free-energy protocol. Our data reveal a compelling trend on the strength of PufX dimerization: species capable of forming a dimeric core complex have PufX helices that show higher propensity to self-associate. Conversely, *Rba. veldkampi*i, which is observed with only monomeric core complexes, has a PufX that exhibits very

little propensity toward homodimerization. These results strongly indicate that differences in PufX dimerization affinity is an important factor for the variability of oligomerization states in Rba. photosynthetic core complexes.

4.2 Materials Methods

4.2.1 Molecular dynamics construction of monomeric and dimeric PufX

As there are currently no structural data available for PufX from *Rba. blasticus, Rba. capsulatus*, and *Rba. veldkampii*, the monomeric PufX models in simulations *blasticus-Monomer-POPE, capsulatus-Monomer-POPE, and veldkampii-Monomer-POPE* (Table 1) were constructed on the basis of that of *Rba. sphaeroides* PufX, for which two solution structures have been reported(11, 21) and were used in previous modeling studies.(23, 25-29) All PufX monomers were modeled with an integral TM helix with the same length as that of *Rba. sphaeroides* PufX.(21) Because we are only interested in the TM interaction of PufX helices, the N- and C-terminal residues that are thought to form loops(11, 21) were not included. These monomeric PufX structures were then placed in a POPE membrane patch, with addition of neutralizing Na+ and Cl– ions at a total ionic strength of 300 mM, as shown in Figure 2a–c. For comparison, the *Rba. sphaeroides* PufX monomer, constructed previously, (23) is shown in Figure 2d.

Equilibrium MD simulations were carried out for the three PufX monomer systems for 15 ns each. The final conformations of the PufX helices resulting from these monomer simulations were used to construct the corresponding PufX dimer models. Each PufX helix was replicated, and the two copies of PufX were placed facing each other by mapping them onto the GpA dimer structure,(22) as was previously done for *Rba. sphaeroides* PufX.(23) Because *Rba. blasticus, Rba. capsulatus*, and *Rba. veldkampii* do not have a GxxxG motif at position 31–35 (which *Rba. sphaeroides* possesses), amino acids 29–33 of *Rba. blasticus*, *Rba. capsulatus*, and *Rba. veldkampii* PufX were mapped onto the GxxxG portion of GpA. Choice of position 29–33 is based on the observation that *Rba. blasticus*, *Rba. capsulatus*, and *Rba. sphaeroides* all have a GxxxA or GxxxG motif at this segment, while *Rba.*

veldkampii does not. In fact, Gly29 is conserved in all four species as shown in Figure 1c.

Table 1. List of Molecular Dynamics Simulations Performed in the Present Study[a]

simulation name	type	number of atoms	time (ns)
blasticus-Monomer-POPE	EQ	32 812	15
capsulatus-Monomer-POPE	EQ	34 004	15
veldkampii-Monomer-POPE	EQ	32 904	15
blasticus-Dimer-POPE	EQ	31 801	50
capsulatus-Dimer-POPE	EQ	30 949	50
veldkampii-Dimer-POPE	EQ	32 336	100
blasticus-Dimer-DODE-1	EQ	20 486	10
capsulatus-Dimer-DODE-1	EQ	20 487	20
veldkampii-Dimer-DODE-1	EQ	20 557	10
blasticus-Dimer-DODE-ABF-1	ABF	20 486	220
capsulatus-Dimer-DODE-ABF-1	ABF	20 487	285
veldkampii-Dimer-DODE-ABF-1	ABF	20 557	185
blasticus-Dimer-DODE-2	EQ	20 496	20
capsulatus-Dimer-DODE-2	EQ	20 559	20
veldkampii-Dimer-DODE-2	EQ	20 503	20
blasticus-Dimer-DODE-ABF-2	ABF	20 496	55
capsulatus-Dimer-DODE-ABF-2	ABF	20 559	105
veldkampii-Dimer-DODE-ABF-2	ABF	20 503	70
sphaeroides-Dimer-DODE-ABF	ABF	20 584	170

[a] Total simulation time: 1.435 μs.

All PufX dimers were also placed in a POPE membrane patch, and similarly neutralized with additional ions at a total ionic strength of 300 mM, as shown in Figure 2e–g. The *Rba. sphaeroides* PufX dimer system(23) is shown in Figure 2h for comparison. An equilibrium MD simulation was performed for each of the resulting PufX dimer systems, designated as *blasticus-Dimer-POPE*, *capsulatus-Dimer-POPE*, and *veldkampii-Dimer-POPE* in Table 1, for at least 50 ns.

4.2.2 Equilibrium molecular dynamics

All simulations were performed using the MD package NAMD(30) with the CHARMM27 force field,(31, 32) including CMAP corrections.(33) Water molecules were described with the TIP3P

model.(34) Long-range electrostatic forces were evaluated by means of the particle-mesh Ewald (PME) summation approach with a grid spacing of <1 Å. An integration time step of 2 fs was used in the framework of the Verlet r-RESPA algorithm.(35) Bonded terms and short-range, nonbonded terms were evaluated every time step, and long-range electrostatics was evaluated every other time step. Constant temperature (T = 310 K) was maintained using Langevin dynamics,(36) with a damping coefficient of 1.0 ps–1. A constant pressure of 1 atm was enforced using the Langevin piston algorithm(37) with a decay period of 200 fs and a time constant of 50 fs.

4.2.3 Free-Energy calculations

To assess computationally the dimerization affinity of the PufX helices, adaptive biasing force (ABF) calculations(38-40) were performed to determine free-energy as a function of helix–helix distance.(40, 41) Prior to conducting ABF simulations, the PufX TM segments were equilibrated in a dodecane patch in a solvent environment neutralized with ions at 300 mM ionic strength. Use of dodecane as a lipid mimetic is dictated by the slow relaxation times of natural lipid molecules as compared to affordable MD time scales.(23, 40, 42) The TM segments of PufX were blocked at the N- and C-termini by Ac– and −NHMe groups, respectively. Two sets of PufX dimer–dodecane systems were constructed (*blasticus-Dimer-DODE-1*, *capsulatus-Dimer-DODE-1*, *veldkampii-Dimer-DODE-1*, *blasticus-Dimer-DODE-2*, *capsulatus-Dimer-DODE-2*, and *veldkampii-Dimer-DODE-2* in Table 1), using slightly different TM segments to test if inclusion of different residues would alter significantly the results of free-energy calculations. Each protein–dodecane system was subject to equilibrium MD for at least 10 ns. An example setup of the dodecan–PufX system is shown in Figure S1 in the **Supporting Information**.

ABF calculations were carried out subsequently in the framework of NAMD(30) for the six

dodecane systems *(blasticus-Dimer-DODE-ABF-1*, *capsulatus-Dimer-DODE-ABF-1*, *veldkampii-Dimer-DODE-ABF-1*, *blasticus-Dimer-DODE-ABF-2*, *capsulatus-Dimer-DODE-ABF-2*, and *veldkampii-Dimer-DODE-ABF-2* in Table 1). The TM portion of a modeled *Rba.sphaeroides* PufX dimer was previously equilibrated in a dodecane patch,(23) and an ABF calculation was also performed for *Rba.sphaeroides* PufX, designated as *sphaeroides-Dimer-DODE-ABF* in Table 1. For each ABF simulation, the model reaction coordinate, ξ, is defined as the distance separating the center of mass of the two helices, in the interval 4.5 Å $\leq \xi \leq$ 27 Å. A small ξ indicates that the PufX helices are associated, with a large ξ indicating their separation. In the course of an ABF simulation, average forces applied on the PufX helices in an unconstrained MD simulation are projected onto ξ, and a "biasing force" is calculated and applied to the helices to overcome local energy barriers.(38-40) The free-energy profile along ξ is then obtained by integrating the average force, with a standard error estimated according to Rodriguez-Gomez et al.(43)

4.2.4 TOXCAT

Vectors and constructs

The TOXCAT vector, pccKAN, and positive controls containing the TM domain of wild type GpA (pccGpA-WT) and the G83I disruptive mutant (pccGpA-G83I) have been described previously.(24) DNA coding for the TM domains of the PufX proteins (Table 2), flanked by 5′*Nhe*I and 3′*Bam*HI restriction sequence, was purchased as synthetic genes (IDT). The sequences were ligated in-frame to *Nhe*I and *Bam*HI sites of the pccKAN vector.

Table 2. Sequences of the TM Regions of ToxR′(TM)MBP Constructs[a]

Species	Amino Acid Sequence
Rba. blasticus	**NRAS**QMVWGAFLAAVGVVVVICLLVGT**GIL**
Rba. capsulatus	**NRAS**QMAYGAFLGSIPFLLGLGLVLGS**GIL**
Rba. sphaeroides	**NRAS**QMMKGAGWAGGVFFGTKKKIGFF**GIL**
Rba. veldkampii	**NRAS**AMGKGMGITAVVFFGTVFFVVAL**GIL**

[a] Boldface residues represent the TOXCAT construct flanking regions including those containing the restriction site codons used for subcloning into the TOXCAT construct.

Expression of ToxR'(TM)MBP constructs

Plasmids encoding ToxR′(TM)MBP chimerae were transformed into Escherichia coli MM39 cells (provided by D. M. Engelman) and plated onto Luria–Bertani (LB) plates (with 100 μg/mL ampicillin and 25 μg/mL streptomycin); colonies were inoculated into LB medium (with 100 μg/mL ampicillin) and stored as glycerol stocks at −80 °C. LB cultures (with 100 μg/mL ampicillin) were inoculated from frozen glycerol stocks and grown overnight (approximately 18 h). Three mL LB cultures (with 100 μg/mL ampicillin) were inoculated using 50 μL overnight cultures and grown to A420 1.0, and 1 mL of cells was harvested by centrifugation and resuspended in 0.5 mL of lysis buffer (25 mM Tris-HCl, 2 mM EDTA, pH 8.0). Cells were then lysed by probe sonication. The lysate was clarified by centrifugation at 17 000*g*, and the supernatant was stored on ice until the spectrophotometric assay was performed.

Spectrophotometric CAT assay

The colorimetric assay used to detect chloramphenicol acetyltransferase activity in cell lysates was described previously.(44, 45) Absorbance was measured using a PerkinElmer Lambda 25 UV/vis spectrophotometer. 40 μL of lysate was mixed with 1 mL of reaction buffer (0.1 mM acetyl-coA, 0.4

mg/mL 5,5′-dithiobis-(2-nitrobenzoic acid), 0.1 M Tris-HCl, pH 7.8), and absorbance at 412 nm was measured for a period of 2 min with intervals of 3 s to establish a basal rate of acetyl-coA hydrolysis in the absence of substrate. At 2 min, 40 μL of 2.5 mM chloramphenicol was added with mixing, and the absorbance was measured at 412 nm for another 2 min in 3 s intervals. CAT activity was calculated as the slope of 412 nm absorbance, after subtracting the basal rate prior to substrate addition. Lysates were assayed in triplicate, and the reported data are the result of three separate experiments.

Maltose complementation assay

To confirm correct membrane insertion, E. coli MM39 cells expressing the ToxR′(TM)MBP constructs were grown overnight in LB (with 100 μg/mL ampicillin) and then streaked onto M9 minimal media plates containing 0.4% maltose as the only carbon source and incubated for 3 days at 37 °C.

Western Blot analysis

TOXCAT protein expression levels were verified by Western blot analysis. Cell lysate was mixed with 2× SDS-PAGE sample buffer, heated to 70 °C for 10 min, run on precast 12% polyacrylamide gels (Invitrogen), transferred onto an Immobilon-P polyvinylidene fluoride membrane (Millipore), and detected with rabbit anti-MPB primary antibodies (New England Biolabs) and antirabbit horseradish peroxidase conjugate secondary antibodies (Millipore).

4.3 Results and Discussion

Below, our computational and experimental results are discussed. First, we report the stability of different species of PufX helices in monomeric and homodimeric conformations as probed by equilibrium MD simulations. Next, we present the dimerization affinity of PufX helices as measured using the TOXCAT assay. Finally, complementing TOXCAT experiments with atomic resolution and quantitative assessment, we report MD-based free-energy calculations conducted to estimate the apparent dimerization free energy, ΔG_{app}, of PufX helices.

4.3.1 Equilibrium molecular dynamics

PufX Monomers

All three PufX monomers were seen to be structurally stable during their respective equilibrium MD simulations. Similar to *Rba. sphaeroides*, the PufX helices of *Rba. blasticus*, *Rba. capsulatus*, and *Rba. veldkampii* were seen to tilt with respect to the normal of the lipid bilayer during simulations. Examining the sequence content of PufX from the different species, it was observed that *Rba. veldkampii* is the only case without either a tyrosine or a tryptophan residue. Tyrosine and tryptophan residues are known to reside preferentially at the lipid–water interface(46) and might contribute to the anchoring of a TM helix to the lipid headgroups.(47-49) As can be seen in Figure 2a–d, for *Rba. blasticus*, *Rba. capsulatus*, and *Rba. sphaeroides* PufX that contain tyrosine and tryptophan, most of these residues appear near the membrane–solvent interface.

The helical structures of all PufX models persisted throughout the simulations, as shown in Figure 3a. Structural stability of each PufX monomer is consistent with the two-stage model of membrane–protein folding, which postulates that TM helices act as independent stable domains and are preformed prior to their association into large protein complexes(50, 51).

PufX Dimers

Each PufX dimer model was constructed using the final conformation from the equilibrium simulations of monomeric PufX, as described in the **Methods**. All three dimer systems were observed to be structurally robust with consistent α-helical content throughout the simulation (Figure 3b). The dimerized PufX helices also maintained a consistent crossing-angle (Figure 3c) and remained in contact during the simulation as indicated by the measurement of the buried solvent-accessible surface area (SASA) (Figure 3d). For all three species, buried SASA of the PufX dimers remained near or above 600 Å2, comparable to that of GpA (52).

The most notable motion was seen in the case of *Rba. veldkampii* PufX, which lacks both tyrosine and tryptophan, and transformed from an originally upright orientation (Figure 3e) to one tilted relative to the membrane at 50 ns (Figure 3f), and with one of the helices submerged in the lipid phase on the C-terminus. This tilted and partially membrane-buried conformation of the *Rba. veldkampii* PufX dimer persisted when the simulation was extended to 100 ns. In comparison, the tyrosine and tryptophan residues in *Rba. blasticus* and *Rba. capsulatus* PufX dimers (Figure 3g and h, respectively) remained at the membrane–solvent interface, preventing strong fluctuations in their helix–membrane orientations. Quantitative measurement of helix tilting with respect to the membrane normal during the simulations *blasticus-Dimer-POPE*, *capsulatus-Dimer-POPE*, and *veldkampii-Dimer-POPE* is shown in Figure S2 in the **Supporting Information**. The instability of *Rba. veldkampii* PufX helices due to the lack of anchorage might be significant in the propensity of the helices to homodimerize. Additionally, it can be seen that the proline residue at position 36 in *Rba. capsulatus* PufX induces a moderate kink in the helix (10–30°) that persisted throughout the simulations for both the mononeric and the dimeric conformations (Figure S3); this residue does not face the dimerization interface in the

modeled *Rba. capsulatus* PufX dimer.

Interhelical interactions contributing to the stability of PufX dimer models are shown in Figure 4a–c for *Rba. blasticus*, *Rba. capsulatus*, and *Rba. veldkampii*, respectively. For *Rba. blasticus* and *Rba. capsulatus*, significant molecular interactions are contributed by residues Gln25 and Met26, which interact with each other, and also with other small amino acids such as glycine and alanine. For example, Gln25 was seen to interact with Ala22, and Met26 interacted with Gly29 in *Rba. blasticus* PufX dimer (Figure 4a). The Met26–Gly29 interaction was also observed for *Rba. capsulatus*, and its Gln25 was observed to interact with Ile22 (Figure 4b). Also, helix packing is achieved through close contact between small residues Gly29 and Ala30 for both *Rba. blasticus* and *Rba. capsulatus* (Figure 4a and b). Notably, while Gly29 is conserved for all four species investigated in the present study, *Rba. veldkampii* is the only species that does not contain Gln25 and Ala30 (Figure 1c), two residues that contribute significantly to interhelical interactions for *Rba. blasticus* and *Rba. capsulatus*. For *Rba. veldkampii* PufX dimer, the helices are held together by a slightly different set of molecular interactions, although Met26, which is conserved in all four PufX sequences (Figure 1c), plays also an important role (Figure 4c). Further away from the dimerization core, bulkier amino acids such as Val37 for *Rba. blasticus*, and Phe37 for *Rba. capsulatus* and *Rba. veldkampii*, provide additional interhelix contact.

Table 3. Geometry of Potential $C_\alpha-H\cdots O$ Hydrogen-Bond Contacts[a]

donor	acceptor	d_H (min value)	d (min value)	ζ	ξ	θ
			Ideal Values			
		≤2.7	≤3.8	180	120	0
			Rba. blasticus			
A22	A22	4.04 (3.03)	4.75 (3.75)	127.06	103.68	28.11
M26	Q25	3.65 (2.54)	4.42 (3.42)	131.82	85.87	29.44
A30	G29	3.06 (2.78)	3.83 (3.13)	129.28	96.57	17.14
A34	A33	3.90 (2.76)	4.69 (3.66)	132.64	96.42	39.62
			Rba. capsulatus			
I22	Q25	3.01 (2.20)	4.03 (3.27)	158.92	110.55	54.45
M26	Q25	2.86 (2.24)	3.80 (3.14)	146.67	120.92	61.52
A30	G29	2.97 (2.21)	3.56 (3.01)	115.23	108.14	15.58
S34	G33	4.79 (2.81)	5.58 (3.80)	133.70	115.98	38.84
			Rba. veldkampii			
M26	A25	2.61 (2.14)	3.51 (3.07)	141.31	115.86	46.91
M30	G29	2.82 (2.17)	3.65 (3.11)	135.74	104.27	13.96

[a] Definitions of distances and angles are given as the following:[54,57] d_H is the distance between the H and O atoms; d is the distance between the C_α and the O atoms; ζ is the $C_\alpha-H-O$ angle; ξ is the $H-O-C$ angle; and θ is the elevation angle between the $C_\alpha-H$ vector and the amide plane. All numbers are average values from the last 10 ns of corresponding simulations (*blasticus-Dimer-POPE*, *capsulatus-Dimer-POPE*, and *veldkampii-Dimer-POPE*). Distances are given in angstroms, and angles are given in degrees.

Interhelical hydrogen bonds are known to be an important factor in mediating helix–helix

association in the membrane.(53) The close packing of the modeled PufX dimers permitted the formation of several interhelical hydrogen bonds. In particular, the side-chain amide group of Gln25 forms an interhelical hydrogen bond with the carbonyl of Ala22 in the Rba. blasticus dimer (Figure 5). The same side chain accepts a Cα–H···O hydrogen bond from Ile22 in the Rba. capsulatus dimer. As mentioned above, *Rba. veldkampii* is the only species that does not contain Gln25. Several backbone-to-backbone Cα–H···O hydrogen bonds were also observed (illustrated in Figure 5 and Table 3), which are a hallmark of GxxxG-mediated transmembrane interactions.(53-58) The Gln25–Met26 and Gly29–Ala30 pairs were seen to be sites for the potential formation of Cα–H···O hydrogen bonds for the cases o f *Rba. blasticus* and *Rba. capsulatus* PufX dimers, and locations 33 and 34, which contain small amino acids such as alanine, serine, and glycine, provide additional hydrogen bonding (Figure 5 and Table 3). For the case of *Rba. veldkampii* PufX dimer, only two Cα–H···O hydrogen bonds were observed and were also formed between amino acid pairs 25–26 (Ala25–Met26) and 29–30 (Gly29–Met30).

4.3.2 TOXCAT

The equilibrium MD simulations of the three PufX dimers conducted here, as well as the one conducted previously for *Rba. sphaeroides*,(23) showed that PufX dimer models for all four species remain associated. Although it appears that the *Rba. veldkampii* PufX dimer has an unstable protein–membrane interaction due to the lack of anchorage, no spontaneous disassociation was observed. It is possible that disassociation of PufX requires longer simulation time than is currently feasible due to the slow relaxation time of a full POPE membrane.

To determine quantitatively the dimerization affinity of the PufX helices, we employed an experimental assay, the TOXCAT method,(24) which measures the association of TM helices in a

biological membrane. Three TOXCAT measurements were performed on each of the four Rba. species, with the average dimerization affinity for each species shown in Figure 6b as percent of the CAT activity of GpA. *Rba. capsulatus* is seen to have the highest propensity for homodimerization, with a relative CAT activity at ~30%, comparable to a prior measurement reported in Aklujkar and Beatty(59). *Rba. blasticus* has the second highest CAT activity, albeit only at ~15% GpA. *Rba. sphaeroides* shows even lower propensity to homodimerize, and *Rba. veldkampii* exhibits no significant CAT activity.

4.3.3 Free-Energy Calculations

Concurrent to the experimental measurement of PufX dimerization affinity with TOXCAT, we also employed free-energy calculations to measure the apparent dimerization free energy *in silico* using the ABF algorithm(38-40) for PufX from four *Rba. species*. The computational treatment is inspired by the atomic resolution of the method, which can reveal great structural details in the dimerization and disassociation pathway.

Two sets of ABF calculations were conducted corresponding to distinct choices of TM residues. In the first set, the same sequences as those used in TOXCAT (i.e., those shown in nonboldface in Table 2) were included. Because the TOXCAT experiments contain also flanking residues and are not identical to the setup of the in silico assays, to test if results from ABF are sensitive to the small difference in the sequence of amino acids, a second set of ABF simulations was conducted, using the sequences identified as the TM region from the dimer simulations carried out in the POPE environment (i.e., *blasticus-Monomer-POPE*, *capsulatus-Monomer-POPE,* and *veldkampii-Monomer-POPE;* Table 1). For *Rba. sphaeroides* PufX, the sequence used in TOXCAT is the same as that identified as the TM region;(23) therefore, only one ABF simulation was performed (*sphaeroides-Dimer-DODE-ABF* in Table 1).

The dimerization pathway of PufX is observed to be more complex than that of GpA,(40) with an example shown in Figure 7 for the case of *Rba. sphaeroides* PufX. At the beginning of the ABF simulation *sphaeroides-Dimer-DODE-ABF*, the two PufX helices are both straight (Figure 7a). However, spontaneous bending occurred after 13 ns (Figure 7b, left), in agreement with prior *in silico* observation on the inherent flexibility of the *Rba. sphaeroides* PufX helix(23). Furthermore, bending of the PufX helix occurs at the same location as that seen for one of the PufX solution structures,(11) and, as a result, the bent conformation seen in simulation *sphaeroides-Dimer-DODE-ABF* is structurally very similar to the solution structure (Figure 7b, right). Helix bending persisted for a few tens of a nanosecond, but eventually the helix spontaneously straightened (Figure 7c). Previously, we had estimated that bending of the *Rba. sphaeroides* PufX only costs a few kcal/mol;(23) our present results support such a low value. We note that the tendency for *Rba. sphaeroides* PufX to bend might complicate self-association, but does not completely prohibit it as the helix quickly straightens back and the straight conformation can possibly be stabilized by dimerization.

The results from the two sets of ABF calculations are compared in Figure 8 in the form of free-energy profiles as a function of helix–helix distance. For the first set of ABF calculations (Figure 8a), all four species of PufX are seen to have energy minima for an associated, dimerized conformation, albeit with different well depths. *Rba. veldkampii* has the most shallow free-energy minimum near a helix–helix separation of 12 Å. *Rba. sphaeroides* has the second-most shallow free-energy minimum. Unlike the GpA dimer, which exhibits a well-defined free-energy well,(40) the free-energy well of *Rba. sphaeroides* PufX is seen to span nearly 5 Å, with the minimum occurring near 8 Å. *Rba. blasticus* and *Rba. capsulatus* have the deepest free-energy wells, and both possess multiple local minima. For *Rba. capsulatus*, two local free-energy minima are found at helix–helix distances of 8 and 11 Å; for *Rba.*

blasticus, its free-energy well has several less well-defined local minima that stretch up to a helix–helix distance of 15 Å. The much wider free-energy well for *Rba. blasticus* PufX is possibly due to additional stabilizing interhelical interactions arising from transient van der Waals contact between the bulkier Leu43, Leu44, and Thr47 residues near the C-terminal end (Figure S4 in the **Supporting Information**). In general, the PufX dimers exhibit more complex free-energy profiles than does the GpA dimer.(40) This extra complexity is possibly due to the usage of modeled dimer systems rather than experimentally derived structures. Alternatively, it is also possible that the complex dimerization scheme is intrinsic to PufX due to its difference to GpA.

In the second set of ABF simulations (Figure 8b), *Rba. veldkampii* appears to have no preference for association. *Rba. capsulatus* PufX is seen to have a deeper free-energy well than that of *Rba. blasticus* and retains the two minima observed in Figure 8a, albeit at closer helix–helix distances (7 and 9 Å). *Rba. blasticus* PufX again exhibits a wide minimum, with the global free-energy minimum occurring at a helix–helix distance of 9 Å. Although the precise free-energy profiles are different in the two sets of ABF simulations, it is reassuring that distinct features in the *Rba. blasticus* and *Rba. capsulatus* free-energy profiles are preserved across the two simulations. Additionally, *Rba. veldkampii* PufX consistently exhibits the lowest propensity toward dimerization.

Table 4. Free Energy of Association[a]

species	ΔG_{app} from ABF1 (kcal/mol)	ΔG_{app} from ABF2 (kcal/mol)
Rba. capsulatus	6.7 ± 0.3	9.4 ± 0.3
Rba. blasticus	6.8 ± 0.4	6.6 ± 0.5
Rba. sphaeroides	5.2 ± 0.4	n/a
Rba. veldkampii	3.8 ± 0.3	0

[a] Two ABF calculations were conducted each for *Rba. blasticus*, *Rba. capsulatus*, and *Rba. veldkampii* PufX segments using slightly different amino acid sequences (Figure 8), and one ABF calculation was performed for *Rba. sphaeroides*.

From the free-energy profiles in Figure 8, we calculated the apparent disassociation free energy, ΔG_{app}, for the four species of PufX in two sets of ABF calculations using the expression utilized by Hénin et al.,(40) with the results shown in Table 4 and Figure 9. Calculation of ΔG_{app} allows comparison of PufX dimerization affinity with that of GpA (Figure 9), which has a ΔG_{app} value of 11.5 ± 0.4 kcal/mol as previously reported using also the ABF method in a dodecane environment.(40) It can be seen that the order of PufX dimerization affinity is similar to the experimental results (Figure 6), in the decreasing order of *Rba. capsulatus* > *Rba. blasticus* > *Rba. sphaeroides* > *Rba. veldkampii*. Differences in experimental and simulation setups might contribute to the consistent overestimate of *in silico* free energies as compared to TOXCAT measurements (Figures 9 and 6). For example, the PufX sequences used in the TOXCAT experiment and the ABF measurements are not exactly identical (Table 2 and Figure 8), and, as shown by comparing Figure 8a and b, small differences in sequence content can lead to varying dimerization affinity. Additionally, while TOXCAT was performed in a biological membrane environment, the ABF measurements were conducted with dodecane. Finally, the reaction coordinate, ξ, chosen in the ABF calculation does not consider the relative orientation of the two helices, including their intrinsic rotation about their longitudinal axis, a degree of freedom important in optimizing helix–helix packing. Considering these factors limiting direct comparison between experiment and simulation results, it is significant that a consensus in the relative strength of dimerization for the four PufX sequences tested here was reached.

4.4 Concluding Remarks

We have shown through experiments and molecular dynamics simulations that PufX from different *Rba. species* of purple photosynthetic bacteria exhibit distinct propensities toward homodimerization. This result can explain in part why core complexes have different oligomerization states in different species, namely, due to the different inherent affinity of the TM regions of PufX to dimerize. In particular, species with PufX shown to be least likely to dimerize, *Rba. veldkampii*, form only monomeric core complexes (13, 17). On the other hand, *Rba. blasticus* that possesses dimeric core complexes(6) is seen to have PufX with a relatively high dimerization affinity.

In addition to the ability for dimerization at the TM region, the presence of aromatic amino acids with polar groups (tyrosine and tryptophan) appears to aid in stabilizing PufX helices in the membrane. *Rba. veldkampii* PufX contains no tyrosine or tryptophan and also shows the lowest tendency for dimerization in its TM region. These two characteristics of *Rba. veldkampii* PufX, the lack of anchoring residues and a TM region with low likelihood for self-association, make *Rba. veldkampii* PufX a poor candidate for forming homodimers. Interestingly, a tryptophan residue on the N-terminal end of the TM region is part of the recently identified PufX motif that is missing in *Rba. veldkampii*, but present in *Rba. blasticus*, *Rba. capsulatus*, and *Rba. sphaeroides* (Figure 1c) (13).

While *Rba. blasticus*, *Rba. capsulatus*, and *Rba. sphaeroides* PufX show some preference for self-association, their dimerization affinity is significantly lower than that of GpA (52, 60). The lower dimerization affinity might be the reason why dimeric and monomeric core complexes are both present in *Rba. blasticus* and *Rba. sphaeroides*,(4, 6, 18) as a subset of PufX helices might be in monomeric forms in the photosynthetic membrane, residing in monomeric core complexes. It is also possible that dimerization of PufX requires additional molecular interactions other than those arising from the PufX

TM region, or between PufX and the rest of the core complex. For *Rba. sphaeroides*, there are experimental reports showing that the N-terminal segment of PufX is critical for the formation of dimeric core complexes,(12, 61) although the molecular role of these residues in PufX-assisted core complex dimerization is unclear. Dimerization of PufX might also be strengthened by interaction between PufX and LH1α helices observed previously for *Rba. sphaeroides* and *Rba. capsulatus*,(62) or by the binding of the light-absorbing pigment bacteriochlorophyll (shown in Figure 1a and b as crosses) to PufX (59, 63, 64). Speculation that different *Rba.* species might have different organizations for their core complexes has also been raised (15, 18).

While identification of a GxxxG motif in the *Rba. sphaeroides* PufX sequence at the 31–35 position is intriguing,(17, 21) the motif by itself does not explain the observed oligomerization states of *Rba.* core complexes. As alluded to above, *Rba. blasticus* lacks this particular sequence motif, yet it has been confirmed to contain dimeric core complexes.(6) It should be noted, however, that *Rba. blasticus*, *Rba. capsulatus*, and *Rba. sphaeroides* actually all feature a GxxxA/G motif at the 29–33 position that is not present in *Rba. veldkampii* (Figure 1c), with GxxxA previously suggested as a motif for dimerization of TM helices (55, 65-69). The glycine residue at position 29 in PufX is actually conserved across the four *Rba.* species, and an alanine residue is found at position 30 except for *Rba. veldkampii* PufX (Figure 1c), providing another small amino acid that allows for potential helix–helix interaction. It is conceivable that the combination of presence of protein–membrane anchoring provided by tyrosine or tryptophan, and small amino acids such as glycine and alanine at the helix–helix contact site, renders a PufX TM segment more prone to homodimerize.

Figure 4.1

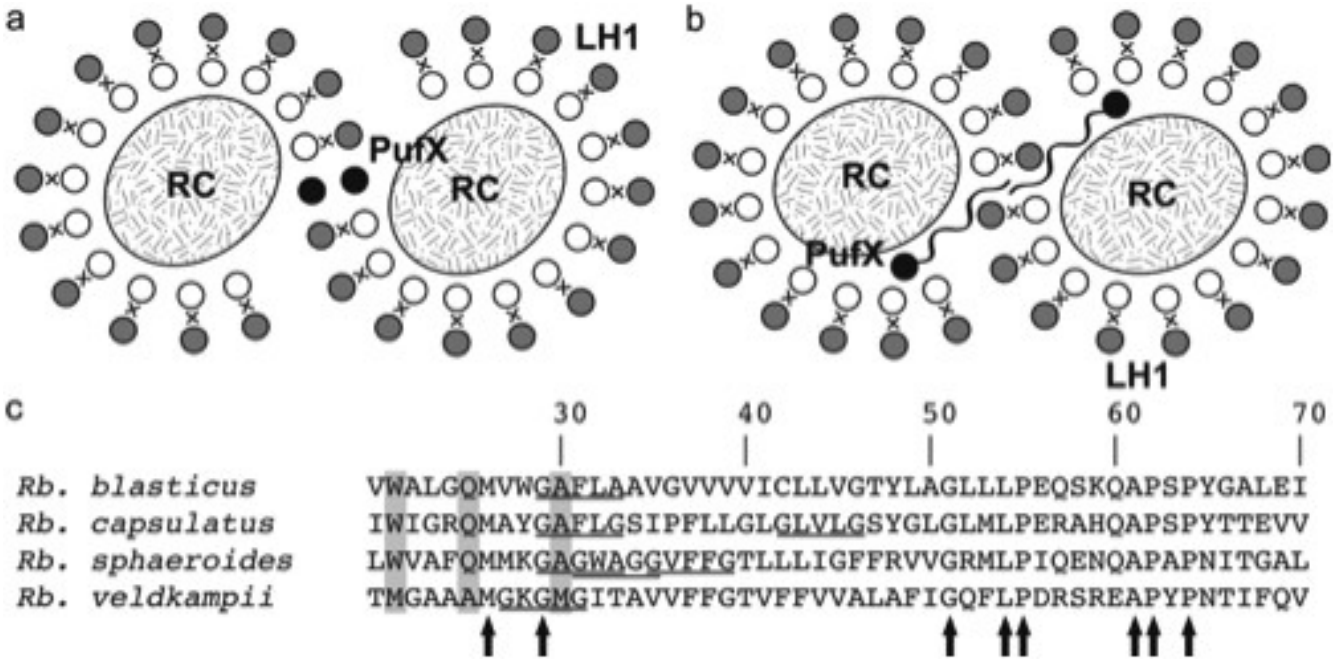

Figure 4.1 Proposed models for the protein organization of a dimeric photosynthetic core complex. (a) Model based on atomic force microscopy imaging studies of *Rba. sphaeroides* and *Rba. blasticus* photosynthetic membrane.(4, 6) PufX is placed at the dimerization interface in the center of the core complex and is itself also thought to be dimerized. (b) Model based on the highest resolution structural data to date of the dimeric *Rba. sphaeroides* core complex,(7) with PufX situated near the gap of the open LH1 ring, and association of PufX is facilitated through a long loop at the N-terminal region.(7, 11, 12) In (a) and (b), PufX helices are represented by black circles, while LH1 helices are shown as gray circles (outer helices, known as LH1β) and white circles (inner helices, known as LH1α), with the embedded pigments between the outer and inner helices denoted by "X". RC is shown as an oval. (c) Aligned sequences of the central region of PufX from four *Rhodobacter* species investigated in the present study. Conserved amino acids are indicated by arrows, and amino acids conserved in *Rba. blasticus, Rba. capsulatus*, and *Rba. sphaeroides*, but not in Rba. veldkampii, are

shaded in gray.(13) GxxxG and GxxxA motifs are underlined.

Figure 4.2

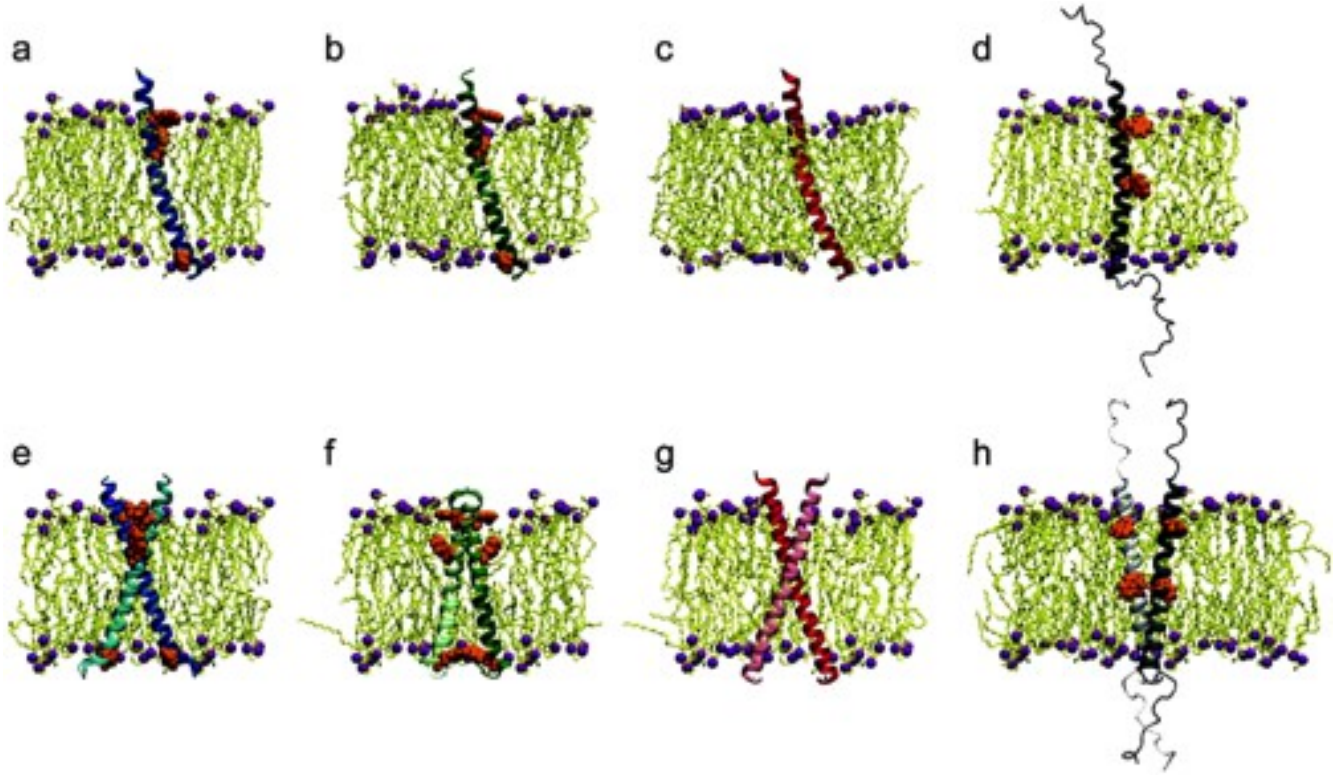

Figure 4.2 Simulated molecular systems with POPE lipid bilayers. Protein–membrane systems with monomeric PufX for (a) *Rba. blasticus*, (b) *Rba. capsulatus*, and (c) *Rba. veldkampii*. (d) Monomeric *Rba. sphaeroides* system is also shown for comparison; the simulation was performed previously.(23) PufX helix is shown in blue ((a) *Rba. blasticus*), green ((b) *Rba. capsulatus*), red ((c) *Rba. veldkampii*), and gray ((d) *Rba. sphaeroides*), lipid is shown in yellow with purple spheres representing the headgroups; polar-aromatic residues tyrosine and tryptophan of PufX are shown in orange. For clarity, water and ion molecules included in all simulations are not shown. (e–g) Protein–membrane systems with modeled homodimeric PufX for (e) *Rba. blasticus*, (f) *Rba. capsulatus*, and (g) *Rba. veldkampii*. (h) Dimeric *Rba. sphaeroides* system is also shown for comparison; the simulation was performed previously. 23). PufX helices in this and subsequent figures are shown with N-termini pointing upward.

Figure 4.3

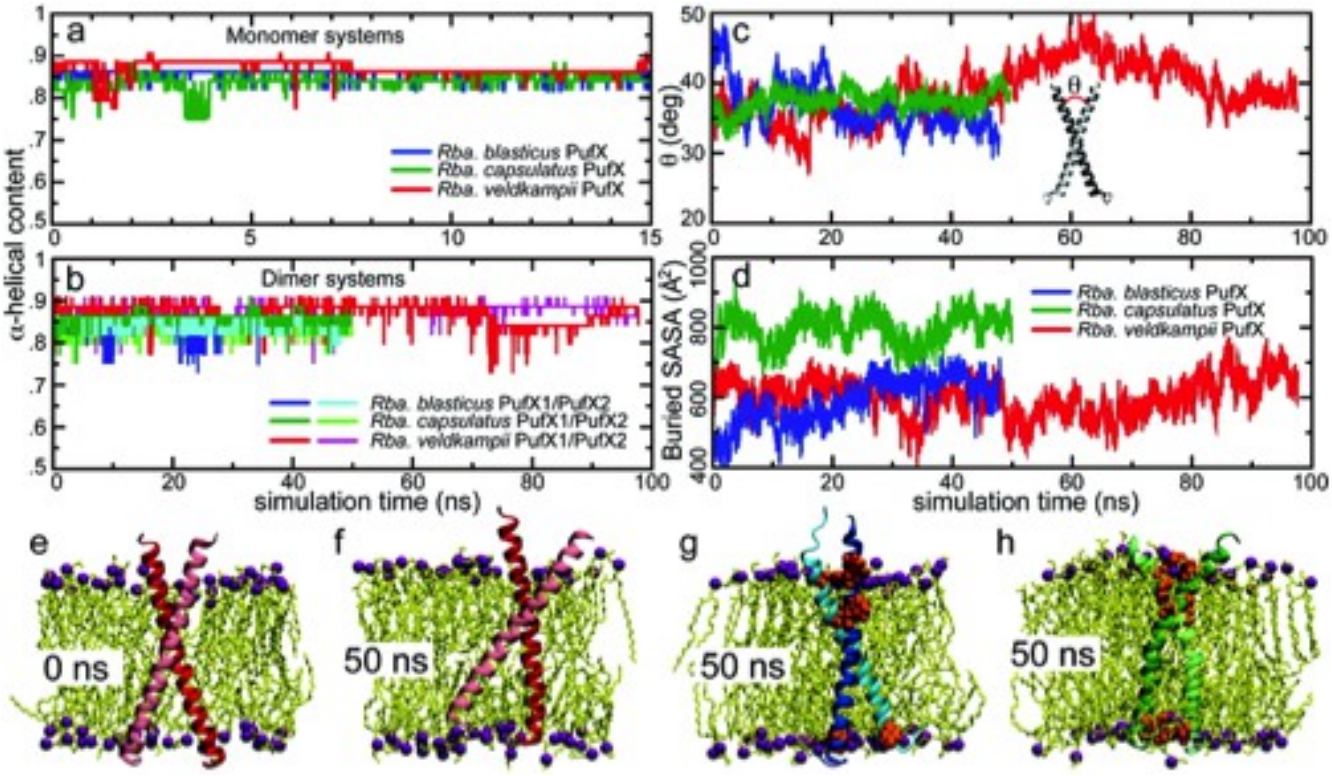

Figure 4.3 Stability of PufX monomeric and homodimeric helices during equilibrium MD simulations. (a) α-Helical content of the modeled PufX monomer in a full POPE membrane. For each of the three species tested (*Rba. blasticus*, *Rba. capsulatus*, and *Rba. veldkampii*), PufX retains its high α-helical content. Similarly, modeled PufX helices in dimeric conformation also remain largely α-helical, as shown in (b). (c) Crossing-angle between the dimerized helices. (d) Buried solvent-accessible surface area (SASA) as a measure for helix–helix interaction. Parts (e) and (f) show the movement of the *Rba. veldkampii* PufX helices. At 50 ns, one of the *Rba. veldkampii* helices can be seen to submerge nearly fully into the membrane on the C-terminus. For comparison, (g) and (h) show the *Rba. blasticus* and *Rba. capsulatus* PufX helices also at 50 ns; in these cases, the tyrosine and tryptophan residues aided in anchoring the helices in the membrane, and these residues remained at the

membrane–solvent interface throughout the simulation.

Figure 4.4

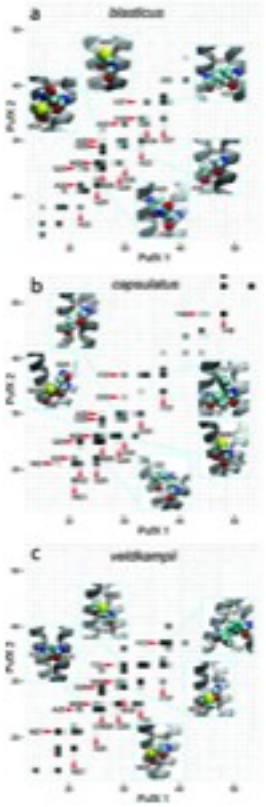

Figure 4.4 Interhelical interactions observed during the equilibrium molecular dynamics simulations (a) *blasticus-Dimer-POPE*, (b) *capsulatus-Dimer-POPE,* and (c) *veldkampii-Dimer-POPE*. In each interaction map, highly interacting amino acid pairs are highlighted with darker grids, and five of such pairs are shown in the insets as examples.

Figure 4.5

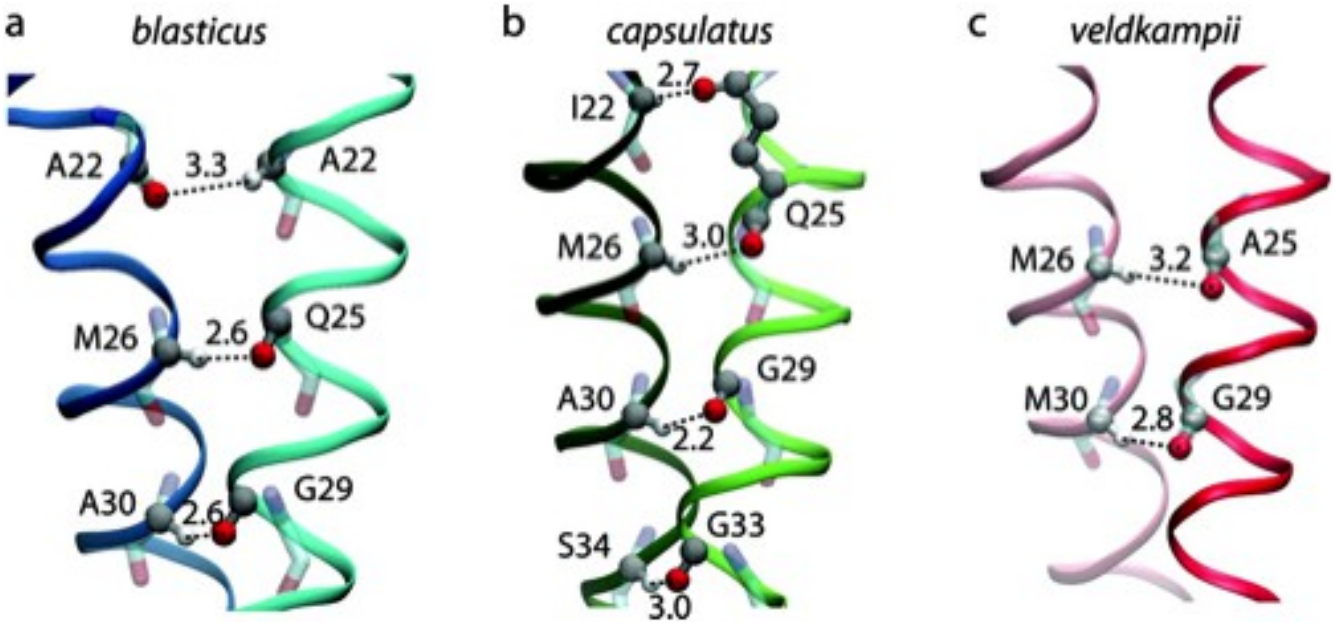

Figure 4.5 Networks of interhelical Cα–H···O hydrogen-bond contacts in the three PufX dimer models identified from simulations (a) *blasticus-Dimer-POPE*, (b) c*apsulatus-Dimer-POPE*, and (c) *veldkampii-Dimer-POPE*. For the amino acids involved in formation of Cα–H···O contacts, carbon atoms are shown in gray, oxygen atoms in red, hydrogen atoms in white, and other backbone atoms are shown in transparent. All H···O distances are shown in angstroms.

Figure 4.6

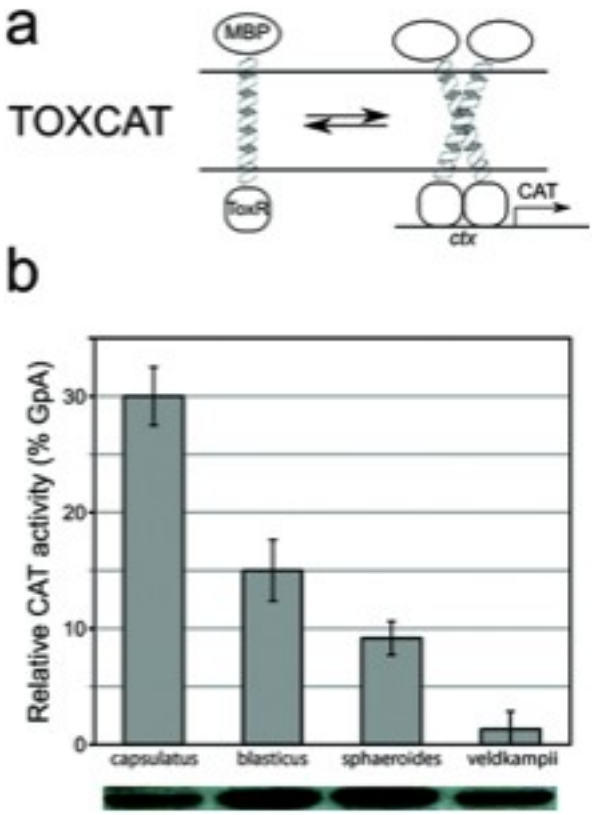

Figure 4.6 Quantification of association of TM constructs in E. coli membranes using TOXCAT. (a) TOXCAT(24) is an in vivo assay based on a fusion construct consisting of the TM domain under investigation, a maltose binding protein, and the ToxR transcriptional activator of V. cholerae. TM association results in the expression of chloramphenicol acetyl transferase (CAT) under the ctx promoter, whose enzymatic activity can be measured. (b) TOXCAT data for the PufX TM domains of *Rba. capsulatus*, *Rba. blasticus*, *Rba*. *sphaeroides*, and *Rba. veldkampii*. The data are reported as percent of the CAT activity of GpA, a strongly dimerizing transmembrane domain (22). The data are the average of three independent measurements, and the error bars report the standard deviation. Protein expression levels were verified by Western blot using anti-MBP antibodies.

Figure 4.7

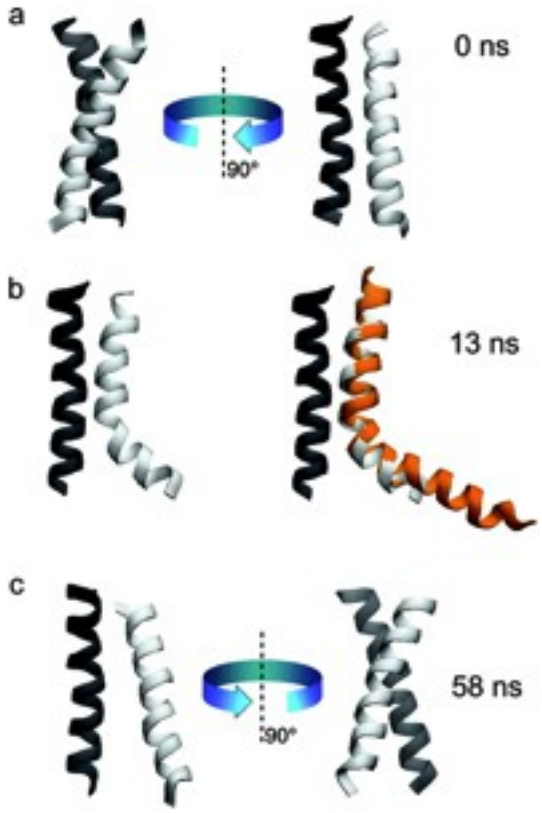

Figure 4.7 Spontaneous bending and straightening of *Rba. sphaeroides* PufX. (a) At the onset of the ABF simulation for *Rba. sphaeroides* PufX, both helices were straight. (b) At 13 ns, one of the helices bent spontaneously. The bending corresponded well to the observed NMR solution structure of PufX (pdb code 2NRG(11)) and persisted for the next ~40 ns. (c) The bent helix was seen to straighten back at 58 ns, suggesting that bending and straightening of the helix occur spontaneously with a low energy barrier, as suggested previously (23).

Figure 4.8

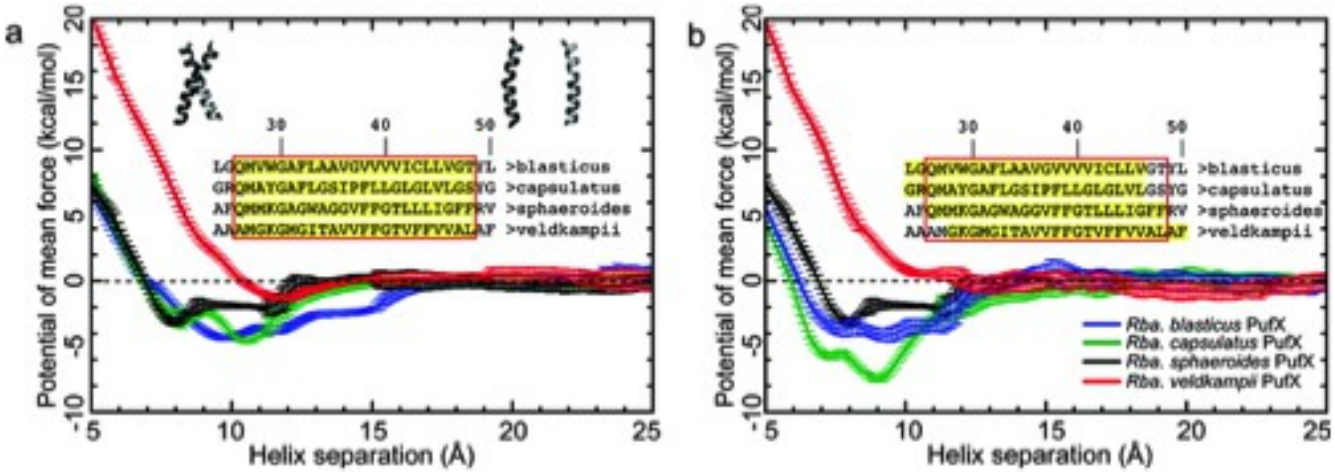

Figure 4.8 Potentiaof meal n force measured in ABF simulations. Highlighted sequences are those included in the ABF simulations; the sequences outlined in the red box are those included in the TOXCAT measurement (Table 2). (a) First set of ABF simulations using the same sequence for TM segments of PufX as that in TOXCAT experiments. (b) Second set of ABF simulations using the sequence identified as the TM segments in the PufX dimer–POPE membrane simulations

Figure 4.9

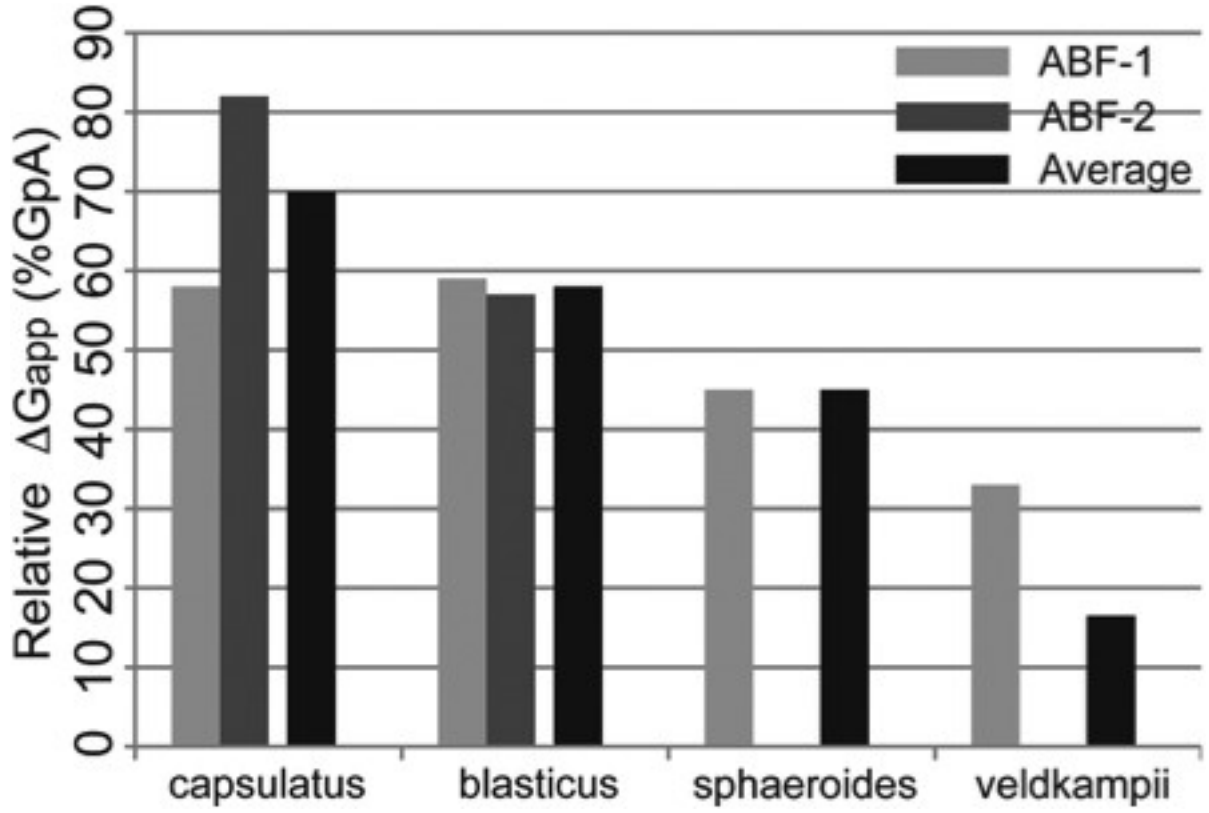

Figure 4.9 Free energy of association, ΔG_{app}, for various PufX sequences as a fraction of GpA ΔG_{app}. GpA ΔG_{app} was calculated in Hénin et al. (40).

4.5 Acknowledgements

We thank C. Neil Hunter and Pu Qian for many helpful discussions, Simon Scheuring for illuminating communications, and Ben Mueller for assistance in performing the TOXCAT assays. This work was supported by Grants NSF MCB-0744057 and NIH P41-RR005969. Computer time was provided by NCSA and TACC via Large Resources Allocation Committee Grant MCA93S028, resources of the Argonne Leadership Computing Facility at Argonne National Laboratory, supported by the Office of Science of the U.S. Department of Energy (Contract DE-AC02-06CH11357), and resources of the Oak Ridge Leadership Computing Facility at Oak Ridge National Laboratory, which is supported by the Office of Science of the U.S. Department of Energy under Contract DE-AC05-00OR22725.

4.6 References

1. Jungas, C.; Ranck, J.-L.; Rigaud, J.-L.; Joliot, P.; Verméglio, A. EMBO J. 1999, 18, 534– 542.

2. Siebert, C. A.; Qian, P.; Fotiadis, D.; Engel, A.; Hunter, C. N.; Bullough, P. A. EMBO J. 2004, 23, 690– 700.

3. Loach, P. A. Proc. Natl. Acad. Sci. U.S.A. 2000, 97, 5016– 5018.

4. Scheuring, S.; Francia, F.; Busselez, J.; Melandris, B. A.; Rigaud, J.-L.; Lévy, D. J. Biol. Chem. 2004, 279, 3620– 3626.

5. Scheuring, S.; Lévy, D.; Rigaud, J.-L. Biochim. Biophys. Acta 2005, 1712, 109– 127.

6. Scheuring, S.; Busselez, J.; Lévy, D. J. Biol. Chem. 2005, 280, 1426– 1431.

7. Qian, P.; Hunter, C. N.; Bullough, P. A. J. Mol. Biol. 2005, 349, 948– 960.

8. Cogdell, R. J.; Gall, A.; Köhler, J. Q. Rev. Biophys. 2006, 39, 227– 324.

9. Qian, P.; Bullough, P. A.; Hunter, C. N. J. Biol. Chem. 2008, 283, 14002– 14011.

10. Scheuring, S.; Sturgis, J. N. Photosynth. Res. 2009, 102, 197– 211.

11. Tunnicliffe, R. B.; Ratcliffe, E. C.; Hunter, C. N.; Williamson, M. P. FEBS Lett. 2006, 580, 6967– 6971.

12. Ratcliffe, E. C.; Tunnicliffe, R. B.; Ng, I. W.; Adams, P. G.; Qian, P.; Holden-Dye, K.; Jones, M. R.; Williamson, M. P.; Hunter, C. N. Biochim. Biophys. Acta 2011, 1807, 95– 107.

13. Liu, L.-N.; Sturgis, J. N.; Scheuring, S. J. Struct. Biol. 2011, 173, 138– 145.

14. Francia, F.; Wang, J.; Venturoli, G.; Melandri, B. A.; Barz, W. P.; Oesterhelt, D. Biochemistry 1999, 38, 6834– 6845.

15. Holden-Dye, K.; Crouch, L. I.; Jones, M. R. Biochim. Biophys. Acta 2008, 1777, 613– 630.

16. Scheuring, S. Curr. Opin. Cell Biol. 2006, 10, 387– 393.

17. Busselez, J.; Cottevielle, M.; Cuniasse, P.; Gubellini, F.; Boisset, N.; Lévy, D. Structure 2007, 15, 1674– 1683.

18. Crouch, L. I.; Holden-Dye, K.; Jones, M. R. Biochim. Biophys. Acta 2010, 1797, 1812– 1819.

19. Gubellini, F.; Francia, F.; Busselez, J.; Venturoli, G.; Lévy, D. Biochemistry 2006, 45, 10512–10520.

20. Milhiet, P.-E.; Gubellini, F.; Berquand, A.; Dosset, P.; Rigaud, J.-L.; Le Grimellec, C.; Lévy, D. Biophys. J. 2006, 91, 3268– 3275.

21. Wang, Z.-Y.; Suzuki, H.; Kobayashi, M.; Nozawa, T. Biochemistry 2007, 46, 3635– 3642.

22. MacKenzie, K. R.; Prestegard, J. H.; Engelman, D. M. Science 1997, 276, 131– 133.

23. Hsin, J.; Chipot, C.; Schulten, K. J. Am. Chem. Soc. 2009, 131, 17096– 17098.

24. Russ, W. P.; Engelman, D. M. Proc. Natl. Acad. Sci. U.S.A. 1999, 96, 863– 868.

25. Chandler, D.; Hsin, J.; Harrison, C. B.; Gumbart, J.; Schulten, K. Biophys. J. 2008, 95, 2822–2836.

26. Hsin, J.; Gumbart, J.; Trabuco, L. G.; Villa, E.; Qian, P.; Hunter, C. N.; Schulten, K. Biophys. J. 2009, 97, 321– 329.

27. Sener, M. K.; Hsin, J.; Trabuco, L. G.; Villa, E.; Qian, P.; Hunter, C. N.; Schulten, K. Chem. Phys. 2009, 357, 188– 197.

28. Hsin, J.; Chandler, D. E.; Gumbart, J.; Harrison, C. B.; Sener, M.; Strumpfer, J.; Schulten, K.

ChemPhysChem 2010, 11, 1154– 1159.

29. Trabuco, L. G.; Schreiner, E.; Gumbart, J.; Hsin, J.; Villa, E.; Schulten, K. J. Struct. Biol. 2011, 173, 420– 427.

30. Phillips, J. C.; Braun, R.; Wang, W.; Gumbart, J.; Tajkhorshid, E.; Villa, E.; Chipot, C.; Skeel, R. D.; Kale, L.; Schulten, K. J. Comput. Chem. 2005, 26, 1781– 1802.

31. MacKerell AD1, Bashford D, Bellott M, Dunbrack RL, Evanseck JD, Field MJ, Fischer S, Gao J, Guo H, Ha S, Joseph-McCarthy D, Kuchnir L, Kuczera K, Lau FT, Mattos C, Michnick S, Ngo T, Nguyen DT, Prodhom B, Reiher WE, Roux B, Schlenkrich M, Smith JC, Stote R, Straub J, Watanabe M, Wiórkiewicz-Kuczera J, Yin D, Karplus M. J. Phys. Chem. B 1998, 102, 3586– 3616.

32. Foloppe, N.; MacKerell, A. D., Jr. J. Comput. Chem. 2000, 21, 86– 104.

33. MacKerell, A. D., Jr.; Feig, M.; Brooks, C. L., III. J. Comput. Chem. 2004, 25, 1400– 1415.

34. Jorgensen, W. L.; Chandrasekhar, J.; Madura, J. D.; Impey, R. W.; Klein, M. L. J. Chem. Phys. 1983, 79, 926– 935.

35. Tuckerman, M. E.; Berne, B. J.; Martyna, G. J. J. Phys. Chem. B 1992, 97, 1990– 2001.

36. Brünger, A. T.; Brooks, C. L., III; Karplus, M. Chem. Phys. Lett. 1984, 105, 495– 500.

37. Feller, S. E.; Zhang, Y.; Pastor, R. W.; Brooks, B. R. J. Chem. Phys. 1995, 103, 4613– 4621.

38. Darve, E.; Pohorille, A. J. Chem. Phys. 2001, 115, 9169– 9183.

39. Hénin, J.; Chipot, C. J. Chem. Phys. 2004, 121, 2904– 2914.

40. Hénin, J.; Pohorille, A.; Chipot, C. J. Am. Chem. Soc. 2005, 127, 8478– 8484.

41. Kim, H.; Hsin, J.; Liu, Y.; Selvin, P. R.; Schulten, K. Structure 2010, 18, 1443– 1449.

42. Stockner, T.; Ash, W. L.; MacCallum, J. L.; Tieleman, D. P. Biophys. J. 2004, 87, 1650– 1656.

43. Rodriguez-Gomez, D.; Darve, E.; Pohorille, A. J. Chem. Phys. 2004, 120, 3563– 3578.

44. Shaw, W. V. Methods Enzymol. 1975, 43, 737– 755.

45. Sulistijo, E. S.; Jaszewski, T. M.; MacKenzie, K. M. J. Biol. Chem. 2003, 278, 51950– 51956.

46. Senes, A.; Chadi, D. C.; Law, P. B.; Walters, R. F. S.; Nanda, V.; DeGrado, W. F. J. Mol. Biol. 2007, 366, 436– 448.

47. Killian, J. A.; von Heijne, G. Trends Biochem. Sci. 2000, 25, 429– 434.

48. Yuen, C. T. K.; Davidson, A. R.; Deber, C. M. Biochemistry 2000, 39, 16155– 16162.

49. de Planque, M. R. R.; Killian, J. A. Mol. Membr. Biol. 2003, 20, 271– 284.

50. Popot, J.-L.; Engelman, D. M. Biochemistry 1990, 29, 4031– 4037.

51. Engelman, D. M.; Chen, Y.; Chin, C.-N.; Curran, A. R.; Dixon, A. M.; Dupuy, A. D.; Lee, A. S.; Lehnert, U.; Matthews, E. E.; Reshetnyak, Y. K.; Senes, A.; Popot, J.-L. FEBS Lett. 2003, 555, 122–125.

52. Fleming, K. G.; Ackerman, A. L.; Engelman, D. M. J. Mol. Biol. 1997, 272, 266– 275.

53. Bowie, J. U. Curr. Opin. Struct. Biol. 2011, 21, 42– 49.

54. Senes, A.; Ubarretxena-Belandia, I.; Engelman, D. M. Proc. Natl. Acad. Sci. U.S.A. 2001, 98, 9056– 9061.

55. Senes, A.; Engel, D. E.; DeGrado, W. F. Curr. Opin. Struct. Biol. 2004, 14, 465– 479.

56. Arbely, E.; Arkin, I. T. J. Am. Chem. Soc. 2004, 126, 5362– 5363.

57. Derewenda, Z. S.; Lee, L.; Derewenda, U. J. Mol. Biol. 1995, 252, 248– 262.

58. Lawrie, C. M.; Sulistijo, E. S.; MacKenzie, K. R. J. Mol. Biol. 2010, 396, 924– 936.

59. Aklujkar, M.; Beatty, J. T. Photosynth. Res. 2006, 88, 159– 171.

60. Duong, M. T.; Jaszewski, T. M.; Fleming, K. G.; MacKenzie, K. R. J. Mol. Biol. 2007, 371, 422–434.

61. Francia, F.; Wang, J.; Zischka, H.; Venturoli, G.; Oesterhelt, D. Eur. J. Biochem. 2002, 269, 1877–1885.

62. Recchia, P. A.; Davis, C. M.; Lilburn, T. G.; Beatty, J. T.; Parkes-Loach, P. S.; Hunter, C. N.; Loach, P. A. Biochemistry 1998, 37, 11055– 11063.

63. Parkes-Loach, P. S.; Law, C. J.; Recchia, P. A.; Kehoe, J.; Nehrlich, S.; Chen, J.; Loach, P. A. Biochemistry 2001, 40, 5593– 5601.

64. Law, C. J.; Chen, J.; Parkes-Loach, P. S.; Loach, P. A. Photosynth. Res. 2003, 75, 193– 210.

65. Senes, A.; Gerstein, M.; Engelman, D. M. J. Mol. Biol. 2000, 296, 921– 936.

66. Schneider, D. FEBS Lett. 2004, 577, 5– 8.

67. Schneider, D.; Engelman, D. M. J. Mol. Biol. 2004, 343, 799– 804.

68. Kairys, V.; Gilson, M. K.; Luy, B. Eur. J. Biochem. 2004, 271, 2086– 2092.

69. Rath, A.; Deber, C. M. Proteins: Struct., Funct., Bioinf. 2008, 70, 786– 793.

4.7 Supporting Information

Figure S4.1

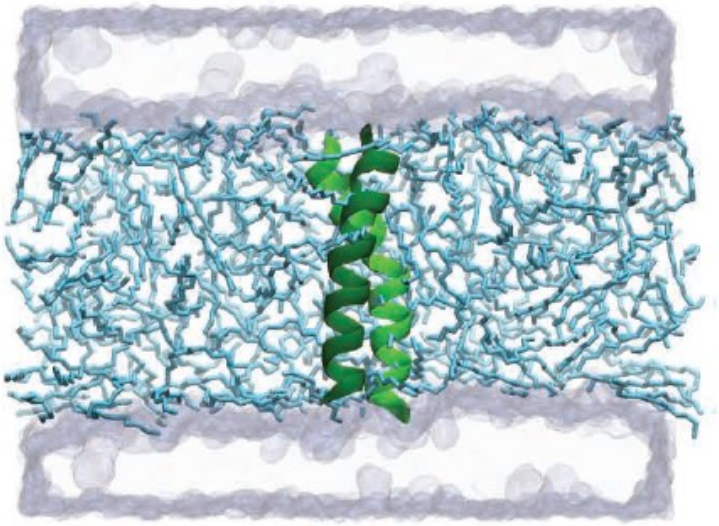

Figure S4.1 An example setup of a molecular dynamics simulation using a dodecane patch as a lipid mimetic. Shown here is the configuration for simulation *capsulatus-Dimer-DODE-1* in Table 1 in the text. Water is shown in transparent blue, dodecane molecules are shown in cyan and the two transmembrane segments of *Rba. capsulatus* PufX are shown in green and dark green.

Figure S4.2

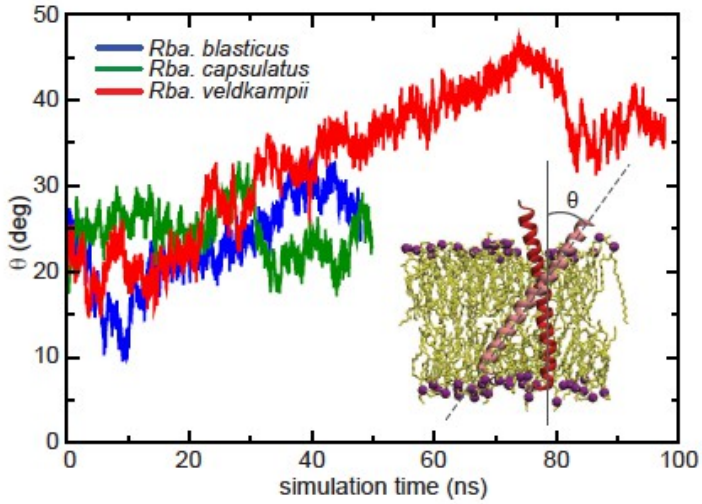

Figure S4.2 Measurement of helix tilt with respect to the membrane normal during the equilibrium simulations *basticus-Dimer-POPE* (blue trace), *capsulatus-Dimer-POPE* (green trace), and *veldkampii-Dimer-POPE* (red trace).

Figure S4.3

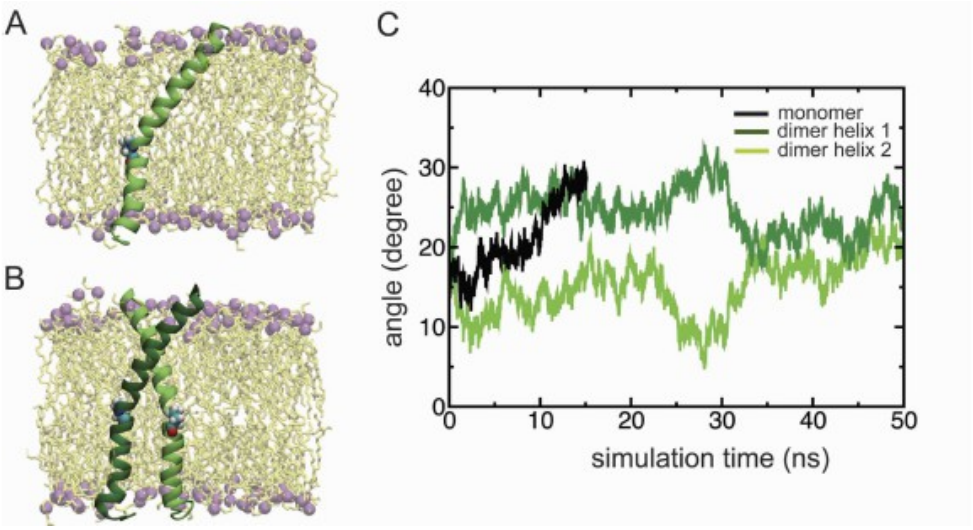

Figure S4.3 Location of the transmembrane proline residue in *Rba. capsulatus* PufX. (A) Protein-membrane system from simulation *capsulatus-Monomer-POPE* at 15 ns. PufX is shown in green, with the proline residue at location 36 (P36) shwon in sphere representation. Membrane is shown in the transparent with the same color scheme as in Figure 2 of the main text. (B) Protein-membrane system from simulation *capsulatus-Dimer-POPE* at 35 ns. The two PufX helices are colored in green and dark green for distinction. The P36 residues can be seen to point away from the helix-helix association interface. (C) Measurement of the helix kink near the P36 residue during simulation *capsulatus-Monomer-POPE* (black trace) and *capsulatus-DIMER-POPE* (dark green and light green traces).

Figure S4.4

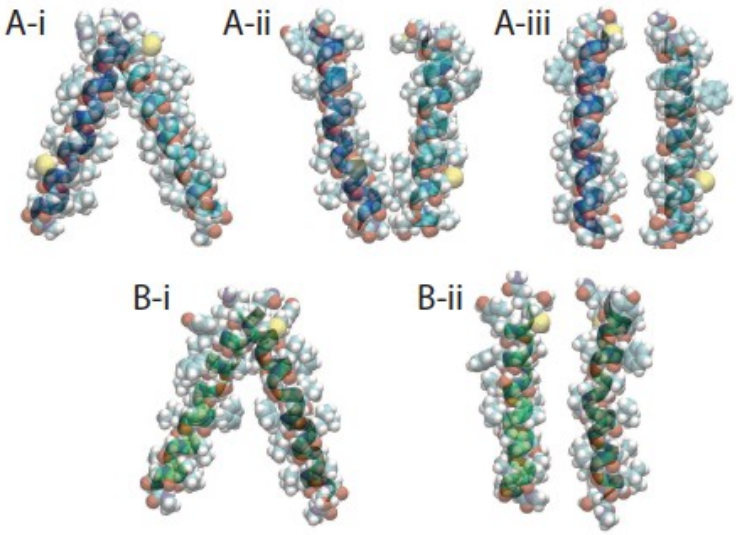

Figure S4.4 Common conformations of PufX helices seen in ABF simulations with a helix-helix separation of 14.9-15.1 Å. (A) The three most common conformations for the transmembrane segments of *Rba. blasticus* PufX seen in *blasticus-DIMER-DODE-ABF-1*. (A-i) Conformation with helices associated at the N-Terminal ends via close contacts near Gly29. (A-ii) Conformation with helices interacting transiently at the C-terminal ends via van der Waals contacts between large side chains (most notably Leu43, Leu44, and Thr47). (A-iii) Conformation with the helices separated. The conformation in A-ii is only observed for the case of *Rba. capsulatus.* For example, for the case of the transmembrane segments of *Rba. capsulatus* PufX seen in *capsulatus-Dimer-DODE-ABF-1*, only two common conformations are observed with a helix-helix separation of 14.9-15.1 Å, one with associated N-terminal ends also mediated by the Gly29 contact (B-i) and another with completely separated helices (B-ii).

Chapter 5
The Oligomeric States of the Purified Sigma 1 Receptor are Stabilized by Ligands

This chapter was prepared for publication as:

Katarzyna A. Gromek,[1] Fabian P. Suchy,[1] Hannah R. Meddaugh,[1] Russell L. Wrobel,[1] Loren LaPointe,[2] Uyen B. Chu,[3] John G. Primm,[1] Arnold E. Ruoho,[3,*] Alessandro Senes[2] and Brian G. Fox[1,2,*] The Oligomeric States of the Purified Sigma 1 Receptor are Stabilized by Ligands. Journal of Biological Chemistry (2014) 289(29):20333-44.

From the [1]Transmembrane Protein Center, Departments of [2]Biochemistry and [3]Neuroscience, University of Wisconsin-Madison, Madison, Wisconsin 53706.

Contribution: I performed the analysis of oligomerization of the transmembrane domain (TM2) in the sigma-1 receptor, including mutagenesis.

Abstract

Sigma 1 receptor (S1R) is a mammalian member of the ERG2 and sigma1 receptor like protein family (pfam04622). It has been implicated in drug addiction and many human neurological disorders including Alzheimer's and Parkinson's diseases and amyotrophic lateral sclerosis. A broad range of synthetic small molecules including cocaine, (+)-pentazocine, haloperidol and small endogenous molecules such as N,N-dimethyltryptamine, sphingosine and steroids have been identified as regulators of S1R. However, the mechanism of activation of S1R remains obscure. Here we provide evidence in vitro that S1R has ligand binding activity only in an oligomeric state. The oligomeric state is prone to decay into an apparent monomeric form when exposed to elevated temperature, with loss of ligand binding activity. This decay is suppressed in the presence of the known S1R ligands such as haloperidol, BD-1047 and sphingosine. S1R has a GxxxG motif in its second transmembrane region, and these motifs are often involved in oligomerization of membrane proteins. Disrupting mutations within the GxxxG motif shifted the fraction of the higher oligomeric states towards smaller states and resulted in a significant decrease in specific [3H]-(+)-pentazocine binding. Results presented here support the proposal that S1R function may be regulated by its oligomeric state. Possible mechanisms of molecular regulation of interacting protein partners by S1R in the presence of small molecule ligands are discussed.

Abbreviations used:

The abbreviations used are: BD-1047, N-[2-(3,4-dichlorophenyl)ethyl]-N-methyl-2-(dimethylamino)ethylamine dihydrobromide; BODIPY, boron-dipyrromethene; CAT, chloramphenicol acetyltransferase; DTG, 1,3-di-(2-tolyl)guanidine; MBP, maltose binding protein; 4-PPBP, 4-phenyl-1-(4-phenylbutyl)piperidine maleate; PRE-084, 2-(4-morpholinethyl)-1-phenylcyclohexanecarboxylate

hydrochloride; S1R, sigma-1 receptor; SKF-83959, 6-chloro-7,8-dihydroxy-3-methyl-1-(3-methylphenyl)-2,3,4,5-tetrahydro-1H-3-benzazepine; TEV, tobacco etch virus; TM2, second transmembrane region; ToxR, Vibrio cholerae toxin transcriptional regulator.

5.1 Background

The mammalian sigma 1 receptor (S1R2) is a unique 223 amino acid membrane bound protein (1-5). S1R is found in the mammalian central nervous system (CNS) and in most peripheral tissues including the immune and endocrine systems. It is primarily localized in the endoplasmic reticulum (6-8), but also in some cellular plasma membranes (9), specialized cisternae-laiden cholinergic synapses of the spinal cord ventral horn motoneuron C-terminals (10,11) and in spinal cord dorsal root ganglia (12). The amino acid sequence of S1R is approximately 95% identical between mammals including the guinea pig, mouse, rat and human. ERG2, a sterol isomerase found in yeast (13) and fungi (2), is an ortholog of the mammalian S1R with an approximately overall 30% sequence homology and 66% homology in the putative S1R ligand binding domain (1). The mammalian S1R does not possess sterol isomerase activity and has been clearly differentiated by sequence and size from the fungal sterol isomerase (1,13).

S1R functions as a molecular chaperone and serves as a partner for a variety of client proteins. It stabilizes the IP3 type 3 receptor (14) in ER mitochondrial associated membranes and has been shown to interact and play an important regulatory role in many cell signaling systems including the molecular chaperone GRP78/BIP (15), several types of G-protein coupled receptors (15-18), and voltage- gated ion channels (9,19-23). S1R suppresses the production of reactive oxygen species in various mouse tissues including the retina, lung and liver, and in cultured mammalian cells possibly by activating antioxidant response element genes (6,24-26).

A broad range of synthetic small molecules with widely varied structures bind with high affinity to S1R, including the (+)–isomer of benzomorphan derivatives such as pentazocine and dextrallorphan, neuroleptics such as haloperidol, fluphenazine and chlorpromazine, the compounds o-ditolylguanidine,

PRE-084, BD-1047 and BD-1063, the beta-blocker propranolol and the presynaptic dopamine D2 agonist (+)-3-PPP (27-29). Several endogenous small molecules such as N, N' dimethyltryptamine (30), sphingosine (31) and steroids such as progesterone (32) and dehydroepiandrosterone (33) have also been identified as regulators of S1R.

Due to the broad contributions of S1R in maintaining cellular homeostasis, the receptor has been identified as a therapeutic target for the treatment of cancer (34) and neurodegenerative diseases including amyotrophic lateral sclerosis (35), Alzheimer's (36) and Parkinson's diseases (37), and for retinal neurodegeneration (38). Several studies have also connected S1R to the possible treatment of drug addiction and toxicity related to derivatives of cocaine and amphetamine (8,16,39,40).

The guinea pig S1R has been purified to homogeneity following expression in E. coli as a fusion to maltose binding protein (MBP, (41)). The ligand binding region of S1R was identified by the use of specific radioiodinated photoprobes (42-45) and by mutagenesis (46,47) to be formed primarily by the juxtaposition of a short C terminal hydrophobic region (residues 176-194) with a portion of TM2 (residues 91-109) and perhaps a portion of TM1. Based on hydrophobicity analyses and the use of S1R-GFP constructs (9) and S1R antibody probes (14), it has been concluded that the S1R contains two putative transmembrane (TM) helices (9) with both the N and C termini occurring on the cytoplasmic side of the cellular membrane (9,14). S1R also has a GxxxG motif in TM2. This motif is often involved in helix-helix oligomerization of integral membrane proteins (48-50). High molecular weight forms (tetramer, pentamer) of the S1R were previously identified using radioiodinated photoaffinity labeling in rat liver microsomal membrane preparations (44), suggesting that S1R may oligomerize under physiological conditions.

Here we report that highly purified S1R forms an oligomeric state, and also show that the

oligomeric state provides specific ligand binding, while the monomeric state does not. Stabilization of the functional oligomeric states occurs via the participation of the GxxxG oligomerization motif. These results are discussed in the context of possible mechanisms of molecular regulation of interacting protein partners by S1R in the presence of small molecule ligands.

5.2 Experimental Procedures

Cloning

Plasmid DNA containing the guinea pig sigma-1 receptor gene was used the template for all cloning work (41). All oligonucleotides were purchased from IDT (Coralville, IA). The MBP-4A- S1R plasmid used in the current work was made using PIPE mutagenesis (51) as previously reported (52) using primers listed in Table S1 of the Supplementary Material. PCR was carried out using Pfu-UltraII polymerase. When the PCR reaction was completed, a DpnI digestion was performed to remove the template. The DpnI-digested PCR product was purified using a Qiagen PCR purification kit and the eluted DNA was transformed into E. coli 10G (Lucigen, Middleton, WI).

To make expression plasmids for the second transmembrane helix (TM2) for TOXCAT analysis, two partially complementary long oligonucleotides corresponding to the S1R-TM2 domain were designed to include 5' NheI and 3' BamHI overhangs (see primer list in Table 1). These single stranded oligonucleotides were allowed to anneal and the resulting dsDNA was ligated into NheI- and BamHI-digested pccKan (53). Correct DNA constructs were verified by DNA sequencing of the entire MBP to ToxR fusion coding region. Mutations in TM2 were made using PIPE mutagenesis.

Protein preparation

Expression and purification of MBP-4A-S1R containing a stabilizing 4-Ala linker between the MBP and S1R domains, a variant with a tobacco etch virus protease site present as the interdomain linker (MBP-TEV- S1R), or with mutations in TM2 were carried out as described previously (52). MBP-TEV-S1R was purified using amylose affinity chromatography (52) and subjected to proteolysis using TEV protease in a ratio of 1 mg of protease per 1 mg of fusion protein. TEV protease was prepared as previously reported (54). The TEV protease reaction was performed at room temperature

for 96 h, and the final cleavage efficiency was greater than 95%. The sample was filtered through a 0.8 μm syringe filter and diluted with 20 mM Tris, pH 7.2, containing 0.031% Triton X-100 and 1 mM 2-mercaptoethanol to reduce the concentration of NaCl to 100 mM. A 5-mL Fast Flow HiTrap Q column (GE Healthcare Life Sciences) was prepared using 5 column volumes of 20 mM Tris, pH 7.2, containing 100 mM NaCl, 0.031% Triton X-100 and 1 mM 2-mercaptoethanol (loading buffer). The protein sample was loaded onto the Q column using the AKTA purifier sample pump at a flow rate of 1 mL/min and then washed with 5 column volumes of 20 mM Tris, pH 7.2, containing 100 mM NaCl, 0.031% Triton X-100 and 1 mM 2-mercaptoethanol (wash buffer). Elution was performed with gradient of NaCl to a final concentration of 1 M over 20 column volumes. The collected fractions were analyzed for protein content by 4-20% gradient SDS-PAGE. Appropriate fractions were combined and concentrated as described before. Protein concentrations were determined using BioRad in-gel densitometry. Samples from all purification steps were assayed for ligand binding activity.

Preparative size exclusion chromatography

This chromatography was conducted on a Shimadzu Prominence HPLC equipped with a DGU-20A5 on- line degasser, LC-20AD solvent delivery module, SIL-20ACHT autosampler, CTO-20AC column oven, SPD-20A UV-vis detector, RF-10AXL spectrofluorometric detector, RID-10A differential refractometric detector, FRC-10A fraction collector module, CBM-20A system controller and LabSolution LCsolution software version 1.24 SP1. The mobile phase, 10 mM HEPES, pH 7.2, containing 150 mM NaCl, 0.3 mM TCEP and 0.018% DDM (2× CMC), was degassed for a minimum of 20 min under vacuum prior to use. The buffer was isocratically pumped at 1 mL/min through a Phenomenex 300 x 7.8 mm Yarra 3μm SEC-3000 column with SecGuard column guard. Protein elution was monitored by UV absorption at 280 and 260 nm. The column temperature was 20.0 ˚C and the

detector flow cell temperature was 35.0 ˚C. Columns were calibrated daily using bovine thyroglobulin, IgA, ovalbumin, myoglobin and uridine as standards (Phenomenex). High volume separation was achieved through repeated 100 µL injections while separating the protein into forty-one 125 µL fractions.

Analytical size exclusion chromatography

Fractions from multiple injections of MBP-4A-S1R were subjected to additional rounds of analytical sizing chromatography to assess whether changes in the distribution of oligomeric states occurred during the repeat chromatography. Elution from the repeat chromatography was monitored using the intrinsic fluorescence of tryptophan with excitation at 280 nm and emission at 340 nm. During the course of the repeated analyses, retention times varied by less than 0.25 min during the 12 min chromatographic run (2%), and were corrected for preparation of figures to correspond to the same apparent molecular weight (determined from the daily calibration) by using the earliest chromatogram as the benchmark for retention times. Similarly, S1R obtained from TEV protease proteolysis of MBP-TEV-S1R was subjected to repeat sizing chromatography. In this case, the forty-one proteolyzed fractions were stored for ~1 month at 4 ˚C before repeat analysis.

Light scattering measurements

Separate fractions containing peaks 1, 2 and intermediate oligomer from Fig. 2A were subjected to size exclusion chromatography coupled to multi-angle laser light scattering, with UV absorbance and refractive index detection. Separation was performed on a Superdex S200 (GE Healthcare Life Sciences) in 150 mM NaCl, 5 mM HEPES, pH 7.2 and 0.018% DDM (2× CMC). Light scattering and refractive index were measured with a DAWN HELEOS II and OPTILab rEX respectively (Wyatt Technology). Data analysis was performed using ASTRA 6.1 (Wyatt Technology).

Chemical cross-linking

Chemical cross-linking with disuccinimidyl suberate (DSS) was performed on the detergent-solubilized and highly purified individual oligomeric states of MBP-4A-S1R. DSS was dissolved in DMSO and the control samples (no cross-linker) contained equivalent amount of DMSO (2%). 5 μM of each protein state was incubated with either 30- or 50- molar excess of DSS (150 μM, 250 μM, respectively) for 2 h at room temperature, in presence or absence of 10 μM BD-1047. The reactions were stopped by addition of Tris-HCl, pH 8.0, to the final concentration of 30 mM. The samples were then subject to SDS-PAGE in 7.5% Tris-HCl BioRad gel and calibrated with commercial molecular weight markers (Spectra Multicolor High Range Protein Ladder, Thermo Scientific). After staining with Brilliant Blue R, the gels were imaged and analyzed using the GelAnalyzer 2010 free software (www.GelAnalyzer.com) to calculate the approximate molecular weight of visualized bands.

Oligomer stability tests

Haloperidol, o-ditolylguanidine, PRE-084, BD-1047, 4-PPBP, SKF-83959, sphingosine, and sphingosine-1-phosphate were from Tocris Biosciences (Bristol, UK). Pentazocine and was from Sigma-Aldrich (St. Louis, MO). Stock solutions of PRE-084 (5 mM) and BD-1047 (10 mM) were prepared in deionized water. A pentazocine stock solution (10 mM) was prepared in 20 mM HCl in deionized water, while stock solutions of 4-PPBP (10 mM), haloperidol (10 mM), ortho-di-tolylguanidine (10 mM) and SKF-83959 (10 mM) were prepared in 100% (v/v) DMSO. Sphingosine and sphingosine-1-phosphate stock solutions (5 mM) were prepared in solution containing 1.8% (w/v) DDM. The sphingosine-1-phosphate stock solution was heated to ~60 °C to aid in solublization. Less than 0.5 mM of free Pi was detected in this sample, indicating the phosphoryl group was not hydrolyzed during solubilization.

Purified peak 1 (see Fig. 2B) from preparative size exclusion chromatography of MBP-4A-S1R was diluted to 15 μg/ml (0.23 μM) and a final volume of 100-300 μL in 10 mM HEPES, pH 7.2, containing 0.3 mM TCEP and 0.018% DDM and incubated for up to 18 h at 4 °C, 25 °C and 37 °C. Analytical size exclusion chromatography was run before and after incubation with various ligands. A typical HPLC injection was 10 μL and intrinsic tryptophan fluorescence was monitored. All experiments included a control sample incubated under the same conditions but with no added ligand. Ligand stock solutions were prepared as described above, and ligands were tested for stabilization at 0.45 μM and 10 μM.

Ligand binding assays

[3H]-(+)-pentazocine (specific activity 36 Ci/mmol) was from Perkin-Elmer (Waltham, MA). Binding assays were performed in 100 μL in a 48-well block format as described previously (41,45) with minor modifications. Protein samples at 1 ng/μL were prepared in 20 mM Tris, pH 8.0, containing 0.1% Triton X-100. The final concentration of [3H]-(+)-pentazocine in both total and non-specific binding assays was 100 nM. Haloperidol (Tocris) was used as the masking agent in the non-specific binding reaction at final concentration of 10 μM. The incubation with ligands was performed for 90 min at 32 ˚C, followed by filtration on a glass fiber filter (Whatman GF/B) performed in Brandel cell harvester. The glass filter was then washed with 50 mM Tris, pH 8.0, and individual filters were transferred into vials containing 3 mL of scintillation cocktail (Ultima Gold, Perkin-Elmer). The level of radioactivity was measured the following day using a Packard scintillation counter. The raw count data were normalized to nmol of protein present in the assay and plotted as the percentage of specific binding activity of the original, control sample, MBP-TEV-S1R.

The stoichiometry of ligand binding was determined using 300 nM of purified peak 1 (see Fig.

2B) supplemented with a range of concentrations of BD-1047 from 0 to 3000 nM in a total volume of 150 μL. The titration was assembled in a 96-well plate, and incubated for 16 h at 37 ˚C. Aliquots (10 μL) from each well were examined with analytical size exclusion chromatography and eluted protein was detected using tryptophan fluorescence. The values for 0% and 100% oligomeric stabilization were normalized using the wells containing either no BD-1047 or the maximal amount, respectively. The binding data were analyzed using KD = [nP][L]/[PL], where n is the number of protein molecules that bind one molecule of ligand, and P, L and PL are the equilibrium concentrations of free receptor, free ligand, and the ligand-bound receptor, respectively. The expression for KD was rewritten as KD = [nPi x][Li x]/[x], where x corresponds to the amount of [PL] formed and also the depletion in concentrations of free receptor and free ligand. Theoretical values for x at each step in the ligand binding titration were determined by solving this latter expression. Best fit values for n and KD were determined using the NonlinearModelFit routine of Mathematica v.8.0.4.0 (Wolfram Research).

TOXCAT

A gene encoding the TM2 domain of S1R was cloned into the NheI-BamHI restriction sites of the pccKAN vector resulting in the following sequence: NRASxxxGILIN. Escherichia coli MM39 cells transformed with pccKan-derived TOXCAT plasmids were inoculated into 3 mL of Luria Bertani medium containing 100 μg/mL of ampicillin and grown overnight at 37 ˚C with shaking. To check for proper membrane insertion of the TOXCAT constructs, overnight cultures of transformed MM39 cell were plated onto M9 minimal medium agar plates containing 0.4% maltose as the only carbon source and grown at 37 ˚C for 48 h (53). Aliquots (3 μL) of the overnight cultures were inoculated into 3 mL of Luria Bertani medium and grown to OD600 of 0.6 at 37 ˚C with shaking. An aliquot (1 mL) of the culture medium was centrifuged for 10 min at 17,000g and the cell pellet was resuspended in 500 mL

of 25 mM Tris- HCl, pH 8.0, containing 2 mM EDTA. The resuspended cells were sonicated at medium power for 10 s and a 50-µL aliquot was removed from each sample and mixed with 4× NuPAGE SDS loading buffer, boiled for 10 min, and saved for western blotting. Lysates were clarified by centrifugation at 17,000g for 10 min. The supernatant was kept on ice and used in chloramphenicol acetyltransferase (CAT) assays.

Chloramphenicol acetyltransferase assays

One mL of 0.1 M Tris-HCl, pH 7.8, containing 0.1 mM acetyl-CoA and 0.4 mg/mL of 5,5'-dithiobis-(2- nitrobenzoic acid) was mixed with 40 µL of supernatant from the cell lysis and the absorbance at 412 nm was measured for 2 min to establish basal activity (55). After this, 40 µL of 2.5 mM chloramphenicol dissolved in 10% ethanol was added and absorbance at 412 nm was measured for an additional 2 min to determine CAT activity. CAT activity was normalized using OD420 measurements of cell aliquots. The relative CAT activities were reported as percentages of the activity given by the strong transmembrane dimer control, glycophorin A (GpA).

Quantification of TOXCAT expression

Boiled cell lysates (10 µL) were loaded onto a NuPAGE 4-12% Bis-Tris SDS-PAGE gel (Invitrogen) and then transferred to polyvinylidene fluoride membranes (VWR) for 1 h at 100 mV. Blots were blocked using 5% bovine serum albumin (US Biologicals) in 50 mM Tris, pH 8.0, containing 150 mM NaCl and 0.5% Tween buffer (TBST) for 2 h at 4 ˚C. Biotinylated anti-maltose binding protein antibody (Vector labs) was diluted 1:1500 in 1% bovine serum albumin in TBST and incubated overnight at 4 ˚C. Blots were washed with TBST for 1 h with three buffer exchanges at room temperature before incubation with secondary antibody in 1% bovine serum albumin in TBST at 1:1500 dilution, peroxidase-conjugated streptavidin (Jackson ImmunoResearch) for 2 h at room

temperature. Blots were again washed for 1 h using three exchanges of TBST. A 1:1 mixture of buffers from the Pierce ECL Western Blotting Substrate Kit was added to the blot and chemiluminescence was measured using an ImageQuant LAS 4000 (GE Healthsciences).

5.3 Results

For these studies, MBP-4A-S1R (Fig. 1A, lane P1) was prepared using an expression method that gives higher yield of purified protein from Escherichia coli (52). In addition, S1R without an MBP tag was prepared by treatment of a MBP-TEV-S1R fusion with TEV protease (Fig. 1B, lane P2). Denaturing SDS-PAGE showed that these protein preparations consisted of a single polypeptide with purity greater than 95%. With these preparations, we investigated the relationship between the oligomerization state of S1R and its ligand binding activity. The results show that an oligomeric form of the receptor is required for specific ligand binding.

5.3.1 Evidence for oligomerization

Analytical size- exclusion chromatography of purified MBP-4A-S1R showed two major peaks, labeled 1 and 2 (solid line, Fig. 2A). After treatment with TEV protease, purified S1R also showed two major peaks, labeled 3 and 4 (dotted line, Fig. 2A). Thus both receptor preparations show evidence for formation of a predominant oligomeric state (peaks 1 and 3) along with a corresponding monomer (peaks 2 and 4). Similar behavior was observed from MBP-4A-S1R prepared in buffer containing n-octyl-beta-D-glucopyranoside or MBP-4A-S1R prepared in buffer containing Triton X-100. A variable amount of an intermediate oligomer state was also observed in the MBP-4A-S1R samples (retention time ~8 min, marked with *). Figs. 2B and 2C show that both the oligomer and monomer peaks were stable (i.e., eluted with the same retention time) when subjected to a repeat round of chromatography. Thus the major peaks shown in Fig. 2A could be obtained in a highly pure form. Fig. 2B shows that peaks 1 and 3, corresponding to the potential oligomeric states, had apparent molecular weights of 460 kDa and 150 kDa, respectively, for the protein-detergent micelle, while Fig. 2C shows that peaks 2 and 4, corresponding to monomeric states, had apparent molecular weights of 80 and 35 kDa, respectively.

The oligomeric assemblies were only dependent on the presence of S1R, as MBP alone did not form an oligomeric state in the conditions used here. Moreover, after removal of the MBP by treatment with TEV protease, S1R remained in the oligomeric state and could be further purified by both adsorption and size exclusion chromatographies (Fig. 2B, peak 3).

The estimation of oligomer stoichiometry using analytical SEC alone is complicated because of uncertainty in how the protein will be accommodated into a protein-detergent micelle and those effects on the hydrodynamic radius. Although static light scattering measurements are often used to assess oligomeric stoichiometry, the presence of detergent micelles creates high background noise and must be accounted for in the mass of the protein-detergent complex. Thus, the fusion protein was sent to the Yale Keck Biophysics Lab, which is specially equipped for these measurements, with combined SEC and light scattering instrumentation. Three peaks were analyzed. The smallest protein molecules detected (Fig. 3A) had a mass within 2% of that predicted for a monomer, while the largest molecular weight protein (Fig. 3B) was polydisperse, with molecular weights corresponding to oligomerization states of 6 to 8. Light scattering also showed that the intermediate oligomer marked with * in Fig. 2A was monodisperse with a molecular weight corresponding to a tetramer (Fig. 3C).

Analysis by SDS-PAGE after cross-linking gave further insight into the light scattering results. Fig. 4A shows the monomer was unchanged in SDS-PAGE either without cross-linker (lanes 1 and 2) or with cross-linker (lanes 3 and 4), suggesting no inter-molecular interactions capable of being captured by the crosslinking reagent. In contrast, Fig. 4B shows that the polydisperse oligomer cross-linked to a size greater than 300 kDa. Furthermore, Fig. 4C shows that the intermediate oligomer, assigned to be a tetramer by light scattering measurements, was cross-linked to a molecule with molecular weight again consistent with a tetramer.

5.3.2 Ligand binding

Pentazocine is a well-studied ligand for S1R (56,57). Fig. 5 shows that only the oligomeric states of MBP-4A-S1R and S1R exhibited specific pentazocine binding activity. For example, peak 1 from Fig. 2 (oligomer of the MBP fusion) bound pentazocine with ~20× higher specific activity than peak 2 (monomer of the MBP fusion). Likewise, the specific binding activity for peak 2 from Fig. 3 (S1R oligomer) was ~15× higher than for peak 4 (S1R monomer). Since some S1R ligands were delivered in DMSO carrier, a sample containing a final concentration of 2% DMSO but no other ligand was tested independently and shown to have no effect on oligomeric state. With these assignments of the active form of the receptor, peak deconvolution of the original samples indicated that active MBP-4A-S1R (solid line, Fig. 2A and B) was ~75% of the original protein sample while active S1R (dotted line, Fig. 2A and B) represented ~50%.

Ligand binding was also tested using the fluorescent ligand BODIPY-sphingosine in analytical SEC experiments. Consistent with the specific pentazocine binding results (Fig. 5), the oligomeric forms of the protein migrated with haloperidol-masked BODIPY fluorescence, while the monomer did not (data not shown). The fluorescent ligand was a gift from Mary L. Kraft PhD (University of Illinois, Urbana-Champaign).

5.3.3 Stability of oligomers

The oligomeric forms of S1R were observed to decay upon incubation in buffer. Thus, after ~18 h at 37 ˚C, the amount of protein in peak 1 decreased by ~40% and the amount in peak 2 increased by a corresponding amount (Fig. 6A). Similar instability of the S1R oligomers was also observed at 25 ˚C and 4 ˚C in the absence of ligand, but to a lesser extent. In all chromatograms, the total integrated area remained constant within 5%, supporting the conclusion that interconversion between oligomer and

monomer states was occurring. Disulfide bonds are apparently not involved in oligomer formation since inclusion of 100 mM 2-mercaptoethanol in the buffer used for S1R purification and repeat analytical size exclusion chromatography did not change the elution profile.

Fig. 6B shows that in the presence of 0.45 μM BD-1047, a known tight-binding ligand of S1R, the relative proportions of peaks 1 and 2 were essentially unchanged after the ~18 h incubation; similar behavior was observed at each of the three temperatures tested. Several other known S1R ligands, including the natural membrane constituent sphingosine, also gave stabilizing interactions. Fig. 7 shows the percentage increase in the monomer form after incubation with these ligands relative to a control containing no ligand, where a larger increase in monomer corresponds to less effective stabilization of the active oligomer. Overall, the tightest binding synthetic ligands (e.g., BD-1047, 4-PPBP) gave the largest stabilizing effect (i.e., least conversion to the monomer). Interestingly, the natural membrane lipid sphingosine gave a stabilizing interaction that was close to that of many of the synthetic ligands. In contrast, another natural membrane lipid, sphingosine-1-phosphate, did not stabilize the receptor even when present at greater than 20× higher concentration than BD-1047 (10 μM versus 0.45 μM).

Fig. 8 shows an analysis of stoichiometry of binding for BD-1047, a tight-binding ligand, as assessed by stabilization of the peak 1 oligomer. In the experiment with receptor-detergent micelles carried out here, the best-fit KD (r2 = 0.998, solid black line) was ~7 nM, which is comparable the value reported elsewhere (58). The best unconstrained fit stoichiometry of ligand bound per receptor, n, was determined to be 0.43, i.e., corresponding to ~1 mol of ligand per 2 mol of receptor. Fits with n held constant at 1 were not compatible with the binding data (dashed line), as acceptable fits could not be obtained at any KD value. Moreover, when n was held constant at 0.25, approximate fits using the

best-fit KD values gave systematic overestimation of the fraction bound at low ligand:protein ratio (dotted line). An analysis assuming n was 0.33, i.e., ligand binds to a trimer, also gave a similar overestimation; increasing the KD value gave a better fit at low ligand:protein ratios but gave under estimation of complex formation at high ligand:protein ratios. An identical experiment was conducted on the intermediate oligomer (Fig. 1A, peak labeled *) yielding the same results.

5.3.4 Role of GxxxG motif in oligomerization

The GxxxG motif is often involved in helix-helix association in integral membrane proteins (49,59). In S1R, TM2 contains this motif in the primary sequence G87-G88-Trp89-Met90-G91. Mutations of the Gly residues in this motif and an adjacent His residue in MBP-4A-S1R were prepared to test their roles in oligomerization. All mutations within the motif (substitutions of either Ile or Leu at G87, G88 and G91) resulted in lower expression and significantly decreased yield for the purified fusion protein. For example, MBP-4A-S1R gave a purified yield of ~3.5 mg per L of culture medium, while G91I MBP-4A-S1R (~0.4 mg/L) and G91L MBP-4A-S1R (~0.6 mg/L) were the best yields for the proteins with mutations in the GxxxG motif. With all of the purified receptor variants, all mutations in the GxxxG motif eliminated the largest oligomer (e.g., peak 1 in Fig. 2) from size exclusion chromatographs. Fig. 9 shows representative behavior for mutation of Gly91 to either Ile (Fig. 9A) or Leu (Fig. 9B). Both mutations strongly shifted the distribution of receptor states to the monomer form (solid lines). With the G91I mutation (Fig. 9A), a smaller oligomeric state (retention time ~8.2 min, marked with †) with an apparent molecular weight of ~180 kDa was observed. All G88 and G89 mutants had similar chromatograms. This peak plausibly represents a dimeric state of the S1R. Fig. 9C shows that the mutation H97A, which is not in the GxxxG motif, yielded a chromatograph almost identical to MBP-4A-S1R, suggesting this residue does not play an important role in oligomerization.

Fig. 10 shows that mutations within the GxxxG motif had a profound effect on specific ligand binding. Among the set of all GxxxG mutations, G91L MBP-4A-S1R exhibited ~20% of specific pentazocine binding activity of the non-mutated receptor, while all other mutations in the GxxxG motif yielded purified receptor variants that had less than 5% specific binding. Corresponding to the modest level of specific binding activity observed, G91L MBP-4A-S1R uniquely stabilized a significant fraction of the purified protein as the intermediate oligomer (Fig. 9B), likely tetramer (Fig. 3C). These results further implicate the role of an oligomer in ligand binding. While H97A MBP-4A- S1R had a distribution of large, intermediate and monomer states that was nearly identical with the non-mutated fusion protein (Fig. 9C), it exhibited only ~50% ligand binding activity (Fig. 10). This result suggests a role for H97 in ligand binding independent of oligomerization.

5.3.5 Oligomerization of TM2

To further assess the propensity of TM2 for self-association, TOXCAT reporter assays were performed by inserting the sequence of TM2 (WVFVNAGGWMGAMCLL- HASL) between MBP and the ToxR receptor (Fig. 11A). With this construct, oligomerization of the TM2 region can be assessed by catalytic assasy of the ToxR-mediated expression of CAT, as ToxR only functions as a transcriptional enhancer when it is present as an oligomer. Fig. 11B shows results from the TOXCAT experiment. All variants were expressed to a comparable level as assessed by western blotting, and non-mutated TM2 from S1R gave rise to a strong positive CAT assay response, corroborating the propensity of the TM2 sequence to self-associate. Interestingly, among the single mutations of the GxxxG motif, only G91I eliminated the positive response in the CAT assay, indicating this mutation strongly destabilized oligomerization of the TM2. Surprising, the G91L mutation gave a positive assay response, albeit attenuated to only 60% of that observed from the non-mutated TM2. Individually,

mutations at either G87 or G88 did not affect the assay response. While this result is apparently contradictory to the results of Fig. 10 obtained with the full length receptor, the adjacent positions of Gly87 and Gly88 in the primary sequence of the TM2 peptide presumably allowed alternative modes for association of the TM2 peptide that could not be achieved with the TM2 present in the MBP-4A-S1R fusion. The double mutation G87L/G88L eliminated the TOXCAT assay response, perhaps corresponding to more effective disruption of alternative TM2 interactions leading to oligomerization.

5.4 Discussion

In this work, we provide biochemical evidence for the importance of an oligomeric state in the ligand binding function of guinea pig S1R, and the essential role of the GxxxG motif from TM2 in this oligomerization. Since amino acid sequences and pharmacological profiles are highly conserved among mammalian S1R (Fig. S1), these results are likely broadly relevant to many studies of this protein family (60). Mutational analysis of putative TM2 in both the full-length receptor and as a transmembrane domain in the TOXCAT studies have identified key residues involved in oligomerization (G87, G88 and G91) and in ligand binding independent of oligomerization (His97). This work adds to the list of other residues in TM2 (S99, Y103 and L105- L106) that are important for ligand binding (61), which this work suggests is intimately related to the ability to form one or more oligomeric states. Although the GxxxG motif within TM2 has an important role in oligomer formation, other studies have implicated additional residues of the S1R receptor sequence in dimerization/oligomerization (17), which could explain the appearance of the 180 kDa peak (Fig. 9A peak labeled †). The S1R ligand binding site in the intact receptor, as identified by photoaffinity labeling, has been localized to a region that juxtaposes a steroid binding domain-like motif (SBDLI) in TM2 (which encompasses the oligomerization sequences identified in this work) and a C-terminal SBDLII hydrophobic sequence (42-44). Although the C- terminus alone does not bind S1R ligands, some of the chaperone functions of S1R have been localized to this region (62). It has been proposed that S1R agonists alter the structure of the receptor in such a fashion that the C-terminal chaperone region becomes accessible to its client proteins. NMR derived structures of the C-terminus have been recently reported (63). Perhaps the oligomeric states of the S1R receptor dictate the availability of the C- terminus for these interactions (64).

Several previous experiments support the conclusion that S1R functions as an oligomer in ligand binding. For example, different molecular weights have been observed by gel filtration chromatography for S1R purified from natural sources (65). Moreover, high molecular weight bands of S1R protected from photo-affinity labeling by (+)-pentazocine were detected by denaturing gel electrophoresis of rat liver microsomes (44,64). Furthermore, gel filtration of ligand-bound S1R purified from human leukemia cells showed that ligand binding activity was associated with a protein of ~100 kDa (2). Many other membrane receptors adopt an oligomeric state (66-68), and recombinant expression often leads to a distribution of these states (69). For example, when human serotonin receptor 3A was overexpressed in E.coli, the protein was detected as a mixture of oligomers and the biologically active pentamer represented only 7% of the total protein (70). The percentage of active S1R protein determined in the study reported here was between 50-75%.

S1R interacts with a large number of synthetic and natural ligands, and has also been documented to interact with a large number of different proteins within the cell (5,30). We found that interactions with the tightest binding synthetic ligands strongly stabilize the oligomeric state (Fig. 6, 7). The stabilizing effects of ligands on many other membrane proteins, including G-protein coupled receptors, is recognized (71,72). Our studies with purified S1R indicate a minimal binding stoichiometry of one ligand per two polypeptide chains (Fig. 8), while reconciliation of gel filtration, light scattering and denaturing gel electrophoresis results obtained with purified S1R suggest the octamer, hexamer and tetramer are the predominant ligand binding forms. A stoichiometry of one ligand bound/dimer is further supported by the work of Chu and Ruoho (64) who showed that a C12 alkyl containing photoprobe selectively and quantitatively derivatized His145 at a proposed S1R dimer interface. Further, dimerization of S1R, as assessed by SDS-PAGE, occurred via intermolecular

disulfide bond formation when a M170C mutant form of the receptor was expressed.

The oligomer can decay to an intermediate tetramer and monomer in the absence of ligands (Fig. 6), while mutations of the GxxxG motif change the distribution of these species. Preliminary efforts to reassemble the monomer into functional oligomers were not successful. However, it is intriguing to consider that protein-protein interactions may be involved in reassembly of the functional receptor. In this regard, monomeric S1R has been reported to interact with ion channels such as Nav 1.5 voltage-gated Na+ channel, acid sensing channels, and dopamine D1 receptor (16,23,73). Interestingly, these interactions were disrupted in the presence of ligands such as haloperidol and/or (+)-pentazocine, so one may speculate that a ligand-gated S1R oligomer/monomer equilibrium defines the availability of monomer S1R for interaction with client ion channels or G-protein coupled receptors. An additional unusual feature of binding of the agonist, (+)-pentazocine, to S1R is the time (>90 min at 30 ˚C) needed to reach equilibrium (41,74). It is possible that formation of stable interactions between oligomeric states of S1R in situ regulate the rate of (+)-pentazocine binding to S1R (perhaps also affected by interactions with accessory protein partners). Fig. 12 provides a schematic of these possibilities.

Figure 5.1

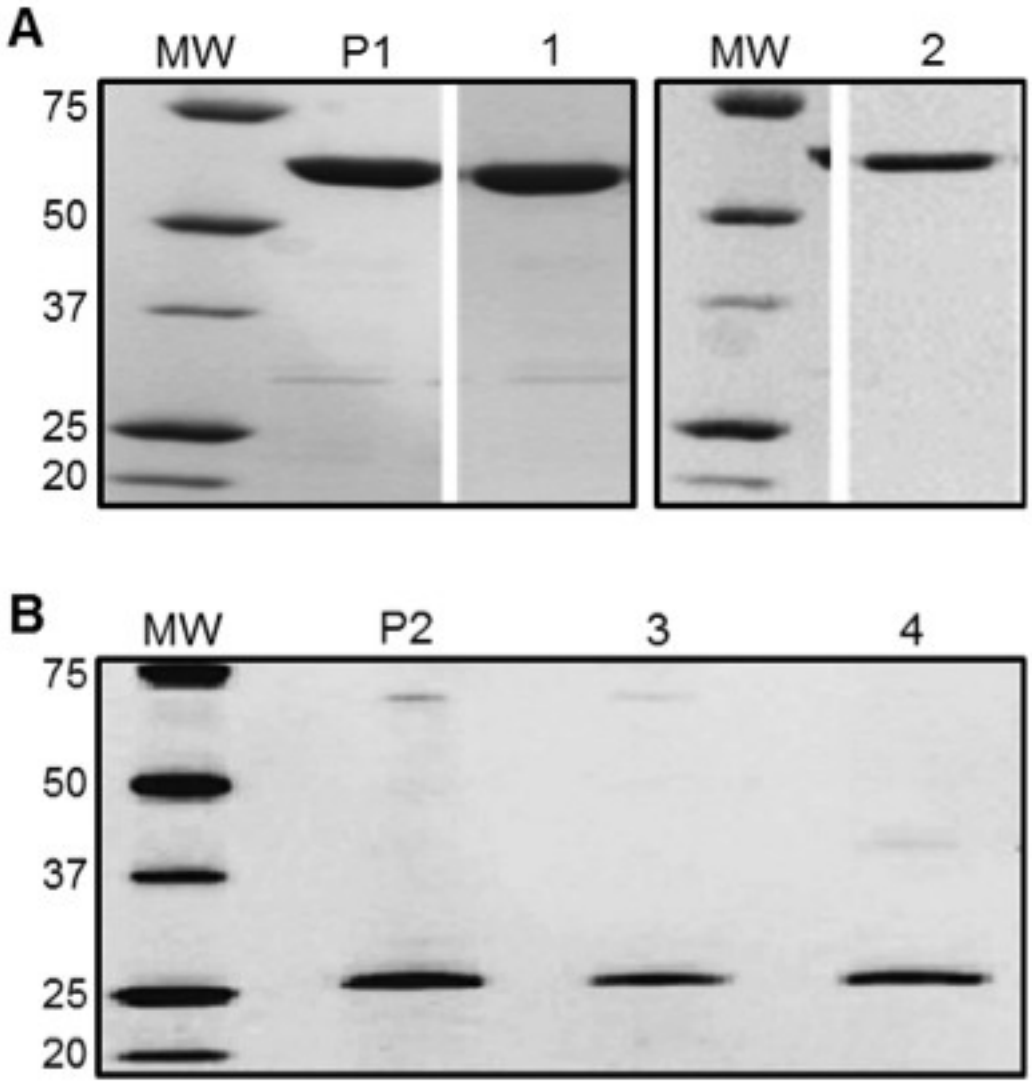

Figure 5.1 SDS-PAGE of MBP-4A-S1R (A) and S1R (B). The starting MBP-4A-S1R and S1R preparations prior to SEC separation are labeled P1 and P2, respectively. Peaks 1-4 from Fig. 2A are labeled respectively. Molecular weight markers (MW) are labeled in kDa.

Figure 5.2

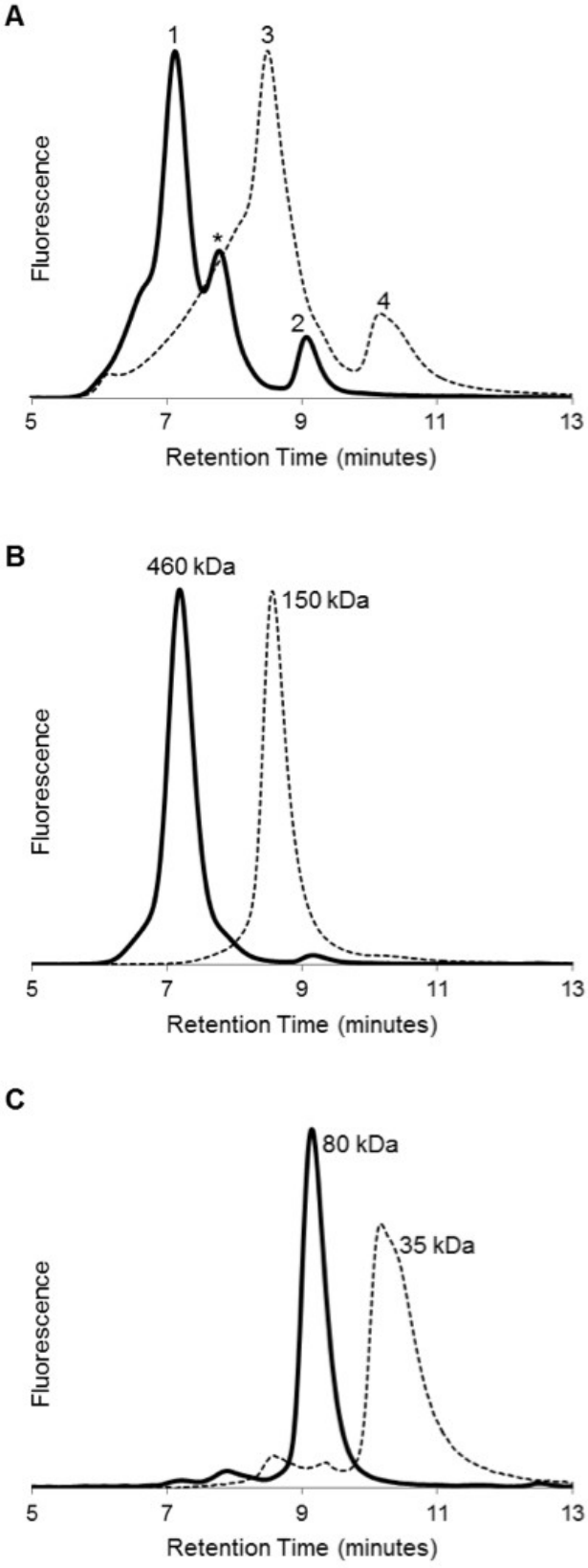
A
1
3
*
2
4
Fluorescence
5
7
9
11
13
Retention Time (minutes)
B
460 kDa
150 kDa
Fluorescence
5
7
9
11
13
Retention Time (minutes)
C
80 kDa
35 kDa
Fluorescence
5
7
9
11
13
Retention Time (minutes)

Figure 5.2 Evidence from size exclusion chromatography for oligomeric states of S1R. A, elution profiles for MBP- 4A-S1R (solid line) and S1R (dashed line). Peaks corresponding to different oligomerization states are marked with numbers 1-4. B, repeat chromatography of peaks 1 (solid line) and 3 (dashed line) from A. C, repeat chromatography of peaks 2 (solid line) and 4 (dashed line) from A.

Figure 5.3

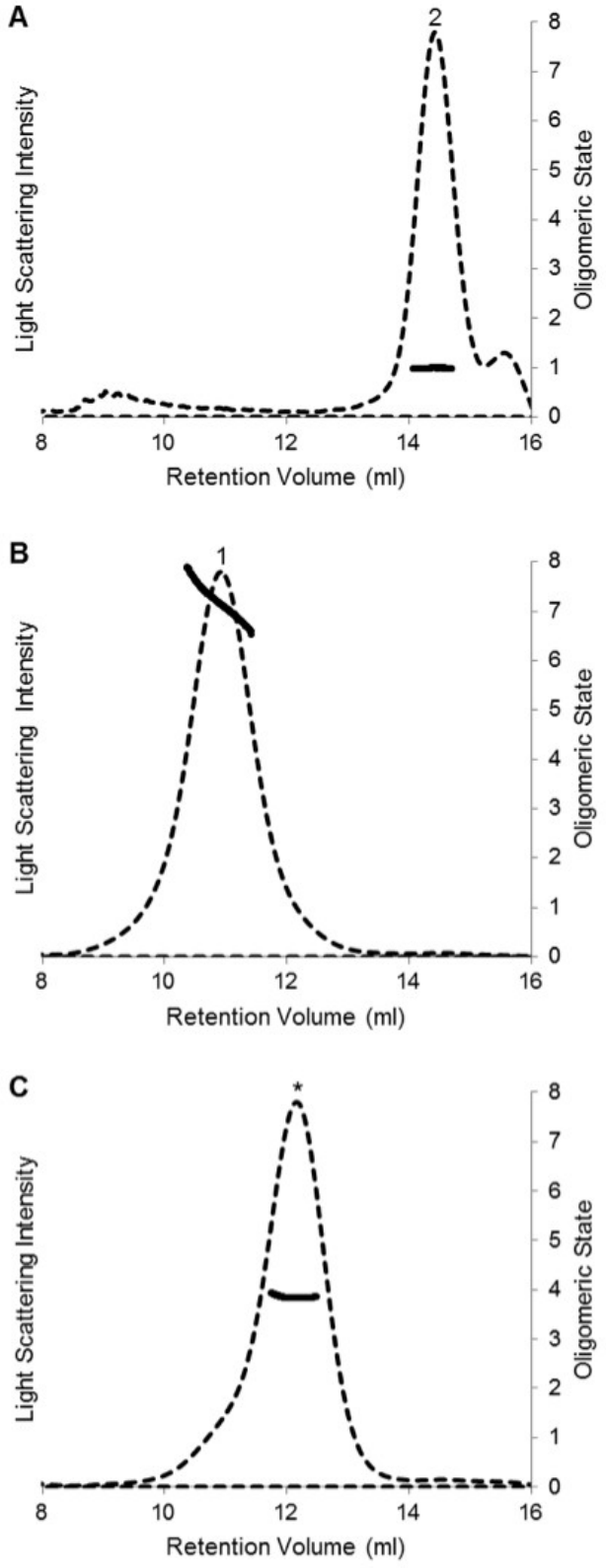
A
2
Light Scattering Intensity
Oligomeric State
Retention Volume (ml)
B
1
Light Scattering Intensity
Oligomeric State
Retention Volume (ml)
C
*
Light Scattering Intensity
Oligomeric State
Retention Volume (ml)

Figure 5.3 Oligomeric molecular weight of MBP-4A-S1R determined by light scattering. Elution profiles detected by 652 nm laser light scattering are shown by dashed lines. Oligomeric stoichiometry across each peak is marked with a solid line. Peaks have the same labeling as in Fig. 1 and 2. A, The apparent monomer is confirmed to be a monomer. B, The largest molecular weight oligomer is polydisperse, with stoichiometry ranging from a hexamer to octamer. C, The intermediate oligomer is a tetramer.

Figure 5.4

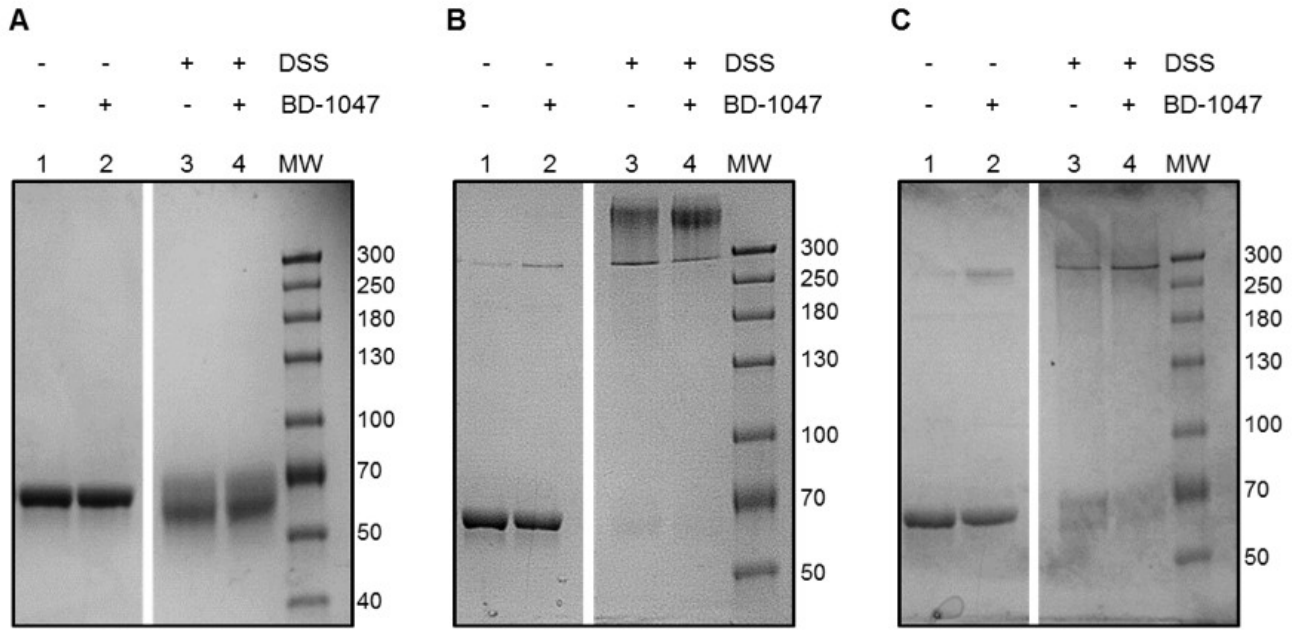

Figure 5.4 Analysis of oligomeric states of MBP-4A-S1R by chemical cross-linking agent disuccinimidyl suberate (DSS). DSS-free controls are shown by lanes 1 and 2, containing 0 and 10 μM high affinity ligand BD-1047 respectively. Lanes 3 and 4 mirror the control with the addition of DSS. A, The addition of cross-linking agent to the monomer (Fig. 2A, peak 2). The bands show slight smearing with no shift in size, signifying only intramolecular cross-linking. B, The addition of cross-linking agent to the oligomer (Fig. 2A, peak 1). The bands show a mass greater than 300 kDa and oligomeric stoichiometry cannot be accurately determined. However, an oligomeric state greater than tetramer is clearly visible. C, The addition of cross-linking agent to the intermediate oligomer (Fig. 2A peak labeled *). The bands show an approximate 4-fold increase in size to a mass between 250 and 300 kDa, suggesting a tetrameric state.

Figure 5.5

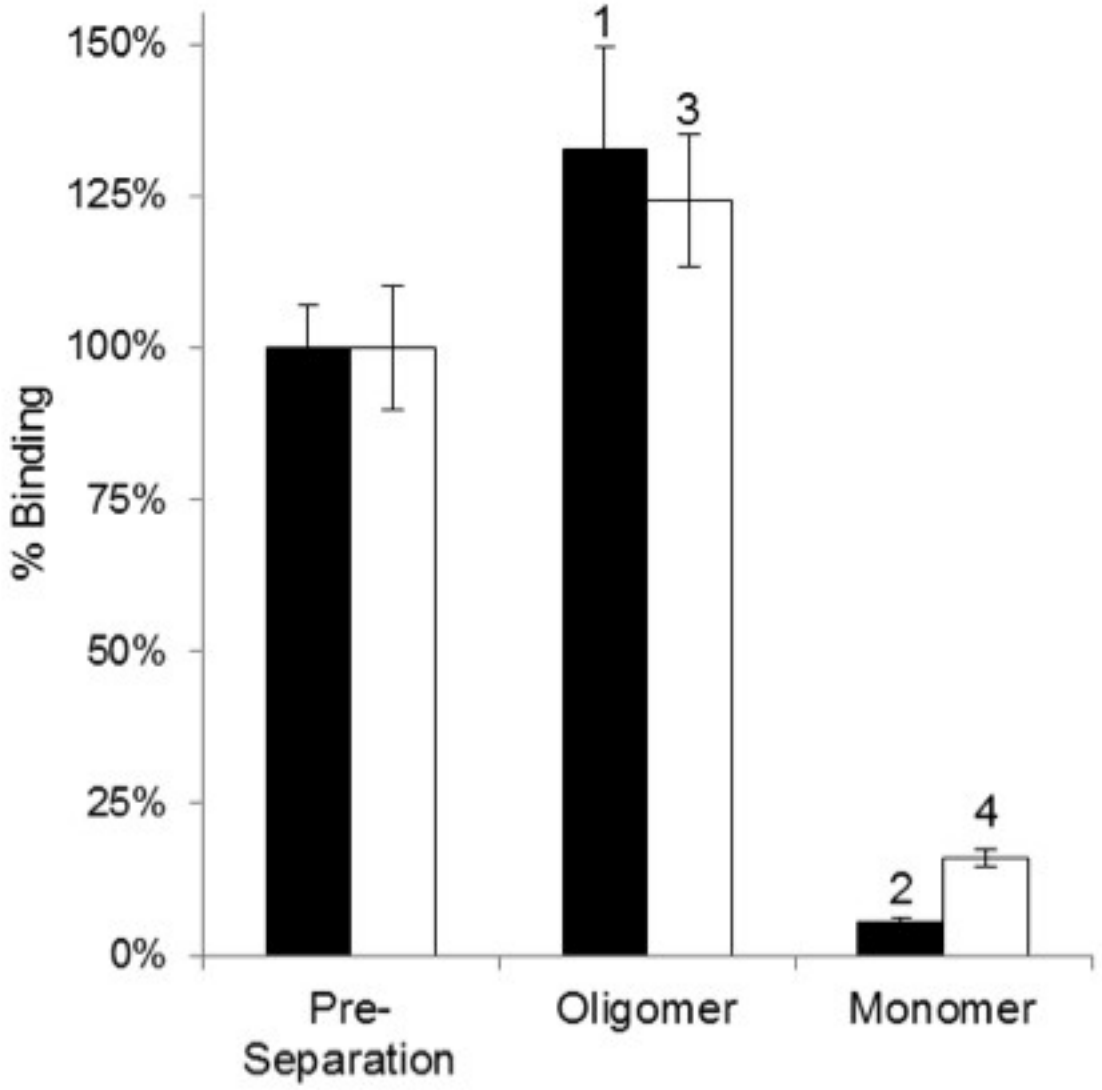

Figure 5.5 Comparison of specific pentazocine binding activity of S1R oligomers before and after repeat chromatography of peaks from Fig. 2B and 2C. The black bars are for assays of MBP-4A-S1R; white bars are for assays of S1R. Binding assays were performed in triplicate and the error bars represent 1σ deviation.

Figure 5.6

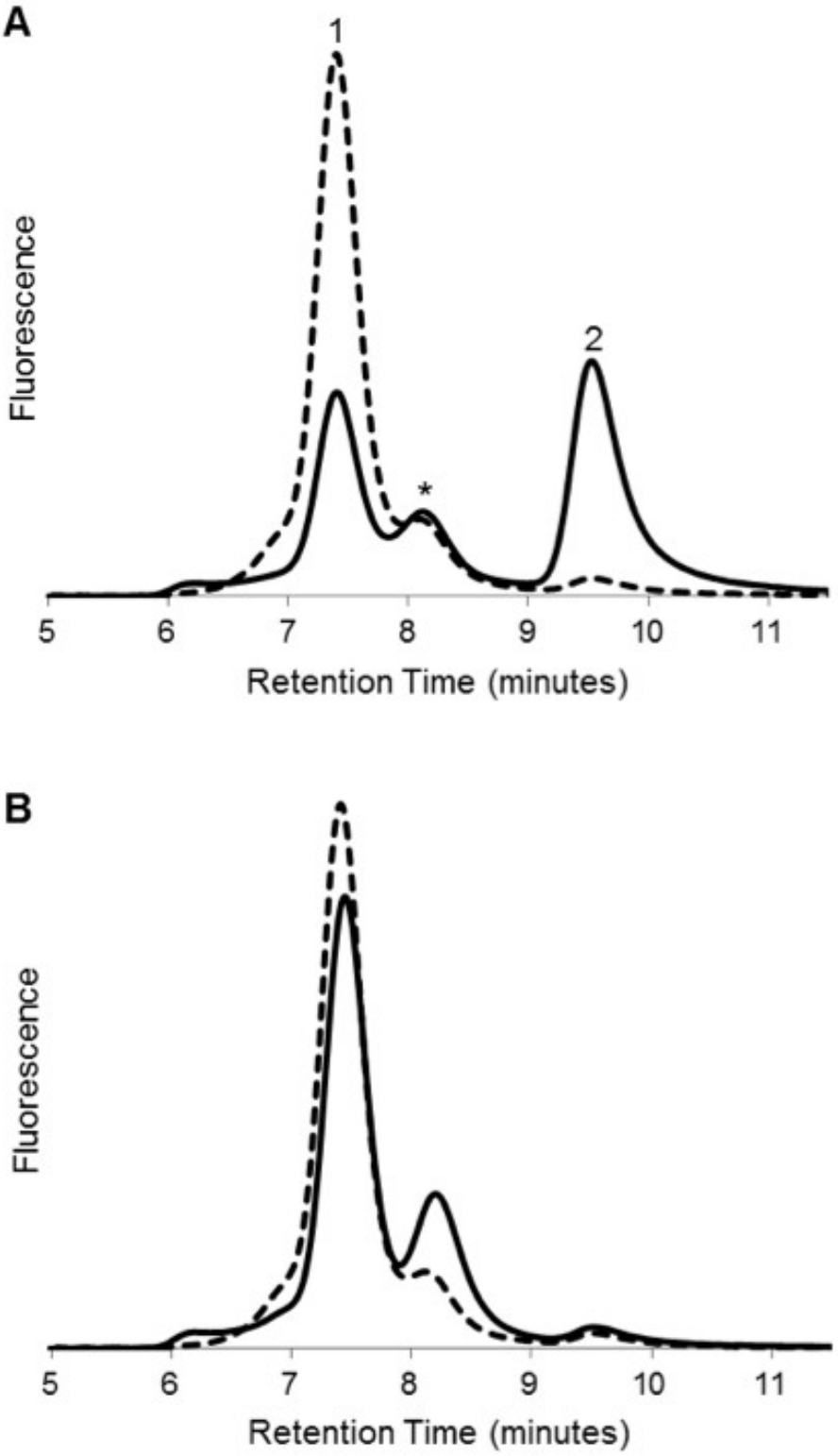
A
1
2
*
Fluorescence
5
6
7
8
9
10
11
Retention Time (minutes)
B
Fluorescence
5
6
7
8
9
10
11
Retention Time (minutes)

Figure 5.6 Stabilization of oligomeric S1R by ligand binding. A, size exclusion chromatogram of MBP-4A-S1R before (dashed line) and after incubation for 1 day at 37 ˚C (solid line) without added ligand. Peaks have the same labeling as in Fig. 1 and 2. B, chromatogram of MBP-4A-S1R before (dashed line) and after (solid line) incubation for 1 day at 37 ˚C in the presence of the tight binding ligand BD-1047 (10 μM).

Figure 5.7

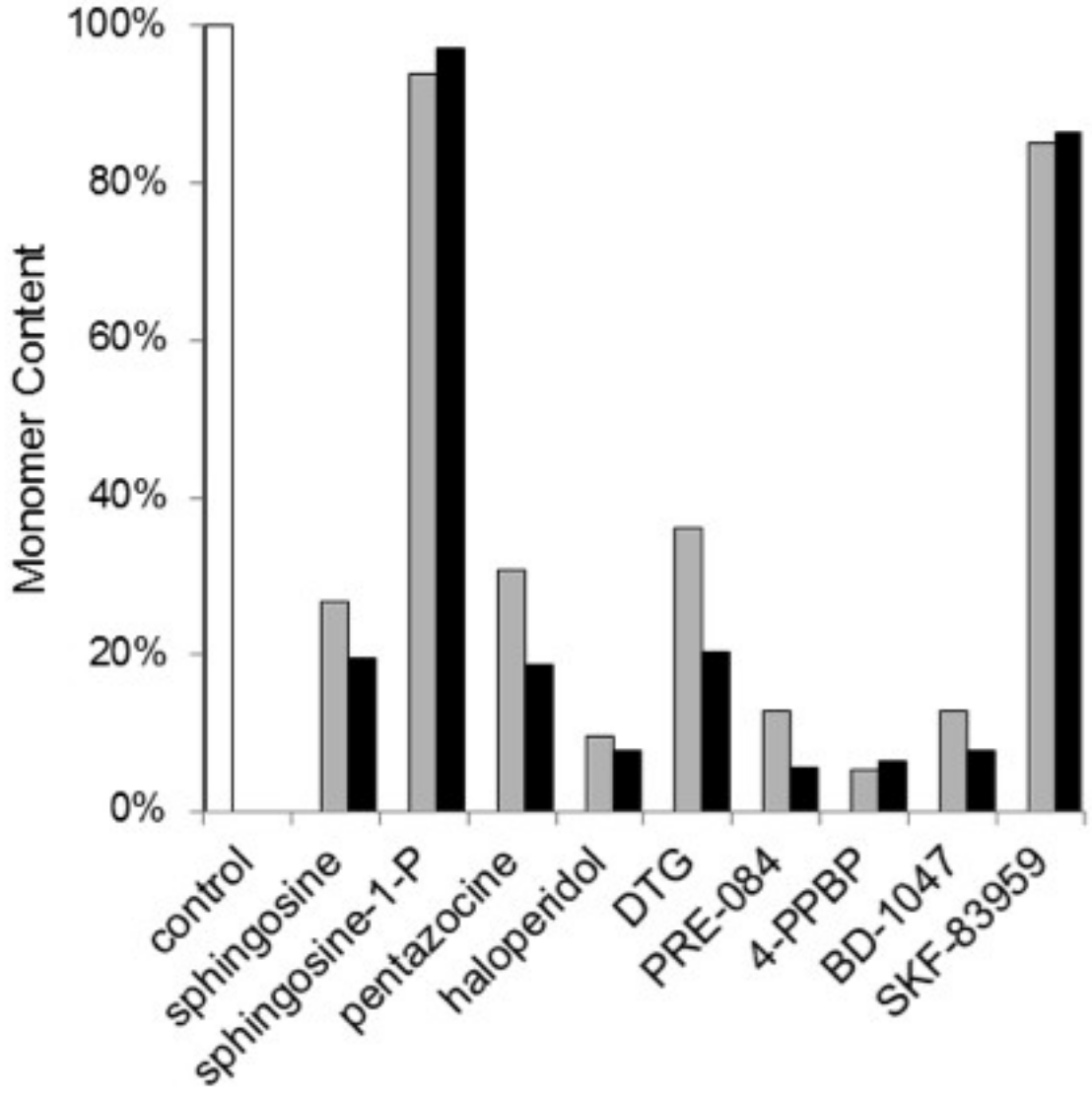

Figure 5.7 Comparison of the ability of various S1R ligands to prevent conversion to the inactive monomer state. The amount of MBP-4A-S1R converted to the monomer (peak 2 from Fig. 2) in the absence of ligands served as the control (white bar). Gray and black bars indicate ligand doses of 0.45 and 10 μM respectively, while the concentration of MBP-4A-S1R was always 0.23 μM. Tight-binding ligands 4-PPBP, BD-1047 and others stabilized the oligomeric states, whereas sphingosine-1-phosphate

allowed conversion to the monomeric state.

Figure 5.8

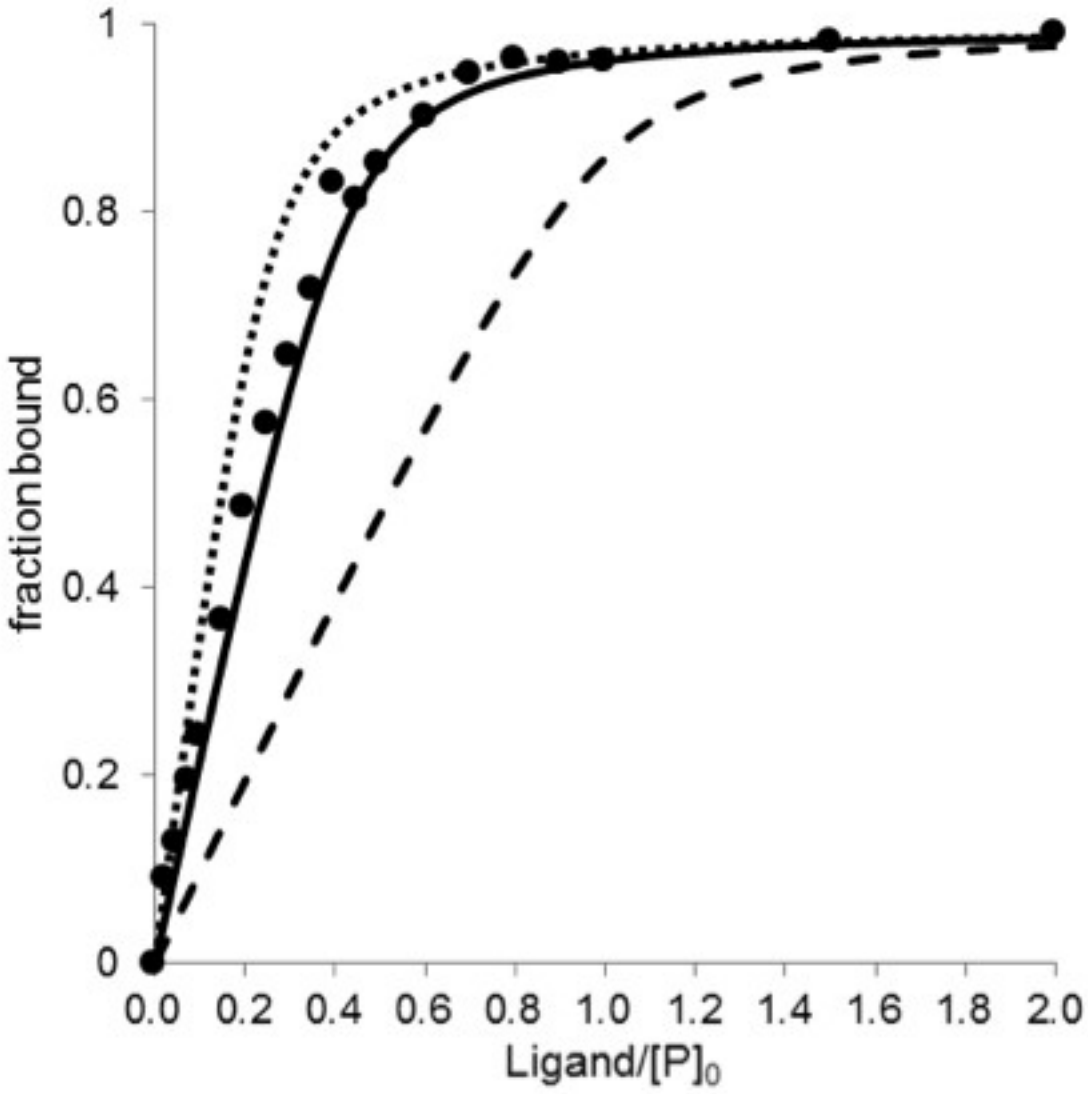

Figure 5.8 Ligand binding stoichiometry determined by titration of BD-1047 into a 300 nM sample of peak 1 (see Fig. 2B). Experimental measurements (solid circles) were made in the concentration range from 0 to 3000 nM, with results shown up to 600 nM ligand. Binding curves were calculated as described in Materials and Methods with best fit values of KD = 7 nM and n = 0.43 (solid

line), fixed KD = 7 nM and n = 0.25 (dotted line), or fixed KD = 7 nM and n = 1 (dashed line).

Figure 5.9

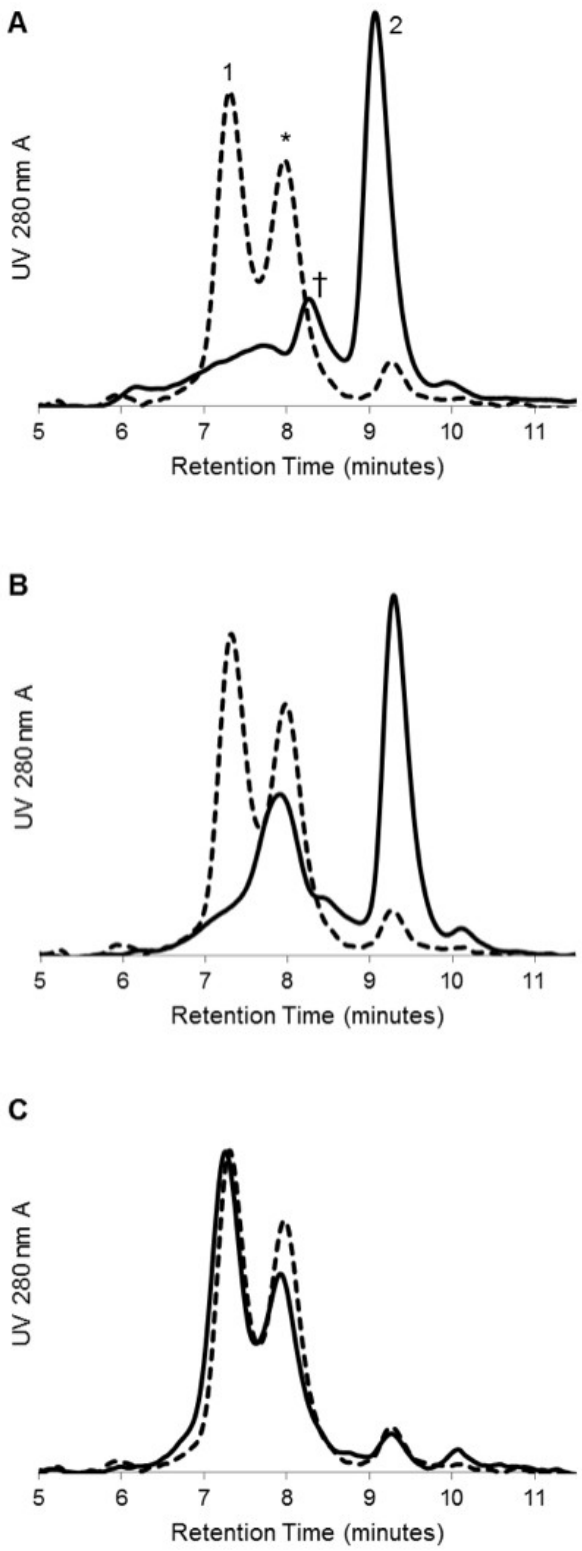
A
1
2
*
†
UV 280 nm A
5
6
7
8
9
10
11
Retention Time (minutes)
B
UV 280 nm A
5
6
7
8
9
10
11
Retention Time (minutes)
C
UV 280 nm A
5
6
7
8
9
10
11
Retention Time (minutes)

Figure 5.9 Size exclusion chromatography of MBP-4A-S1R with mutations in the GxxxG motif. The control chromatogram of MBP-4A-S1R lacking mutations is shown as a dotted line. A, G91I MBP-4A-S1R with defined peaks as in Fig. 2. A significant shift toward the monomeric state is seen, as is a new ~180 kDa peak labeled with †. B, G91L MBP-4A-S1R showing conversion to intermediate oligomeric (*) and monomer (peak 2) states. C, H97A MBP-4A-S1R showed little change in the oligomerization states relative to the non-mutated receptor.

Figure 5.10

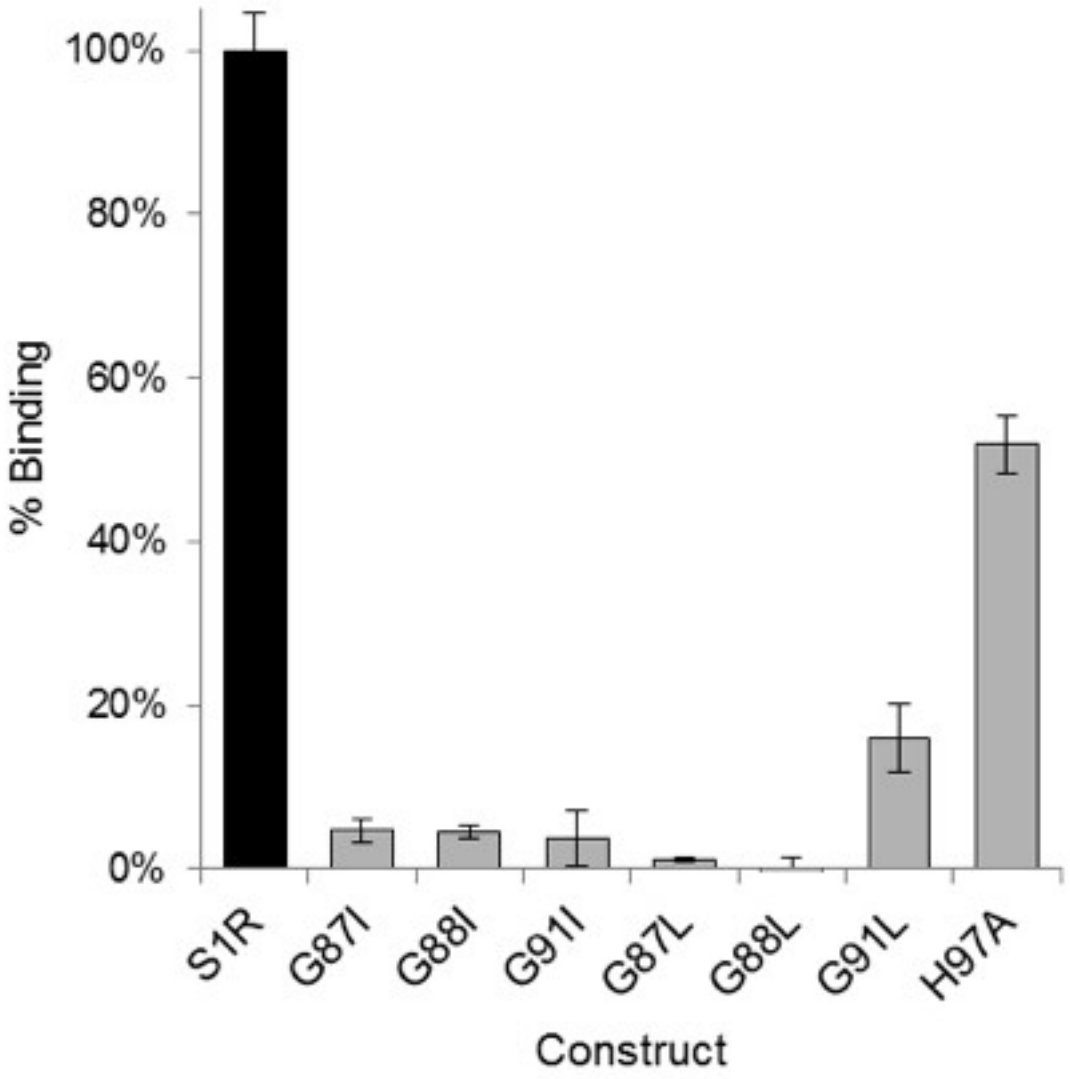

Figure 5.10 [3H]-pentazocine specific binding for MBP-4A-S1R and the variants with mutations in the GxxxG motif. Binding activity is shown relative to MBP-4A-S1R (black bar); n = 3; error bars represent 1 σ deviation.

Figure 5.11

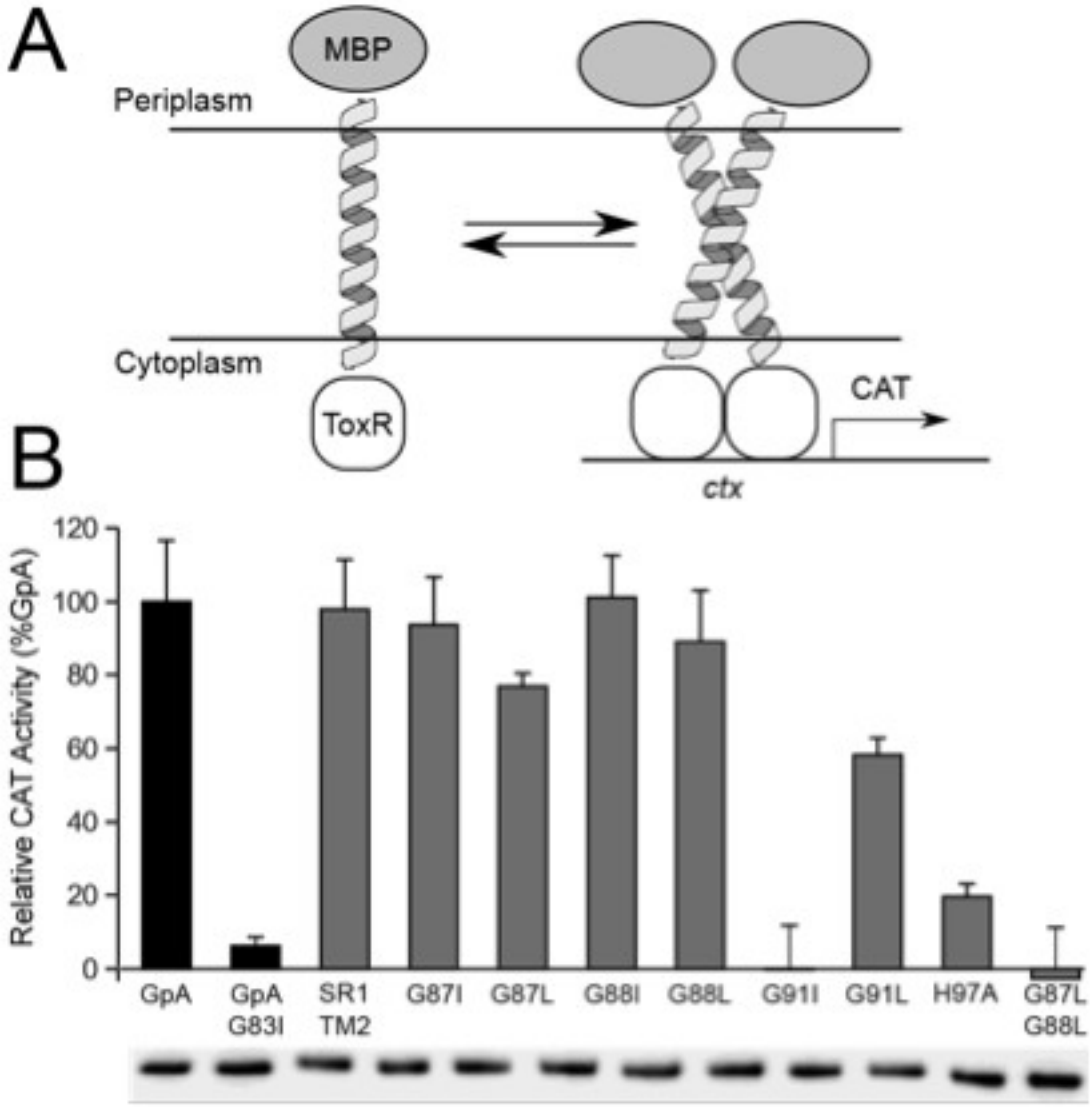

Figure 5.11 TOXCAT measurements for mutations of the TM2 domain of S1R. A, schematic of the TOXCAT experiment, where periplasmic secretion of MBP is used to place a TM domain into the cytoplasmic membrane, while ToxR resides in the cytoplasm. Dimerization of the TM promotes dimerization of ToxR, which then acts as a transcriptional activator, in this case for CAT. B) The TOXCAT response is reported as a percentage relative to the strong transmembrane oligomerization

control, glycophorin A (GpA). Immunoblot results obtained from anti- MBP-HRP are shown below the histogram bars, and indicate equivalent expression of all TM2 domain variants.

Figure 5.12

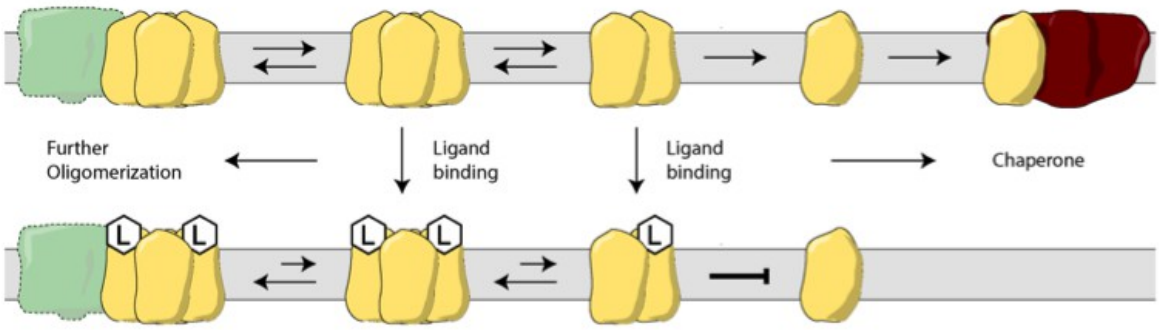

Figure 5.12 A model representing the proposed interconversions of S1R between the monomer form and ligand stabilized oligomeric forms. Protein partners of the monomer form would include voltage-gated Na+ channel, acid sensing channels, and dopamine D1 receptor (16,23,73).

5.5 Supplementary information

Table S5.1 List of primers used in cloning experiments.

Name	Sequence	Notes
Nhe1-TM2 Pair	ctagcTGGGTGTTCGTGAACGCGGGCGGCTGGATGGGCGCCATGTGCCTTCTGCATGCCTCGCTGgg	TM2-ToxCat ultramere
TM2-BamH1 Pair	atcccCAGCGAGGCATGCAGAAGGCACATGGCGCCCATCCAGCCGCCCGCGTTCACGAACACCCAgg	TM2-ToxCat ultramere
G87I For2	GTGAACGCGatCGGCTGGATG	G87I mutation
G87I Rev2	CATCCAGCCGatCGCGTTCAC	G87I mutation
G87L For	GTGAACGCGctCGGCTGGATG	G87Lmutation
G87L Rev	CATCCAGCCGagCGCGTTCAC	G87Lmutation
G88I For2	GAACGCGGGCatCTGGATGG	G88Imutation
G88I Rev2	CCATCCAGatGCCCGCGTTC	G88Imutation
G88L For	GAACGCGGGCctCTGGATGG	G88Lmutation
G88L Rev	CCATCCAGagGCCCGCGTTC	G88Lmutation
G91I For2	GGCTGGATGatCGCCATGTGC	G91Imutation
G91I Rev2	GCACATGGCGatCATCCAGCC	G91Imutation
G91L For	GGCTGGATGctCGCCATGTGC	G91Lmutation
G91L Rev	GCACATGGCGagCATCCAGCC	G91Lmutation
GG87LL For	GTGAACGCGctCctCTGGATGGG	GG87LLmutation
GG87LL Rev	CCCATCCAGagGagCGCGTTCAC	GG87LLmutation
H97A For	GTGCCTTCTGgcTGCCTCGC	H97Amutation
H97A Rev	GCGAGGCAgcCAGAAGGCAC	H97Amutation
GpS1R5' For	ATGCAGTGGGCCGTGGGCCGGCGATG	Creation of the A4 linker
GpS1R-A4 Rev	GCCCACGGCCCACTGCATtgcagctgcagcAGTCTGCGCGTCTTTCAGGGCTTC	Creation of the A4 linker

Figure S5.1

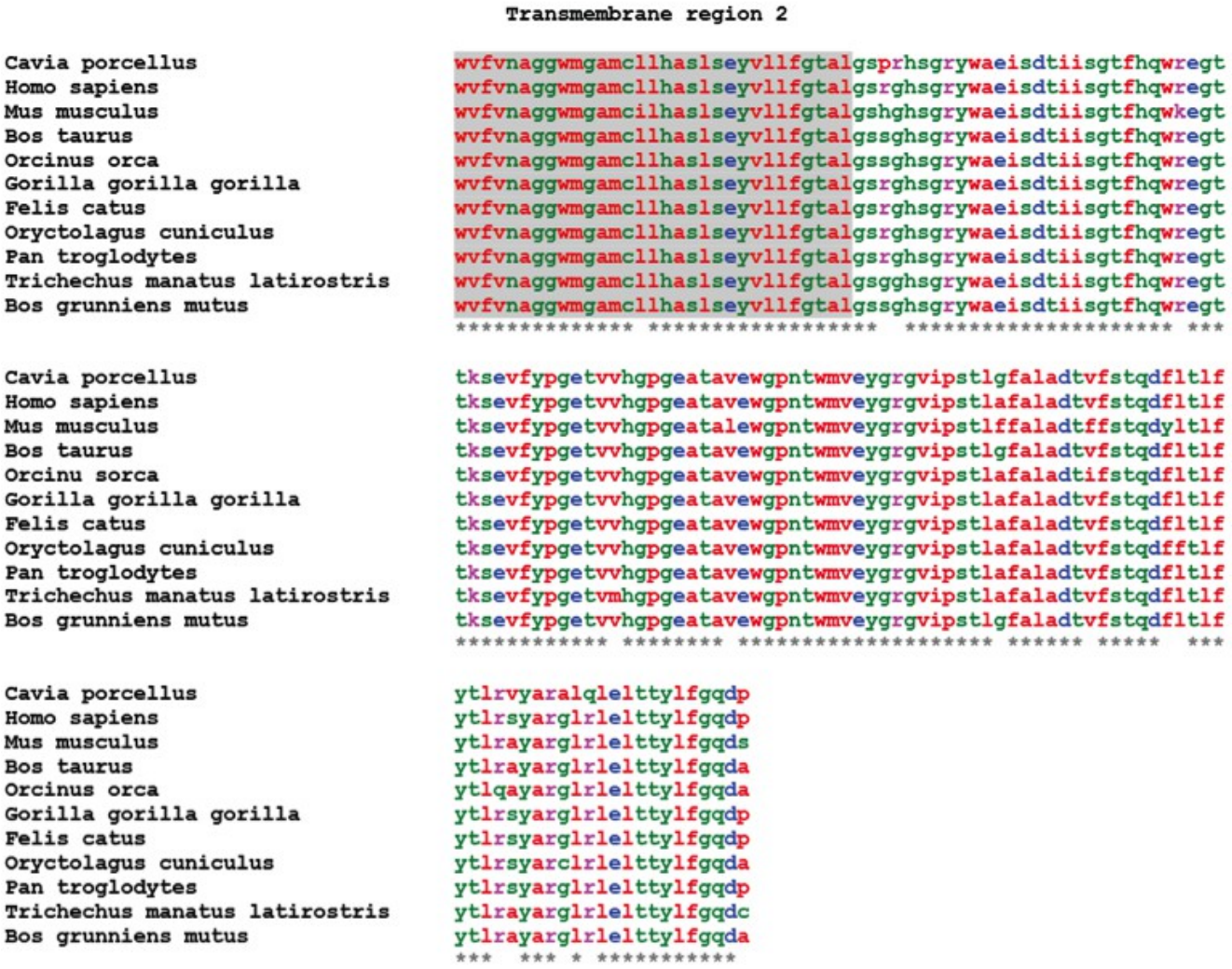

Figure S5.1 Alignment of mammalian amino acid sequences for Sigma 1 receptor protein (variant 1 only). Sequence is shown starting at the predicted second transmembrane region (TM2). Gray shading indicates the predicted transmembrane region 2. Absolutely conserved residues are marked with asterisk. Alignment prepared using Clustal Omega, job # clustalo-I20130415-193556-0648-67762133-pg (1,2).

References for Figure S5.1

1. Goujon, M., McWilliam, H., Li, W., Valentin, F., Squizzato, S., Paern, J., and Lopez, R. (2010) A new bioinformatics analysis tools framework at EMBL-EBI. Nucleic Acids Res 38, W695-699.

2. Sievers, F., Wilm, A., Dineen, D., Gibson, T. J., Karplus, K., Li, W., Lopez, R., McWilliam, H., Remmert, M., Soding, J., Thompson, J. D., and Higgins, D. G. (2011) Fast, scalable generation of high-quality protein multiple sequence alignments using Clustal Omega. Mol Syst Biol 7, 539.

5.6 Acknowledgements

The authors thank Drs Emily T. Beebe, Ronnie O. Frederick, and Shin-ichi Makino for helpful comments on experimental procedures and analysis of results. This work was supported by NIGMS PSI: Biology Network grant U54 GM094584 to B.G.F and NIH NS075820 to A.E.R. H.R.M. received a University of Wisconsin-Madison Hilldale Fellowship. U.C. holds a Pharmaceutical Manufacturer's Postdoctoral Fellowship. A.E.R. was also supported by an Edwin and Dorothy Gamewell UW McPherson Retina Research Foundation Professorship. Light scattering experiments performed at the Yale University W.M. Keck Foundation were supported by NIH Award Number 1S10RR023748-01.

5.7 References

1. Hanner, M., Moebius, F. F., Flandorfer, A., Knaus, H. G., Striessnig, J., Kempner, E., and Glossmann, H. (1996) Purification, molecular cloning, and expression of the mammalian sigma1-binding site. Proc Natl Acad Sci U S A 93, 8072-8077

2. Jbilo, O., Vidal, H., Paul, R., De Nys, N., Bensaid, M., Silve, S., Carayon, P., Davi, D., Galiegue, S., Bourrie, B., Guillemot, J. C., Ferrara, P., Loison, G., Maffrand, J. P., Le Fur, G., and Casellas, P. (1997) Purification and characterization of the human SR 31747A-binding protein. A nuclear membrane protein related to yeast sterol isomerase. J Biol Chem 272, 27107-27115

3. Kekuda, R., Prasad, P. D., Fei, Y. J., Leibach, F. H., and Ganapathy, V. (1996) Cloning and functional expression of the human type 1 sigma receptor (hSigmaR1). Biochem Biophys Res Commun 229, 553-558

4. Seth, P., Leibach, F. H., and Ganapathy, V. (1997) Cloning and structural analysis of the cDNA and the gene encoding the murine type 1 sigma receptor. Biochem Biophys Res Commun 241, 535-540

5. Su, T. P., Hayashi, T., Maurice, T., Buch, S., and Ruoho, A. E. (2010) The sigma-1 receptor chaperone as an inter-organelle signaling modulator. Trends Pharmacol Sci 31, 557-566

6. Ha, Y., Dun, Y., Thangaraju, M., Duplantier, J., Dong, Z., Liu, K., Ganapathy, V., and Smith, S. B. (2011) Sigma receptor 1 modulates endoplasmic reticulum stress in retinal neurons. Invest Ophthalmol Vis Sci 52, 527-540

7. Hayashi, T., and Fujimoto, M. (2010) Detergent-resistant microdomains determine the localization of sigma-1 receptors to the endoplasmic reticulum-mitochondria junction. Mol Pharmacol 77, 517-528

8. Hayashi, T., Justinova, Z., Hayashi, E., Cormaci, G., Mori, T., Tsai, S. Y., Barnes, C., Goldberg, S. R., and Su, T. P. (2010) Regulation of sigma-1 receptors and endoplasmic reticulum chaperones in the brain of methamphetamine self-administering rats. J Pharmacol Exp Ther 332, 1054-1063

9. Aydar, E., Palmer, C. P., Klyachko, V. A., and Jackson, M. B. (2002) The sigma receptor as a ligand-regulated auxiliary potassium channel subunit. Neuron 34, 399-410

10. Mavlyutov, T. A., Epstein, M. L., Andersen, K. A., Ziskind-Conhaim, L., and Ruoho, A. E. (2010) The sigma-1 receptor is enriched in postsynaptic sites of C-terminals in mouse motoneurons. An anatomical and behavioral study. Neuroscience 167, 247-255

11. Mavlyutov, T. A., Epstein, M. L., Liu, P., Verbny, Y. I., Ziskind-Conhaim, L., and Ruoho, A. E. (2012) Development of the sigma-1 receptor in C-terminals of motoneurons and colocalization with the N,N'- dimethyltryptamine forming enzyme, indole-N-methyl transferase. Neuroscience 206, 60-68

12. Gundlach, A. L., Largent, B. L., and Snyder, S. H. (1986) Autoradiographic localization of sigma receptor binding sites in guinea pig and rat central nervous system with (+)3H-3-(3-hydroxyphenyl)-N-(1- propyl)piperidine. J Neurosci 6, 1757-1770

13. Moebius, F. F., Bermoser, K., Reiter, R. J., Hanner, M., and Glossmann, H. (1996) Yeast sterol C8-C7 isomerase: identification and characterization of a high-affinity binding site for enzyme inhibitors. Biochemistry 35, 16871-16878.

14. Hayashi, T., and Su, T. P. (2001) Regulating ankyrin dynamics: Roles of sigma-1 receptors. Proc Natl Acad Sci U S A 98, 491-496.

15. Hayashi, T., and Su, T. P. (2007) Sigma-1 receptor chaperones at the ER-mitochondrion interface regulate Ca(2+) signaling and cell survival. Cell 131, 596-610.

16. Navarro, G., Moreno, E., Aymerich, M., Marcellino, D., McCormick, P. J., Mallol, J., Cortes, A., Casado, V., Canela, E. I., Ortiz, J., Fuxe, K., Lluis, C., Ferre, S., and Franco, R. (2010) Direct involvement of sigma-1 receptors in the dopamine D1 receptor-mediated effects of cocaine. Proc Natl Acad Sci U S A 107, 18676-18681.

17. Kim, F. J., Kovalyshyn, I., Burgman, M., Neilan, C., Chien, C. C., and Pasternak, G. W. (2010) Sigma 1 receptor modulation of G-protein-coupled receptor signaling: potentiation of opioid transduction independent from receptor binding. Mol Pharmacol 77, 695-703.

18. Villard, V., Espallergues, J., Keller, E., Vamvakides, A., and Maurice, T. (2011) Anti-amnesic and neuroprotective potentials of the mixed muscarinic receptor/sigma 1 (sigma1) ligand ANAVEX2-73, a novel aminotetrahydrofuran derivative. J Psychopharmacol 25, 1101-1117.

19. Wilke, R. A., Lupardus, P. J., Grandy, D. K., Rubinstein, M., Low, M. J., and Jackson, M. B. (1999) K+ channel modulation in rodent neurohypophysial nerve terminals by sigma receptors and not by dopamine receptors. J Physiol 517 (Pt 2), 391-406.

20. Johannessen, M., Ramachandran, S., Riemer, L., Ramos-Serrano, A., Ruoho, A. E., and Jackson, M. B. (2009) Voltage-gated sodium channel modulation by sigma-receptors in cardiac myocytes and heterologous systems. Am J Physiol Cell Physiol 296, C1049-1057.

21. Zhang, M. R., Haradahira, T., Maeda, J., Okauchi, T., Kawabe, K., Kida, T., Obayashi, S., Suzuki, K., and Suhara, T. (2002) Synthesis and evaluation of 3-(4-chlorobenzyl)-8-[11C]methoxy-1,2,3,4-tetrahydrochromeno[3,4-c]pyridin-5-one: a PET tracer for imaging sigma(1) receptors. Nucl Med Biol 29, 469-476.

22. Lupardus, P. J., Wilke, R. A., Aydar, E., Palmer, C. P., Chen, Y., Ruoho, A. E., and Jackson, M.

B. (2000) Membrane-delimited coupling between sigma receptors and K+ channels in rat neurohypophysial terminals requires neither G-protein nor ATP. J Physiol 526 Pt 3, 527-539.

23. Carnally, S. M., Johannessen, M., Henderson, R. M., Jackson, M. B., and Edwardson, J. M. (2010) Demonstration of a direct interaction between sigma-1 receptors and acid-sensing ion channels. Biophys J 98, 1182-1191.

24. Bucolo, C., Drago, F., Lin, L. R., and Reddy, V. N. (2006) Sigma receptor ligands protect human retinal cells against oxidative stress. Neuroreport 17, 287-291.

25. Wang, L., Eldred, J. A., Sidaway, P., Sanderson, J., Smith, A. J., Bowater, R. P., Reddan, J. R., and Wormstone, I. M. (2012) Sigma 1 receptor stimulation protects against oxidative damage through suppression of the ER stress responses in the human lens. Mechanisms of ageing and development 133, 665-674.

26. Pal, A., Fontanilla, D., Gopalakrishnan, A., Chae, Y. K., Markley, J. L., and Ruoho, A. E. (2012) The sigma-1 receptor protects against cellular oxidative stress and activates antioxidant response elements. Eur J Pharmacol 682, 12-20.

27. Largent, B. L., Gundlach, A. L., and Snyder, S. H. (1986) Sigma receptors on NCB-20 hybrid neurotumor cells labeled with (+)[3H]SKF 10,047 and (+)[3H]3-PPP. Eur J Pharmacol 124, 183-187.

28. Itzhak, Y. (1987) [3H]PCP-3-OH and (+)[3H]SKF 10047 binding sites in rat brain membranes: evidence of multiplicity. Eur J Pharmacol 136, 231-234.

29. Martin, W. R., Eades, C. G., Thompson, J. A., Huppler, R. E., and Gilbert, P. E. (1976) The effects of morphine- and nalorphine- like drugs in the nondependent and morphine-dependent chronic spinal dog. J Pharmacol Exp Ther 197, 517-532.

30. Fontanilla, D., Johannessen, M., Hajipour, A. R., Cozzi, N. V., Jackson, M. B., and Ruoho, A. E. (2009) The hallucinogen N,N-dimethyltryptamine (DMT) is an endogenous sigma-1 receptor regulator. Science 323, 934-937.

31. Ramachandran, S., Chu, U. B., Mavlyutov, T. A., Pal, A., Pyne, S., and Ruoho, A. E. (2009) The sigma1 receptor interacts with N-alkyl amines and endogenous sphingolipids. Eur J Pharmacol 609, 19-26.

32. Su, T. P., London, E. D., and Jaffe, J. H. (1988) Steroid binding at sigma receptors suggests a link between endocrine, nervous, and immune systems. Science 240, 219-221.

33. Moriguchi, S., Yamamoto, Y., Ikuno, T., and Fukunaga, K. (2011) Sigma-1 receptor stimulation by dehydroepiandrosterone ameliorates cognitive impairment through activation of CaM kinase II, protein kinase C and extracellular signal-regulated kinase in olfactory bulbectomized mice. J Neurochem 117, 879-891.

34. Cobos, E. J., Entrena, J. M., Nieto, F. R., Cendan, C. M., and Del Pozo, E. (2008) Pharmacology and therapeutic potential of sigma(1) receptor ligands. Curr Neuropharmacol 6, 344-366.

35. Al-Saif, A., Al-Mohanna, F., and Bohlega, S. (2011) A mutation in sigma-1 receptor causes juvenile amyotrophic lateral sclerosis. Ann Neurol 70, 913-919.

36. Mishina, M., Ohyama, M., Ishii, K., Kitamura, S., Kimura, Y., Oda, K., Kawamura, K., Sasaki, T., Kobayashi, S., Katayama, Y., and Ishiwata, K. (2008) Low density of sigma1 receptors in early Alzheimer's disease. Ann Nucl Med 22, 151-156.

37. Mishina, M., Ishiwata, K., Ishii, K., Kitamura, S., Kimura, Y., Kawamura, K., Oda, K., Sasaki,

T., Sakayori, O., Hamamoto, M., Kobayashi, S., and Katayama, Y. (2005) Function of sigma1 receptors in Parkinson's disease. Acta Neurol Scand 112, 103-107.

38. Smith, S. B., Duplantier, J., Dun, Y., Mysona, B., Roon, P., Martin, P. M., and Ganapathy, V. (2008) In vivo protection against retinal neurodegeneration by sigma receptor 1 ligand (+)-pentazocine. Invest Ophthalmol Vis Sci 49, 4154-4161.

39. Hiranita, T., Soto, P. L., Tanda, G., and Katz, J. L. (2010) Reinforcing effects of sigma-receptor agonists in rats trained to self-administer cocaine. J Pharmacol Exp Ther 332, 515-524.

40. Ujike, H., Kuroda, S., and Otsuki, S. (1996) sigma Receptor antagonists block the development of sensitization to cocaine. Eur J Pharmacol 296, 123-128.

41. Ramachandran, S., Lu, H., Prabhu, U., and Ruoho, A. E. (2007) Purification and characterization of the guinea pig sigma-1 receptor functionally expressed in Escherichia coli. Protein Expr Purif 51, 283-292.

42. Chen, Y., Hajipour, A. R., Sievert, M. K., Arbabian, M., and Ruoho, A. E. (2007) Characterization of the cocaine binding site on the sigma-1 receptor. Biochemistry 46, 3532-3542.

43. Fontanilla, D., Hajipour, A. R., Pal, A., Chu, U. B., Arbabian, M., and Ruoho, A. E. (2008) Probing the steroid binding domain-like I (SBDLI) of the sigma-1 receptor binding site using N-substituted photoaffinity labels. Biochemistry 47, 7205-7217.

44. Pal, A., Hajipour, A. R., Fontanilla, D., Ramachandran, S., Chu, U. B., Mavlyutov, T., and Ruoho, A. E. (2007) Identification of regions of the sigma-1 receptor ligand binding site using a novel photoprobe. Mol Pharmacol 72, 921-933.

45. Pal, A., Chu, U. B., Ramachandran, S., Grawoig, D., Guo, L. W., Hajipour, A. R., and Ruoho,

A. E. (2008) Juxtaposition of the steroid binding domain-like I and II regions constitutes a ligand binding site in the sigma 1 receptor. J Biol Chem 283, 19646-19656.

46. Ganapathy, M. E., Prasad, P. D., Huang, W., Seth, P., Leibach, F. H., and Ganapathy, V. (1999) Molecular and ligand-binding characterization of the sigma-receptor in the Jurkat human T lymphocyte cell line. J Pharmacol Exp Ther 289, 251-260..

47. Seth, P., Ganapathy, M. E., Conway, S. J., Bridges, C. D., Smith, S. B., Casellas, P., and Ganapathy, V. (2001) Expression pattern of the type 1 sigma receptor in the brain and identity of critical anionic amino acid residues in the ligand-binding domain of the receptor. Biochim Biophys Acta 1540, 59-67.

48. Russ, W. P., and Engelman, D. M. (2000) The GxxxG motif: a framework for transmembrane helix-helix association. J Mol Biol 296, 911-919.

49. Senes, A., Engel, D. E., and DeGrado, W. F. (2004) Folding of helical membrane proteins: the role of polar, GxxxG-like and proline motifs. Curr Opin Struct Biol 14, 465-479.

50. Senes, A., Gerstein, M., and Engelman, D. M. (2000) Statistical analysis of amino acid patterns in transmembrane helices: the GxxxG motif occurs frequently and in association with beta-branched residues at neighboring positions. J Mol Biol 296, 921-936.

51. Klock, H. E., and Lesley, S. A. (2009) The Polymerase Incomplete Primer Extension (PIPE) method applied to high-throughput cloning and site-directed mutagenesis. Methods Mol Biol 498, 91-103.

52. Gromek, K. A., Meddaugh, H. R., Wrobel, R. L., Suchy, F. P., Bingman, C. A., Primm, J. G., and Fox, B. G. (2013) Improved expression and purification of sigma 1 receptor fused to maltose

binding protein by alteration of linker sequence. Protein Expr Purif 89, 203-209.

53. Russ, W. P., and Engelman, D. M. (1999) TOXCAT: a measure of transmembrane helix association in a biological membrane. Proc Natl Acad Sci U S A 96, 863-868.

54. Blommel, P. G., and Fox, B. G. (2007) A combined approach to improving large-scale production of tobacco etch virus protease. Protein Expr Purif 55, 53-68.

55. Shaw, W. V. (1975) Chloramphenicol acetyltransferase from chloramphenicol-resistant bacteria. Methods Enzymol 43, 737-755.

56. Narayanan, S., Bhat, R., Mesangeau, C., Poupaert, J. H., and McCurdy, C. R. (2011) Early development of sigma-receptor ligands. Future medicinal chemistry 3, 79-94.

57. Su, T. P., and Hayashi, T. (2003) Understanding the molecular mechanism of sigma-1 receptors: towards a hypothesis that sigma-1 receptors are intracellular amplifiers for signal transduction. Curr Med Chem 10, 2073-2080.

58. Matsumoto, R. R., Bowen, W. D., Tom, M. A., Vo, V. N., Truong, D. D., and De Costa, B. R. (1995) Characterization of two novel s receptor ligands: antidystonic effects in rats suggests s receptor antagonism. Eur J Pharmacol 280, 301-310.

59. Herrmann, J. R., Panitz, J. C., Unterreitmeier, S., Fuchs, A., Frishman, D., and Langosch, D. (2009) Complex patterns of histidine, hydroxylated amino acids and the GxxxG motif mediate high-affinity transmembrane domain interactions. J Mol Biol 385, 912-923.

60. Colabufo, N. A., Contino, M., Inglese, C., Niso, M., Perrone, R., Roperto, S., and Roperto, F. (2009) In vitro and ex vivo characterization of sigma-1 and sigma-2 receptors: agonists and antagonists in biological assays. Cent Nerv Syst Agents Med Chem 9, 161-171.

61. Yamamoto, H., Miura, R., Yamamoto, T., Shinohara, K., Watanabe, M., Okuyama, S., Nakazato, A., and Nukada, T. (1999) Amino acid residues in the transmembrane domain of the type 1 sigma receptor critical for ligand binding. FEBS Lett 445, 19-22.

62. Wu, Z., and Bowen, W. D. (2008) Role of sigma-1 receptor C-terminal segment in inositol 1,4,5-trisphosphate receptor activation: constitutive enhancement of calcium signaling in MCF-7 tumor cells. The Journal of biological chemistry 283, 28198-28215.

63. Ortega-Roldan, J. L., Ossa, F., and Schnell, J. R. (2013) Characterization of the human sigma-1 receptor chaperone domain structure and binding immunoglobulin protein (BiP) interactions. The Journal of biological chemistry 288, 21448-21457.

64. Chu, U. B., Ramachandran, S., Hajipour, A. R., and Ruoho, A. E. (2013) Photoaffinity Labeling of the Sigma-1 Receptor with N-[3-(4-Nitrophenyl)propyl]-N-dodecylamine: Evidence of Receptor Dimers. Biochemistry 52, 859-868.

65. Schuster, D. I., Arnold, F. J., and Murphy, R. B. (1995) Purification, pharmacological characterization and photoaffinity labeling of sigma receptors from rat and bovine brain. Brain Res 670, 14-28.

66. Casado, V., Cortes, A., Mallol, J., Perez-Capote, K., Ferre, S., Lluis, C., Franco, R., and Canela, E. I. (2009) GPCR homomers and heteromers: a better choice as targets for drug development than GPCR monomers? Pharmacol Ther 124, 248-257.

67. Ferre, S., and Franco, R. (2010) Oligomerization of G-protein-coupled receptors: a reality. Curr Opin Pharmacol 10, 1-5.

68. Rovira, X., Pin, J. P., and Giraldo, J. (2010) The asymmetric/symmetric activation of GPCR

dimers as a possible mechanistic rationale for multiple signalling pathways. Trends Pharmacol Sci 31, 15-21.

69. Low, C., Moberg, P., Quistgaard, E. M., Hedren, M., Guettou, F., Frauenfeld, J., Haneskog, L., and Nordlund, P. (2013) High-throughput analytical gel filtration screening of integral membrane proteins for structural studies. Biochim Biophys Acta 1830, 3497-3508.

70. Na, J. H., Shin, J., Jung, Y., Lim, D., Shin, Y. K., and Yu, Y. G. (2013) Bacterially expressed human serotonin receptor 3A is functionally reconstituted in proteoliposomes. Protein Expr Purif 88, 190-195.

71. Venkatakrishnan, A. J., Deupi, X., Lebon, G., Tate, C. G., Schertler, G. F., and Babu, M. M. (2013) Molecular signatures of G-protein-coupled receptors. Nature 494, 185-194.

72. Vukoti, K., Kimura, T., Macke, L., Gawrisch, K., and Yeliseev, A. (2012) Stabilization of functional recombinant cannabinoid receptor CB(2) in detergent micelles and lipid bilayers. PLoS One 7, e46290.

73. Balasuriya, D., Stewart, A. P., Crottes, D., Borgese, F., Soriani, O., and Edwardson, J. M. (2012) The sigma-1 receptor binds to the Nav1.5 voltage-gated Na+ channel with 4-fold symmetry. J Biol Chem 287, 37021-37029.

74. Brune, S., Schepmann, D., Lehmkuhl, K., Frehland, B., and Wunsch, B. (2012) Characterization of ligand binding to the sigma(1) receptor in a human tumor cell line (RPMI 8226) and establishment of a competitive receptor binding assay. Assay Drug Dev Technol 10, 365-374

Appendix
Self-association of the transmembrane domains of divisome proteins ZipA and FtsN

A1 Introduction

Chapter 1 discusses the importance of the protein protein interactions of the divisome. **Chapter 2** discusses the importance of the self association of the FtsB protein. Many proteins in the divisome have been shown to self associate, but the importance of this oligomerization has not been fully characterized (**section 1.9.2**). Evidence suggests that ZipA self associates prior to its association with the membrane and interaction with FtsZ[1]. There has not been evidence showing that self-association occurs in FtsN in the literature, but we were interested to see whether or not the transmembrane domain had a propensity to self-associate. Because FtsN has so many interaction partners (FtsQ[2], FtsI and FtsW[3]), we thought it would be interesting to see if it also had any tendency to self-interact. TOXCAT is a well known assay for measuring self-association of transmembrane domains of proteins[4], both of which exist in ZipA and FtsN. I determined that both ZipA and FtsN weakly associate via their transmembrane domains in the TOXCAT assay.

A2 Materials and Methods

Vectors and strains

All oligonucleotides were purchased in desalted form Integrated DNA Technologies and used without purification. The expression vectors pccKAN, pccGpA-wt, and pccGpA-G83I, and *malE* deficient *Escherichia coli* strain MM39 were kindly provided by Dr. Donald M. Engelman[4]. Genes encoding the transmembrane domain of FtsB and FtsL were cloned into the NheI-BamHI restriction sites of the pccKAN vector resulting in the following protein sequences:

ZipA "...LILIIVGAIAIIALLVHGFWTS..."

FtsN "...LPAVSPAMVAIAAAVLVTFIFIGGLYFIT..."

All mutagenesis was done with the QuikChange kit (Stratagene).

Expression of Chimeric Proteins in MM39 cells and MalE complementation assay

The TOXCAT constructs were transformed into MM39 cells. A freshly streaked colony was inoculated into 3 mL of LB broth containing 100 μg/mL ampicillin and grown overnight at 37 ˚C. Overnight cultures were inoculated into 3 mL of LB broth at a ratio of 1:1000 and grown to an OD_{420} of approximately 1 at 37 ˚C (OD_{600} of 0.6) at 37 ˚C. After recording the optical density, 1 mL of cells were spun down for 10 min at 17000*g* and resuspended in 500 mL of sonication buffer (25 mM Tris-HCl, 2 mM EDTA, pH 8.0). Cells were lysed by probe sonication at medium power for 10 seconds over ice, and an aliquot of 50 μL was removed from each sample and stored in SDS-PAGE loading buffer for western blotting. The lysates were then cleared by centrifugation and the supernatant was kept on ice for chloramphenicol acetyltransferase (CAT) activity assay. To confirm for proper membrane insertion of the TOXCAT constructs, overnight cultures were plated on M9 minimal medium plates containing 0.4% maltose as the only carbon source and grown at 37 ˚C for 48 hours[4].

Chloramphenicol Acetyltransferase (CAT) spectrophotometric assay

CAT activity was measured as described[5,6]. 1 mL of buffer containing 0.1 mM acetyl coA, 0.4 mg/mL 5,5'-dithiobis-(2-nitrobenzoic acid), and 0.1 M Tris-HCl pH 7.8 was mixed with 40 μL of cleared cell lysates and the absorbance at 412 nm was measured for two minutes to establish basal activity rate. After addition of 40 μL of 2.5 mM chloramphenicol in 10% ethanol were added, the absorbance was measured for an additional two minutes to determine CAT activity. The basal CAT activity was subtracted and the value was normalized by the cell density measured as OD_{420}. All measurement were determined at least in duplicate and the experiments were repeated at least twice.

A3 Results and Discussion

A3.1 ZipA shows weak self-association in TOXCAT with variation across different sequence lengths

Although evidence has suggested that ZipA self association occurs in the divisome, our results showed that the self-association of the transmembrane domain is weak (~20% of strong dimerizing control Glycophorin A, GpA) as shown in **Figure A2.1**. Because it was believed that ZipA self association occurred, we scanned varying lengths of the transmembrane domain of ZipA fairly exhaustively as you can see from the constructs tested. In general, though, the self-association was weak.

A3.2 FtsN shows weak self-association in TOXCAT, but the variation across different C-terminal truncations is profound

As the role of FtsN in the divisome is not fully characterized, we decided to probe the interaction of the transmembrane domain. In order to fully characterize its action with other divisome proteins, the first step would be to determine if the transmembrane domain self associates. I performed truncations on the C-terminus of FtsN and found that the construct that extends to F53 showed a result of self-association at a level 20% of GpA (**Figure A2.2**). Interestingly, this was drastically more TOXCAT activity than the other truncations that were testing. This has been seen consistently in TOXCAT; a deletion of one amino acid can change the signal by a large amount.

Figure A1

A

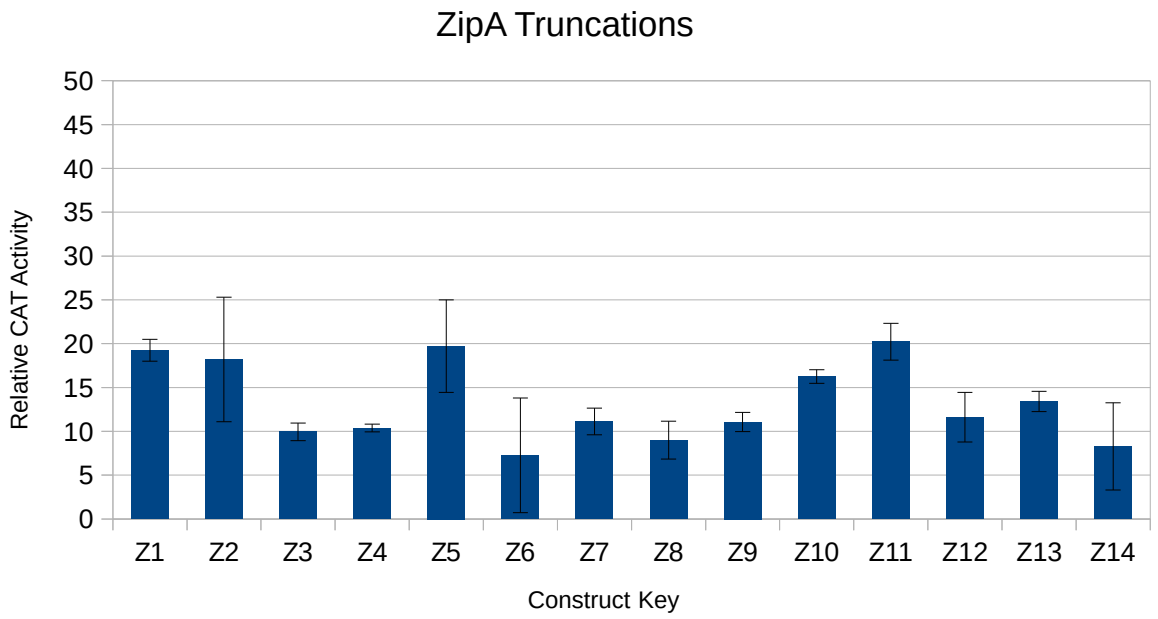

B

ZipA TM Sequence	Key
LILIIVGAIAIIALLVHGF	Z1
LILIIVGAIAIIALLVHGFW	Z2
LRLILIIVGAIAIIALLVHGFWT	Z3
RLILIIVGAIAIIALLVHGFWT	Z4
LILIIVGAIAIIALLVHGFWT	Z5
ILIIVGAIAIIALLVHGFWT	Z6
LIIVGAIAIIALLVHGFWT	Z7
IIVGAIAIIALLVHGFWT	Z8
LRLILIIVGAIAIIALLVHGFWTS	Z9
RLILIIVGAIAIIALLVHGFWTS	Z10
LILIIVGAIAIIALLVHGFWTS	Z11
ILIIVGAIAIIALLVHGFWTS	Z12
LIIVGAIAIIALLVHGFWTS	Z13
IIVGAIAIIALLVHGFWTS	Z14

Figure A1 Self-association of ZipA. A) ZipA self association across multiple constructs with transmembrane domains of varying lengths and B) the transmembrane domain sequence key.

Figure A2

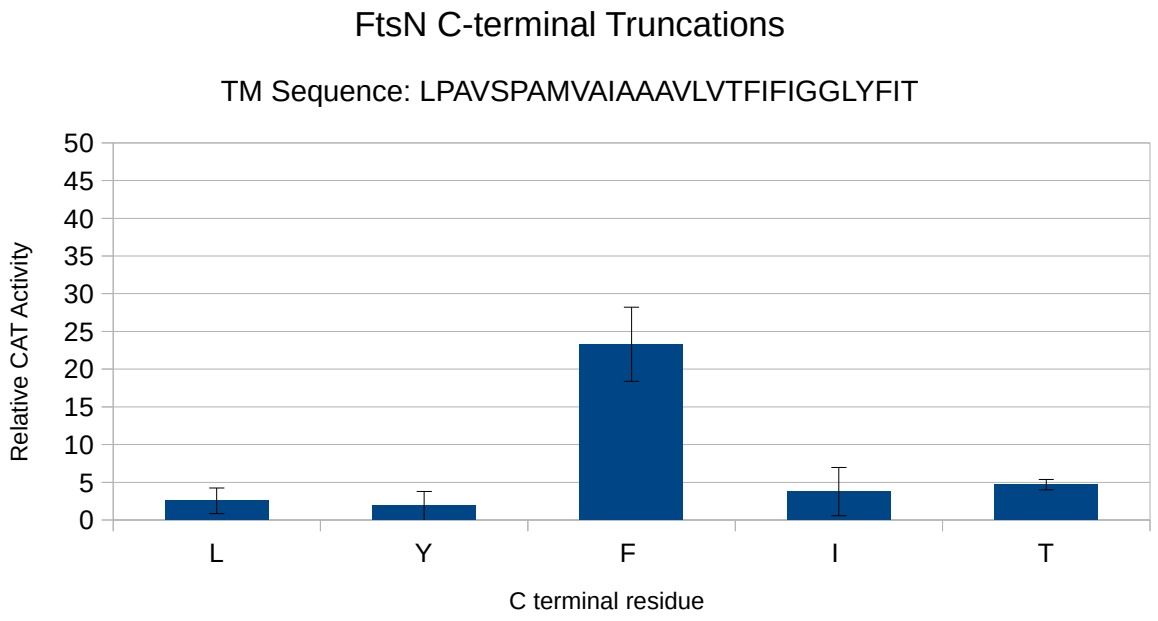

Figure A2 Self-association of FtsN is weak in TOXCAT. Single amino acid truncations of the C-terminus of FtsN were tested for self association and most showed no CAT activity, bu truncation to F53 showed a mild amount of CAT Activity.

A4 Acknowledgements

I would like to thank Claire Armstrong (Senes lab undergraduate student) for her help during the molecular biology of the ZipA construct and TOXCAT assay. I was supported by the WARF Distinguished Fellowship at the time of this research.

A5 References

1. Skoog, K. & Daley, D. O. The Escherichia coli cell division protein ZipA forms homodimers prior to association with FtsZ. *Biochemistry (Mosc.)* **51,** 1407–1415 (2012).
2. Karimova, G., Dautin, N. & Ladant, D. Interaction network among Escherichia coli membrane proteins involved in cell division as revealed by bacterial two-hybrid analysis. *J. Bacteriol.* **187,** 2233–2243 (2005).
3. Alexeeva, S., Gadella, T. W. J., Jr, Verheul, J., Verhoeven, G. S. & den Blaauwen, T. Direct interactions of early and late assembling division proteins in Escherichia coli cells resolved by FRET. *Mol. Microbiol.* **77,** 384–398 (2010).
4. Russ, W. P. & Engelman, D. M. TOXCAT: a measure of transmembrane helix association in a biological membrane. *Proc. Natl. Acad. Sci. U. S. A.* **96,** 863–8 (1999).
5. Sulistijo, E. S. & Mackenzie, K. R. Structural basis for dimerization of the BNIP3 transmembrane domain. *Biochemistry (Mosc.)* **48,** 5106–5120 (2009).
6. Shaw, W. V. Chloramphenicol acetyltransferase from chloramphenicol-resistant bacteria. *Methods Enzymol.* **43,** 737–755 (1975).